

# **The Effect of Oil Properties on Engine Oil Pump Failure Mechanisms**

by

**Farnaz Motamen Salehi**

Submitted in accordance with the requirements for the degree of  
**Doctor of Philosophy**

The University of Leeds  
School of Mechanical Engineering  
Leeds, UK

September, 2016

The candidate confirms that the work submitted is her own, except where work which has formed part of jointly authored publications has been included. The contribution of the candidate and other co-authors in published work from this thesis has been clearly indicated. The candidate confirms that appropriate credit has been given within the thesis where reference has been made to the work of others.

In the paper contributing to this thesis “Corrosive-abrasive wear induced by soot in boundary lubrication regime”, the candidate (first author) carried out all the experiments, analysis and preparation of the manuscripts. All other authors contributed by providing insight on the discussions and proof reading. Raman spectroscopy was undertaken by Dr Doris Khaemba (Institute of Functional Surfaces, The University of Leeds, UK).

This copy has been supplied on the understanding that it is copyright material and that no quotation from this thesis may be published without proper acknowledgement.

© 2016 The University of Leeds and Farnaz Motamen Salehi

## **Papers contributing to this thesis**

- Motamen Salehi, F., Khaemba, D.N., Morina, A. Neville A. “Corrosive-abrasive wear induced by soot in boundary lubrication regime” Tribology Letters, Volume 63, Issue 2, 2016. Featured in Chapter 6

## Conferences and awards

### Conferences presented:

- Motamen Salehi *et al.* Variable Displacement Vane Pump: A tribological study, TriboUK conference, Sheffield 2014
- Motamen Salehi *et al.* The effect of oil contamination on wear and friction in engine oil, 41st Leeds-Lyon Symposium on Tribology, Leeds 2014
- Motamen Salehi *et al.* The effect of diesel and soot contamination on wear and friction in boundary lubrication regime. Loughborough 2015
- Motamen Salehi *et al.* Effect of oil degradation on tribological performance of engine oil pump, TurkeyTrib conference, Turkey 2015
- Motamen Salehi *et al.* Effect of oil degradation on tribological performance of engine oil pump, STLE 71st Annual Meeting USA 2016
- Motamen Salehi *et al.* Corrosive-abrasive wear induced by soot in boundary lubrication regime, 43rd Leeds-Lyon Symposium on Tribology, Leeds 2016

### Awards received:

- First poster award: TriboUK conference, Sheffield 2014
- Third poster award: 41<sup>st</sup> Leeds-Lyon Symposium on Tribology, Leeds 2014
- Second poster award: Postgraduate Research competition, University of Leeds 2014
- First poster award: TriboUK 2015 conference, Loughborough 2015

## **Acknowledgements**

First, I would like to express my deepest gratitude to my supervisors, Professor Anne Neville and Professor Ardian Morina who have been very influential in ensuring the successful completion of this work. It has truly been a pleasure working with both of you and without you this work would not have been possible.

I would like to thank Magna Powertrain and the University of Leeds for funding this PhD study. I am grateful to all my colleagues and technicians in the Institute of Functional Surfaces (iFS), in particular, Mrs Fiona Slade and Mrs Judith Schneider. My special thanks go to all my friends and members of iFS research group in the school of Mechanical Engineering, namely Shahriar, John, Kirijen, Nik, Zahra, Ashely, Kevin, Erfan, Ali, Pourya, Siavash, Joe, Thawhid, MacDonald, Cayetano, Mohsen and Karen for creating a wonderful working environment for me. I am particularly grateful to my two invaluable friends, Dr. Doris Khaemba and Dr. Mahsa Shahi Avadi, for their assistance in managing thoughts and proofreading the text.

I am extremely grateful to all my family and friends in Iran for their support throughout my studies. My very special thanks go to my father (Mohammad Mehdi Motamen Salehi) and my mother (Mehrnaz Anari) for their unconditional love, support and encouragement during my stay in England. This applies not only in this research but also my entire educational journey, without them it would not have been possible. I am also thankful to my sister (Sarvenaz Motamen Salehi) and my brother (Alireza Motamen Salehi) for their continuous support and love.

Last but not least, I would like to express my appreciation to my husband Siamak Taghaboni for his endless love, care and encouragements. His constant support during my PhD has been invaluable.

## To My Family

## Abstract

In recent years, there has been an increasing demand in the automotive industry to improve fuel economy. Poor fuel economy is attributed to the high friction and wear of various engine components. Thus, the automotive industry aims to design fuel efficient vehicles in order to reduce the fuel consumption. A Variable Displacement Vane Pump (hereafter denoted VDVP) is an innovative type of oil pump that has a variable capacity that is adjustable to the engine demand. This type of pump can improve the efficiency of engines. However, high friction and severe wear in the component of this pump is an issue. Oil contamination is one of the factors that influence the friction and wear behaviour of components in VDVP. Many studies have been conducted on the effect of contaminants such as soot on tribological performance of oils. However, the exact mechanism of the oil contaminations is not fully understood yet.

This study aims to investigate the effect of oil contaminants such as soot and diesel on the oil properties and tribological behaviour of oils in the boundary lubrication regime in VDVP. Furthermore, it examines the effect of these contaminants on the oil's properties during the ageing process.

To achieve this, the tribological performance of various oils has been evaluated using ball-on-disc and pin-on-plate test rigs in the boundary lubrication regime. Different surface analysis techniques were used to understand the effect of each of the contaminants on wear and friction behaviour of contacts. A number of surface analysis techniques were employed in this study such as Scanning Electron Microscopy (SEM), Energy- Dispersive X-ray (EDX), Raman spectroscopy, Fourier Transform InfraRed Spectroscopy (FTIR) and Inductively Coupled Plasma (ICP).

The results of this study indicate that Carbon Black (CB) contamination (soot surrogate) increases the wear of components. It has been proposed that a

corrosive-abrasive mechanism is responsible for the high wear observed in fully formulated oil (FFO) when contaminated with CB. The interaction of sulphur- and phosphorus-based additives such as ZDDP with CB resulted in an antagonistic behaviour that enhanced wear. This mechanism is more dominant than the abrasion effect of itself.

This study shows that diesel contamination can reduce the friction and wear under certain condition due to the lubricity of diesel. It also reveals that the contaminants and ageing conditions can change the bulk properties (viscosity and TAN) of the oils. This is found to be dependent on the type of contaminants and ageing duration. When CB is present in the oil during the ageing process, it results in high Total Acid Number (TAN) and severe wear of engine components. These results also reveal that the high wear observed with CB is not solely due to abrasion. Additive depletion and additive adsorption by CB particles during the ageing process are shown to play a significant role in producing high wear.



# Table of Contents

<b>Papers contributing to this thesis .....</b>	<b>iii</b>
<b>Conferences and awards.....</b>	<b>iv</b>
<b>Acknowledgements.....</b>	<b>v</b>
<b>Abstract.....</b>	<b>vii</b>
<b>Table of Contents .....</b>	<b>ix</b>
<b>List of Figures .....</b>	<b>xv</b>
<b>List of Tables .....</b>	<b>xxv</b>
<b>Nomenclature .....</b>	<b>xxvi</b>
<b>List of Abbreviations.....</b>	<b>xxvii</b>
<b>Chapter 1 Introduction.....</b>	<b>1</b>
1.1 Global energy challenges .....	1
1.2 Diesel engine fuel economy .....	2
1.3 Engine oil pumps .....	2
1.4 Aims and objectives.....	4
1.5 Thesis outline .....	5
<b>Chapter 2 Theoretical aspects of tribology.....</b>	<b>7</b>
2.1 Introduction to tribology .....	7
2.2 Friction.....	8
2.3 Contact between surfaces .....	9
2.4 Lubrication .....	11
2.5 Wear.....	15
2.6 Oils .....	18
<b>Chapter 3 Literature review .....</b>	<b>21</b>
3.1 Introduction to hydraulic pumps.....	21
3.1.1 Introduction to VDVP .....	23

3.1.2	VDVP components .....	23
3.1.3	Operation of VDVP .....	24
3.2	Failure of VDVP .....	25
3.3	Tribological behaviour of VDVP .....	26
3.4	Lubrication .....	30
3.5	Lubrication regime in VDVP .....	30
3.6	Role of tribofilm in boundary lubrication regime .....	32
3.6.1	Zinc Dialkyldithiophosphates (ZDDP) tribofilms.....	32
3.6.2	Mechanical properties of ZDDP tribofilm .....	33
3.6.3	Chemical properties of ZDDP tribofilm .....	34
3.7	Parameters that influence ZDDP tribofilm .....	35
3.8	Tribological performance of ZDDP on surfaces .....	36
3.9	Tribochemistry of ZDDP .....	38
3.10	Stability of ZDDP film.....	40
3.11	Interactions of additives.....	43
3.12	ZDDP interactions with dispersants and detergents .....	44
3.13	Role of oil contamination on tribological performance of contacts ....	46
3.13.1	Diesel fuel.....	47
3.13.2	Diesel fuel contamination of engine oils .....	48
3.13.3	Soot.....	49
3.13.4	Effect of soot on friction in boundary lubrication regime .....	52
3.13.5	Proposed wear mechanisms by soot.....	55
3.14	Interactions of additives and oil contaminants .....	59
3.15	Oil ageing .....	62
3.16	Effect of oil ageing on the performance of oils.....	64
3.17	Summary .....	65
<b>Chapter 4</b>	<b>Experimental methodology.....</b>	<b>68</b>
4.1	Introduction.....	68
4.2	Materials.....	68
4.2.1	Fully formulated engine oil.....	68
4.2.2	Base oil and antiwear additive.....	69

4.2.3 Carbon black powder .....	70
4.2.4 Diesel fuel.....	72
4.3 Oil ageing .....	73
4.4 Tribological tests.....	74
4.4.1 High Speed Pin-on-Disc (HSPOD) tribotests.....	75
4.4.2 Pin-on-plate tribometer testing procedure (TE77) .....	78
4.5 Pre-test and post-test sample treatment.....	81
4.6 Wear measurement .....	82
4.7 Scanning Electron Microscope (SEM) and Energy Dispersive X-ray analysis (EDX) .....	84
4.8 Raman spectroscopy .....	85
4.9 Bulk oil analysis .....	86
4.9.1 Viscosity measurement .....	86
4.9.2 Attenuated Total Reflectance/ Fourier Transform InfraRed spectroscopy (ATR/ FTIR) .....	86
4.9.3 Inductively Coupled Plasma spectroscopy (ICP) .....	86
4.9.4 Centrifugation for particle removal.....	87

**Chapter 5 Initial failure analysis of the variable displacement vane  
pump 88**

5.1 Introduction.....	88
5.2 Background .....	88
5.3 Visual inspection of worn surfaces .....	89
5.4 Microscopic characterisation of variable displacement vane pump ..	95
5.4.1 SEM analysis.....	95
5.5 Wear analysis .....	99
5.6 Summary of historical tests.....	102
5.6.1 Design of hydraulic pump.....	102
5.7 Material and treatment.....	103
5.7.1 VDVP lubrication .....	104
5.8 Discussion and conclusions.....	105

**Chapter 6 The effect of soot on lubrication and wear mechanisms 107**

6.1	Introduction.....	107
6.2	Physical properties of oils.....	108
6.3	Calculation of lambda ratio ( $\lambda$ ).....	108
6.4	Friction results.....	109
6.5	Wear results.....	112
6.6	Surface characterisation.....	114
6.7	Wear mechanism.....	117
6.7.1	Abrasion of antiwear tribofilms and steel substrate.....	117
6.7.2	Additive adsorption.....	121
6.8	Summary.....	123
<b>Chapter 7 Antiwear additive adsorption mechanism on soot.....</b>		<b>124</b>
7.1	Introduction.....	124
7.2	Base oil (group III mineral oil) and ZDDP additive.....	124
7.3	Oil degradation in presence of CB.....	127
7.4	ZDDP additive adsorption during the ageing process.....	128
7.4.1	FTIR analysis.....	128
7.4.2	ICP analysis.....	129
7.4.3	Chemical composition of CB particles.....	130
7.5	Summary.....	132
<b>Chapter 8 The effect of diesel contamination on tribological performance of fully formulated engine oils.....</b>		<b>134</b>
8.1	Introduction.....	134
8.2	Physical properties of oils.....	134
8.3	Calculation of lambda ratio ( $\lambda$ ).....	136
8.4	Friction results.....	136
8.5	Wear results.....	138
8.6	Chemical composition of tribofilm.....	140
8.6.1	EDX analysis.....	140
8.6.2	Raman analysis.....	142
8.7	Role of diesel on wear mechanism.....	143

8.8 Physical properties of oils .....	143
8.8.1 Wear results .....	144
8.8.2 EDX analysis .....	145
8.9 Summary .....	146
<b>Chapter 9 The effect of oil degradation on tribological performance of vane-rotor contact .....</b>	<b>147</b>
9.1 Introduction.....	147
9.2 Oil analysis .....	148
9.2.1 Viscosity results.....	149
9.2.2 Total Acid Number (TAN) .....	150
9.2.3 FTIR results.....	151
9.3 Tribotests under reciprocating sliding conditions .....	154
9.3.1 Effect of contaminants on friction and wear.....	154
9.3.2 Effect of oil degradation on friction and wear.....	156
9.4 Surface characterisation.....	158
9.5 The effect of contaminants on wear mechanism .....	162
9.5.1 Effect of abrasion by CB.....	164
9.5.2 Antagonistic effect of contaminants on wear .....	164
9.5.3 Effect of filtration on oil performance .....	166
9.6 Summary .....	168
<b>Chapter 10 Discussion .....</b>	<b>170</b>
10.1 The effect of CB on the bulk properties of oils .....	171
10.2 The link between friction and CB contamination.....	173
10.3 The link between sliding configuration, friction and wear.....	174
10.4 Wear mechanism induced by carbon black .....	176
10.5 The effect of diesel fuel on wear reduction and tribofilm formation.	180
10.6 Effect of ageing on tribological behaviour of oils.....	181
10.6.1 Effects of ageing process and contamination on oil .....	181
10.6.2 Ageing oil with diesel and carbon black.....	187
<b>Chapter 11 Conclusions and future work.....</b>	<b>189</b>

11.1	Conclusions .....	189
11.1.1	Effects of contaminants and ageing on the bulk properties of FFO 189	
11.1.2	Effect of CB on the tribological performance of oil.....	190
11.1.3	Effects of diesel on tribological performance of oil .....	191
11.1.4	Effects of ageing process on the tribological performance of oil 192	
11.2	Recommendations for future work.....	192
	<b>References.....</b>	<b>194</b>

## List of Figures

Figure 1-1. Energy losses in passenger cars [1].	1
Figure 1-2. Friction power comparison between a traditional oil pump and an engine by increasing engine speed. Friction power of the oil pump takes approximately 8% of the friction power of the engine [9].	3
Figure 2-1. Major tribological factors [13].	7
Figure 2-2. Schematic diagram showing two bodies in a point contact [17].	9
Figure 2-3. Schematic diagram showing two bodies in a line contact [13].	10
Figure 2-4. Schematic diagram illustrating the different lubrication regimes (a) hydrodynamic (b) elastohydrodynamic (c) mixed (d) boundary [17].	14
Figure 2-5. Stribeck diagram for some IC engine components. The lubrication regime for VDVP is either boundary or mixed regime [13].	15
Figure 2-6. Schematic of (a) three-body abrasive wear and (b) two-body abrasive wear [26].	16
Figure 2-7. The range of wear coefficient (K) under different conditions [25].	18
Figure 2-8. Interaction between various surface active additives [30].	20
Figure 3-1. Hydraulic pumps classification [31].	22
Figure 3-2. Schematic of (a) single chamber vane pump (b) double chamber vane pumps (c) variable displacement vane pump [31]. Inlet region is represented in blue and outlet region is shown in red.	22
Figure 3-3. Exploded view of VDVP (Provided by Magna Powertrain, Ontario, Canada).	24
Figure 3-4. (a) Full flow and (b) zero flow working condition [37].	25
Figure 3-5. Vane force at vane tip in contact with the slide ring [39].	27

Figure 3-6. The relationship between coefficient of friction and surface roughness. Pump speed is shown by N in the graph [40]. .....	28
Figure 3-7. Change in surface roughness of vane tip after 250 h [36]......	29
Figure 3-8. Changes in contact radius of vane with time due to wear [34]. .	29
Figure 3-9. Lubrication regime between vane tip and slide ring [40]. .....	31
Figure 3-10. The idealised molecular structure of ZDDP [48]......	32
Figure 3-11. Mechanical properties of ZDDP tribofilm. (a) Full antiwear film formed on surface from ZDDP solution. (b) Same antiwear film after washing with solvent. Y-axis shows representative thickness of each layer of antiwear film. $H_0$ indicates initial hardness for each material [60]. .....	33
Figure 3-12. Structure and composition of ZDDP tribofilm [53]. .....	34
Figure 3-13. The MD simulation showing the combined effects of pressure and shear on the behaviour of the iron oxide particles embedded in the zinc metaphosphate [81]......	39
Figure 3-14. The study of stability of ZDDP tribofilm using base oil and dispersant. Test conducted at speed of 0.05 m/s and 80°C [55]. .....	42
Figure 3-15. Removal of ZDDP film in the presence of 0.1 wt% soot. Test conducted at speed of 0.05 m/s and 80°C [55]. .....	42
Figure 3-16. Intermolecular interactions between additives [87]. .....	44
Figure 3-17. Schematic structures of tribofilms formed using (a) ZDDP solution (b) combination of ZDDP+Detergents+Dispersants [96]. .....	46
Figure 3-18. Diameter of wear scar ( $D_w \times s$ ) versus sulphur content ( $C_s$ ) in diesel fuel obtained by two methods. Method 1: High-Frequency Reciprocating Rig (HFRR method) using ISO 12156 standard. Method 2: proposed method in the study [102]. .....	48
Figure 3-19. A typical extracted soot from engine [107]. .....	50
Figure 3-20. Indicates friction coefficient against temperature with different soot mass, showing that the oil with higher soot mass has lower friction coefficient at temperatures 40-80°C [122]. .....	53



Figure 3-21. Friction behaviour of different oils containing 3wt% soot at 40°C [122]. .....	54
Figure 3-22. Indicates friction coefficient behaviour in the presence of 5 wt% CB using three different dispersants. The concentration of dispersant was 9 wt% in all three samples [110]......	56
Figure 3-23. Schematic of wear mechanism in ball-on-flat tribometer test with high level of contamination [137]......	57
Figure 3-24. 3D topographical image of wear scar formed on the ball samples using various oils containing (a) dispersant (b) CB particles (c) detergent+dispersant+ZDDP+CB [147]......	61
Figure 3-25. Effect of CB particles on wear in the presence of antiwear /EP additives [114]. .....	61
Figure 3-26. Schematic of the oxidative degradation diagram in the oil [151]. .....	63
Figure 3-27. Oil degradation cycle [152]......	64
Figure 3-28. Schematic of the effect of contaminants in the lubrication system (source: author)......	67
Figure 4-1. The main additive elements detected in FFO used in this study using ICP.....	69
Figure 4-2. High resolution image of CB particles, showing the diameter of particles.....	71
Figure 4-3. Raman spectra of the carbon black used in this study.....	71
Figure 4-4 Raman spectra of CB and diesel soot extracted from Vehicle Test (VT) and Engine Dynamometer Test (EDT). Exhaust soot from a pipe was also analysed referred to as ET soot [112]......	72
Figure 4-5. Raman spectra of the FFO and diesel used in this study, showing a similarities in the spectra for the FFO and diesel, with the difference of a larger peak at 1609 cm <sup>-1</sup> for diesel, attributed to higher sulphur content.....	73
Figure 4-6. Schematic set-up for oil degradation.....	74

Figure 4-7. Schematic of the actual contact in pin-on-disc tribometer [164]	75
Figure 4-8. Image of the high speed pin on disc tribometer used in this study, in the setup position. The disc was submerged in an oil bath and the ball was lowered onto the disc during the experiments. ....	76
Figure 4-9. Examples of wear scars generated on the (a) disc and (b) ball after tests on the HSPOD tribometer.....	78
Figure 4-10. Schematic of a TE77 reciprocating pin-on-plate tribometer [165] .....	79
Figure 4-11. Images of the vane (left) and rotor (right) samples fixed in TE77. ....	79
Figure 4-12. Wear tracks generated on the vane (left) and rotor (right) after TE77 tribotests .....	81
Figure 4-13. Wear measurements of the ball sample after HSPOD tests ...	83
Figure 4-14. Wear measurements of the vanes after TE77 tests. ....	84
Figure 5-1. Variable displacement vane pump- the marked contacts are explained in Table 5-2. ....	90
Figure 5-2. Failure of rotor and clamped vanes in rotor slots. ....	93
Figure 5-3. Wear on the opposite sides of the same vane sample which is in contact with rotor. ....	93
Figure 5-4. Wear on slide ring, resulting in plastic deformation of the ring. .	94
Figure 5-5. SEM images of (a) unused slide ring (b) used slide ring in the failed pump. The wear debris is shown by circle and the arrow is demonstrating the direction of sliding.....	96
Figure 5-6. SEM images of the slide ring around deformation at (a) low magnification 76x and (b) high magnification 663x showing plastic deformation of slide ring. ....	97
Figure 5-7. SEM image of the slide ring away from the deformation, showing a typical wear scar formed on the slide ring. Arrow shows direction of sliding. ....	97

Figure 5-8. Profile of step on the slide ring.....	97
Figure 5-9. SEM image of the unused vane, showing the surface is smooth and there is no debris on the surface .....	98
Figure 5-10. SEM images of the vane from the failed pump (a) low magnification (b) high magnification.....	99
Figure 5-11. Wear volume loss on different components of a failed pump. High wear was measured on the vanes, and least amount of wear was measured on spring. ....	100
Figure 5-12. 2-D Image and X-Y profile of wear scar on the rotor groove obtained with white light interferometry. ....	100
Figure 5-13. 2-D Image and X-Y profile of wear scar on the vane (in contact with rotor) obtained with white light interferometry. ....	101
Figure 5-14. Images and X-Y profile of wear and plastic deformation on slide ring, obtained with white light interferometry. ....	101
Figure 5-15. White light interferometry image showing signs of abrasive wear on the casing of VDVP. There are also signs of existence of third particles inside the sytem, as shown with yellow arrow. ....	102
Figure 5-16. Vane-rotor and vane-slide ring contact. ....	104
Figure 6-1. Viscosity of oils at varying CB levels as a function of temperature. ....	108
Figure 6-2. Friction coefficient as a function of time for various CB levels in FFO. Tests were conducted at 500 rpm, 0.83 GPa, 40°C. ....	110
Figure 6-3. Friction coefficient as a function of time for various CB levels in FFO. Tests were conducted at 500 rpm, 0.83 GPa, 100°C. ....	110
Figure 6-4. Friction as a function of CB content in FFO. The friction values are an average of friction coefficient during the last 30 minutes of tests. The error bars on the each points show the repeatability of tests. ....	111
Figure 6-5. Wear volume loss on balls at varying CB content in FFO for tests conducted at 40°C and 100°C. The error bars on the each points demonstrate the repeatability of tests. ....	113

Figure 6-6. Optical images of the wear scars formed on balls after tests with FFO, 1wt% CB and 5wt% CB at 40°C and 100°C. ....	113
Figure 6-7. Raman spectra obtained from different positions on tribopair samples after tests with FFO at (a) 40°C and (b) 100°C. ....	115
Figure 6-8. EDX spectra obtained from wear scar formed by FFO at (a) 40°C and (b) 100°C. ....	115
Figure 6-9. Raman spectra of tribopair wear scars after tests with FFO containing 5 wt% CB for tests conducted at (a) 40°C and (b) 100°C. ....	116
Figure 6-10. EDX spectrum obtained from wear scar formed by FFO containing 5 wt% CB at (a) 40°C and (b) 100°C. ....	117
Figure 6-11. (a) Wear results of BO and FFO with 5wt% CB (b) proportion of wear accounted by abrasion in FFO + 5wt % CB- The black bar for No CB in (b) cannot be seen in the bar chart since the wear volume is very small in comparison to the overall wear volume. All tests were conducted at 100°C for 2h. ....	118
Figure 6-12. Optical images of the wear scars formed on balls after tests with (a) BO+5wt% CB and (b) FFO+5wt% CB at 100°C. ....	119
Figure 6-13. Wear results of BO and FFO with 5wt% CB. ....	120
Figure 6-14. Wear volume loss for tests conducted with H&F and FFO containing various CB levels. Tests were conducted at 100°C for 2h. ....	122
Figure 7-1. FTIR spectra of BO and ZDDP additive concentrate. ....	125
Figure 7-2. FTIR spectra of model oils containing various concentration of ZDDP. It shows that P-O-(C) band appears by increasing the concentration of ZDDP in BO. ....	126
Figure 7-3. ICP results showing zinc concentration in BO as a function of ZDDP in BO. ....	126
Figure 7-4. Aged oils (BO+ 1wt% ZDDT) containing 1wt% and 5wt% CB. the oils were aged for 2 and 96 hours. The images were taken after removal of CB particles using the centrifuge. ....	127

Figure 7-5. FTIR spectra of oils after 2 h and 96 h of ageing. The oil is BO containing 1wt% ZDDP which is then mixed with 1wt% CB and 5wt% CB. FTIR spectra of (a) base oil, and aged oils containing (b) 1 wt% CB (c) 5wt% CB (d) 1wt% CB and (e) 5wt% CB. ....	129
Figure 7-6. Zinc concentration in oil (BO+1wt% ZDDP) in the presence of 1wt% and 5wt% CB particles after ageing for 2 h and 96 h using ICP. CB particles were removed from the oil samples by centrifuging before ICP analysis. ....	130
Figure 7-7. Phosphorous content in CB particles after ageing for 2 and 96 hours .....	131
Figure 7-8. Zinc content in CB particles after ageing for 2 and 96 hours ..	132
Figure 8-1. Viscosity of oils at varying diesel levels as a function of temperature.....	135
Figure 8-2. Friction curves obtained during tests with various diesel levels in FFO. Tests were conducted at 0.83 GPa, 40°C. ....	137
Figure 8-3. Friction curves obtained during tests with various diesel levels in FFO. Tests were conducted at 0.83 GPa, 100°C. ....	137
Figure 8-4. Friction as a function of diesel content in FFO. The friction values are an average of friction coefficient during the last 30 minutes of tests. The error bars on the each points show the repeatability of tests. ....	138
Figure 8-5. Wear volume loss on balls at varying diesel content in FFO for tests conducted at 40°C and 100°C. The error bars on the each points show the repeatability of tests. ....	139
Figure 8-6. Optical images of ball wear scars after two hour tests with FFO and 10 wt% diesel- contaminated oil. ....	140
Figure 8-7. EDX mapping of the Zn, P and S on ball wear scars formed by FFO and FFO + 10 wt% diesel. ND-not detected.....	141
Figure 8-8. Raman spectra obtained from different positions on tribopair samples with FFO containing 10 wt% diesel after tests at (a) 40°C and (b) 100°C.....	142
Figure 8-9. Viscosity of oils as a function of temperature.....	143

Figure 8-10. Wear volume loss on balls with BO and BO+5wt% diesel for tests conducted at 40°C and 100°C. The error bars on the each points show the repeatability of tests. ....	144
Figure 8-11. EDX mapping of the ball wear scars formed by BO and BO + 5 wt% diesel. Sulphur element was detected on the samples diluted with diesel. ND-not detected. ....	145
Figure 9-1. Visual inspection of (a) fresh FFO and oils after different oxidation time: (b) 24h, (c) 48h, (d) 72h, (e) 96h. ....	148
Figure 9-2. Dynamic viscosity of aged oil samples at different ageing time at 40°C. ....	149
Figure 9-3. Dynamic viscosity of aged oil samples at different ageing time at 100°C. ....	150
Figure 9-4. TAN value comparison for aged oil samples. ....	151
Figure 9-5. FTIR spectrum of fresh FFO and aged FFO after 96 hours. ...	152
Figure 9-6. FTIR spectrum of fresh FFO and aged FFO fingerprint region. ....	153
Figure 9-7. FTIR spectrum of fingerprint region for diesel contaminated oil at 0 h and 96 h. ....	153
Figure 9-8. FTIR spectrum of (a) fresh FFO, (b) aged oil with 1wt % CB and diesel and (c) aged oil with 2 wt% CB and diesel. ....	154
Figure 9-9. The effect of contaminants on friction and wear at 0 h oil ageing. The error bars on the each points demonstrate the repeatability of tests. All tests were conducted at 100°C. ....	155
Figure 9-10. Steady state friction coefficient as a function of ageing time of the oil with aged oil due to oxidation, 1wt% diesel, 1wt% CB, 1wt% CB and diesel ,and 2wt% CB and diesel. The error bars on the each points show the repeatability of tests. All tests were conducted at 100°C. ....	157
Figure 9-11. Wear coefficient as a function of ageing time of the oil with aged oil containing various contaminants. Wear measurements were conducted on the vane samples. All tests were conducted at 100°C. ....	157

Figure 9-12. SEM images of wear scar formed by (a) FFO (b) 1wt% diesel-contaminated oil at 0 h and 96 h of oil ageing. ....	159
Figure 9-13. Raman spectra of wear scars after tests with aged FFO at 0 h and 96 h of oil ageing. ....	160
Figure 9-14. Raman spectra of wear scars after tests with 1wt% diesel-contaminated oil at 0 h and 96 h. ....	160
Figure 9-15. SEM images of wear scar with aged oil with 1wt% CB at (a) 0 h, (b) 96 h, (c) aged oil with 1wt% CB and diesel (d) aged oil with 2wt% CB and diesel. ....	161
Figure 9-16. Raman spectra of wear scars after tests with (a) 1wt% CB and (b) 1wt% CB and diesel contaminated oil. ....	162
Figure 9-17. Friction and wear coefficient of tests. Wear measurements were conducted on vane samples. Error bars show repeatability of tests. ....	163
Figure 9-18. SEM images of wear scar on vane with (a) aged oil with 1wt% CB for 96 and aged FFO for 96h then adding(a) 1 wt% CB (b) 2wt% CB - Wear coefficient unit is ( $\times 10^{-16}$ m <sup>3</sup> /Nm). ....	164
Figure 9-19. SEM images and wear scar depth for tests (a) T3 and (b) T4. ....	165
Figure 9-20. Wear coefficient for tests conducted with unfiltered and filtered FFO containing 2 wt% CB and diesel. ....	167
Figure 9-21. The wear scar formed on vane samples by aged oil with %2wt CB and diesel (a) non-filtered (b) filtered. ....	167
Figure 9-22. Raman spectra of wear scar of vane sample after tests with the filtered oil (T5). ....	168
Figure 10-1. Variation in viscosity of FFO and FFO+5wt% CB at different temperatures. ....	171
Figure 10-2. Comparison of viscosity of different oils in the presence of soot. Experiments were conducted in engine tests with different oils [191]. ....	172
Figure 10-3. Friction comparison of FFO and FFO+1wt% CB at different sliding configurations. Two hours tests at 100°C. ....	175

Figure 10-4. Geometric configuration of tribosystems used in (a) unidirectional sliding (b) reciprocating tests.....	175
Figure 10-5. Wear performance of FFO and FFO+1wt% CB at different sliding configurations under two hour tests at 100°C.....	176
Figure 10-6. Schematic image of corrosive-abrasive wear mechanism by CB particles- adopted from Booth <i>et al.</i> [147].....	178
Figure 10-7. Important factors in corrosive-abrasive wear mechanism. ....	178
Figure 10-8. Effect of CB concentration and temperature on wear. ....	179
Figure 10-9. Wear and friction behaviour of oil under 10 hours of oxidation [123] .....	183
Figure 10-10. Wear coefficient and average wear depth of wear scar of vane samples using aged FFO with 1wt% CB, aged FFO then adding 1wt% and 2wt% CB. ....	186
Figure 10-11. Comparison of wear results and potential wear mechanism between T3 (aged diesel-contaminated oil then adding 1wt% CB) and T4 (aged CB-contaminated oil Then adding 1wt% diesel).....	188



## List of Tables

Table 2-1. Oil additives and their functions [30]. .....	19
Table 3-1. Summary of results obtained from previous studies.....	52
Table 4-1. Physical properties of FFO sourced by Fuchs Lubricants. ....	69
Table 4-2. Model oils used in the study. ....	70
Table 4-3. Chemical composition of samples.....	76
Table 4-4. Material properties of tribopair samples used in HSPOD tribotests .....	77
Table 4-5. Test conditions during HSPOD tribotests .....	77
Table 4-6. Specification of materials using in TE77 tests provided by Magna Powertrain, Ontario, Canada.....	80
Table 4-7. Test conditions used during TE77 tribotests .....	80
Table 5-1. Most common source of hydraulic pump failures [168]. ....	89
Table 5-2. Summary of contact between different components in VDVP. ....	90
Table 6-1. Lambda ratio for oils containing various levels of contamination. .....	109
Table 7-1. ZDDP concentration in base oil.....	125
Table 8-1. Lambda ratio for oils containing various levels of diesel contamination.....	136
Table 9-1. Contaminants and their level in the test matrix.....	148
Table 9-2. Text matrix for ageing the oil. ....	163
Table 9-3. Summary of antagonistic effect of contaminants on wear .....	166

## Nomenclature

Terms	Definition	Units
$\mu$	Friction coefficient	-
$F$	Friction force	N
$W$	Load	N
$V$	Wear volume loss	mm <sup>3</sup>
$K$	Dimensional wear coefficient	mm <sup>3</sup> N <sup>-1</sup> mm <sup>-1</sup>
$L$	Sliding distance	M
$H$	Hardness	N/m <sup>2</sup>
$\lambda$	Lambda ratio	-
$h_{\min}$	Minimum film thickness	nm
$R_q$	Root mean square surface roughness	nm
$E_1, E_2$	Young's Modulus of body 1 and 2	Pa
$E^*$	Effective Young's Modulus	Pa
$R_1, R_2$	Radius of body 1 and 2	m
$R^*$	Reduced radius of curvature	m
$U$	Entrainment speed $U = (U_1 + U_2)/2$	m/s
$\nu_1, \nu_2$	Poisson ratio of body 1 and 2	-
$\eta_0$	Dynamic viscosity	Pa s
$\alpha$	Pressure-viscosity coefficient	Pa <sup>-1</sup>
$P$	Pressure	Pa
$P_{\max}$	Maximum Hertzian contact pressure	Pa
$P_{\text{mean}}$	Maximum Hertzian contact pressure	Pa
$T$	Temperature	°C
$t$	time	min

## List of Abbreviations

---

<b>Abbreviation</b>	<b>Definition</b>
ATR	Attenuated Total Reflectance
AW	Antiwear
BL	Boundary Lubrication
BO	Base Oil
CB	Carbon Black
EDT	Engine Dynamometer Test
EDX	Energy Dispersive X-ray analysis
EGR	Exhaust Gas Recirculation
EHD	Elastohydrodynamic Lubrication
EP	Extreme Pressure
FFO	Fully Formulated oil
FTIR	Fourier Transform InfraRed Spectroscopy
HFRR	High-Frequency Reciprocating Rig
HL	Hydrodynamic Lubrication
HRC	Rockwell hardness
HSAB	Hard and Soft Acids and Bases
HSPOD	High Speed Pin on Disc
IC	Internal Combustion
ICP	Inductively Coupled Plasma
MD	Molecular Dynamics
NMR	Nuclear magnetic resonance spectroscopy
PD	Positive Displacement
PPM	Parts Per Million
SEM	Scanning Electron Microscopy
TAN	Total Acid Number
VDVP	Variable Displacement Vane Pump
VI	Viscosity Index
VT	Vehicle Test
ZDDP	Zinc Dialkyldithiophosphates

---

# Chapter 1 Introduction

## 1.1 Global energy challenges

Friction, lubrication and wear have a significant impact on the efficiency and lifetime of components in automotive industry and thus on the global economy. A considerable amount of energy is being lost to overcome friction. Figure 1-1 illustrates the breakdown of energy losses in a typical passenger car. As can be seen a large portion of friction losses, approximately 11.5%, are attributed to friction losses in the internal combustion engine (hereafter denoted IC engine). Friction losses in engines occur in the piston, bearings, valve train, pumping and hydraulic systems [1].

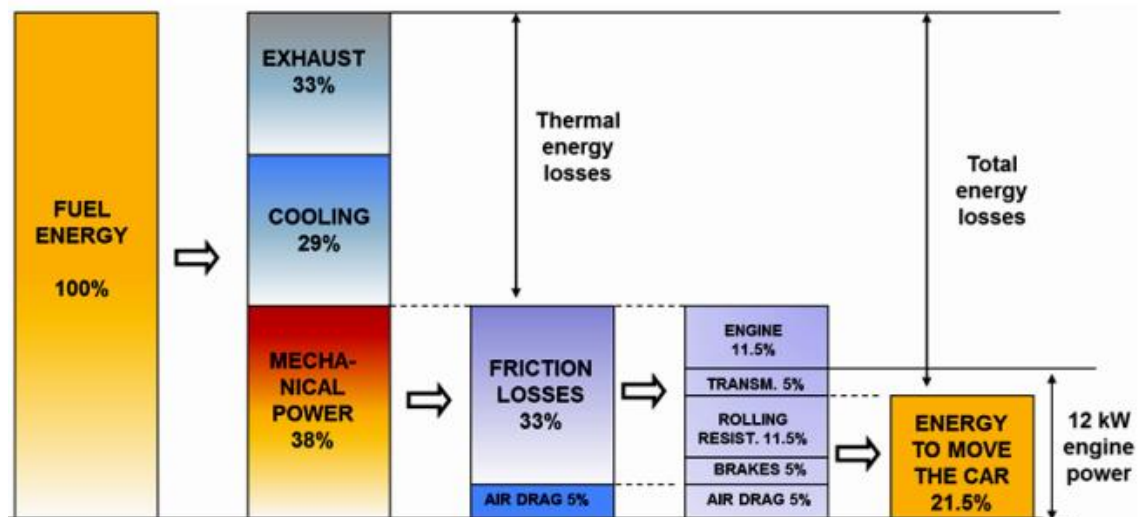


Figure 1-1. Energy losses in passenger cars [1].

Another main concern is the wear of the engine components which induces substantial costs for the industry and car users [1]. In addition, the stringent exhaust emission legislation has led to more focus on producing energy-efficient vehicles in automotive industry over the recent decades. As a result, the automotive industry aims to improve the powertrain performance and design the fuel-efficient vehicles in order to reduce the fuel consumption [2].

## **1.2 Diesel engine fuel economy**

In recent decades, there has been a great concern towards improving fuel economy in passenger cars. Vehicle emission levels need to meet strict standards and fuel standards. There are some factors that can potentially affect the quality of vehicle exhausts such as the fuel used, driving mode and the engine oil used. Different improvements have been introduced to diesel engines to reduce friction losses and exhaust emissions [3]. Engine oil can contribute in improving the fuel economy. Oil formulation is one of the factors that has a significant effect on legislated emissions. In gasoline engines, low viscosity oils have been effective in reducing internal engine friction and improving fuel economy without affecting engine lifetime. However, in diesel engines vehicle fuel economy and emissions are still a tough challenge [4]. There are many studies [5-7] that show that lubricant viscosity and lubricant additive packages can be optimized to reduce the friction losses in the engine and improve fuel economy. For instance, friction modifiers have been used to further reduce the friction between engine components.

Many other technologies have been utilized to improve fuel efficiency such as Exhaust Gas Recirculation (EGR). EGR is one of the most effective techniques to decrease emissions in diesel engines. However, this technique has its own disadvantages due to returning exhaust product to the diesel engine combustion chamber. This results in the formation of increasing amounts of soot in the diesel engines. Thus, engine durability might be affected due to the acceleration of oil contamination and degradation of the oil engine oil [8].

## **1.3 Engine oil pumps**

A portion of the energy losses in a typical IC engine is caused by the internal friction of the oil pump [9]. The role of the oil pump in IC engine is to provide power to lubricate and cool the other moving parts in automotive and provides

pressure for hydraulic-pressure parts. In traditional oil pumps, the volume of oil pumped into the system rises with increasing engine speed; this can result in inefficiency for two reasons. Firstly, the pump consumes more energy to pump more oil into the system; and secondly the oil pumped into the system may not be necessarily required by the system. Figure 1-2 illustrates the trend of friction power in a traditional oil pump at different engine speeds. It can be seen that the friction power of engine and oil pump increase with increasing engine speed.

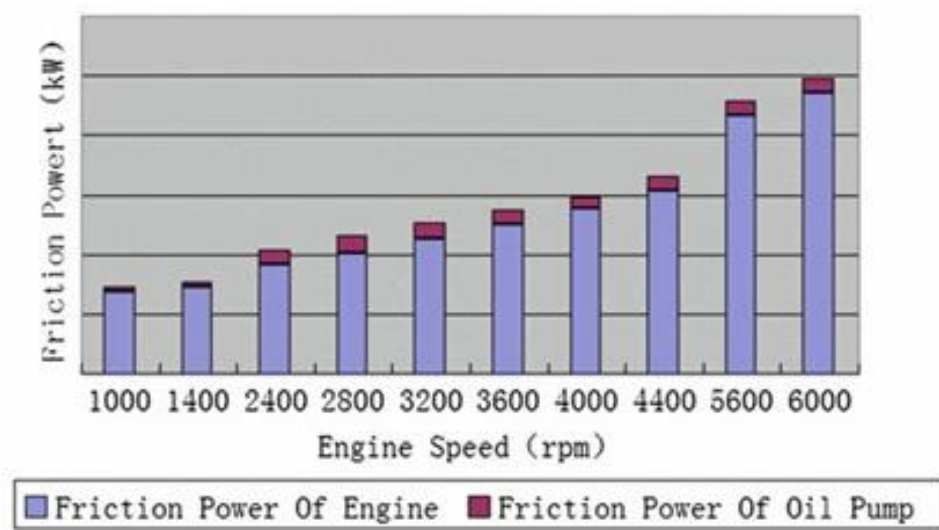


**Figure 1-2. Friction power comparison between a traditional oil pump and an engine by increasing engine speed. Friction power of the oil pump takes approximately 8% of the friction power of the engine [9].**

The variable displacement vane pump is one of the most innovative types of oil pump that has been introduced to automotive industry to improve the efficiency of engines. VDVP has a variable capacity that is adjustable to the engine demand, *i.e.* it only generates the flow rate required at any one time. This results in reduction of energy loss in the engine [9, 10].

The VDVP has a complex design and tribological loaded surfaces in VDVP operate under high loading condition. One of the issues with this type of pump is high friction and severe wear in the components of the pump such as vanes,

slide ring and rotor. Reducing the wear and frictional losses in VDVP can increase its lifetime. Thus, it is crucial to understand the potential factors that produce wear in this pump.

One source of failure in VDVP is improper lubrication. This pump is sensitive to contamination due to the small clearances between the contact areas. Contaminants accelerate the ageing process and degradation of oils and reduce its performance, ultimately leading to failure of the pump. It is therefore necessary to investigate the effect of contaminants such as soot and diesel in the lubrication system.

Based on above, the aim and objectives of this study will be defined.

## **1.4 Aims and objectives**

The aim of this study was to understand the effect of oil contamination such as those produced by soot and diesel on oil properties and tribological performance of oils in the boundary lubrication regime. The objectives of the study were as follows:

### **(1) Understanding the wear mechanisms caused by contaminants**

- To investigate the influence of soot contamination on the wear mechanism and how temperature and various levels of soot in the oil influence the wear;
- To investigate antiwear additive adsorption by soot; and
- To investigate the effect of diesel contamination in oils on tribological behaviour of contacts

### **(2) Understanding the effect of ageing on the tribological performance of oil**

- To investigate the effect of ageing the oils with various contaminants on the bulk properties of oils; and
- To investigate the effect of aged oils on tribological behaviour of contacts, particularly on the vane-rotor contact

## 1.5 Thesis outline

An in-depth review of fundamental theories and hypotheses, literature, experimental procedures used in this study and the results is presented in this thesis. The outline of the thesis as follows:

- Chapter 2: This chapter outlines the fundamental theory of science of tribology relevant to this study.
- Chapter 3: This chapter provides a summary of relevant literature on variable displacement vane pump and tribological behaviour of this pump. It also presents literature review on the role of oil contamination and oil ageing on oil properties and tribological behaviour of contacts.
- Chapter 4: This chapter provides the details of the experimental procedures used in this study.
- Chapter 5: This chapter presents a detailed failure analysis of VDVP and potential causes of failure of this pump.
- Chapter 6: The effect of carbon black contamination on tribological behaviour of oils under boundary lubrication regime is investigated in this chapter.
- Chapter 7: The antiwear additive adsorption by carbon black contamination in the oil is explored in this chapter.
- Chapter 8: The effect of diesel contamination on tribological behaviour of oils under boundary lubricated condition is investigated in this chapter.



- Chapter 9: The effect of aged oil containing carbon black and diesel contamination on the tribological performance of vane-rotor contact is investigated in this chapter.
- Chapter 10: This chapter provides a detailed discussion on the influence of carbon black and diesel contamination and effect of ageing on the tribological performance of oils in boundary lubrication regime.
- Chapter 11: This chapter outlines the main conclusions of study and provides recommendations for future studies and research work on this subject.

## Chapter 2 Theoretical aspects of tribology

### 2.1 Introduction to tribology

Tribology is a relatively new term in science and it made its first debut to the UK science literature after the Second World War in 1966 [11]. Tribology is derived from the Greek word “Tribos” meaning “rubbing”; and “ology” which means “the study of”. This science may be considered as gathering previous known subjects such as friction, lubrication and wear [11].

Leonardo da Vinci (1452-1519) studied the science of friction for the first time and understood the importance of friction in the machines. Lubrication science was then studied by Sir Isaac Newton (1642-1727). In the mid- twentieth century, the study of wear was conducted by Burwell, Strang and Archard [12]. Tribology is the study of friction, lubrication and wear; these three phenomena define the process of “rubbing” surfaces. In other words, it is the science of interacting surfaces under applied load and relative motion [12].

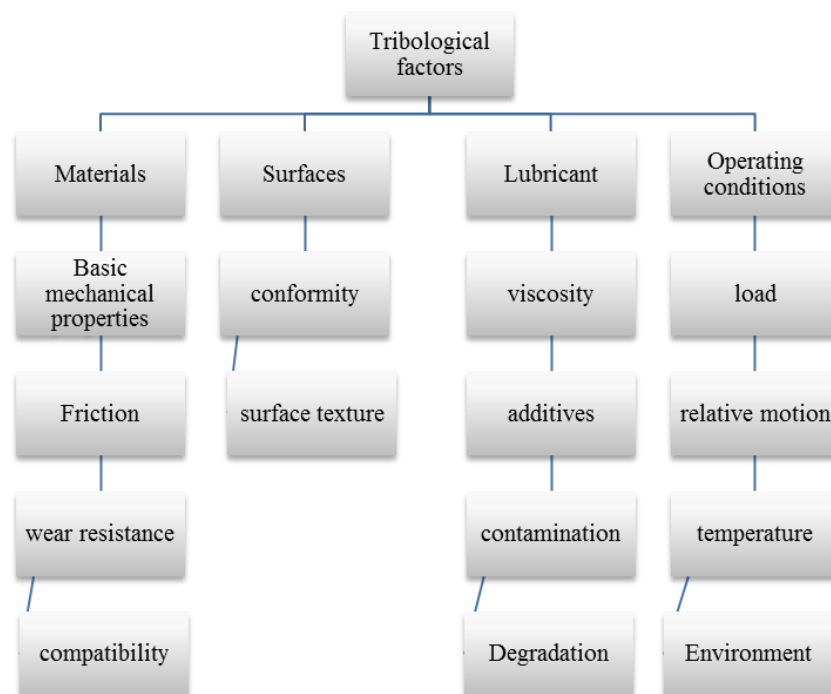


Figure 2-1. Major tribological factors [13].

Tribology has a significant effect on the operation of industry and society as a whole. Tribology is fundamental to every engineering design of machine elements. Tribological factors can play a significant role in the efficiency of machine element. Thus, taking tribology into consideration as well as design stress and deformation would result in a successful long-term performance of engine elements [14]. Figure 2-1 indicates the major tribological factors that need to be considered in any tribological problems, some of which will be discussed in more details in the following sections.

## 2.2 Friction

Friction is a resistance to motion occurring when one body moves tangentially over another. In engine design, low friction surfaces are desirable since they lead to more efficient operation and less energy loss. However, in some applications such as brakes and clutches low friction is not a desired condition [13]. The source of friction in IC engine needs to be fully understood to allow for maximisation of fuel economy. The majority of power loss in engines is due to the friction between components. Engine friction can be generally divided into two groups: dry friction, which occurs between two moving surfaces in which the asperities are in contact; and fluid friction, which occurs between layers of fluid moving at different velocities. Friction in engine components is somewhere between these two groups which are dependent on many factors such as surface roughness, normal loads, properties of oil, component geometry and velocities of moving surfaces [2].

The coefficient of friction is defined by the ratio of the friction force (F) and the normal load (W) as shown in Equation 2-1.

$$\mu = \frac{F}{W} \quad \text{Equation 2-1}$$

## 2.3 Contact between surfaces

When a load is applied to two bodies which are in contact with each other, either elastic or plastic deformation can occur. Stresses below the elastic limit of the materials in contact will lead to elastic deformation. Stresses above the elastic limit of the materials will lead to plastic deformation. Plastic deformation leads to the permanent damage of the element [13]. To determine the possible damage or life of components in contact, it is pertinent to consider the true stress [15]. In 1881, Hertz was the first to consider the stresses and deformations in elastic contacts between two solid surfaces. Therefore, contact between two surfaces with low conformity and significant curvature under an applied load is defined as Hertzian contact [15]. In reality surfaces are not smooth. When two surfaces are pressed, they will touch each other at a single point or along a line at the beginning. Although the area of contact is small compared with the dimensions of surfaces themselves, they deform at the vicinity of the first contact. The Hertz theory predicts the shape of this area of contact and how it grows with the increasing load. It also enables us to calculate the deformation and stresses of both surfaces in the vicinity of the contact area [16]. Figure 2-2 shows the schematic diagram of two bodies in a point contact. The mean and maximum Hertzian contact pressures are calculated using Equation 2-2 and Equation 2-3.

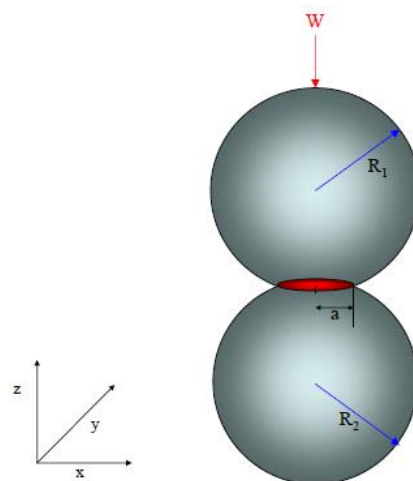
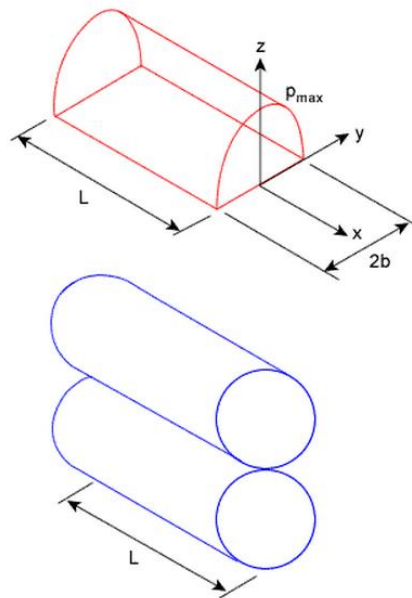


Figure 2-2. Schematic diagram showing two bodies in a point contact [17].

$$P_{max} = \frac{1}{2\pi} \left( \frac{3WE^{*2}}{R^2} \right)^{\frac{1}{3}} \quad \text{Equation 2-2}$$

$$P_{mean} = \frac{2}{3} P_{max} \quad \text{Equation 2-3}$$

Where  $W$  is the applied load [N],  $R^*$  is the reduced radius of curvature and  $E^*$  is the effective Young's Modulus [Pa]. Hertz also analysed the stresses generated around two cylinders in contact over a length of  $L$  for a contact region which is rectangular (Figure 2-3).



**Figure 2-3. Schematic diagram showing two bodies in a line contact [13].**

The mean and maximum Hertzian pressures are defined by Equation 2-4 and Equation 2-5 respectively.

$$P_{mean} = \left(\frac{\pi WE^*}{32RL}\right)^{1/2} \quad \text{Equation 2-4}$$

$$P_{max} = \left(\frac{WE^*}{2\pi RL}\right)^{1/2} \quad \text{Equation 2-5}$$

## 2.4 Lubrication

Lubrication is the effective application of a solid, liquid or gas between two surfaces to reduce friction and wear of the rubbing surfaces. Oils provide smooth running by formation of a layer of material with low shear strength between surfaces. Mineral oils are the most common oil type, however a wide range of materials are included as the description of oil such as synthetic oil, grease, vegetable oil, water, air, process fluid and solid. The form of lubrication involved in a tribological interface depends on the surface conformity and texture, oil properties, materials of the surfaces and operating conditions (e.g. load, speed, temperature and environment) [13]. Lubrication is also very much correlated to wear of interacting surfaces under applied load. An ideal scenario that minimises wear of contacting surfaces is expected to have the two articulating surfaces separated by lubricating film. The most appropriate way to determine the form of lubrication regime in which the system is operating is by calculation of the minimum film thickness [13].

The Lambda ratio ( $\lambda$ ), which is defined as the ratio of film thickness to the composite surface roughness, helps to determine the mode of lubrication regime. Lambda ( $\lambda$ ) is represented by the mathematical relation shown in Equation 2-6, where  $h_{min}$  is the minimum film thickness (m),  $R_{q1}$  and  $R_{q2}$  are the root mean square surface roughness values (m) of each surface. Depending on the value of the lambda ratio different types of lubrication regimes can be characterised [13].

$$\lambda = \frac{h_{\min}}{[(R_{q1})^2 + (R_{q2})^2]^{\frac{1}{2}}} \quad \text{Equation 2-6}$$

Dowson and Higginson [18] pioneered the prediction of minimum film thickness. In the current study the testing is carried out based on both line and point contact. The minimum film thickness is defined for line contact in Equation 2-7 and point contact in Equation 2-8.

$$\frac{h_{\min}}{R^*} = 2.65 \left( \frac{U\eta_0}{2E^*R^*} \right)^{0.7} (2\alpha E^*)^{0.54} \left( \frac{W}{E^*R^*2l} \right)^{-0.13} \quad \text{Equation 2-7}$$

$$\frac{h_{\min}}{R^*} = 3.63 \left( \frac{U\eta_0}{E^*R^*} \right)^{0.68} (\alpha E^*)^{0.49} \left( \frac{W}{E^*R^*} \right)^{-0.073} (1 - e^{-0.68k}) \quad \text{Equation 2-8}$$

In these equations,  $R^*$  is the reduced radius of curvature as defined by Equation 2-9 and  $E^*$  is the effective Young's Modulus [Pa] defined by Equation 2-10.  $\alpha$  is the pressure-viscosity coefficient [ $\text{Pa}^{-1}$ ],  $W$  is the normal contact load [N],  $2l$  is the contact length and  $k=1$ .  $U$  is the entrainment speed [m/s] which is the average speed of the two bodies in contact,  $U = (U_1 + U_2)/2$ .  $\eta_0$  is the dynamic viscosity of the oil at ambient conditions [Pas], the viscosity of the oil is influenced by temperature and pressure [19].

$$\frac{1}{R^*} = \frac{1}{R_A} + \frac{1}{R_B} \quad \text{Equation 2-9}$$

$$\frac{1}{E^*} = \frac{1 - \nu_A^2}{E_A} + \frac{1 - \nu_B^2}{E_B} \quad \text{Equation 2-10}$$

Lubrication regimes enable the evaluation of the general performance of the tribological system in relation to wear and friction. There are four lubrication regimes:

**Hydrodynamic Lubrication (HL) regime:** This lubrication regime is the most desirable form of lubrication since the two surfaces in contact are completely separated by an oil film such that there is no asperity- asperity contact (Figure

2-4(a)). This desired condition occurs at  $\lambda > 10$  and the load is supported by the fluid film. Engine components in this lubrication regime do not experience wear since the surfaces are completely separated from each other. Therefore, the friction is the main concern in this regime. Bulk oil properties of the oil, particularly the viscosity, play an important role in friction performance [13].

**ElastoHydroDynamic (EHD) regime:** This lubrication regime occurs at  $4 < \lambda < 10$ . The two surfaces are completely separated by an oil film although the film is thinner than that of the HL regime, as shown in Figure 2-4(b). The contact experiences high pressures which can result in elastic deformation of the surfaces [13]. Surfaces are separated in this regime thus friction is considered more than wear. Similar to the HL regime, the bulk oil properties play an important role in friction performance with regards to lubrication in this regime.

**Mixed lubrication regime:** This lubrication regime occurs at  $1 < \lambda < 4$ . Asperities from both surfaces are separated by a fluid film in some regions and in other regions there is asperity-asperity contact, as shown Figure 2-4(c). The lubrication film provides partial separation between surfaces. The load is thus supported by both the fluid film and the asperities. The bulk properties of the oil are not enough to provide wear protection and friction reduction. Additives present in the base oil play also a big role in this regime. The characteristics of both EHL and boundary lubrication are influential [13].

**Boundary Lubrication (BL) regime:** This lubrication regime occurs at  $\lambda < 1$ . In this regime the thickness of the oil separating the two surfaces is less than the roughness of the two surfaces in contact. As a result, the surfaces are in contact at a large number of places (see Figure 2-4(d)). The load in the rubbing contact is thus shared partially between the asperities peaks and the oil film resulting in a high friction coefficient. In fact, of all the lubrication regimes, boundary lubrication exhibits the highest friction coefficient [20]. Boundary lubrication regime normally occurs under low speed and high load conditions. This regime is normally observed in IC engine components such



as piston ring/liner interface, cam/tappet interface, gears, bearings, pumps and transmissions. In this regime, the chemical properties of the oil and chemical properties of surfaces in contact are more important than the physical properties of the bulk oil [21, 22]. Lubrication in boundary lubrication regime is achieved by formation of thin boundary films (also known as tribofilms) through physical or chemical adsorption or by a chemical reaction between the oil and the rubbing surfaces [23]. Physical layers are gaseous, liquid and solid which are produced by inter-molecular forces. Chemically adsorbed layers are produced by adding additives to the base oils. The strength of the films formed by these chemical reactions may vary due to the affinity of additives to metals on the surface. These layers are normally formed at high temperature. Tribochemical reactions between rubbing surfaces form films under high load and sliding speed [24].

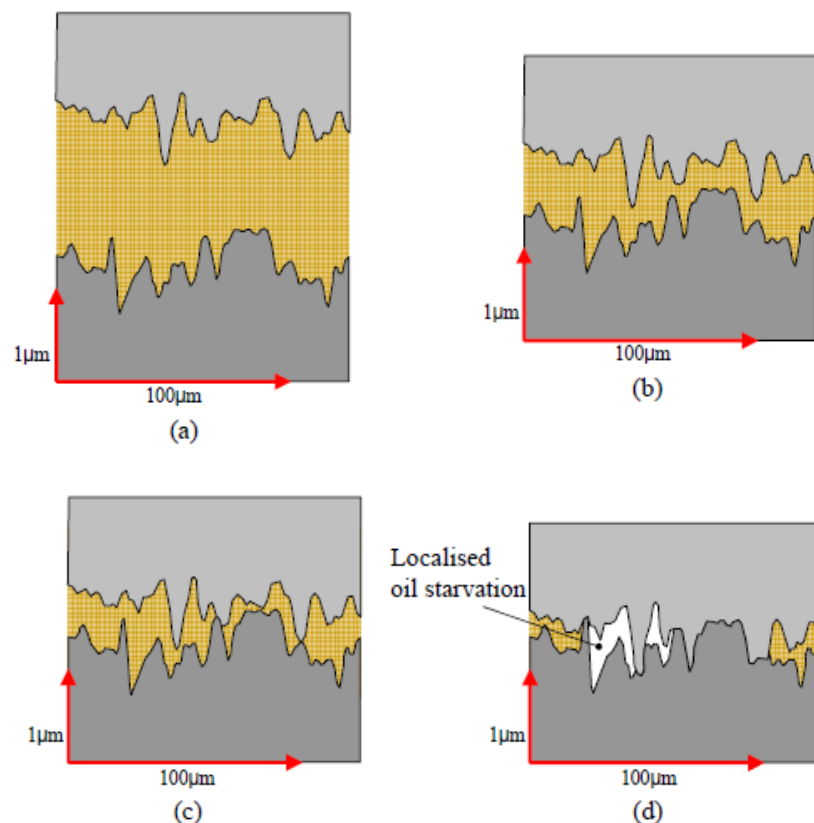


**Figure 2-4. Schematic diagram illustrating the different lubrication regimes (a) hydrodynamic (b) elastohydrodynamic (c) mixed (d) boundary [17].**

The Stribeck diagram in Figure 2-5 illustrates the relation between the friction coefficient ( $\mu$ ) and the ratio of film thickness to surface roughness ( $\lambda$ ). The friction coefficient is a function of oil viscosity, speed and contact pressure. These parameters demonstrate the position of lubrication regimes in Stribeck diagram [13].

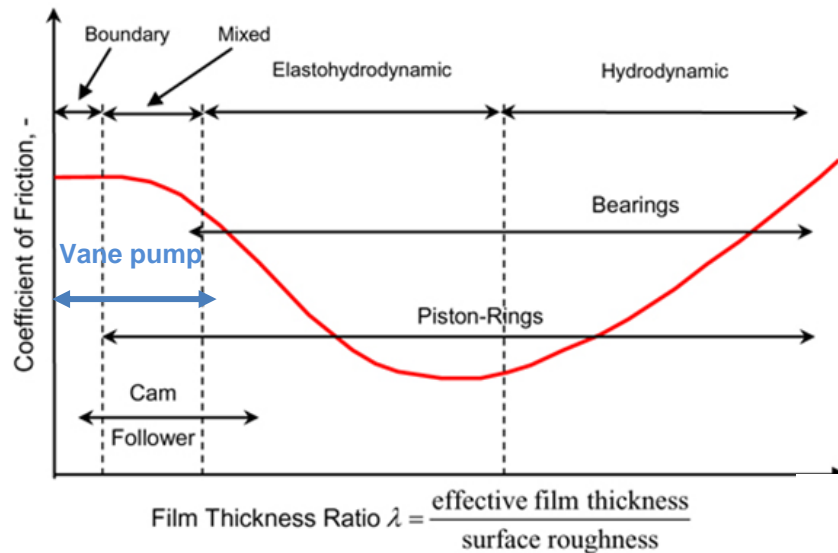


Figure 2-5. Stribeck diagram for some IC engine components. The lubrication regime for VDVP is either boundary or mixed regime [13].

## 2.5 Wear

Wear is a progressive damage, involving material degradation, which occurs on the surface of components under load as a result of their motion. The removal of materials causes changes in surface properties and topography, resulting in loss of mechanical performance of components [25]. Researchers around the world have investigated wear and mechanisms by which it may occur. Some frequently discussed wear mechanisms are explained as follows:

**Adhesive wear:** Severe wear due to the direct contact of bodies that adhere to each other through asperity contact. Adhesion mostly occurs in the boundary and mixed lubrication regimes.

**Abrasive wear:** There are two types of abrasive wear, known as “two-body abrasive wear” and “three-body abrasive wear” as shown in Figure 2-6. The two-body abrasive wear occurs when a harder material is rubbing against a softer material by a ploughing or microcutting mechanism. The three-body abrasive wear occurs due to the cutting of a metal by hard particles that exist in the system. This causes plastic deformation and the formation of parallel furrows and ridges in the direction of movement. In both cases, a high level of metal content in the oil is expected. Abrasive wear typically occurs in boundary lubrication regimes because of inadequate lubrication, excessive surface roughness and oil contamination [26].

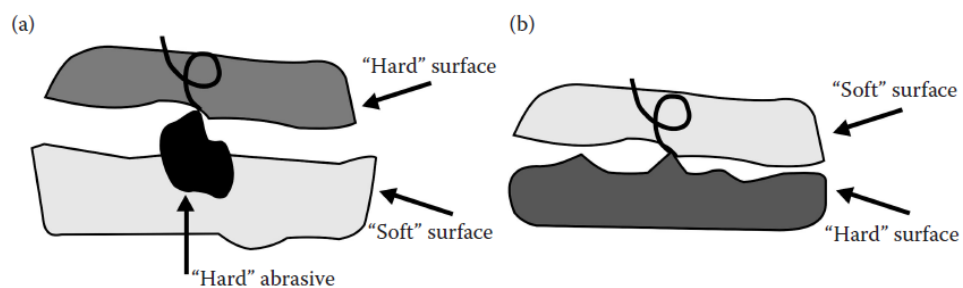


**Figure 2-6. Schematic of (a) three-body abrasive wear and (b) two-body abrasive wear [26].**

**Erosive wear:** Wear due to impingement of solid particles which remove fragments of materials from surfaces due to momentum effect. It normally occurs at high velocity with solid particles in oil. In this type of wear, metal-on-metal contact is not necessarily needed. Erosive wear typically happens in the elastohydrodynamic lubrication regime in rolling bearing [27].

**Fatigue wear:** Failure of material after cyclic straining resulting in the cracks, delamination and small cavities [27].

**Corrosive wear:** Wear due to the chemical reactions with the environments and rubbing at the same time. This type of wear typically occurs by formation

of chemical oxide layers on metal surfaces and following removal by rubbing. There is no need of metal-on-metal contact in this type of wear [27].

**Polishing wear:** Wear generated as a results of mechanical-chemical interaction between the surfaces. This type of wear leads to a very smooth, mirror-like, surface texture. This can lead to the failure in lubricated components since the polished surface is unable to preserve enough oils on surfaces [28]. For instance, polishing wear occurs when there is a high concentration of soot in the engine oil.

In general, wear is a complex process since sometimes it involves more than one mechanism. Wear rates are normally quoted by Archard's wear equation (Equation 2-11);

$$V = K \frac{WL}{H} \qquad \text{Equation 2-11}$$

Where:

$V$  is wear volume loss from the surface per unit sliding distance in  $\text{m}^3$ ;

$K/H$  is the dimensional wear coefficient ( $\text{m}^3\text{N}^{-1}\text{m}^{-1}$ ), with  $H$  being the surface hardness of the wearing material;

$W$  is the contact load in  $\text{N}$ ; and

$L$  is the sliding distance in  $\text{m}$ .

Archard's wear model indicates that volumetric material loss depends on the hardness, sliding distance and contact force. It is worth noting that Archard law does not reflect the influence of oil chemistry and it is usually valid when mechanical mechanisms, adhesive wear or abrasive wear in particular, are dominant.

Figure 2-7 describes the range of wear coefficients under different conditions. The highest value of  $K$  is seen when hard particles are present in the system. It means that wear occurs due to either abrasion or erosion. The wear

coefficients for unlubricated sliding condition and wear by hard particles are greatly high for engineering applications. Even boundary lubrication, which is the least effective lubrication regime on wear, can decrease the wear rate several times less than unlubricated conditions. It is also clear that the values of  $K$  reduces quickly as the thickness of lubrication film increases [25]. In automotive engines, wear unavoidably occurs while the engines are running and studies have been focused on keeping the wear rate at a very low level.

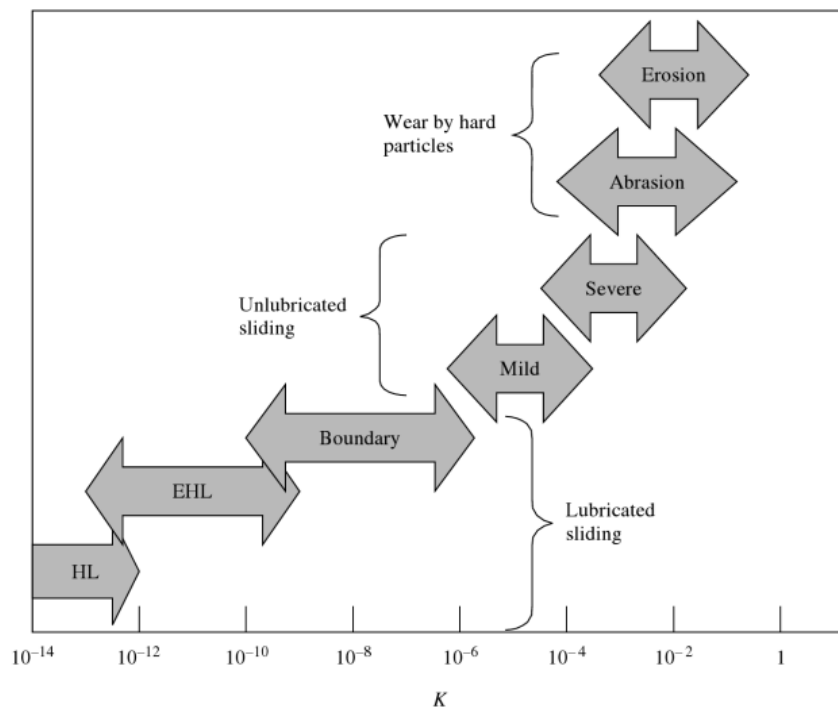


**Figure 2-7. The range of wear coefficient ( $K$ ) under different conditions [25].**

## 2.6 Oils

Engine oils are used to reduce friction and wear in IC engines. An oil is composed of many additives that have been blended together into a base oil. The base oil is usually obtained through refining petroleum products or by synthesis of hydrocarbon molecules [29]. Chemical additives are added to the base oils in order to modify or improve the performance of the base oil. The

oil can consist of more than 20 additives with a total weight concentration of about 20% in the base oil [29]. Based on their functionality, oil additives are either chemically active or chemically inert. Chemically active additives normally interact chemically or physically with the surface or other chemically active additives to protect the surfaces. These additives are antiwear , anti-rust, anti-corrosion additives, friction modifiers, detergents and dispersants[30]. Chemically inert additives reinforce base stock performance to improve the physical characteristics of base oils such as foam inhibitors, viscosity modifiers and pour point dispersants. Table 2-1 shows a list of additives typically adopted in oils and explains their primary function.

**Table 2-1. Oil additives and their functions [30].**

	Oil additive	Function
Chemically inactive additives	Pour point depressant	Control wax crystals formation
	Viscosity index improver	Increases VI of oil
	Foam inhibitor	Destabilizes foam in oil
Chemically active additives	Oxidation inhibitor	Prevents or slow oxidation of base oil at high temperatures
	Storage stabilizer	Prevents or slow oxidation at low temperatures over long periods
	Corrosion inhibitor	Limits corrosion of non-ferrous metals
	Rust inhibitor	Limits rusting of ferrous metals
	Detergent	Prevents build-up of varnishes on surfaces. If basic also neutralizes acids.
	Dispersant	Prevents formation of solid deposits in cold engine
	Friction modifier	Lowers friction of rubbing surfaces
	Antiwear (AW)	Reduces wear of rubbing surfaces
	Extreme pressure (EP)	Prevents seizure of rubbing surfaces

A combination of different additives can result in either synergy or antagonism effects compared to the performance of each additives individually. These interactions respectively lead to enhanced performance or reduced performance of the additive [30]. Figure 2-8 illustrates the most common synergetic and antagonistic interactions of additives. Synergy occurs when the combined effects of additives are beneficial. In this case, the effect of combined additives is more than the effects of individual additives. Antagonism occurs when the presence of one additive represses the function of the other additives. Antagonistic effects of additives are harmful for the system [30].

	VI-IMPROVER	POURPOINT DEPRESSANT	DETERGENT DISPERSANT	OXIDATION INHIBITOR	CORROSION INHIBITOR	ANTIWEAR	EXTREME PRESSURE	ANTI-FOAM
VI-IMPROVER	□ (+)	○	○	○	○ (+)	○	○	□ (-)
POURPOINT DEPRESSANT	□	○	○	○	○	○	○	○
DETERGENT DISPERSANT		□	+	+	-	-	□ (-)	
OXIDATION INHIBITOR			□	+	(+)	○	○	
CORROSION INHIBITOR				□	-	-	○	
ANTIWEAR					□	+	○	
EXTREME PRESSURE						□	○	
ANTI-FOAM							□	□

+ = synergism  
 - = antagonism  
 ○ = no influence

Figure 2-8. Interaction between various surface active additives [30].

## Chapter 3 Literature review

In this chapter, a comprehensive review of the Variable Displacement Vane Pump (VDVP) and the tribological performance of this pump will be provided. Furthermore, the role of tribofilm and oil contamination on tribological performance of contacts under boundary lubrication regime will be reviewed.

### 3.1 Introduction to hydraulic pumps

Hydraulic pumps play a key role in the mechanical systems such as IC engines and automatic transmissions. Hydraulic pumps are classified based on their working principle as shown in Figure 3-1. Dynamic pump is a variation of hydraulic pump. This pump gives energy to the fluid by increasing the flow velocity and converting the velocity to pressure. Positive displacement pump (hereafter denoted PD) generates a fluid's movement from an inlet port to an outlet port by trapping a fluid volume. Vane pumps are classed as PD and rotary pumps. The principle of PD rotary pumps is rotation. This means that the rotation of the pump creates a vacuum in the inlet region which forces liquid inside the pump.

Vane pumps have been classified in three subcategories as listed below [31]. Figure 3-2 shows these three groups of vane pumps.

1. Single chamber vane pump: in this pump the circular pressure ring (slide ring) is eccentrically located in the system that enables one cycle for each vane space per rotor revolution (Figure 3-2(a)).
2. Double chamber vane pump: also known as balanced vane pump, in this type the pressure ring is elliptical. Therefore, double eccentricity enables each vane space a double cycle from inlet to outlet port per rotor revolution (Figure 3-2(b)).



3. Variable displacement vane pump; the pressure ring is circular which can modify its eccentricity with respect to the engine's requirement [31] (Figure 3-2(c)).

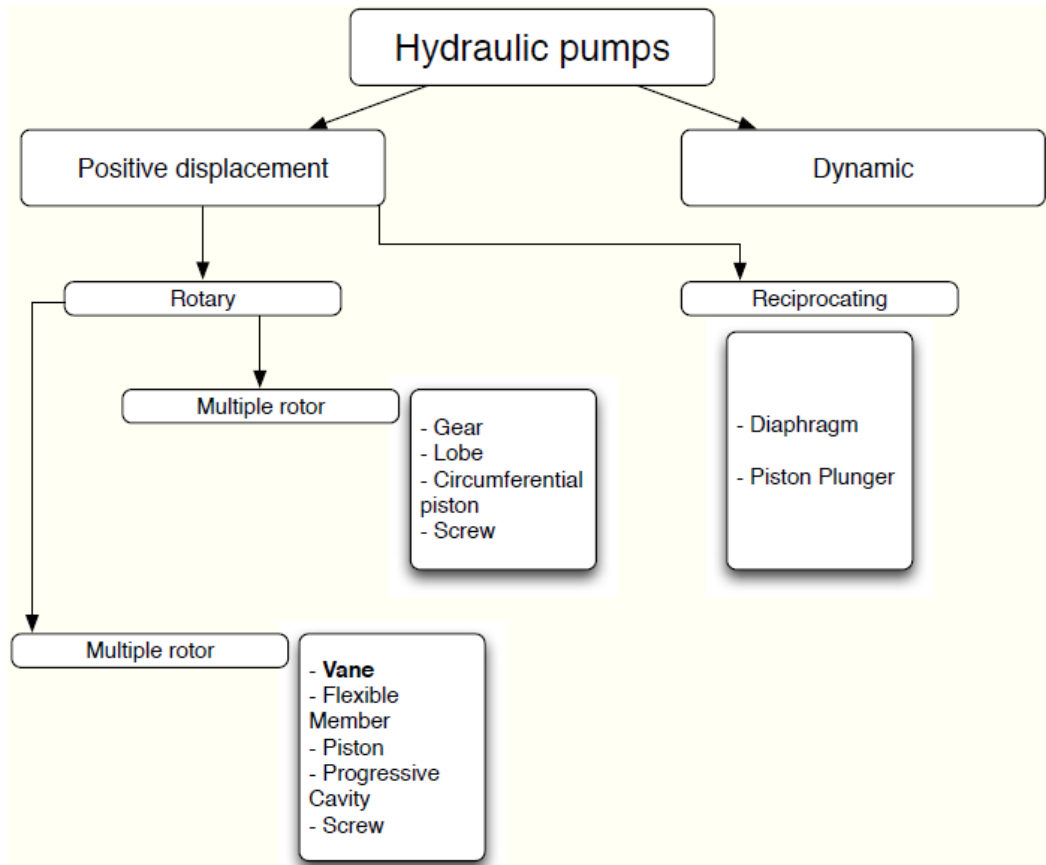


Figure 3-1. Hydraulic pumps classification [31].

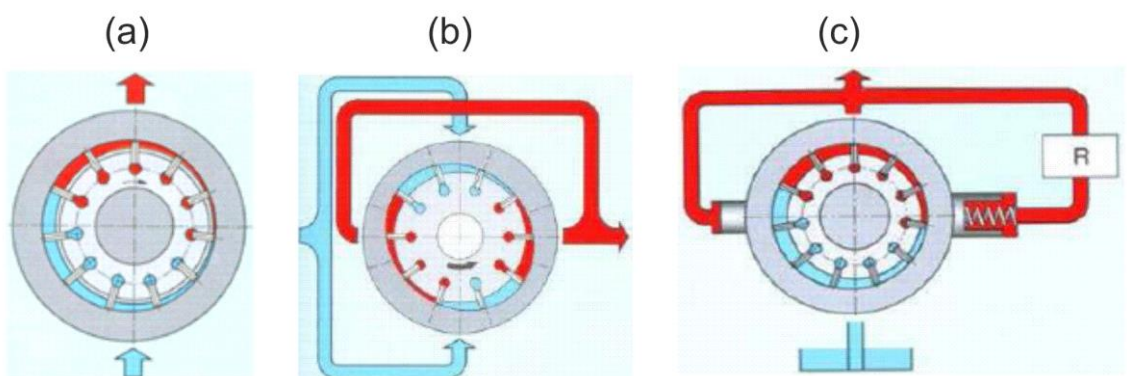


Figure 3-2. Schematic of (a) single chamber vane pump (b) double chamber vane pumps (c) variable displacement vane pump [31]. Inlet region is represented in blue and outlet region is shown in red.

### **3.1.1 Introduction to VDVP**

The oil pump in an IC engine provides lubricating oil, which is under high pressure, to the other moving components of the mechanical system. The oil pump is usually linked to the engine and the operating speed of the pump changes with the operating speed of the engine. For this reason, the lubrication requirements of the system alter with the operating speed of the system.

In some operating conditions, the amount of pressurised oil pumped to the other components is significantly more than the demand of the system. In this case, a significant amount of energy is used to pressurise the excessive lubricating oil to the components. This results in a significant energy loss in the system. VDVP, which is one of the most advanced types of hydraulic pumps, has been invented to overcome this problem [32].

The operation of VDVP will be discussed in detail in the following sections.

### **3.1.2 VDVP components**

VDVP, as shown in exploded view in Figure 3-3, is studied in this research. The pump is mainly composed of a slide ring with a circular inner bore, a rotor with several radially disposed vanes, a shaft, a spring and a casing. This pump is connected to the motor by shaft. The rotor is eccentrically located in the housing with respect to the shaft axis. The eccentricity between the rotor and the slide ring is controlled by the spring. This causes the capacity variation of the pump. It means that the oil flow can be adjusted to the system's need in working conditions. There are also some carvings designed on the casing at the side facing the rotor in order to gradually introduce the delivery pressure to the bottom of the vanes [33-35].

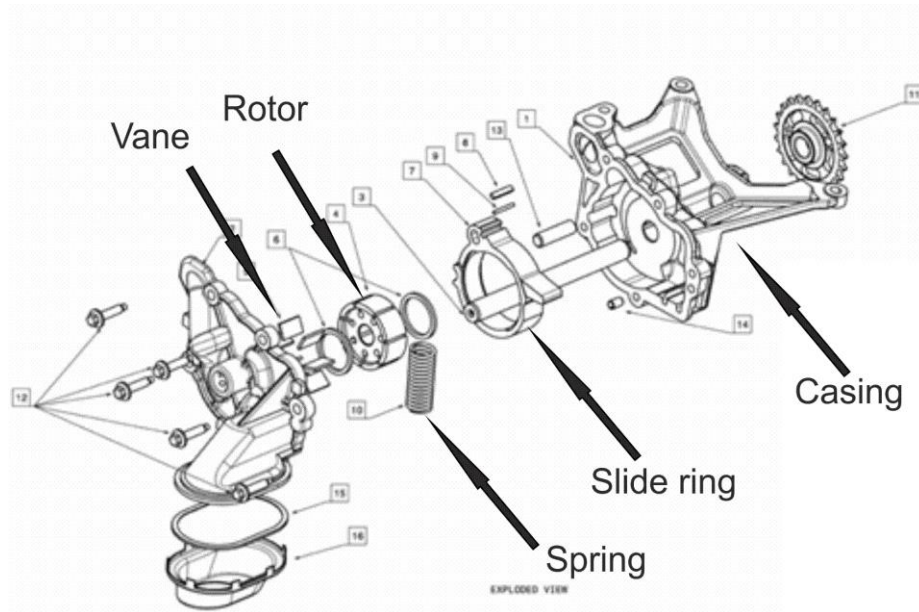


**Figure 3-3. Exploded view of VDVP (Provided by Magna Powertrain, Ontario, Canada).**

### 3.1.3 Operation of VDVP

When the pump rotates, it creates a low-pressure zone at the inlet that in return vacuums the fluid into the pump. The oil moves from the inlet port to the outlet port and passes through the compressed area which is derived by the eccentricity of the slide ring and the rotor. This action generates a high pressure zone at the outlet of the pump. The pressurised oil is then circulated through the bearings in the engine [31-33]. To be more precise, the vanes slide in and out into the rotor slots and follow the outlines of the inner surface of the slide ring due to the centrifugal force and the hydraulic pressure. The pressure acting on the head and bottom of vanes is the hydraulic pressure. The delivery pressure acting on the bottom of the vanes pushes the vanes through the slide ring. The vane faces are also under stress due to the pressure of the fluid [33].

VDVP is commonly used in hydraulic systems and car engines owing to their capability to control the flow. The spring can change the eccentricity between the rotor and the slide ring in different working conditions. Figure 3-4 illustrates

two extreme working conditions in VDVP. Figure 3-4(a) shows the maximum eccentricity that generates the maximum output flow. When the desired pressure level is obtained, the spring alters the displacement of the pump back to the zero eccentricity, *i.e.* zero flow, in order to reduce the resulting pressure force (see Figure 3-4(b)). VDVP also has the ability to work in intermediate condition, when the eccentricity is between the minimum and maximum conditions. The full flow condition is the most critical condition for the pump in terms of wear and fatigue, due to high fluid pressure acting on components with very small clearance [35, 36]. It should also be noted that there are still inefficiencies and energy losses in VDVP which requires further improvement. This will be discussed in the next section.

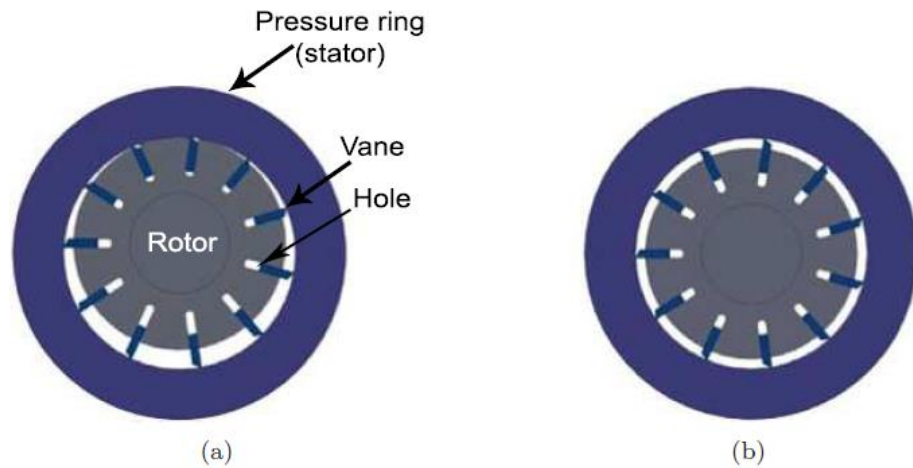


Figure 3-4. (a) Full flow and (b) zero flow working condition [37].

### 3.2 Failure of VDVP

Despite high efficiency and reduced power consumption, VDVP has its own disadvantages in terms of high wear and friction. The wear mechanism is an important aspect of this pump that needs to be carefully considered. The design of VDVP requires very tight tolerances and small clearances between the components. This can increase the probability of metal-on-metal contact in different parts. Excessive wear and high friction in the key components of

the system, such as vane tips, the slide ring and rotor, can lead to failure of the pump [38]. The failure analysis of the VDVP in this study will be discussed in detail in Chapter 5.

### **3.3 Tribological behaviour of VDVP**

Mechanical efficiency of the pump is an important factor to be considered in the evaluation of the pump performance. One of the critical aspects of VDVP is described by the high friction and wear that occurs on the contact surfaces [38]. There are two main tribological contacts in VDVP: vane-slide ring contact and vane-rotor contact.

During the operation of the pump, the vanes are in contact with the inner surface of the slide ring due to the effect of centrifugal loads. The wear occurring between vane tip and slide ring is a critical aspect of VDVP [38]. As shown in Figure 3-5, delivery pressure ( $p_d$ ) always acts on the vane base, however the pressure acting on the vane tip depends on the angle of the vane. The latter can be either suction pressure ( $p_s$ ) or delivery pressure ( $p_d$ ) or the combination of both [39].

Another critical contact is attributed to the vane and rotor. During the operation of the pump, vanes stick in rotor grooves, causing high wear on the vanes and a sudden increase in contact load. Frendo *et al.* [10] showed that one of the critical aspects of VDVP is high friction between vanes and rotor leading to severe wear. They believed that high friction forces between vanes and rotor apply high torque on the vanes followed by an abrupt rise in the vane contact load. Thus, vanes cannot easily slide in and out into the rotor slots. This undesired sticking condition can significantly increase wear between vane and rotor. In this case, an asymmetrical wear pattern is detected on the vane's head [10]. In general, less studies have been conducted on the vane-rotor contact compared to vane-slide ring contact.

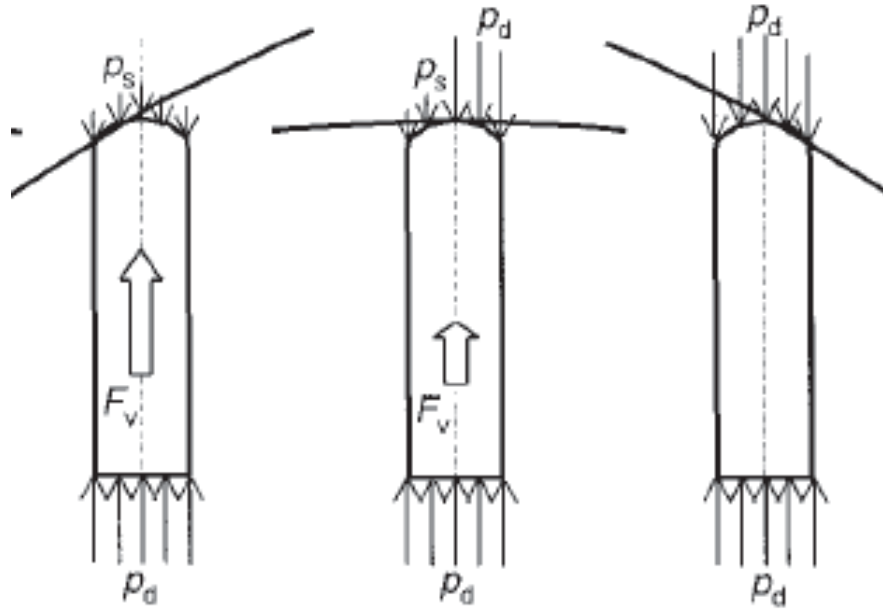


**Figure 3-5. Vane force at vane tip in contact with the slide ring [39].**

Inaguma *et al.* [39] studied the effect of friction between the vane tip and the slide ring on the mechanical efficiency of the balanced vane pump. It has been stated that the friction force between the slide ring and the vane tip is proportional to the pressure difference between the pressure acting on vane base and vane tip. The results indicated that the friction force reduces slightly by increasing the sliding speed. This can be justified by the running-in effect of smoothing the surfaces at sliding parts. Inaguma *et al.* [39] demonstrated that to have a high mechanical efficiency in the vane pump, the friction coefficient of sliding surfaces needs to be reduced.

The effect of surface roughness on the mechanical efficiency of vane pump by reducing the surface roughness of the slide ring has been studied by Inaguma *et al.* [40]. They showed that the coefficient of friction significantly depends on the surface roughness. As shown in Figure 3-6, coefficient of friction ( $\lambda$ ) increases with increasing surface roughness, however it becomes independent of surfaces roughness for value above  $0.7 \mu\text{m}$ . This constant value still dependant on sliding speed, *i.e.* higher sliding speed, has lower friction for the surface roughness above  $0.7 \mu\text{m}$ . This trend can be explained

by the elastohydrodynamic lubrication theory. Inaguma *et al.* [40] conducted a set of experiments and also confirmed these results in the actual pump. It was concluded that the reduction of surface roughness in the slide ring to  $0.4 \mu\text{m}$  reduces the friction torque of the vane to about half and improves the mechanical efficiency by about 5 per cent.

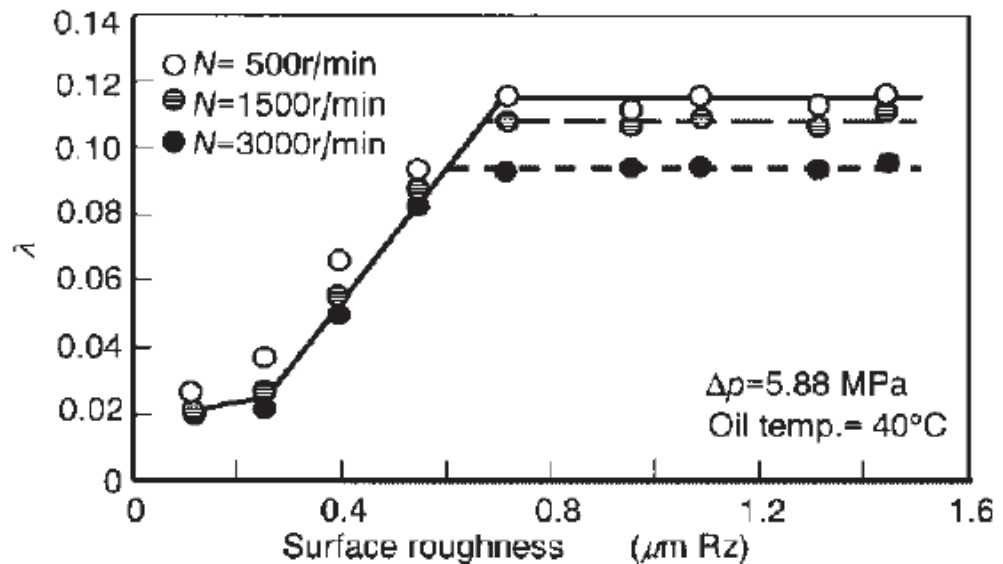


**Figure 3-6. The relationship between coefficient of friction and surface roughness. Pump speed is shown by N in the graph [40].**

The surface roughness of the slide ring becomes smoother after a long time by sliding of vanes which results in wear in the system and probably changes in the lubrication mode. In other words, the surface peaks are removed due to wear. This causes a reduced friction coefficient, therefore the vane loads can be supported by a well-formed oil film [41]. Kunz *et al.* [36] indicated that the surface roughness of the vane tip changed after 250 h tests distinctively (see Figure 3-7) which is a good representative of wear happening in the system.

The influence of changes in contact radius of vanes on load has also been studied by Gellarich *et al.* [34]. They stated that the Hertzian pressure acting on the vane-slide ring tribo-contact is an important factor for the wear

calculation. Hertzian pressure decreases with time due to the change of the vane tip shape. To be more precise, the wear debris on the vanes changes the shape of vanes leading to an increased contact radius of vanes with time (see Figure 3-8). The changes in the geometry of the vanes can lead to unpredicted stresses on the tribo-contact between the vane and slide ring.

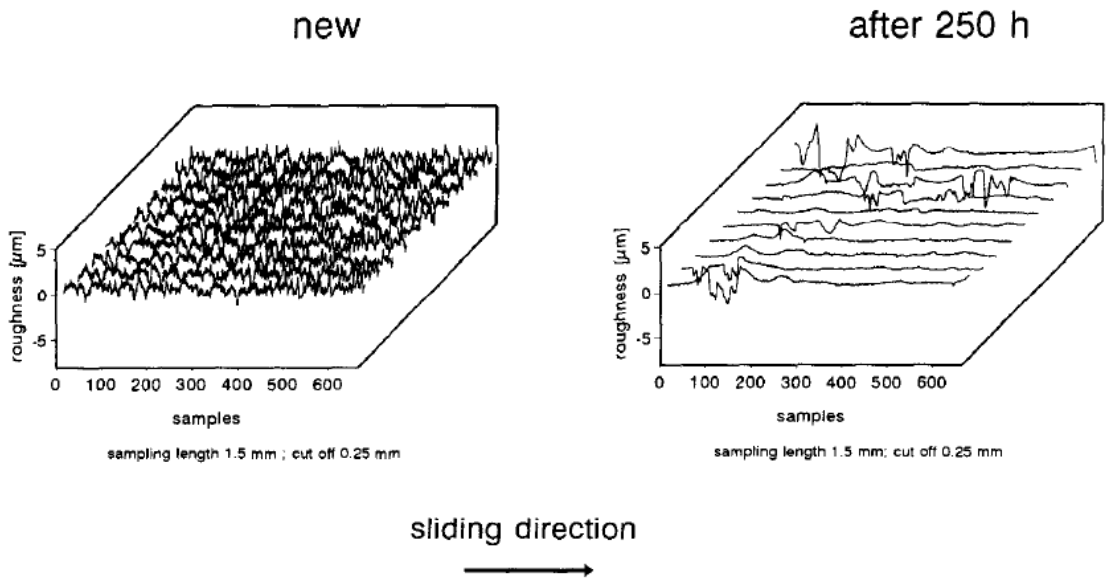


Figure 3-7. Change in surface roughness of vane tip after 250 h [36].

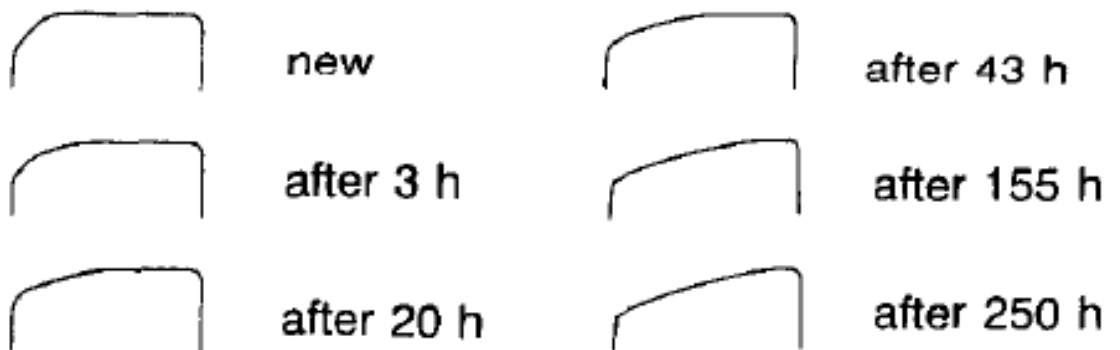


Figure 3-8. Changes in contact radius of vane with time due to wear [34].



### **3.4 Lubrication**

Oil provides a fluid film between moving parts; this reduces friction and wear and improves fuel economy in an engine [42]. It appears that the higher viscosity of oil would provide better lubrication in the VDVP since the thicker film is achieved between surfaces. However, since it is more viscous, it requires more power to be pumped. If an engine is sufficiently lubricated it needs less power to operate resulting in less fuel consumption. The properties of oil can influence the tribological performance of the engine components. These properties such as viscosity, additives and density are different from one oil type to another [43]. Viscosity plays an important role in the performance of oil. Oil viscosity is sensitive to temperature, it decreases rapidly with increasing temperature. On the other hand, viscosity can increase at the high temperature of the operation of engine due to the oxidation of oil, base stock polymerisation and accumulation of soot. This variation in viscosity affects the oil film thickness between components [24, 44].

### **3.5 Lubrication regime in VDVP**

A thin oil film is formed between the slide ring and vane tip in VDVP as shown in Figure 3-9. The height of the oil film ( $h_f$ ) depends on the viscosity of the oil, the sliding speed and force loaded on the vane. As Figure 3-9(a) illustrates, when the surface roughness of slide ring is exceptionally fine, for example below  $0.3 \mu\text{m}$ , the lubrication regime between vanes and the slide ring is 'hydrodynamic lubrication regime'. In this case, the oil film can support the vane forces, resulting in the friction coefficient being very low. 'Mixed lubrication regime' occurs when some of the surface peaks are larger than the oil film thickness (Figure 3-9(b)), in this case resulting in increase of the coefficient of friction. When the surface roughness of the slide ring becomes larger than the height of the oil film, this film cannot support the vane load (see Figure 3-9(c)). This condition happens in the 'boundary lubrication regime', in

which the friction coefficient increases and remains constant due to the increase in the surface roughness. The reduction of friction by decreasing the surface roughness can be justified by the existence of oil film which can support the vane force [40].

Inaguma *et al.* [45] stated that the lubrication regime between the vane tip and the slide ring should be considered as a mixed lubrication regime as it has partial metal-on-metal contact. They noted that the effect of oil temperature on friction should not be ignored as coefficient of friction rises by increasing the oil temperature. This can be explained by the reduction of oil viscosity at high temperatures. In other words, the oil film between the slide ring, vane tip and rotor becomes thinner. As a result, the lubrication regime goes to the boundary condition, the area of metal-on-metal contact increases and the friction rises. In general, the lubrication regime in the tribological contacts of this pump is either boundary or mixed. Thus, the surfaces are in contact in this hydraulic system. As such, the use of antiwear additives in the engine oils can help to protect the surfaces. Maintaining the cleanliness of the oil is also required in this application. The contacts in VDVP are sensitive to contamination due to the small clearances between the components [46].

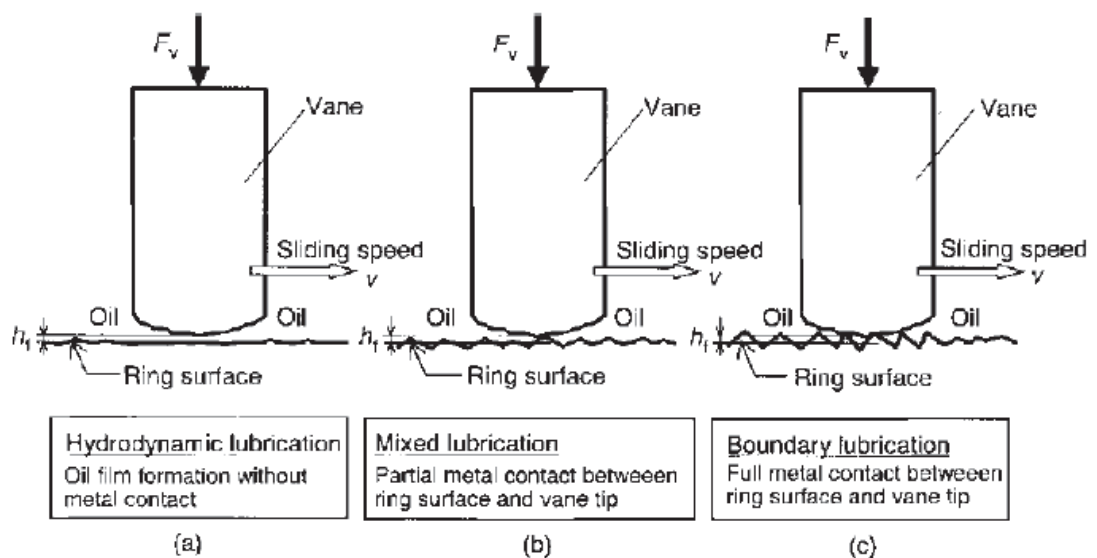


**Figure 3-9. Lubrication regime between vane tip and slide ring [40].**

### 3.6 Role of tribofilm in boundary lubrication regime

Additives are used in the engine oil to protect the rubbing surfaces by formation of a solid-like film, called tribofilm. This protects the rubbing surfaces from excessive wear [42, 47, 48]. The importance of the tribofilm under boundary lubrication has been discussed in studies by Willermet *et al.* [49], Martin *et al.* [50] and Bancroft *et al.* [51]. Wear under boundary lubrication regime is very severe if the antiwear film is weak. The significance of antiwear additive and tribofilm formation on friction and wear mechanisms are discussed in the following sections.

#### 3.6.1 Zinc Dialkyldithiophosphates (ZDDP) tribofilms

Zinc Dialkyldithiophosphates (ZDDP) are one of the most common antiwear additives in engine oils that reacts with the metal surface to form a tribofilm [52]. ZDDP was initially introduced as an antioxidant additive however soon after its antiwear ability was discovered [53]. Figure 3-10 shows the idealised molecular structure of ZDDP. The alcohol group (O-R) can be alkyl or aryl and help to increase the solubility of additive in the base oil. When lubricated surfaces are under severe friction conditions, the ZDDP additives undergo thermal and oxidative degradation forming a thin protective film (approximately 50-150 nm) on the surfaces [54, 55]. ZDDP tribofilm contains sulphide and phosphate which are responsible for reducing wear by minimising the asperity contact between surfaces [56]. This film is known to protect the surfaces from adhesion and abrasion [54].

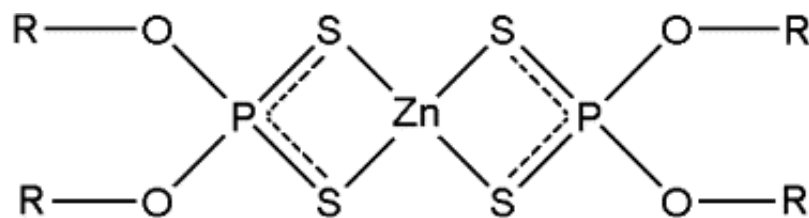
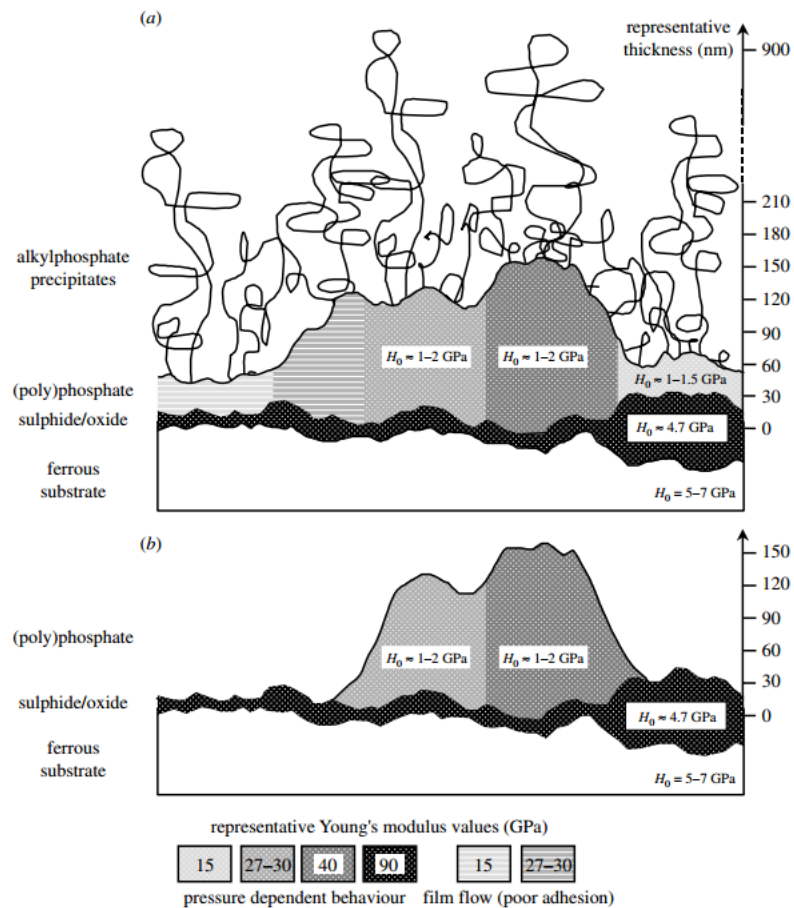


Figure 3-10. The idealised molecular structure of ZDDP [48].

### 3.6.2 Mechanical properties of ZDDP tribofilm

There have been several studies [52, 57-59] on the mechanical properties of ZDDP tribofilms in boundary lubrication regimes. Aktray *et al.* [57] found that morphology and mechanical properties of ZDDP tribofilm vary from point-to-point and film-to-film. They also showed that the morphology of tribofilms change with rubbing time. It was shown that tribofilm has a patchy structure at the low rubbing time and as rubbing time increases tribofilms become smoother and more uniform over the steel substrate. ZDDP tribofilms have a layered structured as shown in Figure 3-11.



**Figure 3-11. Mechanical properties of ZDDP tribofilm. (a) Full antiwear film formed on surface from ZDDP solution. (b) Same antiwear film after washing with solvent. Y-axis shows representative thickness of each layer of antiwear film.  $H_0$  indicates initial hardness for each material [60].**

These layers have different chain length at various positions [58, 59]. A viscous layer of physically-adsorbed additives is formed on the top layer of tribofilms (Figure 3-11(a)) which can be easily removed by solvents and washing. Under this viscous layer, a chemically adsorbed layer of amorphous zinc and iron phosphate with different chain length is present (Figure 3-11(b)). The chain length of the glassy polyphosphates affect the mechanical properties of ZDDP. Longer chain of polyphosphates exits on top of tribofilm, close to the body interfaces, and shorter chain are present close to the tribofilm interface [52, 57-59]. Mosey *et al.* [61] reported that shorter chain polyphosphates are harder than the longer chain polyphosphates. The hardness of ZDDP tribofilms was assumed to be between 2 to 6 GPa [62].

### 3.6.3 Chemical properties of ZDDP tribofilm

In order to understand the friction and wear behaviour observed for ZDPP, it is important to identify the chemical elements of ZDDP tribofilms. ZDDP tribofilm contain inorganic polymer materials containing zinc, sulphur, phosphorous and oxygen [63]. The tribofilm formed on the steel surfaces contain zinc sulphide, iron sulphide, zinc oxide and/or iron oxide very close to the substrate with a thick layer of glassy phosphates and a thin layer of zinc polyphosphate on top (see Figure 3-12).

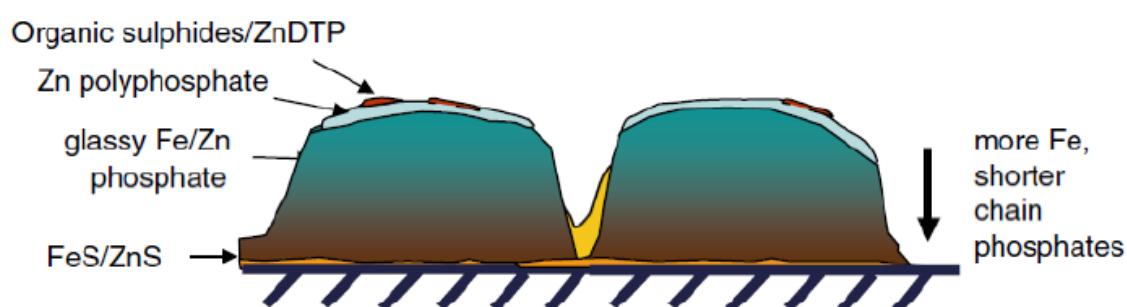


Figure 3-12. Structure and composition of ZDDP tribofilm [53].

Aktray *et al.* [64] demonstrated that ZDDP tribofilms contain long chain polyphosphates. In addition, they reported that the short chain of

polyphosphates were detected beneath the top layer. The ZDDP tribofilm is formed on the surfaces as a mixture of white patches and dark strips along the sliding direction [65]. It has been suggested [66] that white patches contain long chain polyphosphates and dark strips are composed of short chain polyphosphates.

### 3.7 Parameters that influence ZDDP tribofilm

Different physical and chemical parameters can influence the chemical composition, morphology, topography, friction and wear behaviour of the ZDDP tribofilm. Some of these factors will be discussed in this section.

**Concentration of ZDDP:** The concentration of ZDDP has various impacts on the properties of ZDDP tribofilm, such as the film thickness, friction, wear and the chemical composition of the tribofilm. Nicholls *et al.* [48] found that the concentration of ZDDP in the oil influences the tribofilm thickness. Fujita *et al.* [55] observed that by increasing the concentration of ZDDP from 0.01wt% P to 0.12wt% P, the thickness of tribofilm increased from 80 nm to 100 nm. Willermet *et al.* [67] showed that wear decreased as ZDDP concentration increased. It has also been stated that the higher concentrations of ZDDP in the oil help to improve the faster film formation on the surfaces. The rate of tribofilm's formation is a very important factor that needs to be understood in order to prevent wear [56].

**Influence of temperature:** The bulk temperature of oils containing ZDDP has been found to affect the rate of ZDDP tribofilm formation, tribofilm thickness, durability of tribofilms, chemical composition and wear properties of the tribofilm [48, 55, 68, 69]. Nicholls *et al.* [48] found that oil temperature influences the tribofilm thickness. Fujita, *et al.* [55] also found that the rate of tribofilm formation increases with rise in the bulk temperature, resulting in increased tribofilm thickness. Yin *et al.* [69] studied the formation of tribofilm at 100°C, 150°C and 200°C. They observed that decomposition of ZDDP

occurs faster at higher temperatures. Choa *et al.* [68] also indicated that more thick tribofilms are formed at high temperatures than at low temperatures. However, the films formed at high temperatures were found to be less durable than those tribofilms formed at room temperature. This can be attributed to the reduced mechanical strength and structural changes of the thick film.

**Influence of load:** The load applied on the surfaces during tribotests has been found to influence the rate of ZDDP decomposition and the thickness of the tribofilms. Rossi *et al.* [70] reported that ZDDP film thickness increased from 4.2 nm to 5.0 nm by increasing load from 0.05 N to 10 N. Yin *et al.* [69] found that ZDDP decomposed more rapidly at 400 N than at 40 N. However, Palacios [71] stated that the increase in film thickness due to increase in load is only valid up to 600 N, beyond this load the film thickness decreases. Hu *et al.* [72] demonstrated that as the speed and load increase in a system, the film thickness reduces. This results in the oil film to breakdown, which leads to an increase in the wear and friction. The high load applied on the surfaces can break down the tribofilm in a relatively short period of time [52]. Also, friction coefficient was found to increase with increase in load.

### **3.8 Tribological performance of ZDDP on surfaces**

As mentioned above, various factors such as temperature, ZDDP concentration and load influence tribological performance of ZDDP. Therefore, the operating conditions play a significant role in providing the improved antiwear performance by ZDDP.

**Effect of ZDDP on wear:** It is believed that ZDDP can protect the surfaces from wear. From the literature, several mechanisms have been suggested that ZDDP can act as an antiwear agent to reduce wear [53]. These mechanisms are as follows:

1. Formation of a mechanically protective film can act as a barrier to reduce the direct asperity contacts;
2. Reduction of three body abrasion due to digestion of hard and abrasive oxide particles; and
3. Formation of glassy phosphates tribofilm that can act as a viscous lubricant on the surfaces [53].

The most well-known and accepted mechanism is that ZDDP tribofilm can act as a mechanically protective barrier in boundary lubrication regime. The formation of this phosphate film prevents the direct contact between surfaces. This film can also reduce the stresses on the asperity contacts. It has also been reported [53] that ZDDP tribofilms are fairly resistant to wear. Williams *et al.* [73] suggested that ZDDP tribofilm is softer than the substrate and could reduce the asperities in contact. The thickness of tribofilm is dependent on the temperature and the ZDDP concentration in the lubricant [68, 74].

**Effect of ZDDP on friction:** There have been contradictory reports on the effect of ZDDP on the friction performance of contacts. It has been reported that the presence of ZDDP in the lubricants increases friction [75, 76]. It was suggested [76] that the formation of ZDDP film on the surfaces leads to increase in roughness that could promote boundary lubrication and increase the friction values.

Besides the effect of higher roughness of ZDDP tribofilm, Taylor *et al.* [77] found that friction enhancement was because the tribofilms formed prevented the lubricant from being entrained into the rolling/sliding contacts. It is not exactly clear how the tribofilm inhibits entrainment of the lubricant in the rubbing contact. However, the authors suggested that the inlet of the contact region can be blocked due to formation of ZDDP tribofilms resulting in lubricant starvation at the contact. Thus, these contacts operate in the



boundary lubrication regime with consequently high friction. In contrast, other studies have reported that the addition of ZDDP to the lubricant had either neutral effect [78] or decreased the friction [79]. The differences in the reported results can be attributed to different test conditions such as material, temperature, additive mixture used in each study.

### **3.9 Tribochemistry of ZDDP**

Tribochemistry refers to the chemical reactions that occur between the rubbing surfaces and its environment under boundary lubrication conditions. The role of tribochemistry in boundary lubrication regime is significant. Tribofilms are formed not only when the additives are present near the surface, but also when sliding takes place. It means that the rubbing action initiates the formation of tribofilm due to the additive decomposition. Thus, both rubbing action and additive result in the formation of protective film [80].

It is believed [81] that thermo-oxidative decomposition of ZDDP results in the formation of phosphate film on a steel substrate which results in reducing wear. This will be followed by a reaction between the phosphate and iron oxide layer. This reaction provides an inter-grown layer based on the hard and soft acid-based chemical reaction (HSAB). Iron oxide particles that are formed during the wear process can react with the nascent surface after the thermal film is disrupted. These iron oxide particles can cause severe damage by abrasive wear. As explained in Section 3.8, ZDDP tribofilms are capable of reducing wear by digesting the abrasive particles of iron oxides through tribochemical reactions [53, 81].

Martin *et al.* [81] have developed a Molecular Dynamics simulation (MD) to investigate the reactions occurring in the antiwear chemistry of ZDDP. The results showed that pressure and shear effect is crucial for the digestion of iron oxide embedded in the zinc. It was shown that after 300 ps of simulation, the oxygen and iron atoms diffuse into phosphate glass. Thus, they concluded

that the effect of pressure and shear is essential for the tribochemistry reaction of ZDDP (Figure 3-13) [81]. They also demonstrated that the chemical reaction of ZDDP can be activated at a very low contact pressure (1 MPa), and very short time (2.5 ns). Another study [82] using MD simulations showed that the mixing of zinc phosphate and iron oxide on ferrous substrate prevent wear due to increasing mechanical hardness of the tribofilm material and its adhesion to the iron oxide substrate. The results also indicated that zinc metathiophosphate prevents the abrasive wear due to the atomistic digestion of the wear particles in the tribofilm [82].

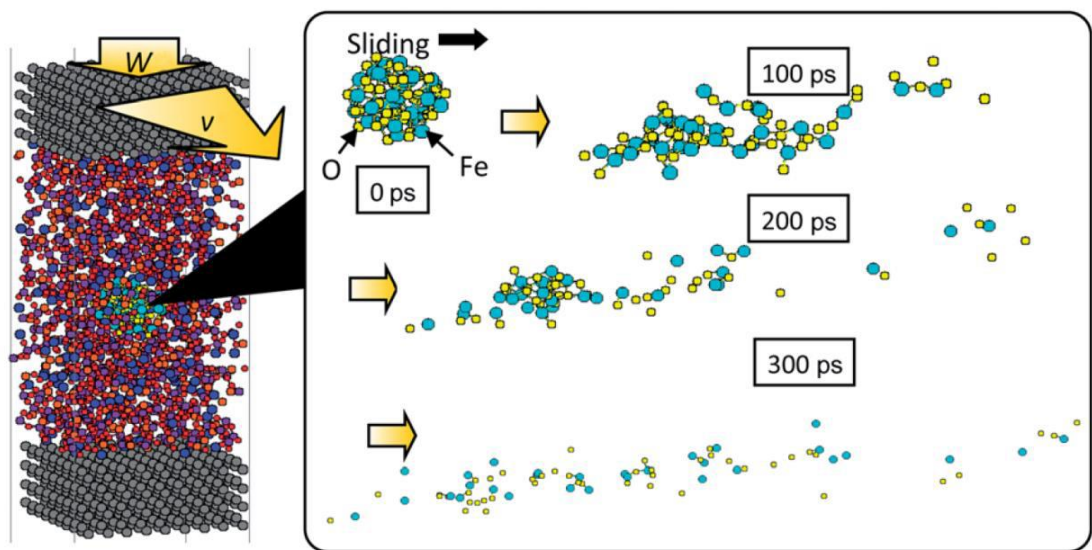
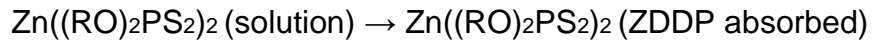


**Figure 3-13. The MD simulation showing the combined effects of pressure and shear on the behaviour of the iron oxide particles embedded in the zinc metaphosphate [81].**

Fuller *et al.* [83] suggested several chemical reactions for ZDDP formation during the tribological conditions. They indicated that the existence of iron oxide is not necessary for the formation of ZDDP tribofilm. They showed that hydrolysis of polyphosphates is involved in the formation of short chain polyphosphates. It was also showed that the existence of a linkage isomer of ZDDP (LI-ZDDP) is important for the formation of ZDDP tribofilm.

The proposed ZDDP film formation processes are as follows:

1. At first, ZDDP is adsorbed on the rubbing surfaces:



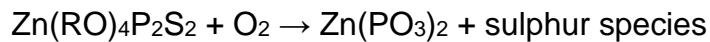
2. Then ZDDP in solution becomes a LI-ZDDP:



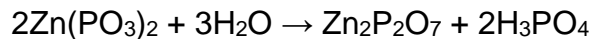
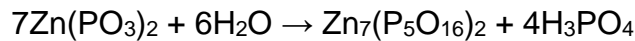
3. After some time the LI-ZDDP in the solution is adsorbed onto the metal surface:



4. In this stage thermal degradation happens and long chain polyphosphate chains are produced:



5. As the rubbing continues long chain polyphosphate interact with the water present in the base oil to form short chain polyphosphates:



The exact tribochemical reactions occurring at the surfaces with ZDDP additives are not well understood yet. The full understanding of these reactions is very difficult due to the complicated nature of boundary lubrication regime.

### 3.10 Stability of ZDDP film

Tribofilms are regularly being removed and reformed when in rubbing contact. ZDDP tribofilms are very stable once they are formed. Fujita, *et al.* [55] studied the influence of factors such as dispersants and soot on the removal of ZDDP tribofilms. In their experiments, first the ZDDP tribofilm was formed then the

oil was replaced by ZDDP-free base oil. The results showed that the thickness of ZDDP tribofilm was not affected even after rubbing with base oil (Figure 3-14). These results confirmed ZDDP tribofilm had a very good durability. This can explain the good performance of ZDDP acting as an antiwear additive. In contrast, ZDDP tribofilms were easily removed in the base oil containing a dispersant (Figure 3-14). This mechanism was explained by the antagonistic behaviour of dispersant and ZDDP that promotes the removal of antiwear films.

Fujita, *et al.* [55] studied the effect of soot on the removal of ZDDP tribofilm further. Their results showed that the rate of tribofilm removal was greatly increased when soot was added to the base oil containing the dispersant (Figure 3-15). In another study, Fujita, *et al.* [84] found that the ratio of dispersant to soot is influential on the removal of ZDDP tribofilm. It was shown that when the ratio of dispersant to soot was low, soot rapidly removed ZDDP tribofilm. In addition, the reformation of ZDDP tribofilm was prevented.

On the other hand, Spikes *et al.* [85] showed that functionalized polymers and dispersants are able to form boundary films depending on the structure and type of polymers. Devlin *et al.* [86] observed that in the absence of contaminants such as soot, ZDDP has a higher rate of boundary film formation than functionalized polymer. However, in the presence of soot, the dispersants and polymers have higher film formation than ZDDP. It has been explained that dispersants can prevent wear by preventing soot agglomeration. Also, dispersants adsorb to the soot particles and reduce the ability of soot particles to contact metal surfaces. Thus, Devlin *et al.* [86] proposed that it is possible to achieve the desired wear performance in the presence of both soot particles and dispersants by optimizing polymer structure.

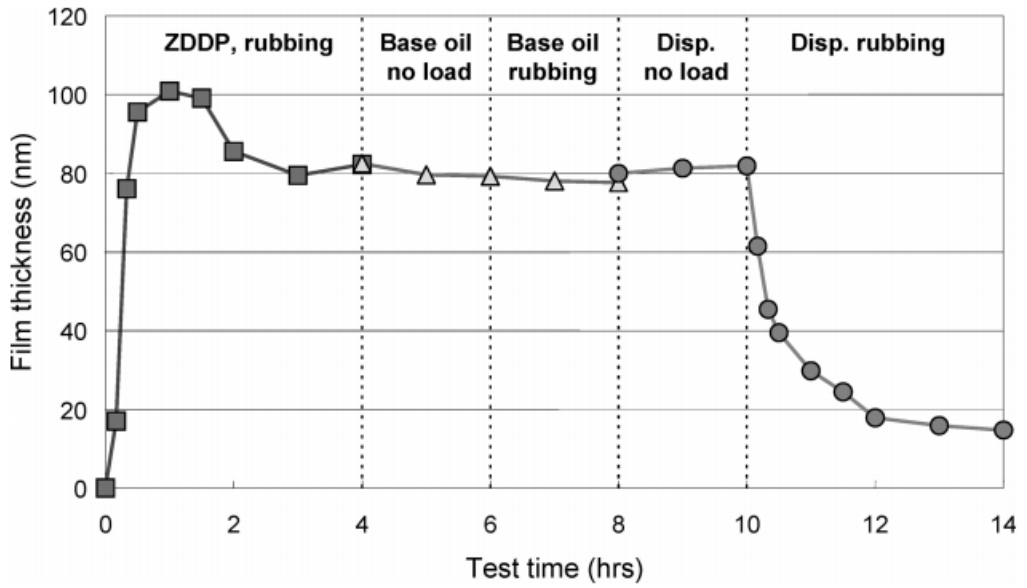


Figure 3-14. The study of stability of ZDDP tribofilm using base oil and dispersant. Test conducted at speed of 0.05 m/s and 80°C [55].

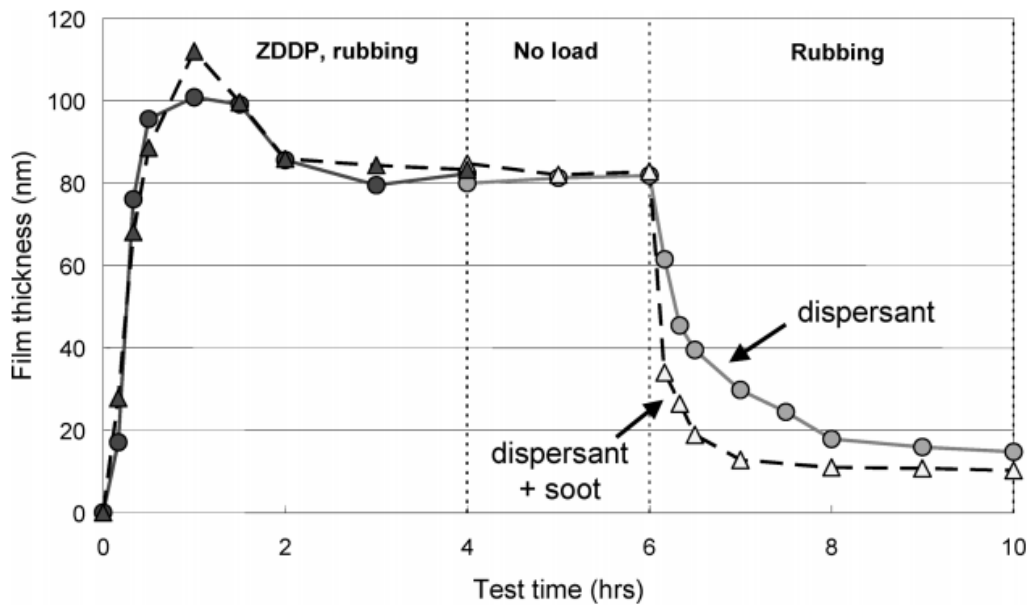


Figure 3-15. Removal of ZDDP film in the presence of 0.1 wt% soot. Test conducted at speed of 0.05 m/s and 80°C [55].

### 3.11 Interactions of additives

As explained in section 2.6, all modern engine oils are composed of base oils and a number of additives to meet demanding performance requirements. These additives are not neutral compounds and could interact with one another in the oil [87]. Interactions of two or more additives can lead to either synergistic or antagonistic effects on the tribological performance of component in contact.

Additive interactions occur either in lubricating oil formulation or at the surfaces. In the oil phase, additive interactions occur to prevent or slow down the oxidation of the oils at high temperature, reduce the variation in viscosity with temperature, control soot thickening and deposit formation. At the contact, additive interactions take place to protect the surfaces from friction, wear and prevent the agglomeration of particles [87]. Figure 3-16 shows the summary of the most common observed interactions between additives. The presence of these additives in the oil can create unexpected and complex interactions.

Rounds [88] reported that the combination of ZDDP and metallic dithiocarbamate oxidation inhibitors, primary alkyl amine friction modifiers, sulphur and chlorine containing EP agents revealed a negative effect on the wear performance. However, ZDDP in combination with detergents, dispersants, oxidation inhibitors, VI improvers and EP agents showed little or no effect on the wear performance. These interactions could change the properties of additives in ways that are not fully understood.

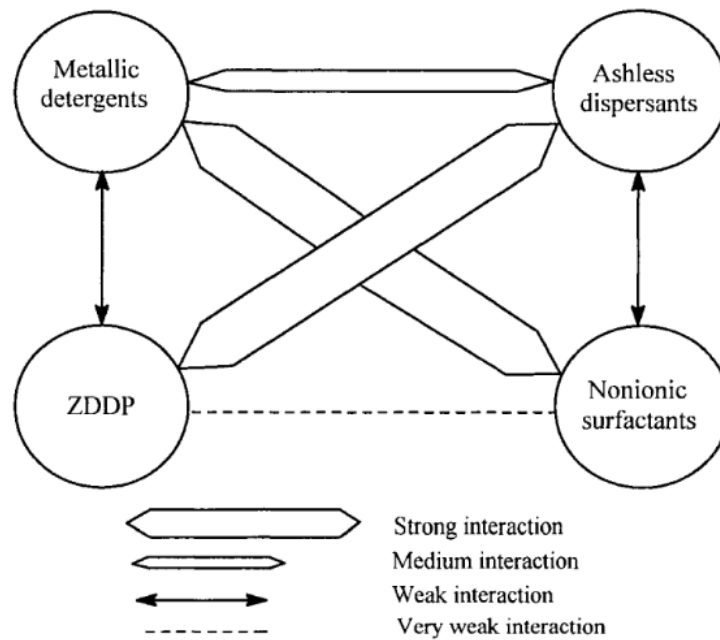


Figure 3-16. Intermolecular interactions between additives [87].

### 3.12 ZDDP interactions with dispersants and detergents

Detergents and dispersants are two important additives in FFO. The role of these additives is to keep the insoluble products in suspension. It has also been reported that detergents can offer antiwear properties by formation of carbonates in the wear scar [88-90]. Metallic detergents were seen to have an antagonistic effect on the wear performance of ZDDP [90, 91]. There is a weak interaction between metallic detergents and ZDDP as shown in Figure 3-16.

The interaction of metallic detergents and ZDDP was shown to deteriorate the effectiveness of ZDDP. This negative interaction was attributed to the competition between these two additives for surface sites. Wan *et al.* [89] demonstrated that  $\text{Ca}^{2+}$  ions from detergent overcame the  $\text{Zn}^{2+}$  ions from ZDDP in the polyphosphate structure of tribofilms leading to the formation of short chain polyphosphate. This was in line with previous results presented by Willermet *et al.* [90] which showed that the formation of ortho- and pyro-phosphates with lower molecular weight than phosphates when Zn was

partially replaced with Ca. Kasrai *et al.* [92, 93] also showed the formation of calcium phosphate instead of long chain polyphosphates in the presence of detergent along with ZDDP. In these experiments, higher wear was observed with combination of detergent and ZDDP than the wear resulted from ZDDP alone. This was related to the higher hardness of calcium phosphate formed from detergent.

It was also found [94] that addition of detergent to the oil affected the mechanical properties of the ZDDP tribofilm formed. It was shown that the indentation modulus was lower for the tribofilm formed with the combination of ZDDP and detergent than ZDDP tribofilm alone. The contribution of  $\text{CaCO}_3$  in the tribofilm was thought to be the main reason for these results [94].

As can be seen from Figure 3-16, there is a strong interaction between antiwear additives and dispersants. Rounds [88] reported that when dispersants were added to ZDDP solutions in the experiments wear increased. Shiomi *et al.* [95] reported the same effect on wear in the presence of both dispersant and ZDDP. This antagonistic effect of ZDDP and dispersants on wear was explained by the lower amount of ZDDP available for film formation by forming a complex. The strength of the complexes formed with various dispersants and with amines affected the wear results.

Smith *et al.* [96] showed that in a simple ZDDP mineral oil solution the tribofilm formed was mostly composed of phosphate on the ferrous substrate (Figure 3-17(a)). However, when both detergent and dispersant were used the tribofilm had a patchy structure with no underlying sulphide layer. This result was explained by the competition between the wider ranges of surface-active additives to form on the surface site. In this case, the substrate was almost covered with the tribofilm. The tribofilm was mainly composed of Ca and Zn as shown in (Figure 3-17(b)). Fe element was not observed in the phosphate film. A thin layer of nitrogen-containing material was detected on the outer



surface formed by dispersant. Thus, it was concluded that dispersant did not mainly contribute in the film structure [96].

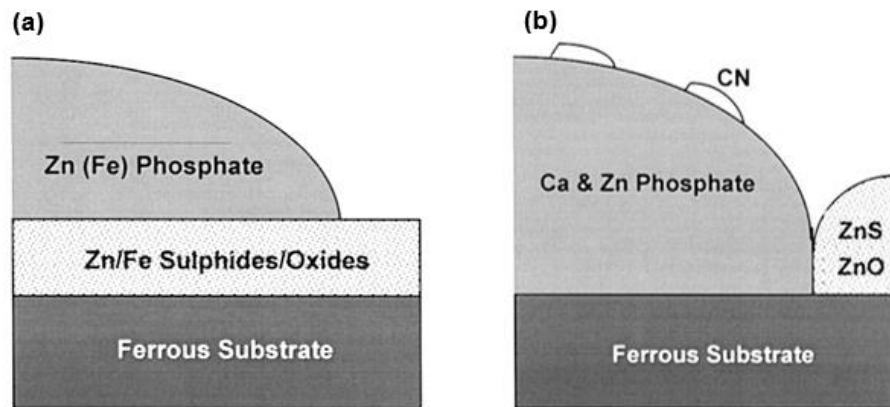


**Figure 3-17. Schematic structures of tribofilms formed using (a) ZDDP solution (b) combination of ZDDP+Detergents+Dispersants [96].**

### **3.13 Role of oil contamination on tribological performance of contacts**

Many studies have been conducted to improve the efficiency of VDVP with the specific focus on factors such as design parameters and operating conditions [97-99]. One source of failure in VDVP is improper lubrication, a factor that has not been studied in detail.

In IC engines, lubricating oil loses its original properties due to contaminations and ageing. Oil degradation and additive depletion form substances that are corrosive and insoluble. In severe operating condition, the oil degradation occurs more rapidly than normal condition. The four main types of contamination in the IC engine are as follows:

- Water contamination
- Coolant contamination
- Fuel contamination

- Soot contamination

Oils are designed to manage the contamination such as soot, water, wear particles, and combustion by-products. Fodor *et al.* [100] conducted a research on the influence of reducing oil contamination on the fuel economy in a six-cylinder diesel engine. The results indicated that the reduction of contamination reduces the fuel consumption, wear and friction by 5%, 93% and 2.9% respectively. These results show that oil contamination has a significant impact on the wear in a system. Fuel and soot contamination are the main focus of this study.

### **3.13.1 Diesel fuel**

Diesel fuels are complex mixtures of hydrocarbons with minor properties of nitrogen, oxygen and sulphur. The compositions of diesel fuels depend on the sources of crude petroleum, methods of separation and the purification techniques [101]. In order to have green environments, new rules and regulations have been formed to limit the amount of harmful components such as sulphur and nitrogen in the fuels. During these modifications in the diesel fuels, other components which are responsible for lubricity of diesel also are removed [101]. Azev *et al.* [102] showed that the wear of the plunger-sleeve pair rises by approximately 50% when the sulphur content in diesel is reduced from 2000 to 10 ppm (see Figure 3-18). Thus, additives are used to enhance the fuel properties and regain the lubricity characteristic.

These additives are composed of a long chain hydrocarbon “tail” similar to diesel itself which dissolves in the fuel. They are also composed of another element at the “head” that has a beneficial effect on diesel. This head contains atoms of nitrogen, oxygen, sulphur or phosphorus in addition to carbon and hydrogen. Unlike the hydrocarbon tail, this head is polar. The polar heads tend to escape from the non-polar hydrocarbons and form a bond with other polar elements such as additives in FFO, metal and degradation particles [103].

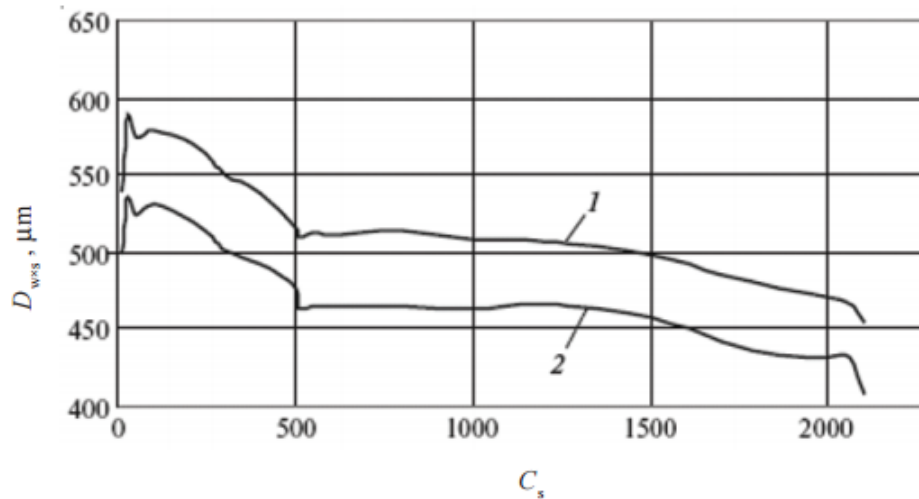


**Figure 3-18. Diameter of wear scar ( $D_{wxs}$ ) versus sulphur content ( $C_s$ ) in diesel fuel obtained by two methods. Method 1: High-Frequency Reciprocating Rig (HFRR method) using ISO 12156 standard. Method 2: proposed method in the study [102].**

### 3.13.2 Diesel fuel contamination of engine oils

The effect of fuel contamination on the performance of oil is normally underestimated compared to the other contaminants such as soot and water. Fuel normally enters the engine oil through internal leakage of the injector and contaminates the oil. The presence of fuel in the engine oil can create several issues such as reduction of viscosity, acceleration of oxidation in the oil, increase of wear due to the reduction of oil film thickness. Diesel fuel contamination can also cause starvation and deposits which reduce the functionality of the oil [104]. Cesur *et al.* [105] reported that engine oil diluted with 50% diesel increased wear when compared to pure engine oil.

The stability of oil contaminated by fuel depends on the type of oil and dilution range. It has been reported [106] that synthetic oils showed better stability resistance when diluted by fuel when compared to mineral oils. The effect of diesel on viscosity of oils are significantly different for mineral and synthetic oils. Mineral oils can lose their properties even with 1% dilution rate, however 7% was the limit reported in the case of synthetic oils.

On the other hand, the existence of sulphur in diesel fuel can play a role in reducing wear and friction losses due to the good lubricating properties of fuel [101]. It has been reported that sulphur lubricity properties can protect surfaces from tribological issues [101]. In summary, the influence of diesel fuel on the oil's properties depends on dilution rate, diesel components and oil's composition. The effect of diesel fuel on tribological behaviour of contacts is not yet fully understood.

### **3.13.3 Soot**

Black carbonaceous soot forms due to the incomplete combustion of hydrocarbons during the combustion process. Soot consists ash, carbon and unsaturated hydrocarbons. The unsaturated hydrocarbons are typically acetylene and polycyclic aromatic hydrocarbon which only consist of the elements of carbon (C), hydrogen (H) and at least one carbon-carbon double or triple bond. All of these components have high levels of acidity and volatility [107]. Soot contains 90 percent carbon, 4 percent oxygen, 3 percent hydrogen and the remaining part consists of nitrogen, sulphur and traces of metal [108].

The presence of soot particles is more common in diesel engines than in gasoline engines. This is due to the difference in combustion mechanism. Diesel engines are operated at higher air-to-fuel ratios, which tend to produce greater levels of engine soot [109]. As the ratio of air-to-fuel increases, the concentration of soot particles produced rises. The soot particles are either exhausted into the atmosphere or adsorbed by the oil. This contamination reduces the life of the engine. Soot has a huge surface activity which can change the chemical properties of oil resulting in the oil losing its functionality, which is also known as oil breakdown. Soot in the oil is one of the major drivers in the wear of engine components. However, the exact wear mechanisms caused by soot and influence of oil additives on these changes are not fully understood [72, 107]. There are different hypotheses regarding the wear

mechanism caused by soot contamination which are explained in Section 3.13.5 [110].

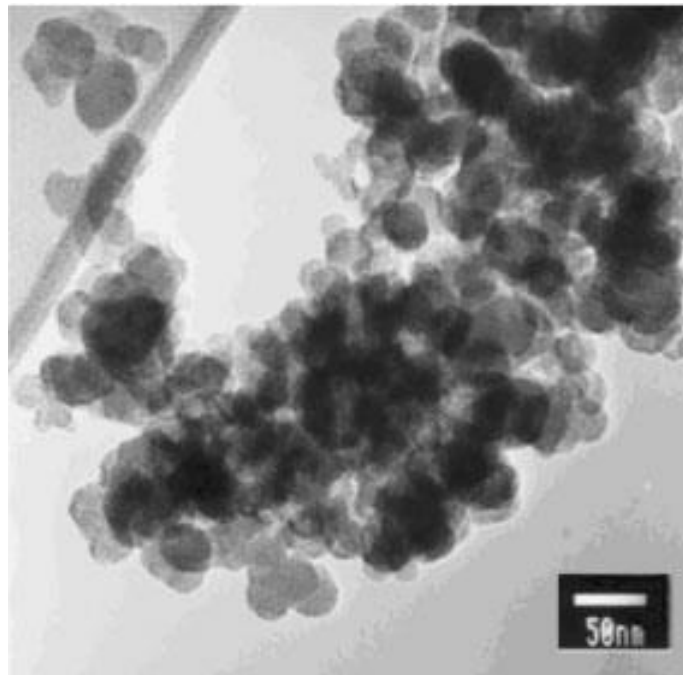


**Figure 3-19. A typical extracted soot from engine [107].**

There are two main obstacles to using soot in experimental studies. Firstly, it is very hard and time-consuming to extract soot from used engine oils. Secondly, the quality of soot extracted from used oils varies greatly with regards to the level of carbon graphitisation, size and chemical composition [111]. Sharma *et al.* [112] studied the structure, morphology and chemistry of different soot samples extracted from a vehicle test, engine test and exhaust. They concluded that different soot particles have different chemical structures. The exhaust soot only revealed C and O elements, however elements of P, S, Ca, Zn and O were detected in the crankcase soot. The variation in the chemistry of soot particles are attributed to their interaction with the lubricant additives (e.g. detergent and antiwear) in the crankcase and tribological contacts in the engine [112]. Uy *et al.* [113] also reported that soot extracted from different engines are different in morphology and chemical composition that can affect the hardness and polarity of soot particles. These differences

can significantly affect the wear mechanism. Thus, results obtained from tests conducted with soot extracted from engines cannot be easily compared to each other.

To overcome this problem, the use of carbon black (hereafter denoted CB) has been adopted to simulate engine soot in several reported studies [72, 110, 114, 115]. This has allowed repeatable experiments to be carried out and reliable data to be obtained. In the literature, there have been concerns regarding the use of CB to simulate soot. These concerns mainly question the similarity between CB particles and soot obtained from diesel engines since they are formed as a result of different processes. Unlike soot, which is an unwanted by-product of combustion, CB is produced under controlled conditions [116]. Uy *et al.* [113] indicated that the main similarities between CB and soot extracted from vehicle are the particle sizes. Jao *et al.* [117] reported that the primary size of soot particles is between 20 and 40 nm, however some larger particles are seen as a result of combining a few primary soot particles together. In general, the size of soot particles from diesel combustion is reported in the range of 40-45 nm in diameter [114, 118]. It has been reported [119] that the size of the carbon black particles is approximately 40 nm which is similar to soot. Jao *et al.* [117] also studied the hardness of a wide range of soot particles from diesel engines. It has been reported that soot particles are hard enough to abrade engine metal parts.

Uy *et al.* [113] believed that the main difference between CB and soot is the chemical composition. This difference can be attributed to the environment and process that these particles are formed. However, Clague *et al.* [120] have demonstrated that the CB particles have the ability to simulate the soot behaviour from engine oils. They believed that CB particles and soot extracted from vehicle engine have many common features. It should be noted that there has been no attempt to investigate the differences between soot and CB in this study as this is not the focus of the study.

### 3.13.4 Effect of soot on friction in boundary lubrication regime

The effect of soot on friction behaviour of contacts have been studied and various results have been reported [72, 118, 121-123]. There have been contradictory views regarding the effect of soot on friction. Table 3-1 shows the summary of results obtained from the previous studies.

**Table 3-1. Summary of results obtained from previous studies.**

Tribometer	Lubricant	CB (wt %)	Friction coefficient ( $\mu$ )	Test conditions	Reference
Four- ball	15W-40	0–8	0.01-0.05	30 min, 25°C, 100–1200rpm, 2.51GPa,	[72]
Pin-on-disc	Model oil +additive package	0–10	0.14	18-23°C, 5 m/s, 2 GPa	[118]
Reciprocating	10W-40	0–5	0.075	20 min, 0.21 m/s	[121]
SRV	10W-30	0–4	0.06-0.15	30 min, 40–130°C	[122]
Pin-on-disc	-	0–10	0.11-0.13	60 min, 28°C, 5 m/s, 2 GPa,	[124]
Reciprocating	5W-30 and Model oil +additive package	0–1.72	0.08-0.15	60 min, 105°C, 0.04 m/s, 1.3 GPa	[115]

Liu *et al.* [122] argued that soot may act as a friction modifier and reduce friction since the structure of soot is relatively similar to graphite and it can act as a solid oil. Figure 3-20 shows that adding soot to oil reduced friction. This suggests that soot has a specific physical and chemical property that can generate lower friction. They showed that the oil with the higher level of soot results in lower friction coefficient (Figure 3-20) and concluded that soot can act as a friction modifier under certain lubricating conditions since both soot

and graphite have similar chemical compositions (high level of carbon around 85%). Hu *et al.* [72] also reported that the low levels of CB that could be uniformly dispersed in the oils can reduce friction between two surfaces during rubbing. Fujita *et al.* [125] explained that soot can reduce friction in two ways: 1) by partially removing the high friction ZDDP tribofilm and 2) by passing through the contacts and acting as a friction modifier.

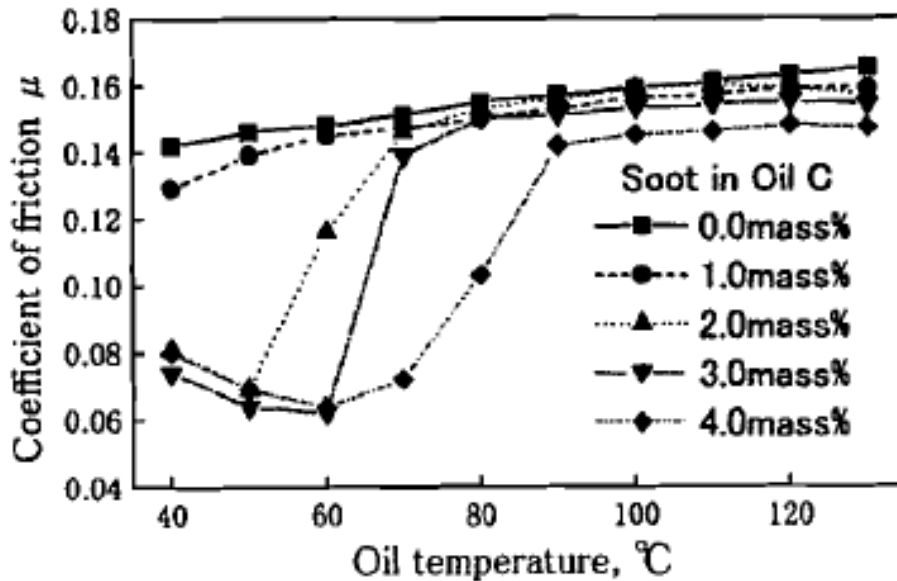


Figure 3-20. Indicates friction coefficient against temperature with different soot mass, showing that the oil with higher soot mass has lower friction coefficient at temperatures 40-80 $^{\circ}\text{C}$  [122].

On the other hand, Ramkumar *et al.* [118] conducted several pin-on-disc experiments with different soot levels in the oil. The results showed that the friction coefficient increases with increasing level of soot. Green *et al.* [121] demonstrated a similar trend using TE77 ball-on-flat reciprocating test rig. Chinas-Castillo *et al.* [126] concluded that soot particles adhering to the surfaces influence the friction behaviour of the system especially when the size of soot particles are greater than the oil film thickness. Hu *et al.* [72] also studied the effect of soot contamination on the tribological behaviour of engine oil. The results indicated that when more than 2% soot was added to the oil,



the friction coefficient increased. The similar trends were observed by Green *et al.* [121]. It has been explained that at lower CB levels the particles were uniformly dispersed throughout the oils. Therefore, CB particles could enter the contact and reduce the friction. However, beyond 2wt% concentration the friction coefficient increases due to the agglomeration of CB particles. Liu *et al.* [122] also demonstrated that in the same test conditions, two oils with varying chemical compositions showed completely different friction behaviour when 3 wt% soot was added to the oils (Figure 3-21). Uy *et al.* [115] showed that the friction behaviour of oils in the presence of CB depends on the oil formulations and CB content. Similar results have been obtained by other researchers [84]. In general, Uy *et al.* [115] concluded that the boundary friction coefficients were not significantly affected by CB.

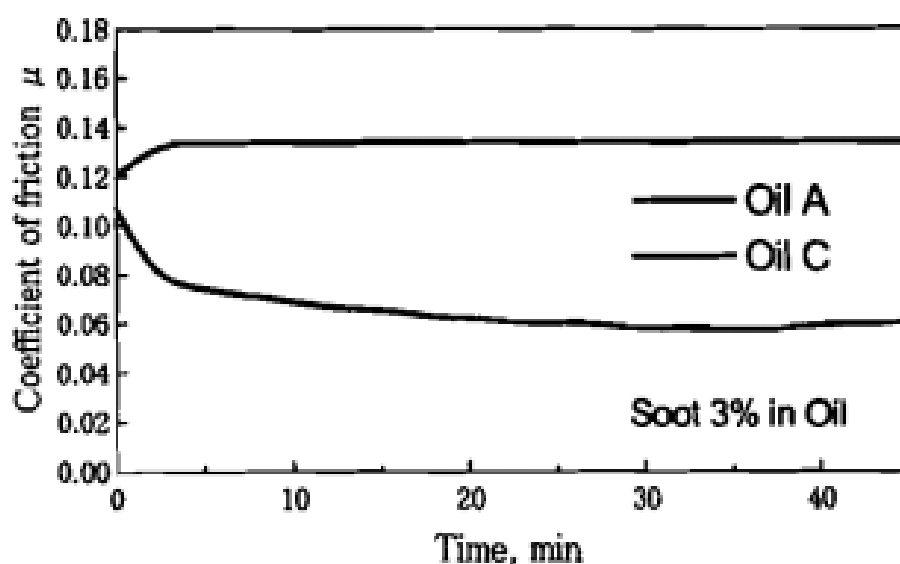


Figure 3-21. Friction behaviour of different oils containing 3wt% soot at 40°C [122].

In summary, it can be concluded that the influence of soot on friction is dependent on many factors such as type of oil, test condition, soot concentration and temperature.

### 3.13.5 Proposed wear mechanisms by soot

Soot is known to induce high wear in engine components. The effect of soot contamination in engine oils on wear of engine components have been investigated in many studies [121, 127-129]. Several mechanisms have been suggested by which soot induces high wear.

#### 3.13.5.1 Abrasion

Abrasion is the most accepted mechanism. Ryason *et al.* [130] stated that soot particles cause abrasive wear based on the wear scars and debris formed between interacting surfaces. Kuo *et al.* [119] reported that abrasive wear by primary soot particles is the main wear mechanism in diesel engines. Other products of wearing process such as wear debris are abraded from the surfaces either by soot or sliding metal-on-metal contact. Kuo *et al.* [119] also believed that these particles further accelerate the abrasive wear process. Cadman and Johnson [131] also concluded that soot acts as the third body enhancing wear either through directly abrading the metallic parts of the engine [110, 129, 130, 132] or by abrasion of antiwear tribofilms formed on the surfaces [114, 132]. Jao *et al.* [117] studied the hardness of a wide range of soot particles from diesel engines. The results showed that the hardness of all types of soot was close to the hardness of metal engine components. Devlin *et al.* [133] also studied the hardness of both biodiesel soot and diesel soot particles and the results showed that the hardness of both types of soot are comparable to engine metal hardness. It was thus concluded [117, 133] that soot is hard enough to abrade both tribofilm and metal engine parts. The same conclusion was also reported in other studies [107, 134].

Nagai *et al.* [132] proposed that antiwear film is removed through abrasion. Torrance [129] also backed up this theory and proposed another potential mechanism. Torrance [129] postulated that soot removes the antiwear tribofilm formed on the surfaces and exposes a fresh reaction underlying

metallic surface. Cadman *et al.* [131] proposed the same mechanism. Ratoi *et al.* [110] showed that addition of CB particles in oil containing various dispersants had different results. In some of the dispersants blends (CD and ED), ZDDP tribofilm was rapidly removed as shown in Figure 3-22. This rapid removal of ZDDP tribofilm was not observed in oil containing another dispersant (AD). They concluded that dispersant additives play a key role in protecting abrasion of ZDDP tribofilm in the presence of CB. This statement has also been confirmed with Devlin *et al.* [86] They have shown that in the presence of soot, functionalized polymers and dispersants form boundary film more rapidly than ZDTP. Kuo *et al.* [119] also reported that the use of dispersant VI improver are found to be effective in reducing wear. It has been explained that this additive increases the thickness of tribofilm which will limit the soot particle's opportunity to contact the surfaces. In contrast, Gautam *et al.* [135] stated that the effect of dispersant level on wear was not significant.

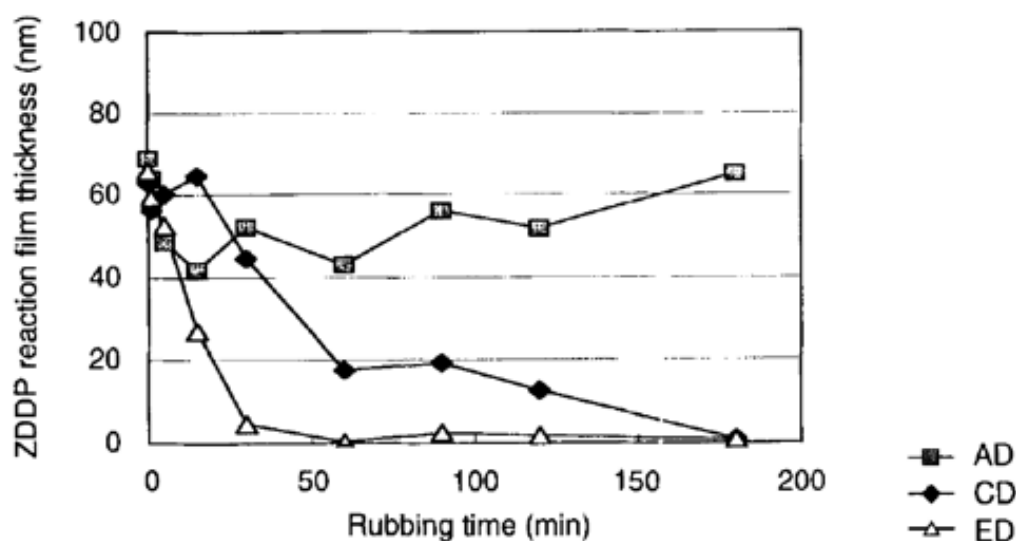


**Figure 3-22.** Indicates friction coefficient behaviour in the presence of 5 wt% CB using three different dispersants. The concentration of dispersant was 9 wt% in all three samples [110].

### 3.13.5.2 Oil starvation

Some studies [107, 136, 137] suggested that soot causes high wear due to the starvation of oil in the contact. Soot in the oil can accumulate at the contact inlet restricting oil supply to the contact [107, 136]. Sato *et al.* [138] conducted a number of experiments by a four-ball wear tester and explained that the starvation wear can occur when the diameter of agglomeration soot is larger than the oil film thickness. Green *et al.* [137] also showed that at high CB levels wear occurred due to high levels of abrasion and starvation (shown in Figure 3-23). In this mechanism, the high levels of soot particles and greater size of particles than film thickness due to agglomeration result in blocking the oil entry to the contact [107]. Thus, the absence of the oil film at the contact leads to metal-on-metal contact and high wear, this is also known as starvation.

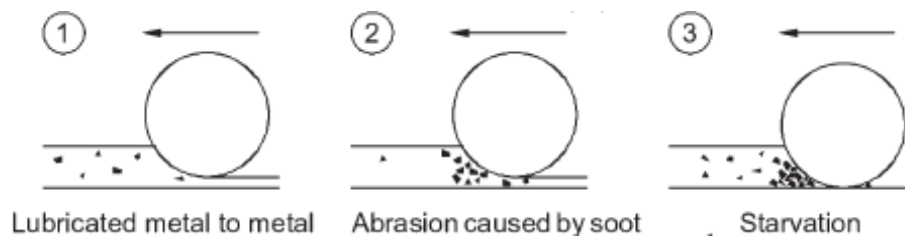


**Figure 3-23. Schematic of wear mechanism in ball-on-flat tribometer test with high level of contamination [137].**

### 3.13.5.3 Competitive adsorption

It has been suggested that soot competes with antiwear additives in adsorbing on surfaces. The adsorption of soot on the surface prevents the adsorption of antiwear additives and their subsequent decomposition to form antiwear films [139]. Barbeizer *et al.* [140] also believed that abrasion was not the only factor producing high wear. It was proposed that the surface coverage rate by antiwear additives reduces due to the physical adsorption of CB on the surfaces.

It has also been reported [141] that the adsorption of soot on surfaces can limit the amount of oxygen reaching the contact surface resulting in the formation of pro wear FeO instead of antiwear Fe<sub>3</sub>O<sub>4</sub>. Unlike Fe<sub>3</sub>O<sub>4</sub>, FeO does not have antiwear properties and as such promotes wear of the metallic surfaces in contact.

#### **3.13.5.4 Additive adsorption on soot**

The adsorption of antiwear additive, ZDDP, on soot particles in diesel engine oils is a great concern. Soot has a tremendous surface activity, so it entraps the effective ZDDP decomposition products and results in dramatic wear [87]. Soot also adsorbs other active additives in the oils and results in wear. This effect of soot is in addition to its abrasion characteristic that removes the tribofilm on surfaces.

It has also been reported [107, 127] that soot adsorbs antiwear additives in the oil phase reducing the concentration of the additives in the oil. Consequently, less antiwear additives adsorb at the contact interface to form antiwear films. This reduces oil's ability to protect the surfaces.

Rounds [127] postulated that soot particles adsorb the decomposition products of antiwear additives leading to high wear. This is to say, before the formation of tribofilm, soot absorbs the antiwear additives. Hosonuma *et al.* [142] also showed that soot preferentially adsorbs zinc-containing compounds and some phosphorous compounds. They agreed with the Rounds theory of additive adsorption by soot. However, they believed that the oils could still perform with the remaining phosphorus compounds within the oils. Berbezier [140] and Gautam [143] also believed that there was no noticeable adsorption of phosphorus compounds on soot particles. However, James and John [144] showed the existence of phosphate and thiophosphates from ZDDP on soot particles using nuclear magnetic resonance spectroscopy (NMR).

### **3.13.5.5 Corrosive–abrasive wear**

Oxygen and hydrogen concentrate on the surface of the CB particles making them polar. Thus, these particles have a great tendency to interact with other polar species [107]. Olomolehin *et al.* [114] demonstrated that the interaction of CB and ZDDP in the oil can lead to aggressive wear. It has been shown that wear increased by 100-2000 times when phosphorus (P-) and sulphur (S-) based antiwear and/or extreme pressure additives were added to a mineral base containing CB. High concentrations of soot can also increase the local acidic level where the temperature is high and volatile gases exist. Corrosion may then happen [107]. In the mentioned study [114], it was concluded that the high wear observed when P- and S-based additives were present was due to the corrosive-abrasive mechanism. This mechanism has also been suggested in other previous studies [110, 129]. Uy *et al.* [115] also showed that fully formulated oil containing P- and S-based additives had much higher wear than a model oil (BO+dispersant+viscosity modifier) in the presence of CB. They explained these results with antagonistic effects of ZDDP and dispersant in FFO. The antagonistic behaviour of dispersant and ZDDP was also reported by Fujita *et al.* [55].

From the above literature on the potential wear mechanisms, it can be concluded that the wear mechanisms are dependent on factors such as soot content, temperature and oil type. The tribological mechanism of soot in oil has been mainly described by abrasion and agglomeration effects on oils. However, the actual mechanisms of wear caused by soot and its interaction with additives in the system are not clearly understood.

## **3.14 Interactions of additives and oil contaminants**

Several studies have reported interactions between fuel and oil additives [145, 146]. As mentioned in Section 3.13.1, diesel fuel contains additives that enhance its lubricity. Stehouwer *et al.* [145] reported that additives in diesel

fuel are composed of organic acids. It was reported that these acidic components in fuel interact with oil additives which result in deposit formation. On the other hand, Fang *et al.* [146] reported that the interaction between fuel and dispersant additives in oil can be beneficial to reduce the deposit formation from fuel. In general, there is a lack of research and literature on the interaction of diesel fuels and additives in engine oils.

Booth *et al.* [147] studied the interactions between carbon black particles and additives such as detergents, dispersants and ZDDP. Figure 3-24 shows that the wear was severe when both ZDDP and CB were present in the oil. The wear scar was small when the oil did not contain ZDDP and CB (Figure 3-24(a)). Figure 3-24(b) showed higher wear and signs of abrasion for oil containing CB without ZDDP. In the presence of both ZDDP and CB the sample was severely worn (Figure 3-24(c)). These results showed that combination of additives in the presence of CB had an antagonistic effect on wear.

Olomolehin *et al.* [114] studied the interaction between additives and CB particles in oil using various additives. They observed that the combination of additives and CB particles showed significantly higher wear (Figure 3-25). This suggests that there was a negative interaction between CB and ZDDP which promoted wear. This mechanism is called corrosive-abrasive wear as explained in Section 3.13.5.5. In general, the interaction between soot and additives is a complex subject and the exact mechanism of these interactions are not fully investigated.

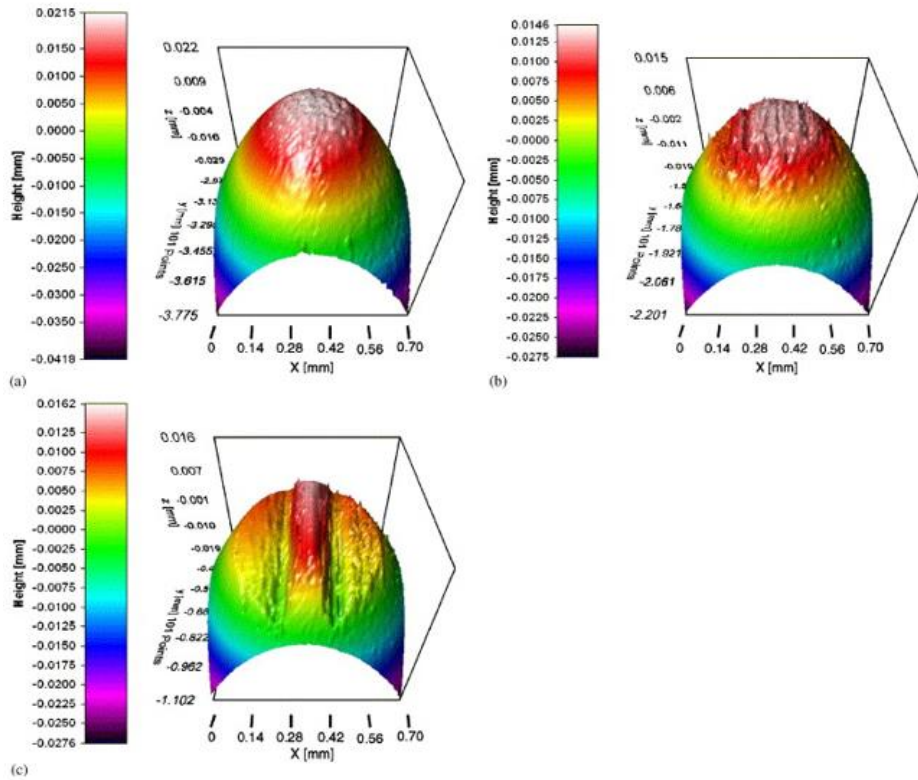


Figure 3-24. 3D topographical image of wear scar formed on the ball samples using various oils containing (a) dispersant (b) CB particles (c) detergent+dispersant+ZDDP+CB [147]

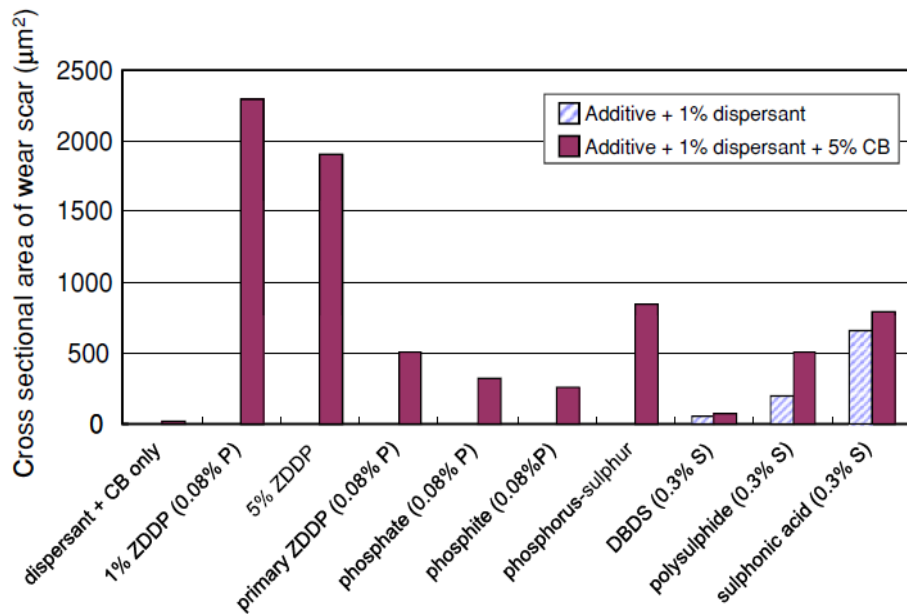


Figure 3-25. Effect of CB particles on wear in the presence of antiwear /EP additives [114].



### 3.15 Oil ageing

The main problem associated with oils in IC engines is the interaction of oils with combustion products. As a result of this, oxidation, oil contamination and formation of deposits on the interacting surfaces can be seen in the systems, causing severe wear and corrosion [42, 47, 48]. Oil ageing is a destructive mechanism that can significantly affect the physical and chemical properties of an oil and reduce its performance. Some factors such as temperature, metal content, type of base oil and additives, contamination content and the rate of air circulation influence the ageing rate of oil [148].

The following processes in the bulk properties of oil can be determined during the ageing process:

- Oxidation and polymerisation of hydrocarbons,
- Production of acids and resins,
- Reduction in the content of additives due to precipitation of their oxidised products,
- Drop in the viscosity index
- Increase in the concentration of solid contaminants due to wear
- Increase in the concentration of contaminants from the environment [148]

It is thus necessary to understand the mechanisms of degradation and its impact on the oil properties and performance. There are three main mechanisms in the degradation process:

**Oxidation:** Oxidation is the primary mechanism and the most common form of degradation. Oxidation occurs due to the chemical reactions between the oils and oxygen from the air. One of the first signs of oxidation is the change in the colour of the oil due to the by-products of the oxidation. The viscosity of oils is also affected following formation of deposits and organic acids as by-

products of oxidation. Oxidation will also change the chemical structure of the base oil during the ageing process [149].

In general, oxidation produces acids, depletes additives and forms harmful sludge due the chemical reactions. Figure 3-26 indicates the three main stages of oxidation of oil. In the initial stage, the hydrocarbons react with oxygen. In this stage hydrocarbon free radicals are formed. The existence of metal ions can catalyse this reaction in this stage. In the propagation stage, hydrocarbon free radicals react with oxygen forming peroxide radicals. These are highly reactive and consequently interact further with oxygen and hydrocarbons from oil. In the final stage, the hydroperoxides form oxygenated compounds and form organic acids.

Temperature significantly affects the oxidation mechanism; higher temperature leads to higher oxidation rate and acid production. The presence of some other factors such as contaminants and reactive metals accelerate the oxidation rate [150]. The ageing stability of the oil depends on its chemical composition and additives [149].

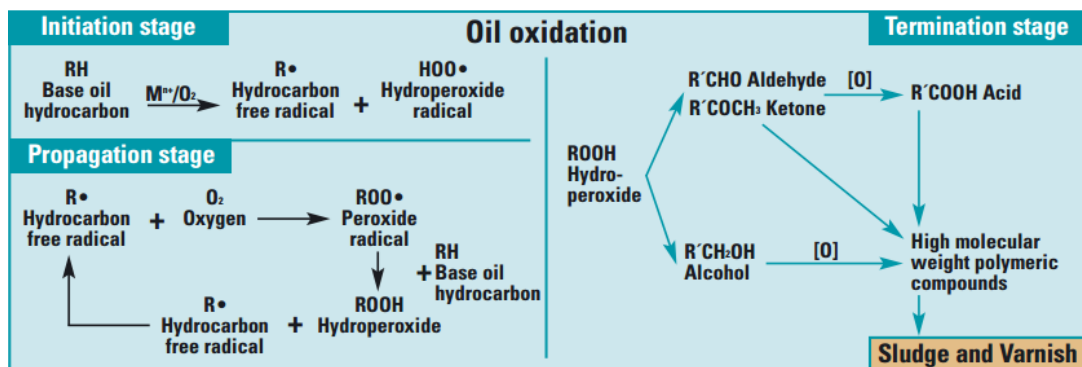


Figure 3-26. Schematic of the oxidative degradation diagram in the oil [151].

**Additive depletion:** additive depletion is one of the leading causes of oils failure. It occurs during the ageing process and reduces the performance of oils. Additive depletion, like oxidation, is accelerated by catalysts such as

metal, acids and contaminants. As the additive levels decrease, the acid levels and oil oxidation increase thus the oil reduces its ability to protect the surfaces.

**Contamination:** contamination can significantly accelerate the oil degradation and acid production. The contaminants are strong oxidisers that can accelerate fluids oxidation and acid production. For example, wear metals act as catalysts and accelerate the oxidation process of the oils [87]. Figure 3-27 shows the cycle of oil degradation.



Figure 3-27. Oil degradation cycle [152].

### 3.16 Effect of oil ageing on the performance of oils

Ageing can significantly affect the performance of oils. Many studies have been conducted on the effect of ageing on the oil properties. Kreuz *et al.* [153] showed that the high engine temperature significantly affected the ageing process of the oil. Zhang *et al.* [154] also showed that the ageing process accelerated at high temperature and resulted in the higher formation of decomposition products. They also demonstrated that the acid content within the oil increased with the increase of temperature, however viscosity did not change considerably.

Beyer-Faiss *et al.* [155] showed that the increase of temperature accelerated the bearing failure due to the thick layers formed on the running surface of the

bearing's cylindrical bore. The formation of these layers was believed to be due to the organic reaction products within the lubrication system. Most oils form acidic oxidation products during the ageing procedure. These acids are either weak or strong depending on the type of oils [156].

Several studies [83, 157] have investigated the performance of antiwear additives, ZDDP, during the ageing process. Willermet *et al.* [49, 158] reported that the by-products of degradation of antiwear additive (ZDDP) were less effective than ZDDP itself. Spedding and Watkins [159] believed that the anti-wear ability of ZDDP is mainly due to its degradation product from decomposition of ZDDP which are alkyl sulphides and zinc polyphosphates. Uy *et al.* [160] backed up this statement and showed that lower wear was observed with aged oils compared to fresh oils in valve-train experiments. They suggested [160] that the film formed from aged oil would provide superior wear performance than the film formed from fresh oil. The reason for this is still unclear.

### **3.17 Summary**

In this chapter, a comprehensive review of the relevant literature on variable displacement vane pumps was presented and operation, advantages, failure mechanisms and tribological behaviours of VDVP were discussed in detail. Most of these studies have purely focused on the vane-slide ring contact and there has been no focus on the vane-rotor interaction. Frendo *et al.* [10] showed that high friction between vanes and rotor applies high torque on the vanes followed by an abrupt rise in this contact. This condition can significantly increase wear between vanes and rotor and affect the performance of VDVP. However there is a clear lack of research and literature on vane-rotor contact compared to vane-slide-ring contact. In this study, the tribological behaviour of vane- rotor contact will be considered.

Inappropriate lubrication can influence the performance of VDVP resulting in high wear. A number of studies have been conducted to investigate the effect of design parameters of VDVP and their impact on the performance of this pump. It was reported that VDVP is sensitive to contamination due to the design of this pump. However, there is no specific study on the effect of oil contamination on the wear and friction of VDVP.

Oil contaminations such as soot and diesel influence the physical and chemical properties of the oil thus changing the tribological performance of VDVP. Soot is also known to induce high wear in engine components. Many studies have investigated the effect of soot contamination on friction and wear of contacts. Although several mechanisms have been suggested, there is still no consensus. The mechanism by which soot induces wear is not well understood.

The effect of diesel fuel contamination on the performance of oil is underestimated compared to the other contaminants. The effect of diesel contamination on the oil is related to the type of oil, stability of oil and dilution range, which can then affect the tribological performance. There is a clear lack of literature on the effect of diesel contamination in oil on friction and wear performance of contacts. In this study, the effect of diesel contamination in oil under boundary lubrication regime will be investigated.

The effect of ageing on the performance of oils was also reviewed. Some factors such as temperature, oxygen, metal and contamination were shown to be the key factors in the ageing process of an oil. It was found that ageing could reduce or increase the wear in different test conditions. There have been several studies on the effect of oil contamination such as soot on wear and friction. However there has been no focus on the aged oil in the presence of contaminants on friction and wear.

It is vital to consider the factor of ageing on wear and friction behaviour which is a more realistic condition. There is still a knowledge gap in the understanding of oil contamination and ageing on the tribological performance. In this study, the influence of soot and diesel on the properties of oil and tribological performance of oil during the ageing process will be investigated. In general, contaminants can affect the oils and tribological performance within the tribosystem and a literature review of their effects can be summarised as shown in Figure 3-28.

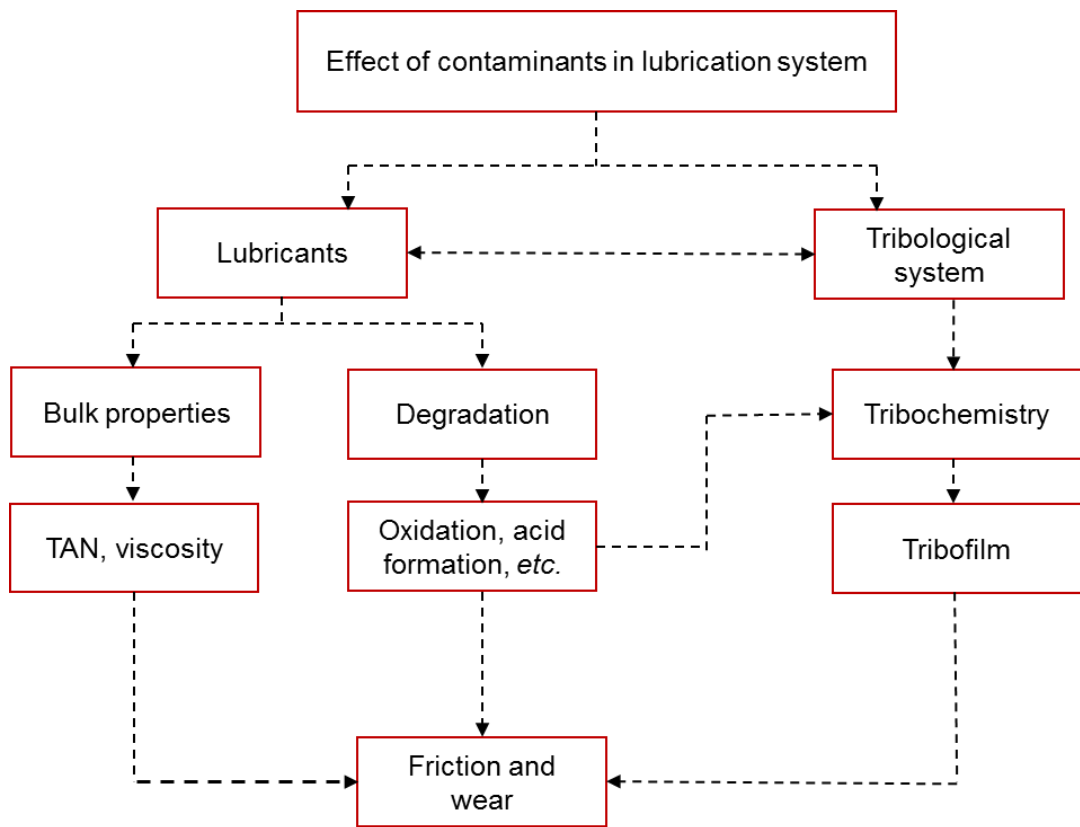


**Figure 3-28. Schematic of the effect of contaminants in the lubrication system (source: author).**

## **Chapter 4 Experimental methodology**

### **4.1 Introduction**

This chapter outlines details of the main experimental procedures undertaken in this project. It explains the details and properties of oil, sample and preparation procedure. This chapter also describes the surface analysis techniques employed to establish the modification of oil during the ageing process, wear mechanism and interaction between additives and contaminants.

### **4.2 Materials**

This section provides information on the oils, CB and diesel used in this study.

#### **4.2.1 Fully formulated engine oil**

A commercially available fully formulated engine oil, hereafter referred to as FFO, with a viscosity grade of 5W-30 was selected for the tribological tests. FFO was sourced from Fuchs Lubricants, Stoke-on-Trent, UK. FFO consists of a synthetic base oil and different additives such as extreme pressure, antiwear, anti-oxidants and additives containing metallic elements.

Inductively Coupled Plasma (ICP) analysis on the fresh oil revealed that the primary additives in the oil are calcium, zinc and boron (see Figure 4-1). Other elements such as magnesium, molybdenum, silicon and sodium were also detected with low concentration less than 10 ppm. All ICP analysis were conducted by Millers Oils, Brighthouse, UK. Table 4-1 shows the physical properties of the oil used in this study.

**Table 4-1. Physical properties of FFO sourced by Fuchs Lubricants.**

Item	5W-30
Density at 15°C	0.860 g/ml
Flash point, CoC	250°C
Kinematic viscosity at 40°C	57 mm <sup>2</sup> /s
Kinematic viscosity at 100°C	10.0 mm <sup>2</sup> /s

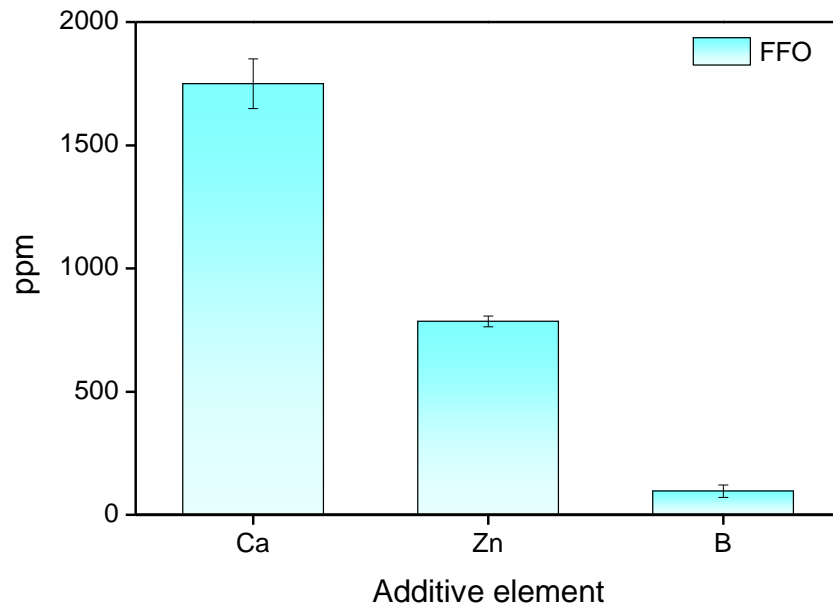


**Figure 4-1. The main additive elements detected in FFO used in this study using ICP.**

#### **4.2.2 Base oil and antiwear additive**

A base oil, hereafter referred to as BO, along with an antiwear additive were also used in this study in order to create a series of model oils. The base oil was a Group III mineral oil. The antiwear additive was a secondary Zinc Dialkyldithiophosphates (ZDDP). The model oils were prepared by blending the antiwear additives in the base oil at various concentrations using stirrer and hot plate for 30 minutes. Table 4-2 shows the model oils used in this study



and their designation. The additive concentrates and the mineral base oil were sourced from Total Raffinage, Solaize, France.

**Table 4-2. Model oils used in the study.**

Description	Oil
BO	Group III mineral oil
Model oil	0.5,1, 3 and 5 wt% ZDDP + Group III mineral oil

#### **4.2.3 Carbon black powder**

A commercially available Monarch 120 carbon black (Cabot Corporation, Massachusetts, USA) was used to simulate engine soot in this study. The Monarch 120 has been previously used in other studies and showed consistent results [86]. Figure 4-2 shows a high resolution image of the CB used in this study. The structure of these CB particles is very similar to a typical soot extracted from an engine as shown in Figure 3-19. The individual CB particles used in this study were approximately 50 nm in diameter. The rounded particles were agglomerates of smaller particles and were 100-200 nm in size as shown in Figure 4-2. As mentioned in section 3.13.5.1, the hardness of Monarch 120 carbon black is close to the range metal engine components [86]. The hardness of Monarch 120 carbon black used in this study is reported around 67.7 HRC provided by Cabot Corporation, Massachusetts, USA.

Although CB was not the exact replicate of engine soot, it was an ideal surrogate for soot since it allowed repeatable experiments to be carried out and reliable data to be obtained. Contaminated oils for experiments were prepared by blending the CB particles in the oils at various concentrations

using stirrer and hot plate for 30 minutes. An ultrasonic bath was also used for 30 minutes prior to tests in order to uniformly distribute the CB in the oil.

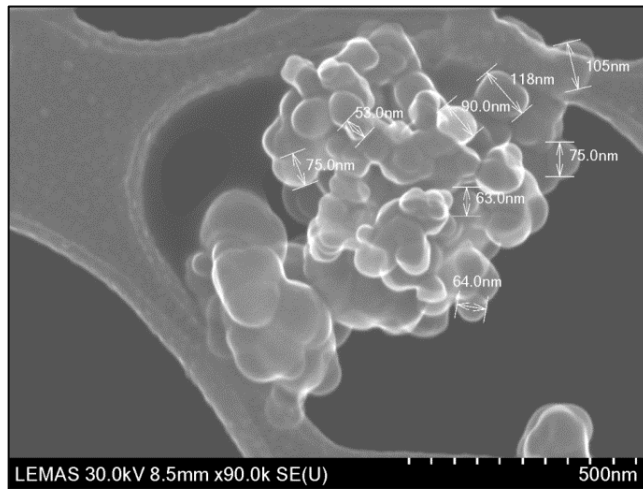


**Figure 4-2. High resolution image of CB particles, showing the diameter of particles.**

Raman spectra obtained from these powders were used as reference. The spectrum for CB was obtained with the 488 nm laser as shown in Figure 4-3. The CB spectra has broad peaks at  $1365\text{ cm}^{-1}$  and  $1580\text{ cm}^{-1}$  similar to those observed in soot extracted from vehicle and engine test as shown in Figure 4-4 [112, 161].

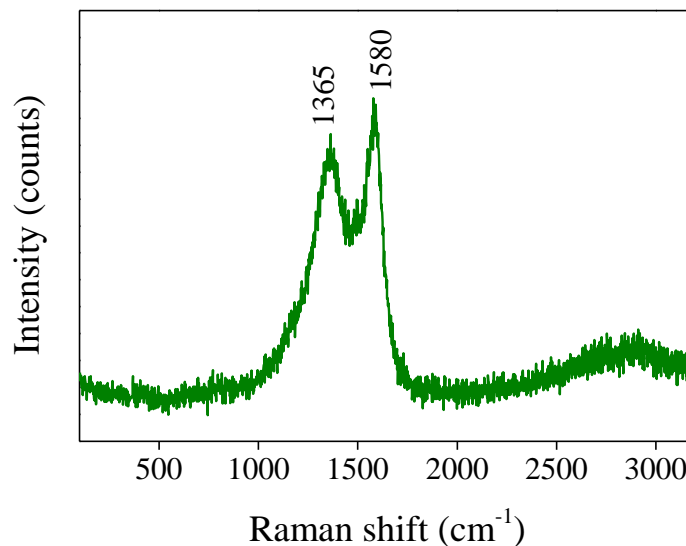


**Figure 4-3. Raman spectra of the carbon black used in this study.**

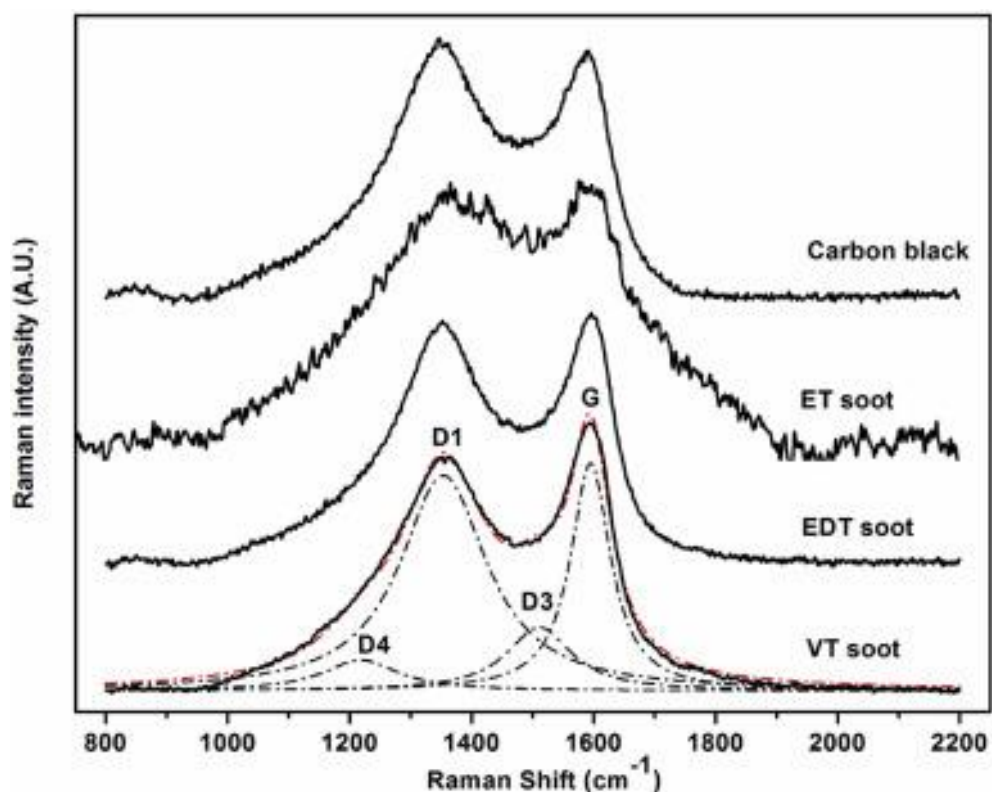


Figure 4-4 Raman spectra of CB and diesel soot extracted from Vehicle Test (VT) and Engine Dynamometer Test (EDT). Exhaust soot from a pipe was also analysed referred to as ET soot [112].

#### 4.2.4 Diesel fuel

The diesel fuel used in this study was Shell City Diesel, sourced from a local petrol station (Shell Fuel Station, Leeds, UK). Figure 4-5 shows the Raman spectra of the diesel and FFO used in this study. Raman spectra of the diesel and FFO were obtained with the 785 nm laser. The 488 nm laser showed signs of high fluorescence and also very broad peaks. Raman spectra of diesel and FFO were relatively similar to each other with the exception of the peak at  $1609\text{ cm}^{-1}$  in the diesel spectra. Both diesel and the oil are distillation products of crude oil and thus they are primarily composed of hydrocarbons. This explains the similarity in Raman spectra. The main difference between diesel and oil is that diesel contains a higher amount of sulphur. The peak at  $1609\text{ cm}^{-1}$  in the diesel spectra was attributed to sulphur content in the hydrocarbon.

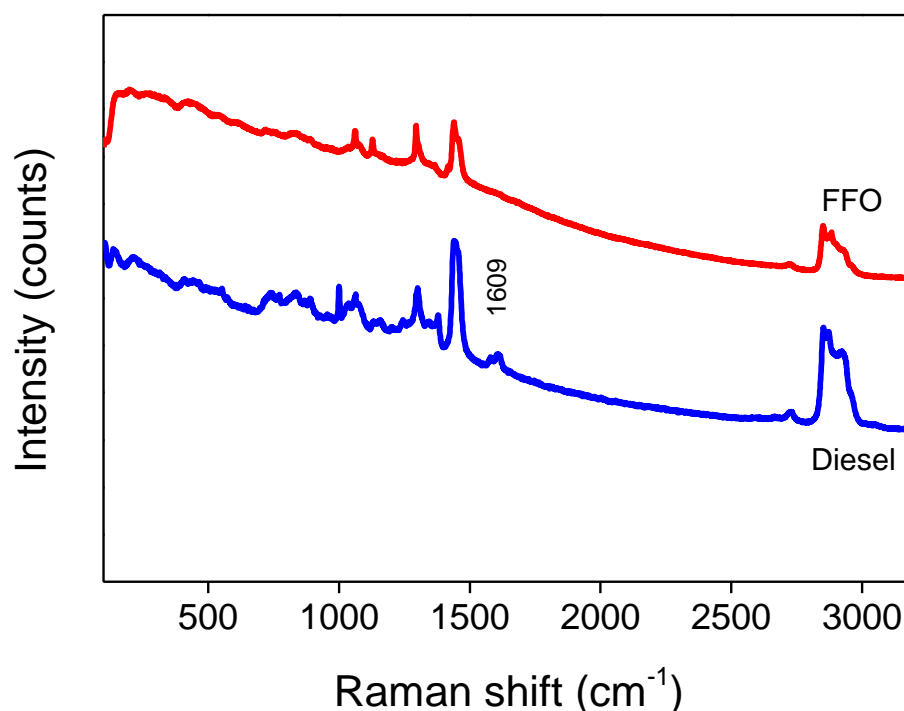
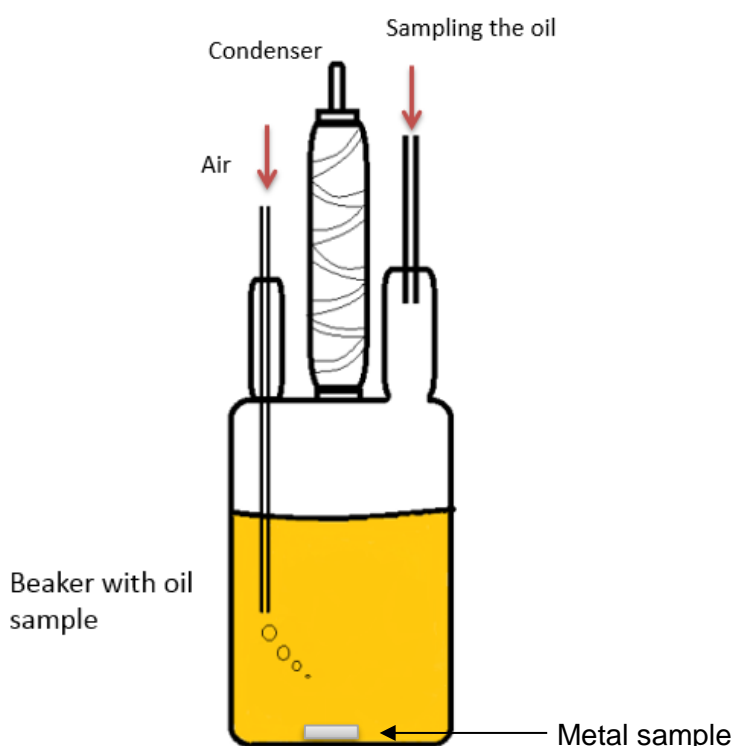


Figure 4-5. Raman spectra of the FFO and diesel used in this study, showing a similarities in the spectra for the FFO and diesel, with the difference of a larger peak at  $1609\text{ cm}^{-1}$  for diesel, attributed to higher sulphur content.

### 4.3 Oil ageing

One of the main focuses of this study was to understand the effects of oil contamination on the performance of VDVP. In order to have reliable and repeatable results, oil with consistent properties was required for the experiments. Therefore, used engine oil extracted from operational vehicles could not be used in this study since it could vary from car to car. To overcome this problem, an alternative approach was taken which was based on degrading the engine oil artificially in the lab in accordance to ASTM D4636- 99 standard [162]. As shown in Figure 4-6, 200 ml of FFO was placed in a PTFE bottle covered with a five-neck lid. The middle neck was equipped with a condenser to prevent the evaporation of the oil. Air was also passed to the beaker with the airflow of 10 L/h to provide a source of oxygen. Metal

samples were also used to provide catalytic reactive surfaces. The largest neck was allocated to the sampling of the oil and condition monitoring of the system. The beaker containing oil was placed on a hot plate in a constant temperature at 160°C. Since the main degradation of oil occurs in the combustion chamber this temperature was selected to simulate the same conditions. This method created a harsh condition in order to accelerate degradation of the oil. This ageing method takes 96 hours and stresses the oil similar to 10,000 miles of severe vehicle service [163].



**Figure 4-6. Schematic set-up for oil degradation.**

#### **4.4 Tribological tests**

The tribological experiments in this project were mainly divided into two phases. In the first phase of this study, the primary experiments were conducted under pure unidirectional sliding conditions in a ball-on-disc rig using various oils. This part aimed to purely investigate the effect of each of the contaminants on friction and wear under boundary lubrication condition.

In the second phase, the other experiments were carried out under reciprocating sliding conditions in a TE77 test rig. This part aimed to understand the effect of aged oil on friction and wear of vane-rotor contact under boundary lubrication regime.

#### 4.4.1 High Speed Pin-on-Disc (HSPOD) tribotests

These experiments were conducted to investigate the effect of contaminants on the oil behaviour in the boundary lubrication regime. This condition simulates the vane-slide ring contact under boundary lubrication regime in VDVP. The disc is placed on top of the motor and the ball was fixed on the loading arm. The loading arm located on top of the disc so that the ball, which was fixed, contacted with the rotating disc as shown in Figure 4-7. This simulated the linear unidirectional sliding conditions. Figure 4-8 shows images of the HSPOD tribometer used in this study. Appropriate weights were applied to the loading arm to provide the desired contact pressure on ball. The oil bath was filled with the oil until the disc was fully submerged. The desired temperature was set and controlled by a heat controller. The oil bath was then heated to the set temperature. The oil bath was covered with a lid to prevent oil spillage during tests. The output of the HSPOD rig was friction voltage which was recorded every second using a LabView program and then the voltage was converted to friction coefficient.

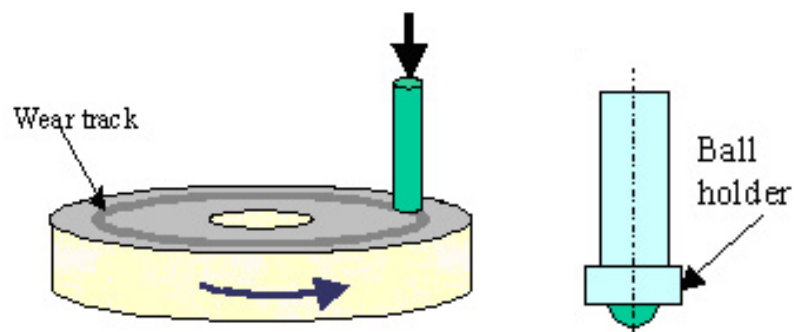
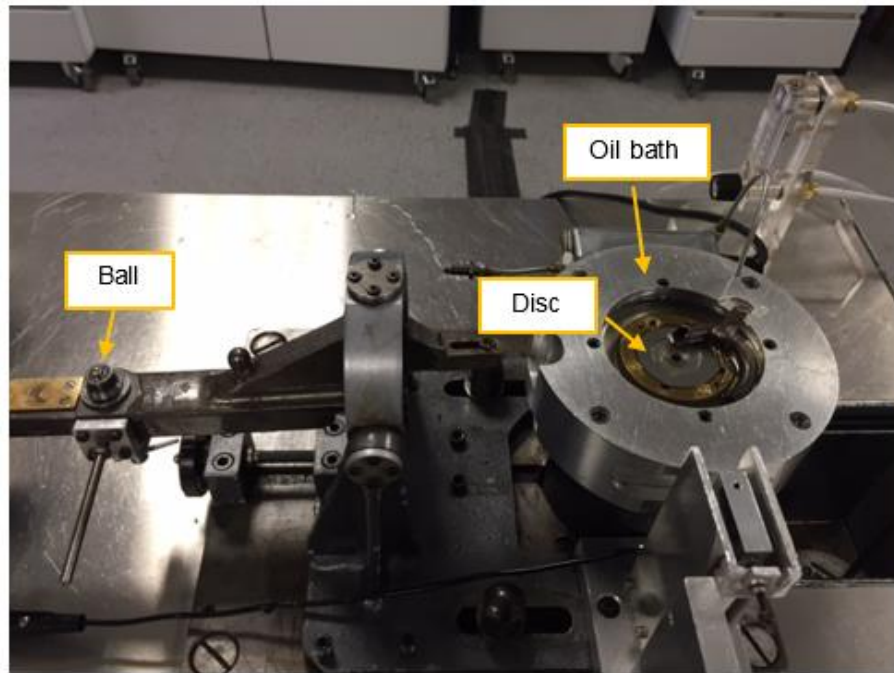


Figure 4-7. Schematic of the actual contact in pin-on-disc tribometer [164]



**Figure 4-8.** Image of the high speed pin on disc tribometer used in this study, in the setup position. The disc was submerged in an oil bath and the ball was lowered onto the disc during the experiments.

#### 4.4.1.1 Test conditions for HSPOD tribotests

Balls and discs used in HSPOD tribometer were AISI 52100 high Chromium alloy and Carbon steel AISI 1050 steel respectively. The chemical compositions of these materials are shown in Table 4-3. The information on material properties and dimensions of the balls and discs samples are summarised in Table 4-4

**Table 4-3. Chemical composition of samples**

	<b>Material</b>	<b>C (%)</b>	<b>Mn</b>	<b>Si</b>	<b>P</b>	<b>S</b>
<b>Ball</b>	AISI 52100	0.95– 1.10	1.10% max	0.10– 0.35%	0.05% max	0.05% max
<b>Disc</b>	AISI 1050	0.48– 0.55	0.60– 0.90%	N/A	0.04% max	0.05% max

**Table 4-4. Material properties of tribopair samples used in HSPOD tribotests**

	<b>Ball</b>	<b>Disc</b>
<b>Material</b>	AISI 52100	AISI 1050
<b>Dimensions</b>	Diameter: 6.5 mm	Inner diameter: 25 mm Outer diameter: 42 mm Thickness: 1 mm
<b>Hardness</b>	60-67 HRC	60-64 HRC
<b>Surface roughness</b>	13 nm	112 nm
<b>Young's Modulus</b>	190-210 GPa	190-210 GPa

Tribotests were carried out at test conditions shown in Table 4-5. The initial contact pressure and film thickness were calculated using Hertzian initial point contact equation shown in Chapter 2. For these calculations, the elastic modulus and Poisson's ratio of the ball and disc were taken as 210 GPa and 0.28, respectively.

**Table 4-5. Test conditions during HSPOD tribotests**

Test condition	Parameters
Oils	Variable
Temperature	40-100°C
Contact pressure	0.83 GPa
Film thickness ratio( $\lambda$ )	< 0.09
Sliding speed	500 rpm (0.75m/s)
Test duration	2h

Figure 4-9 shows images of the tribopair after HSPOD tribotests. A circular wear track was generated on the disc and a wear scar several hundred micrometres in diameter was generated on the ball. The wear scars generated



after HSPOD tests were further analysed to determine chemical composition and morphology. It is worth noting that only the wear on the ball is taken into account. Because the initial roughness of the disc was higher than ball, it was thus difficult to distinguish the wear scar on the disc from the unworn surface.

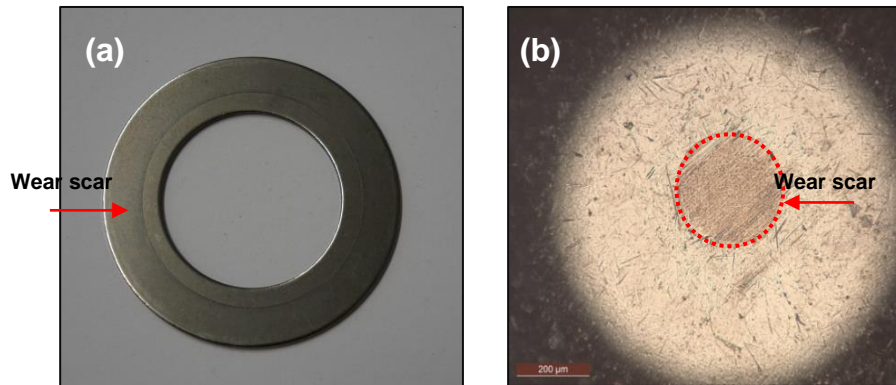


**Figure 4-9. Examples of wear scars generated on the (a) disc and (b) ball after tests on the HSPOD tribometer**

#### **4.4.2 Pin-on-plate tribometer testing procedure (TE77)**

In the second phase of this study, all experiments were conducted using a TE77 tribometer test rig operating under reciprocating sliding conditions. This contact simulated the severe conditions that occur at vane-rotor contact in VDVP. Figure 4-10 shows the schematic view of a TE77 reciprocating pin-on-plate tribometer. Vane and rotor samples used in the experiments were provided by Magna powertrain, Ontario, Canada. These samples were cut from an actual vane pump. The rotor was fitted on the shaft while the vane was fixed at the bottom of the oil bath as shown in Figure 4-11.

Oil in the oil bath is heated using a heater. The heater plate was positioned below the sample holder and temperature was controlled by a thermocouple. The frictional force transducer measures the frictional force generated horizontally while testing was underway. The frictional force was the average

measurement read at five-minute intervals for a set number of hours. All these variables were controlled through a LabView-based software.

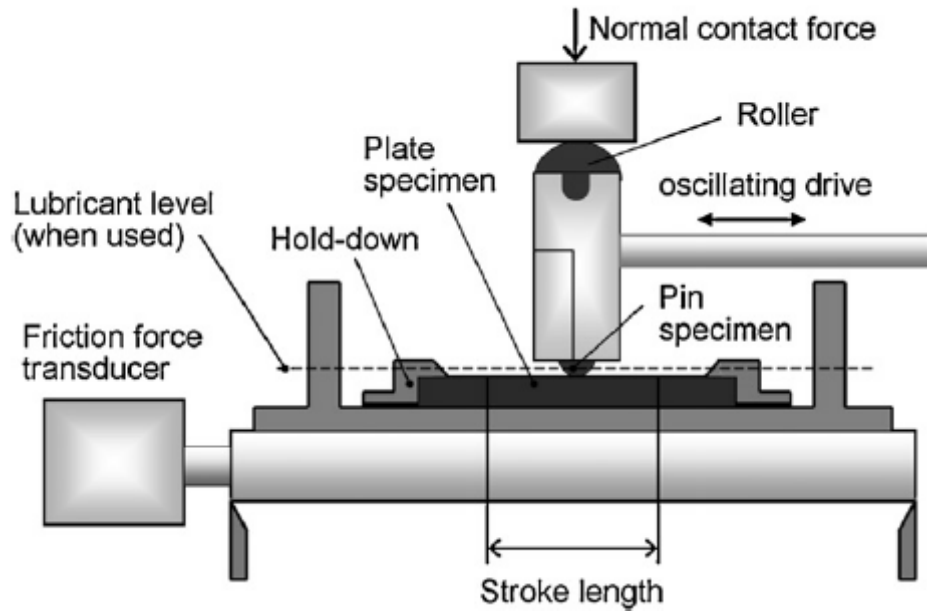


Figure 4-10. Schematic of a TE77 reciprocating pin-on-plate tribometer [165]

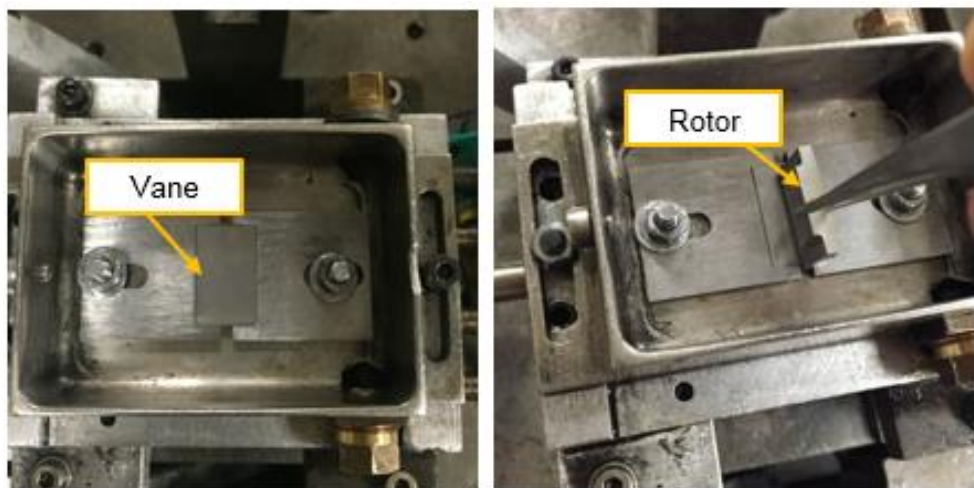


Figure 4-11. Images of the vane (left) and rotor (right) samples fixed in TE77.

#### 4.4.2.1 Test conditions for TE77 tribotests

Tests in TE77 were conducted using SAE 52100 vane samples with 57- 67 HRC hardness. Rotor was sintered metal (MP IF FD-0408-50) with 73- 93 HRB hardness. Table 4-6 shows the specifications and dimensions of samples. TE77 Tests were conducted at test conditions shown in Table 4-7.

**Table 4-6. Specification of materials using in TE77 tests provided by Magna Powertrain, Ontario, Canada**

Component	Material	Hardness	Roughness	Dimension
Vane	SAE 52100	Harden and temper to 57-67 HRC	1.6 Ra	19.98mm×12.56mm
Rotor	MP IF FD-0408-50	73-93 HRB	0.8 Ra	Length 20mm Curvature 0.33mm

**Table 4-7. Test conditions used during TE77 tribotests**

Test condition	Parameters
Temperature	100°C
Contact pressure	0.83 GPa
Oil	Variable
Frequency	25 Hz
Stroke length	7 mm
Test duration	2 h

Figure 4-12 shows an example of the wear scar generated on tribopair immediately after a TE77 test. It can be seen that higher wear was observed on the vane in comparison to the rotor. This is due to the greater hardness of the rotor material when compared with the vane materials (Table 4-6). Also, due to the complex shape of deformation and lower wear, the wear volume loss could not be accurately measured on the rotors. Therefore, the wear track

on vane samples were only measured and further analysed in terms of chemical composition.

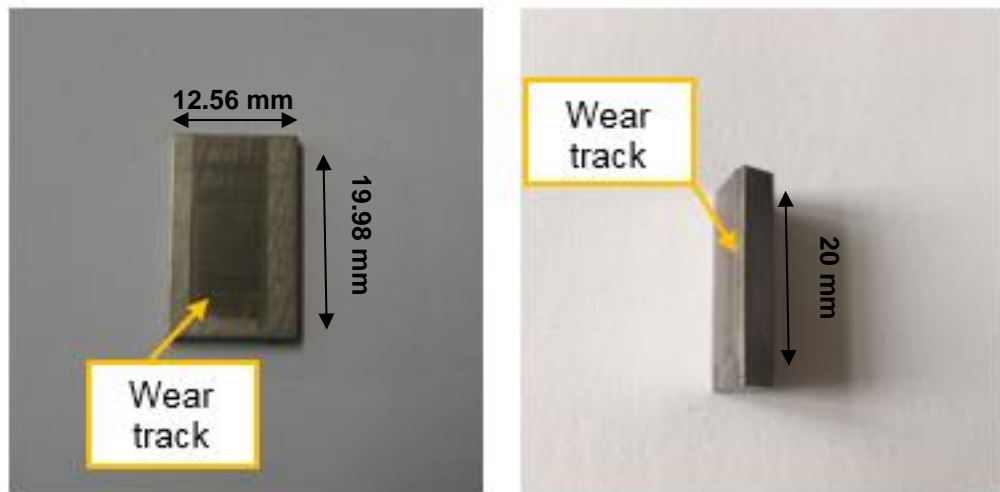


**Figure 4-12. Wear tracks generated on the vane (left) and rotor (right) after TE77 tribotests**

#### **4.5 Pre-test and post-test sample treatment**

Before any tribotests, samples were cleaned with acetone in an ultrasonic bath for five minutes. The samples were then dried with tissue paper before being fixed in the tribometer rig.

At the end of testing, the tribopair samples were rinsed with heptane to remove excess oil. In tests conducted by CB contaminated oils, samples were covered with a layer of black oil. It was therefore difficult to observe the wear debris around the wear scar. Rinsing the disc in heptane removed the wear debris from the surface and the wear track became distinct.

## 4.6 Wear measurement

Optical white light interferometer using NPFLEX from Bruker was used to measure the volume loss on ball and vane samples allowing assessment of wear after the tribotests.

Basic theory of how images are obtained using the equipment is as follows. Interferometer uses a single source of light to generate two white beams of light by a beam-splitter: a reference beam and an object beam. The reference beam reflects from a reference mirror and the object beam reflects from the sample being measured. The reflected light of each beam is then recombined. The recombined beams generate fringes (bright and dark bands) that create an interference pattern and show the topography of the object surface. In this study, interference images obtained from NPFLEX were analysed using Vision64 software from Bruker.

Wear volume of the ball ( $V_{\text{wear-ball}}$ ) was calculated using Equation 4-1 and Equation 4-2. In these equations,  $h$  is the height of wear of the ball,  $r$  the radius of wear scar and  $R$  the radius of the ball.

$$V_{\text{wear-ball}} = \frac{\pi h}{6} (3r^2 + h^2) \quad \text{Equation 4-1}$$

$$h = R - \sqrt{R^2 - r^2} \quad \text{Equation 4-2}$$

Wear coefficient was calculated for vane samples using Archard wear equation, as shown in Equation 4-3.  $V$  is the wear volume ( $\text{m}^3$ ),  $K$  is the dimensionless wear coefficient,  $L$  is the sliding distance (m) and  $V$  is the load (N).

$$K = \frac{V}{LW}$$

Equation 4-3

The typical data of the cross sectional area of the wear scar formed on the balls and vanes are shown in Figure 4-13 and Figure 4-14, respectively.

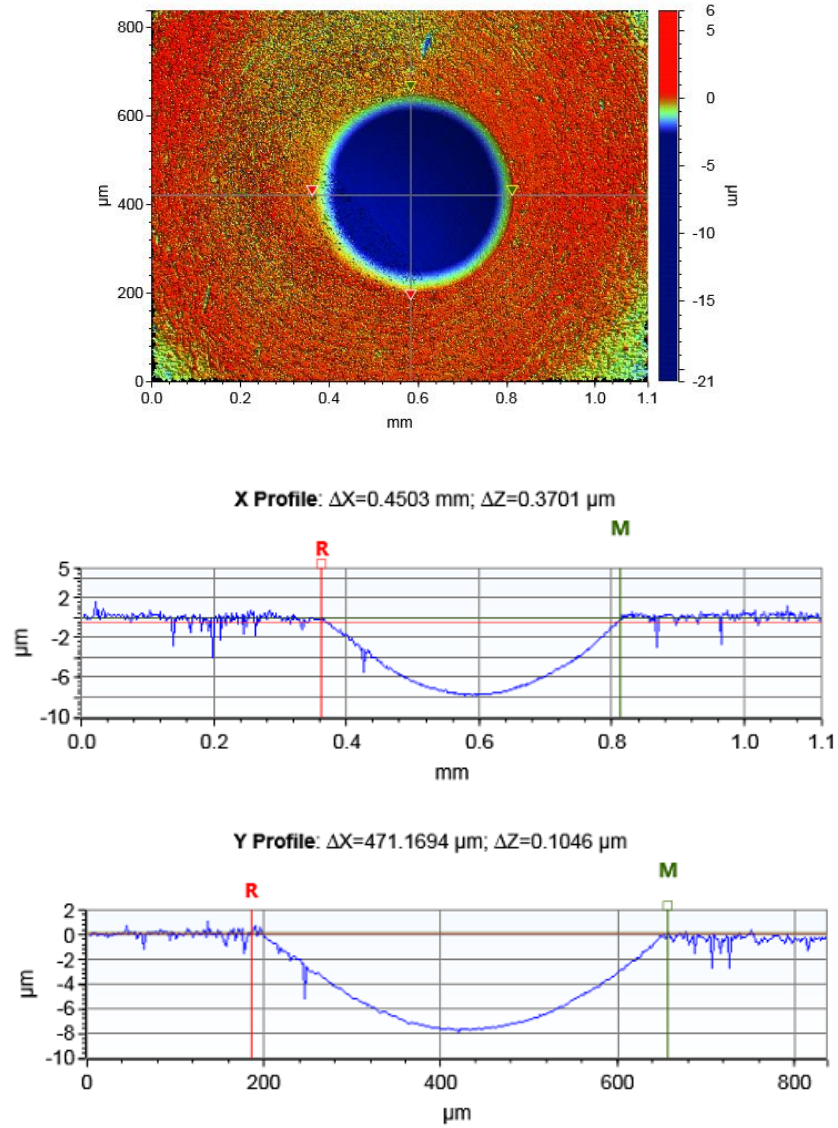


Figure 4-13. Wear measurements of the ball sample after HSPOD tests

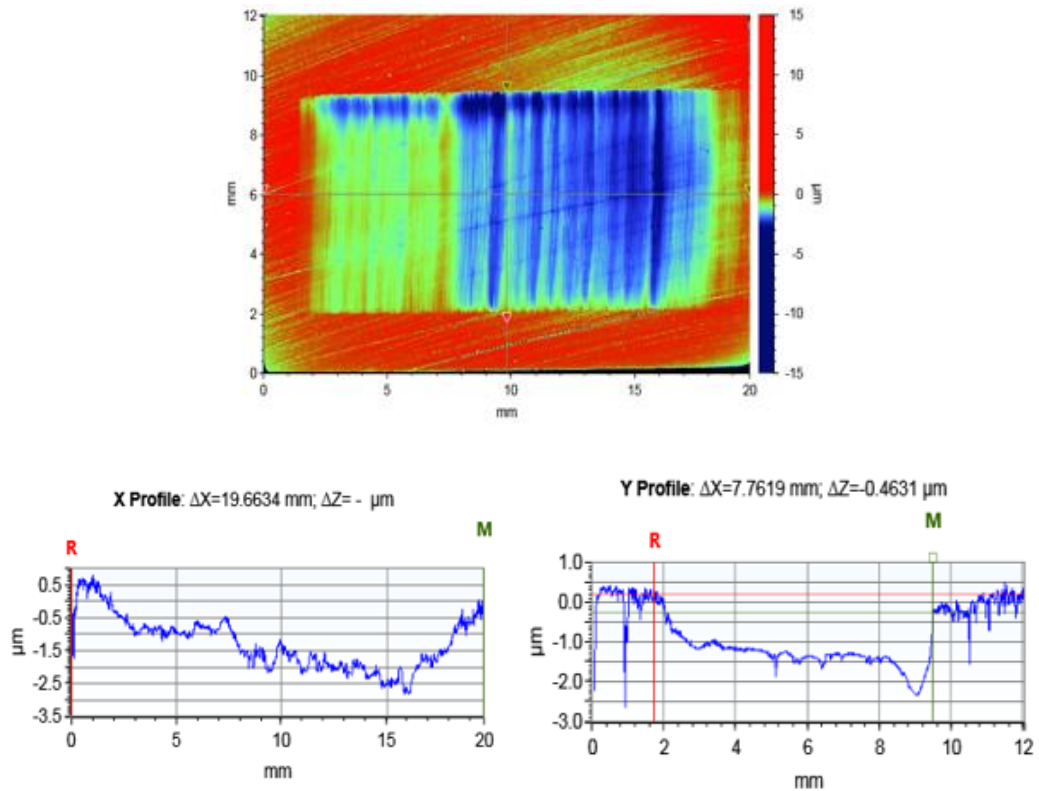


Figure 4-14. Wear measurements of the vanes after TE77 tests.

## 4.7 Scanning Electron Microscope (SEM) and Energy Dispersive X-ray analysis (EDX)

A Carl Zeiss (Oberkochen, Germany) EVO MA15 Scanning Electron Microscope (SEM) was used in this study in order to take high magnification images of the sample surfaces. This microscope was also equipped with an Oxford Instruments (Abingdon, UK) XMAX Energy Dispersive X-Ray (EDX) spectrometer to enable chemical analysis of the tribofilm. SEM images and EDX spectra were recorded at both 20 keV and 10 keV incident beam energy.

SEM produces high resolution images by scanning a focused beam of high-energy electrons at the surface of a sample. Electrons are then emitted from surface and can be detected to produce very high-resolution images of the sample surface. During EDX analysis, the sample is bombarded with a high-

energy electron beam inside the scanning electron microscope. X-rays are then emitted from the surface during electron beam bombardment. The energy of the x-rays are characteristic of different elements. As the structure of each element is unique the EDX can produce a spectrum highlighting the elemental composition of the area in question.

In this study, SEM analysis was utilised to investigate the wear mechanism on the components of VDVP after failure. This technique was also used to determine wear mechanism after tribotests. EDX analysis was utilised to investigate the surface chemistry of a specimen after experiments. Both EDX spot and EDX mapping modes were conducted to provide information about the chemical composition of tribofilm within the wear scars.

#### **4.8 Raman spectroscopy**

Raman analysis in this study was carried out using a Renishaw InVia spectrometer (UK). This Raman spectrometer is equipped with two lasers; 488 nm and 785 nm wavelength lasers operating at a maximum laser power of 10 mW and 220 mW at the source, respectively. The spectra reported in this study were obtained with 488 nm wavelength laser at room temperature, with the exception where laser 785 nm wavelength was used to analyse the diesel fuel. The Raman equipment has 5x, 20x and 50x short distance objectives and 50x long distance objective. Samples were placed on the stage and analysed with lasers focused through the objective lenses. The Raman equipment was connected to a PC which is used to collect spectral data during the analysis. Samples on the stage can be viewed through the eye piece or on the PC. In this study, spectra were obtained using the single spot analysis option. To check for uniformity in chemical composition, different regions of the sample were analysed. All spectra were obtained at the room temperature.



## **4.9 Bulk oil analysis**

### **4.9.1 Viscosity measurement**

The viscosity of the oils were measured by a test kit applying ASTM D7042 standard which covers the measurement of both the density ( $\rho$ ) and the dynamic viscosity ( $\eta$ ) of the oil. The kinematic viscosity ( $\nu$ ) can be obtained by dividing the dynamic viscosity by the density at the test temperature. In this study, viscosities of the oil samples were measured after adding contaminants and following the ageing procedure in order to compare the change in viscosity and the influence of this change on wear. The accuracy of this method is approximately  $\pm 0.1\%$  of the measurement value.

### **4.9.2 Attenuated Total Reflectance/ Fourier Transform InfraRed spectroscopy (ATR/ FTIR)**

FTIR is an analytical technique that works with the infrared region of the electromagnetic spectrum. FTIR was equipped with a horizontal Attenuated Total Reflectance (ATR) zinc selenide (ZnSe) sample cells accessory. This technique is used to identify different chemical bonds of samples from measuring the absorption of various infrared light wavelengths [166]. The sample is radiated with a broad-band source of light in the infrared region. In this study, this analysis was used to identify the chemical composition in bulk oils during the ageing process. A Perkin Elmer FT-IR spectrometer within the range of  $650\text{-}4000\text{ cm}^{-1}$  was used and the resolution of collected spectra was  $4\text{ cm}^{-1}$ .

### **4.9.3 Inductively Coupled Plasma spectroscopy (ICP)**

ICP is an instrumental technique capable of performing chemical assays on given samples, to within parts per trillion accuracy. Samples are usually liquids, however, some gaseous samples and solids may also be analysed using specific preparation techniques. Liquid samples are vaporised by a nebuliser forming a

fine aerosol. The aerosol is then subjected to a high-energy plasma beam, which ionises the atomic species. An ion lens focuses the charged particles onto a detector; this beam consists of species ionised in the spectrometer and species that were present as dissolved ions in the initial sample. Species are then separated based on their mass/charge ratio and directed towards the detector. Ions strike the detector causing a release of electrons. This enables quantification to be made based on the current produced when compared to a calibration curve of known standards. ICP was used in this study to measure the concentration of different chemical elements in the engine oil. Fully formulated engine oil consists of different additives such as extreme pressure, antiwear, anti-oxidants and additives containing different metallic elements (phosphorus, zinc, etc). Additive depletion can be monitored using ICP. It is worth noting that the concentration of additive elements does not necessarily represent the existence of active chemical compounds [167]. All ICP analysis were conducted by Millers Oils, Brighthouse, UK.

#### **4.9.4 Centrifugation for particle removal**

Centrifugation was used to separate CB particles from the engine oil prior to ICP measurement. The centrifuge used was an Eppendorf 5415C with a maximum rotation speed of 14,000 rpm, giving a centripetal acceleration 15,996g. All tests were conducted at speed of 12,000 rpm.

## **Chapter 5 Initial failure analysis of the variable displacement vane pump**

### **5.1 Introduction**

This chapter investigates the potential causes of failure of a variable displacement vane pump. This pump was used in a diesel engine passenger car and failed after 54000 km. The investigation mainly includes the visual and microscopic analysis in order to determine the root cause of the problem. All visual observations are collated along with the microscopic analysis to inform the decision regarding the next phases of the study.

### **5.2 Background**

There are various modes of failure in every system. Failure analysis aims to investigate the reasons that prevent a system from performing properly. It also assists with finding the cause of the failure and the effect of that on the function of the system. Failure analysis is therefore an important aspect of design and development in the automotive and manufacturing industries [168].

Pumps play a significant role in hydraulic systems. Pump failures are rarely caused by manufacturing defects and are normally an indication of other problems in the system. Table 5-1 shows the common sources of failure of hydraulic pumps. As can be seen from this table, nearly 80% of the reported failures have been a result of inappropriate operation and maintenance [168]. Based on this information, there is a demand for improving the operation of the pump in order to reduce failure rates and increase service life.

As explained in the literature review, VDVP is an innovative type of engine oil pump, and is used in diesel engine passenger cars. This pump has a complex design and it consists of various components such as a rotor, slide ring, vane,

vane ring, shaft, spring, casting body, casting cover and so on. The failure of this pump was reported in several cases during the operation. It is vital to investigate the failure modes and take necessary measures to eliminate similar failures in future. However, this will be challenging since this failure may be associated with various factors such as material, physical and chemical characteristics of oils, roughness of the components, design and production. Approximately 85% to 95% of pump failures are attributed to the following causes:

- foaming and aeration;
- cavitation;
- contamination;
- fluid oxidation;
- over-pressurisation; and
- improper oxidation [168].

**Table 5-1. Most common source of hydraulic pump failures [168].**

Source	Failure frequency (%)
Design	2
Manufacture	6
Installation	12
Operation and maintenance	80

### 5.3 Visual inspection of worn surfaces

When confronted with a failed system, one of the first actions is to disassemble the system and observe the failed component of the pump to identify non-conformance root causes. On this basis, a visual inspection on the failed VDVP pump was undertaken and compared to a new VDVP. The purpose of the visual inspection was to gain a better understating of the pump

geometry, the contact surfaces between components, inspection of visible wear scars and comparison of the failed components with the brand new samples.

Figure 5-1 displays the VDVP and the marked points show the parts in contact. The nature of these contact surfaces has been summarised in Table 5-2.

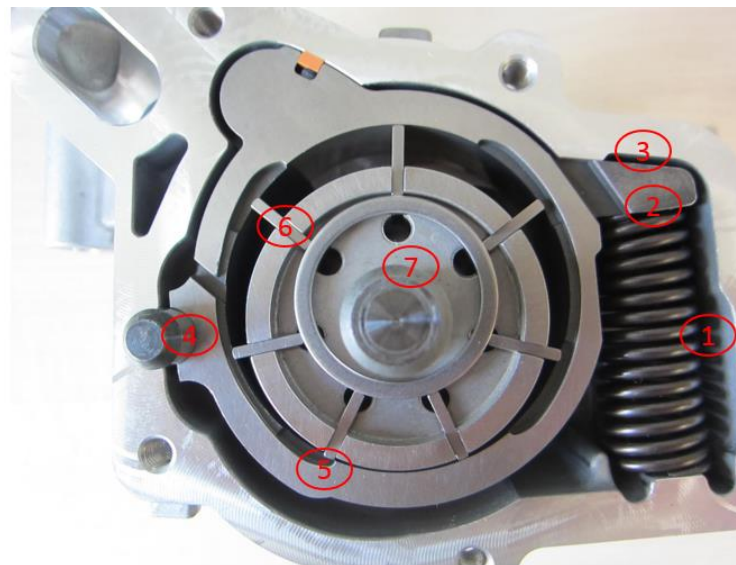
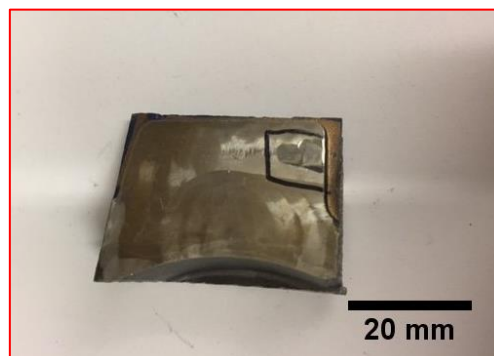


**Figure 5-1. Variable displacement vane pump- the marked contacts are explained in Table 5-2.**

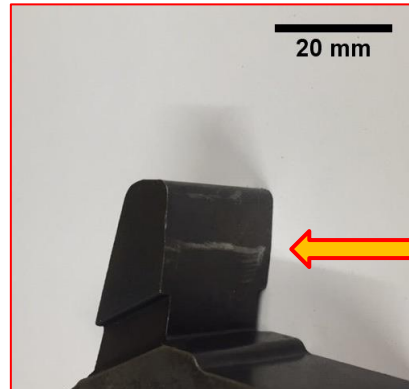
**Table 5-2. Summary of contact between different components in VDVP.**

Contact	Visual inspection of wear
---------	---------------------------

**1 Spring & casing**



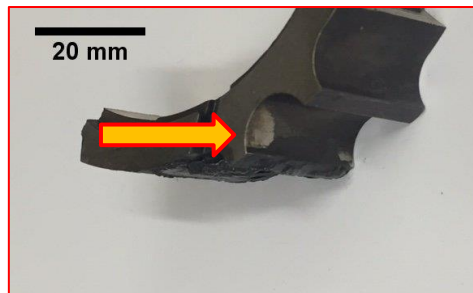
2 Spring & slide ring



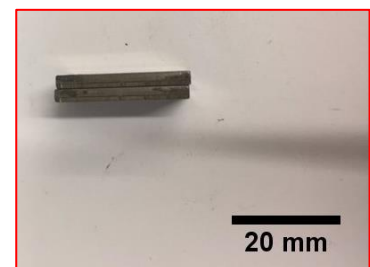
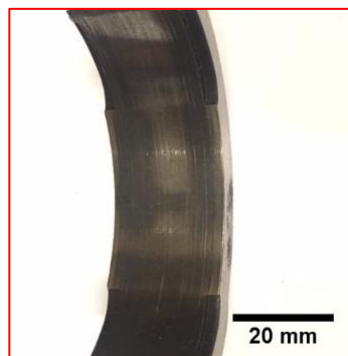
3 Slide ring & casing



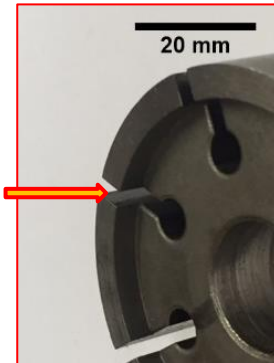
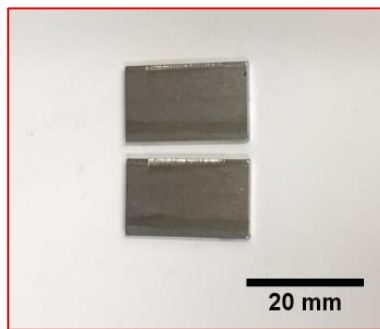
4 Slide ring & pivot pin



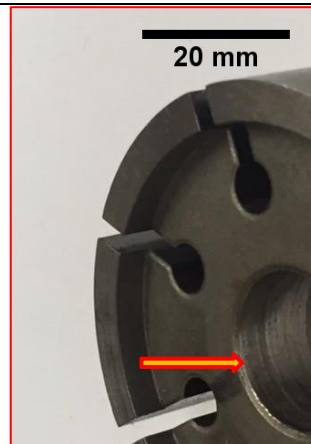
5 Slide ring & vanes



## 6 Vanes &amp; rotor



## 7 Rotor &amp; shaft



As can be seen from Table 5-2, wear was observed generally in all components of VDVP; however it was more significant in some parts such as in the slide ring, rotor and vanes.

The key issue with the failed pump appears to be a large crack within the rotor and excessive wear on the vanes and the slide ring. Figure 5-2 shows the rotor and vanes that are trapped inside the rotor slots. There may be various causes for the failure.

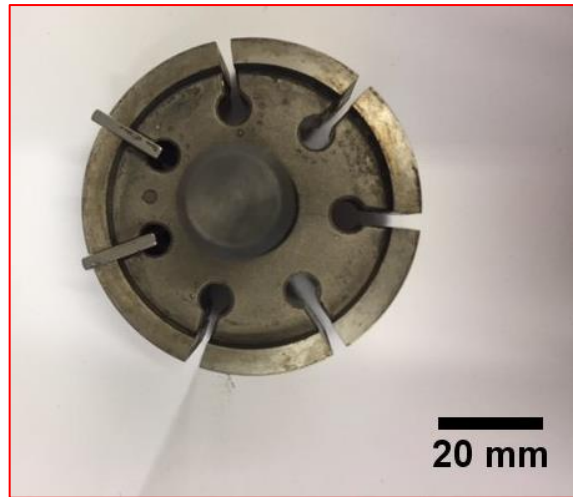


**Figure 5-2. Failure of rotor and clamped vanes in rotor slots.**

The failure of the rotor can be due to fatigue. This can be related to a weak material, torsional vibration, loading changes over time which goes above the fatigue limit (high load). Failure of the rotor due to high load can also be related to the tilt angle. For instance, the contact between the vane and rotor is designed to be a flat-on-flat reciprocating sliding contact however when the vane tilts, this contact will change to a line contact which causes a severe wear on the vane faces as shown in Figure 5-3. This causes a sudden high load on the rotor. Tilt angle also leads to high friction and severe wear on the rotor and vanes and changes the slot clearances. Based on the visual observations on vanes and rotor slots, this can be a very likely reason for the failure of VDVP.

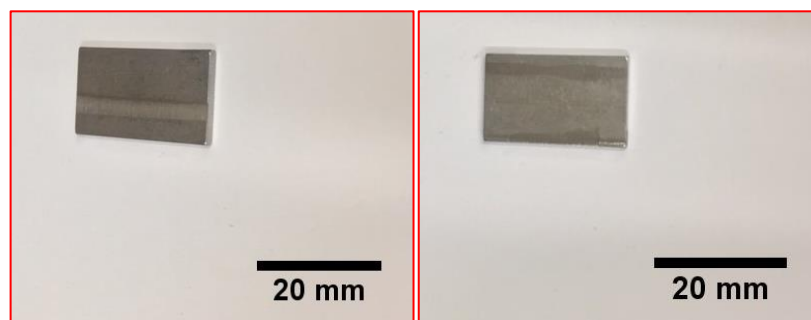


**Figure 5-3. Wear on the opposite sides of the same vane sample which is in contact with rotor.**



Another observation is the step or plastic deformation of the internal surface of the slide ring which is created by the operation of the pump (Figure 5-4). Because of this deformation the vane can get blocked on the slide ring; this would apply a sudden high load on the rotor. This may also be related to the tilt angle of vane; since the edge of the vane tip causes the step (outside the intended contact angle on tip of the vane).

Moreover, high friction forces between rotor and vane prevent the smooth motion of vane in the rotor grooves and force the vanes against the slide ring. The high force against the slide causes a step or deformation on the slide ring. This can be due to the lack of lubrication film between vane and rotor contact. In addition, the reduction in the quality of oil during the operation of the pump, due to contaminations and ageing, can cause the lack of lubricating film. Therefore, rotor and vane interactions along with oil ageing and contamination can be the root causes of this problem.

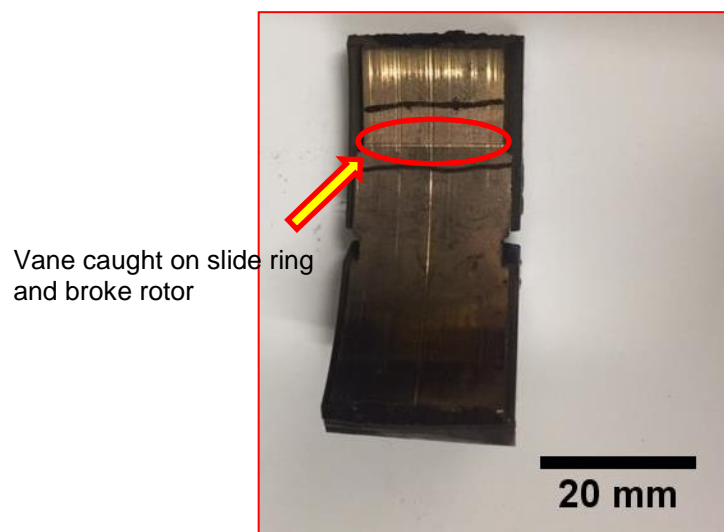


**Figure 5-4. Wear on slide ring, resulting in plastic deformation of the ring.**

In summary, the failure analysis of pump through visual inspection indicates the following:

- Medium wear on slide ring, with one notable deep scratch;
- Wear in housing caused by spring and slide ring;

- Deep wear on vanes caused by rotor;
- Deep wear on rotor slots caused by movement of vanes;
- Wear on the tip of the vanes at the contact with slide ring; and
- Visible crack across the rotor.

## **5.4 Microscopic characterisation of variable displacement vane pump**

Following visual inspection for failure analysis, the nature of the wear mechanisms in VDVP was investigated in order to perform a more detailed failure analysis. To do this, the failed pump sample was disassembled. Scanning electron microscopy (SEM) and the white light interferometer were used to inspect the wear mechanism on the surfaces.

### **5.4.1 SEM analysis**

Since the samples were contaminated by oil (slide ring is a porous material and contains oil) and SEM is sensitive to any type of liquid, some enabling works were required on the sample. The contaminated samples were left in the acetone for one day and dried out in an oven for several hours. However, these samples were not used for any tribochemical assessment, as the third particles or tribofilm formed on the samples which are important factors in this study were removed by acetone.

Microscopic analysis was conducted on the components of both failed and brand new pumps, in order to compare the structure of the surfaces. Figure 5-5 shows the structure of the new and used slide rings. In Figure 5-5(a) the porosity of the surface of the slide ring material can be observed. Although the used slide ring sample was cleaned by acetone, Figure 5-5(b) shows the dark spots remaining from the oil. Wear debris were also observed in the wear scar.

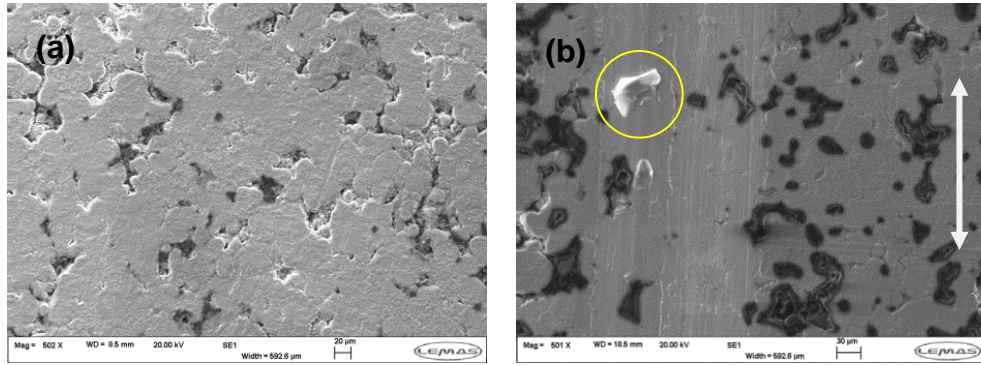
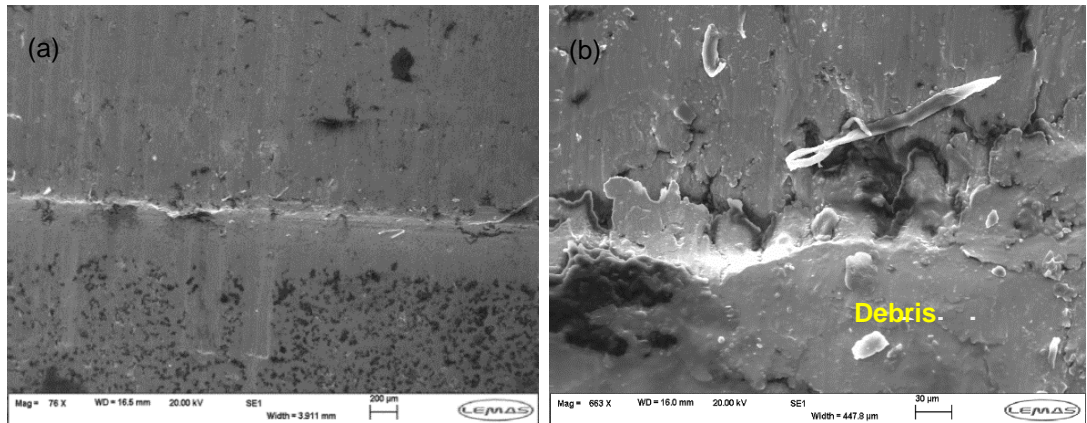


**Figure 5-5. SEM images of (a) unused slide ring (b) used slide ring in the failed pump. The wear debris is shown by circle and the arrow is demonstrating the direction of sliding.**

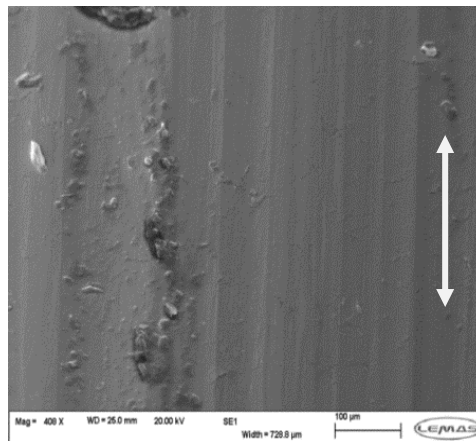
As shown in Figure 5-4, severe wear was observed on the slide ring. Figure 5-6(a) shows a plastic deformation on the slide ring. Figure 5-6(b) shows higher magnification of the same area. The results show that material has been removed from the slide ring.

Figure 5-7 also shows the typical wear scar formed all around the slide ring due to the unidirectional sliding contact between vane tip and slide ring. However, these images do not clarify whether the surface steps along the deformed length. It is important to know the exact profile of the deformation in order to determine how failure has occurred; hence contact profilometer (Talysurf) was used to plot the profile of this section.

The profilometry result (Figure 5-8) shows that the slide ring has a V-shape re-entrant deformation and surfaces around it are levelled. This suggests that vanes are hammered back to the inner surface of the slide ring during the operation of pump and create a step on the slide ring.



**Figure 5-6. SEM images of the slide ring around deformation at (a) low magnification 76x and (b) high magnification 663x showing plastic deformation of slide ring.**



**Figure 5-7. SEM image of the slide ring away from the deformation, showing a typical wear scar formed on the slide ring. Arrow shows direction of sliding.**



**Figure 5-8. Profile of step on the slide ring**

Figure 5-9 and Figure 5-10 show the SEM images of unused vane and used vane in the failed pump, respectively. Severe wear on the vane in contact with rotor groove was observed. The sign of particles, either wear debris or oil contaminants, was also seen on the wear scar as shown in Figure 5-10(b). Parallel furrows and scratches can be easily seen on the used vane and they can be related to abrasive wear. The severe wear observed on the vanes support the potential hypothesis that the vane tilts and creates a line contact with the rotor groove. In summary, the formation of grooves along the direction of the sliding implies that abrasive wear by asperities or third body particles on the pump components may be the dominant wear mechanism. Insufficient metal hardness, hard metal with rough surface against soft metal, and hard particles in oil can stimulate abrasive wear. In general, there are two types of abrasive wear, known as “two-body abrasive wear” and “three-body abrasive wear”. The two-body abrasive wear can be generated by rough surfaces acting in direction of sliding. The three-body abrasive wear can be due to the existence of hard particles in the system. In both cases, a high level of metal content in the oil can be expected. This is consistent with the results of oil analysis, discussed later in 5.7.1. It can be concluded that wear in VDVP is mostly due to the abrasion.

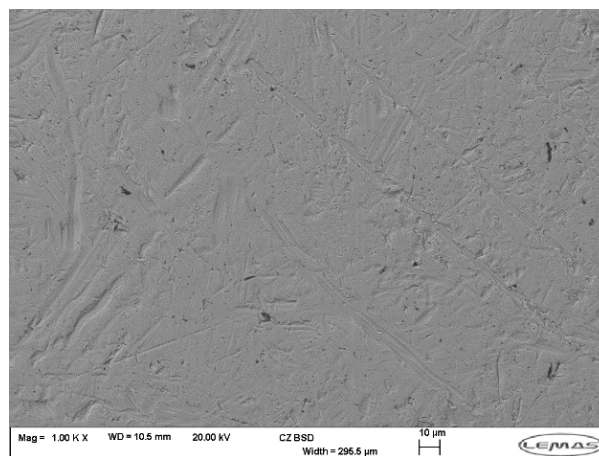


**Figure 5-9. SEM image of the unused vane, showing the surface is smooth and there is no debris on the surface**

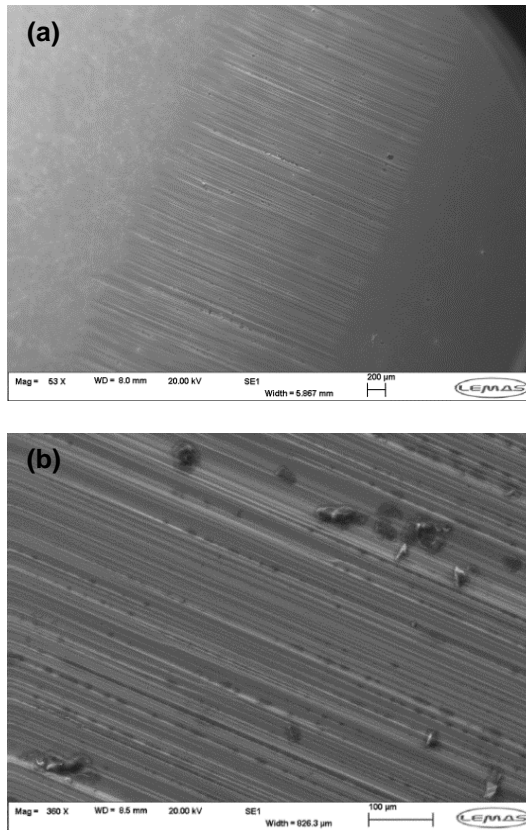


**Figure 5-10. SEM images of the vane from the failed pump (a) low magnification (b) high magnification**

## **5.5 Wear analysis**

White Light Interferometry was used to measure wear scar depth, cross sectional area and wear volume. Wear volume loss was measured for all components which had a sign of wear scar. Figure 5-11 provides an estimate of volume loss on the main components of VDVP. It was not possible to calculate the exact wear volume loss in the VDVP due to the complex geometry of the pump. However this calculation provided a better understanding about the material loss of each component. A higher level of volume loss was observed in the vanes and the rotor slots. The white light interferometer technique was conducted on the other components such as spring and casing.

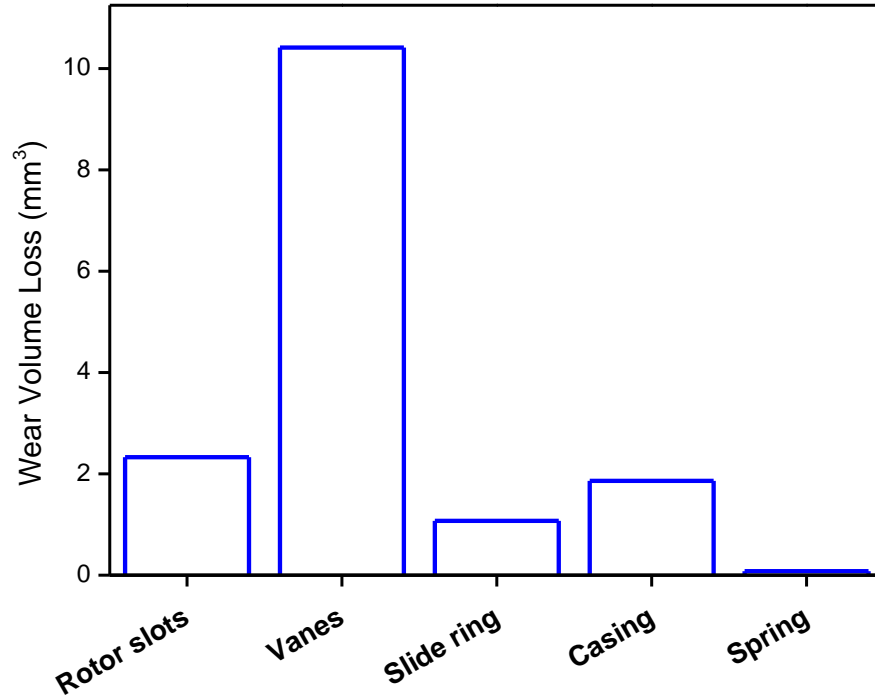


Figure 5-11. Wear volume loss on different components of a failed pump. High wear was measured on the vanes, and least amount of wear was measured on spring.

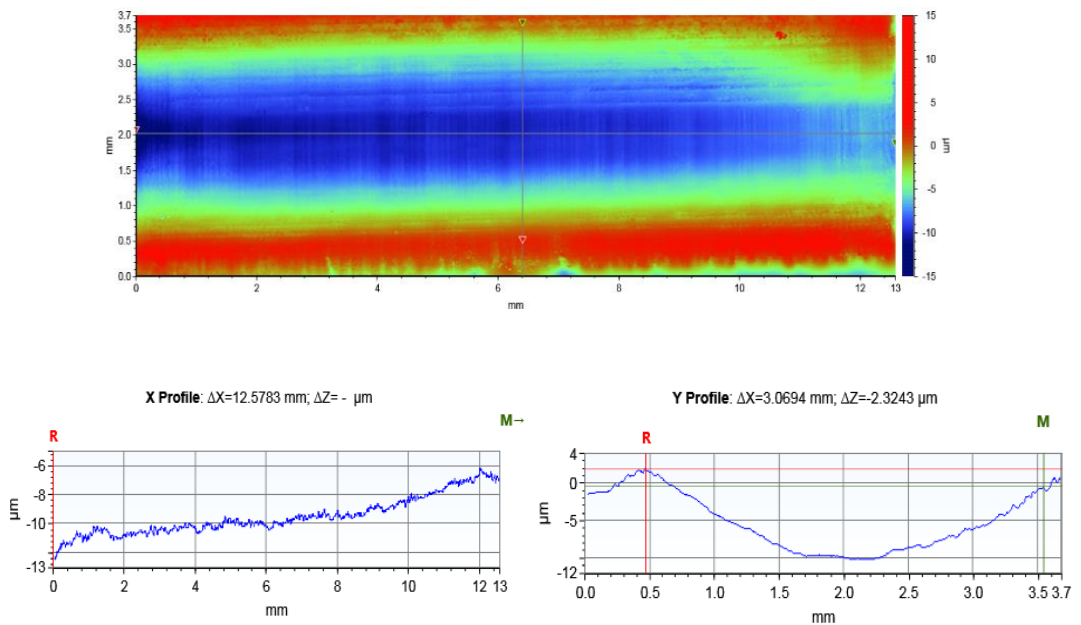
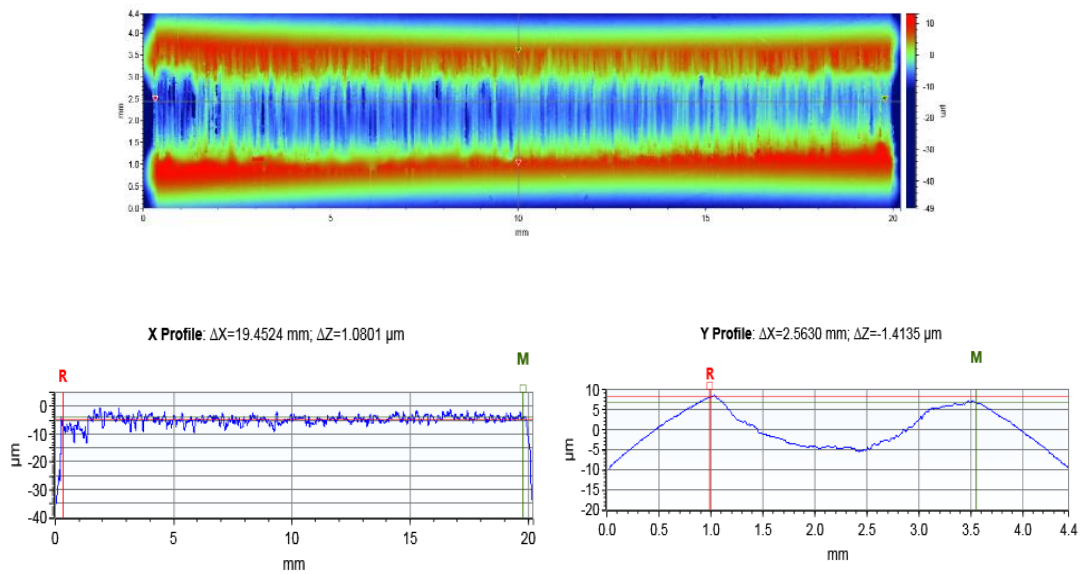
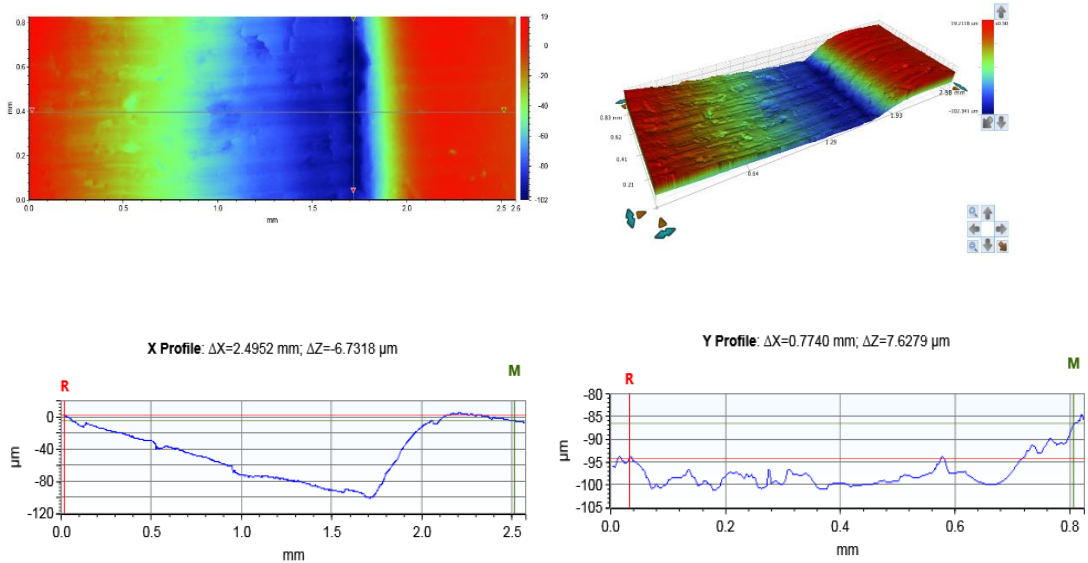


Figure 5-12. 2-D Image and X-Y profile of wear scar on the rotor groove obtained with white light interferometry.



**Figure 5-13. 2-D Image and X-Y profile of wear scar on the vane (in contact with rotor) obtained with white light interferometry.**



**Figure 5-14. Images and X-Y profile of wear and plastic deformation on slide ring, obtained with white light interferometry.**

The results of white light interferometry also reveals signs of third particles in the component of VDVP, see Figure 5-15. As aforementioned, these particles



can be either wear debris from material removal and/or oil contamination such as soot.

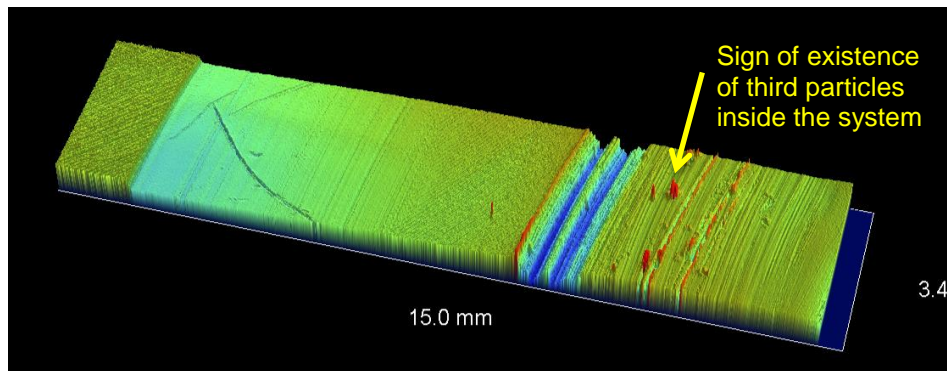


**Figure 5-15. White light interferometry image showing signs of abrasive wear on the casing of VDVP. There are also signs of existence of third particles inside the system, as shown with yellow arrow.**

## **5.6 Summary of historical tests**

In section 5.2 it was discussed that the failure of VDVP can be due to a variety of reasons. Preliminary tests were undertaken by Magna Powertrain (Ontario, Canada) to investigate the root cause of the failures and to examine the factors that had the most significant impact. All tests were conducted with the vane pump at 100 hours, pressure of 4.2 bar and speed of 3000 rpm.

### **5.6.1 Design of hydraulic pump**

As discussed earlier in this chapter, a small percentage of the failures of hydraulic pumps have been due to design issues (see Table 5-1) [168]. Magna Powertrain (Ontario, Canada) has previously explored several changes to the design parameters; such as altering vane spacing, modifying vane tip radius, changing vane ring design and increasing vane tip clearances. The proposal of change in the vane ring reduced the pump performance and caused a high wear on the rotor slot. The increase in vane tip clearances significantly increased the wear on the slide ring; it increased the distance between the

vane tips and the side rings and as a result the vanes jumped and hit the slide ring at a higher speed.

In general, the change in the design of VDVP has not shown any positive impacts on wear of the system. As mentioned previously, it is unlikely that the failure is from the design of the pump.

Apart from the design of VDVP components, Magna Powertrain (Ontario, Canada) also revisited the design loads and drive speed. However these had no significant influence on the wear on pump components. Therefore, it has been assumed that variation in pump load and drive speed does not have a substantial impact on the wear in VDVP. The main conclusions of the results from design modifications are as follows:

- Design changes on vane ring have no positive influence on wear.
- Increase in tip clearance leads to unacceptable performance reduction, and an increase in wear on the slide ring.
- Uneven vane spacing has no positive influence on wear.
- Pumps with larger slot clearances show higher wear.
- Reduction in vane tip radius results in increase of wear.
- Change in design load and drive speed does not affect the wear.

## **5.7 Material and treatment**

Material selection is an important aspect in the design of any system. As mentioned earlier, weak material can lead to fatigue failure. To achieve optimised wear, a careful attention to selection of materials will be required. As such Magna Powertrain (Ontario, Canada) has explored several material and treatments for the main component of the pump. Sintered-hardened slide ring, in conjunction with standard vanes, reduced wear on the slide ring and rotor, however had no influence on the vanes. Steam-treated rotor reduced wear of all main components. However the combination of gas nitride vane

and rotor steam treatment caused the failure after 34 hours. In addition, other changes to increase the robustness of vanes reduced wear on the vanes, but increased the wear in the rotor slot significantly.

### 5.7.1 VDVP lubrication

One source of the pump failure in VDVP is inappropriate lubrication. Most components in vane pumps are in pure sliding contact. The critical sliding contacts are the vane-slide ring and vane-rotor groove surfaces as illustrated in Figure 5-16. Anything that causes a change in these clearances (such as lubrication failure or wear) can significantly influence the pump performance [168]. Therefore, oil contamination can be an important factor in failure of VDVP that needs to be carefully considered.

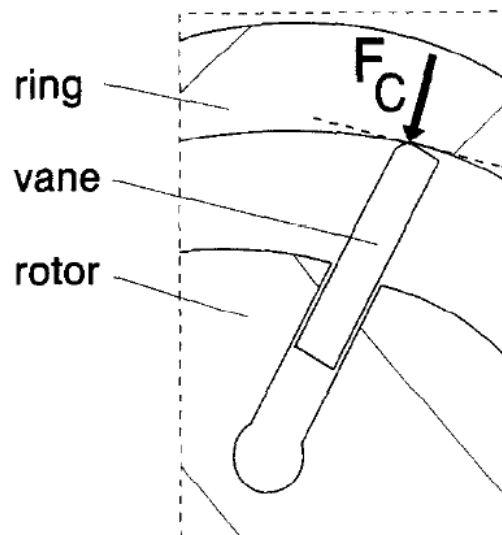


**Figure 5-16. Vane-rotor and vane-slide ring contact.**

Magna Powertrain (Ontario, Canada) has also examined the effects of different engine oils on the failure of VDVP. In order to investigate the effect of contamination, such as soot and iron, these contaminants were added to the oil. Then the results compared with the fresh oil. The results showed that the wear on the component of vane pump is strongly oil dependant, as different types of oils gave different results. It was observed that the soot

contamination is the main factor producing wear. Also, reduction of contamination lessens the wear on the vanes and rotor considerably. In addition, changing the contaminated oil to fresh oil eliminated nearly 100% of the wear on the parts. Therefore, contamination can be the main cause of wear on all parts.

From the results provided by Magna Powertrain (Ontario, Canada), it can be noted that the contamination of oil has a significant impact on the performance of the system. Therefore, oil analysis was conducted on the oil which was used in the failed pumps. The oil analysis indicated a high level of contamination such as iron (354 ppm) and aluminium (24ppm) which are from the wear of the components. Nickel and Silicon were also observed. Nickel is mostly from wear of the exhaust or the shaft. Silicon is mostly an indication of dust, but sometimes also indicates non-abrasive materials containing silicon like the assembly aids or elastic seals. Furthermore, high level of diesel fuel (6.61%) and soot (2.9%) were observed in the oil analysis. These contaminants were found to be the most dominant contaminations in the oil analysis.

## **5.8 Discussion and conclusions**

Based on the results presented in this chapter and the review of the literature presented in Chapter 3; it appears that abnormal wear and high friction forces in the failed pump prevented the smooth sliding motion of the vanes in the rotor slots. It is possible that the vanes stuck in the rotor slots as a result of high friction between surfaces. Once the vanes reached the high pressure regions (i.e. near the outlet), they were released due to higher pressure applied on the bottom of the vane. Consequently, the vanes hammered into the slide ring. This repeated hammer action created a V-shaped deformation and a very severe wear on the slide ring. This deformation could block the movement of the vanes on the slide ring, which could generate an unanticipated load on the rotor which could break the rotor. Therefore,

although wear is not deemed to be the direct cause of failure per se, it could lead to a change in the performance and ultimately failure of the system.

The oil analysis in VDVP also indicated the presence of particles in the oil. These particles could be soot and wear debris. The review of literature highlights the lack of information on the influence of oil contamination on the performance of VDVP. Therefore, the focus of this project will be on the influence of oil contamination on the component of the pump which will be discussed in the following chapters.

## Chapter 6 The effect of soot on lubrication and wear mechanisms

### 6.1 Introduction

As discussed in Chapter 3, soot is known to induce high wear in engine components. The mechanism by which soot causes high wear is not well understood. Although several mechanisms have been suggested [114, 129-132, 136, 139], there is still no consensus among scientists about this. This chapter aims to experimentally investigate the mechanism in which soot-induced wear occurs under boundary lubrication conditions using fully-formulated engine oils (FFO).

Based on the published literature, most studies have been conducted using model oils (containing one or combination of additives) rather than more realistic FFO. It is worth noting that the interaction between various additives and contaminants in FFO can result in synergistic or antagonistic effects. This can affect the tribological behaviour of contacts in a real engine. Therefore, in this study, FFO has been used to provide a more realistic condition.

In this chapter, tribological tests were conducted using the ball-on-disc tribometer under unidirectional sliding conditions. Steel samples were used in the tests to examine the wear mechanism caused by soot contamination in FFO. As mentioned in Chapter 4, carbon black (CB) particles were used to simulate soot. The variable parameters in the experiments were temperature and CB concentration. Tribological tests were conducted using 1 to 5 wt% of CB concentration at 40°C and 100°C, at the speed of 500 rpm, under 0.83 GPa pressure for two hours. These are reasonable CB levels as the level of soot in a real engine oil can vary between 1 and 8 wt% [114]. The properties of materials, geometry of samples and oil compositions used in the test were explained in detail in Chapter 4. All tests were conducted for at least two times to check repeatability.

## 6.2 Physical properties of oils

CB was mixed in FFO in an ultrasonic bath for 30 minutes prior to tests to uniformly distribute the CB particles in oil. Figure 6-1 shows the viscosity of the oils at different CB levels. Overall, the viscosity of the oils decreased with increase in temperature from ambient to 100°C, as expected. At ambient temperature (20°C), the viscosity of the oils increased by adding more CB in oil. At higher temperatures, there was a slight increase in the viscosity of the oils with increase in CB levels.

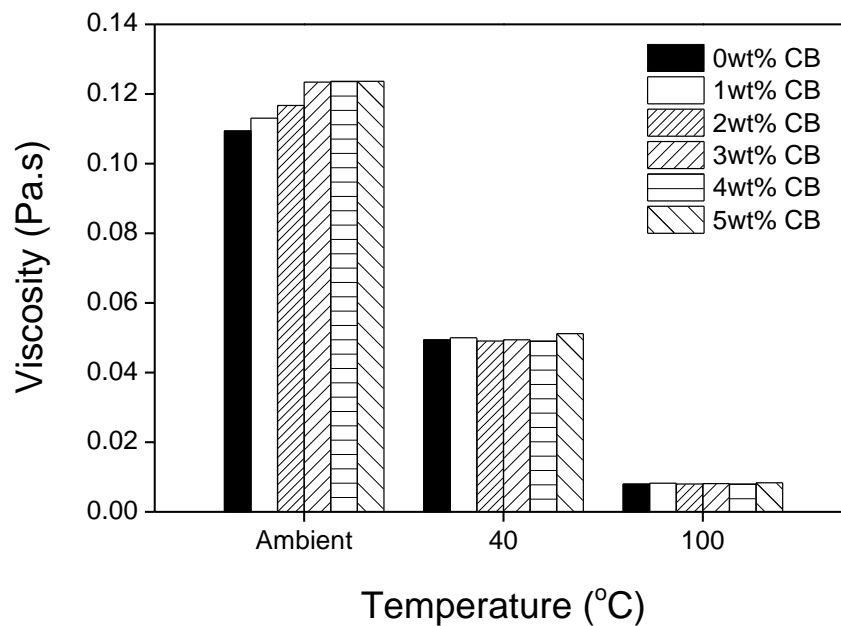


Figure 6-1. Viscosity of oils at varying CB levels as a function of temperature.

## 6.3 Calculation of lambda ratio ( $\lambda$ )

Lambda values were calculated for all oil samples containing various levels of CB at both 40°C and 100°C using Equation 2-6 and Equation 2-8. Table 6-1 shows that the initial lambda values for all samples were less than one ( $\lambda < 1$ ) at both temperatures. This indicates that all tests were started in boundary lubrication regime. The Lambda values also remained relatively unchanged

by increasing CB levels in oil at both 40°C and 100°C. It can be seen that lambda values are almost three times less at 100°C than 40°C. The lower lambda values at 100°C indicate the greater extent of surface contact and the likelihood of wear.

**Table 6-1. Lambda ratio for oils containing various levels of contamination.**

CB level in oil (wt%)	$\lambda$ at 40°C	$\lambda$ at 100°C
0	0.68	0.19
1	0.69	0.20
2	0.68	0.19
3	0.68	0.20
4	0.68	0.19
5	0.70	0.20

## 6.4 Friction results

Figure 6-2 and Figure 6-3 indicate the friction coefficient values obtained during two hours tests at varying CB levels at 40°C and 100°C respectively. In all experiments containing CB particles, the friction was high at the beginning of the tests however it decreased with rubbing time. This can be attributed to the existence of CB particles in the contact. This will be discussed in detail later in section 10.2.

The average friction coefficient values for the last 30 minutes of tests (steady-state condition) are shown in Figure 6-4. It can be seen that FFO showed the highest friction coefficient at both temperatures. There was a sharp decrease in friction, about 50%, when 1 wt% CB was added to the oil at both 40°C and 100°C. The friction further decreased when the level of CB was increased to 5 wt%.



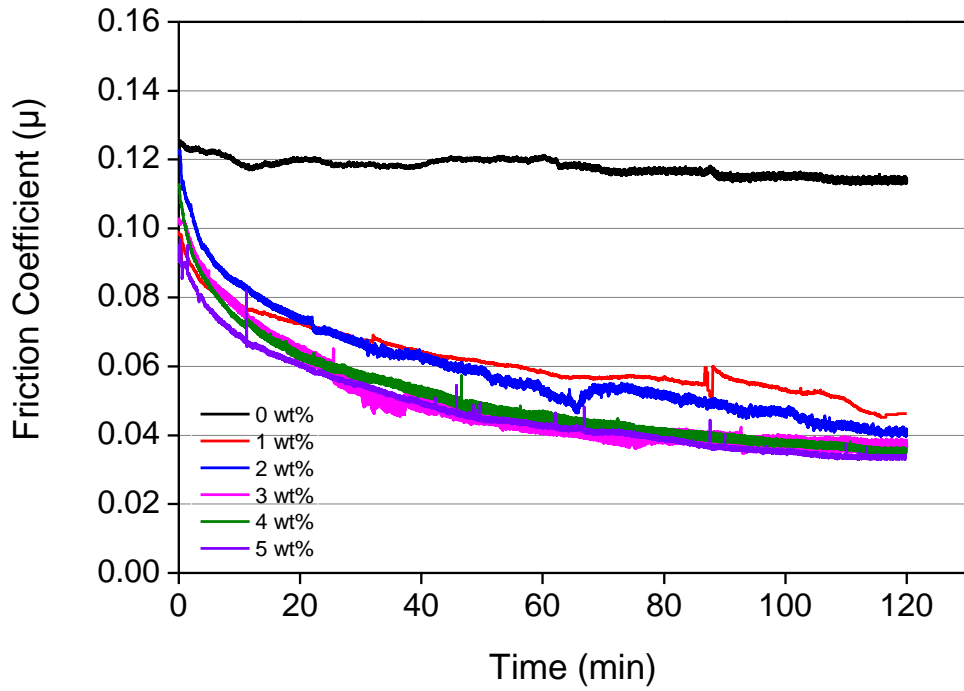


Figure 6-2. Friction coefficient as a function of time for various CB levels in FFO. Tests were conducted at 500 rpm, 0.83 GPa, 40°C.

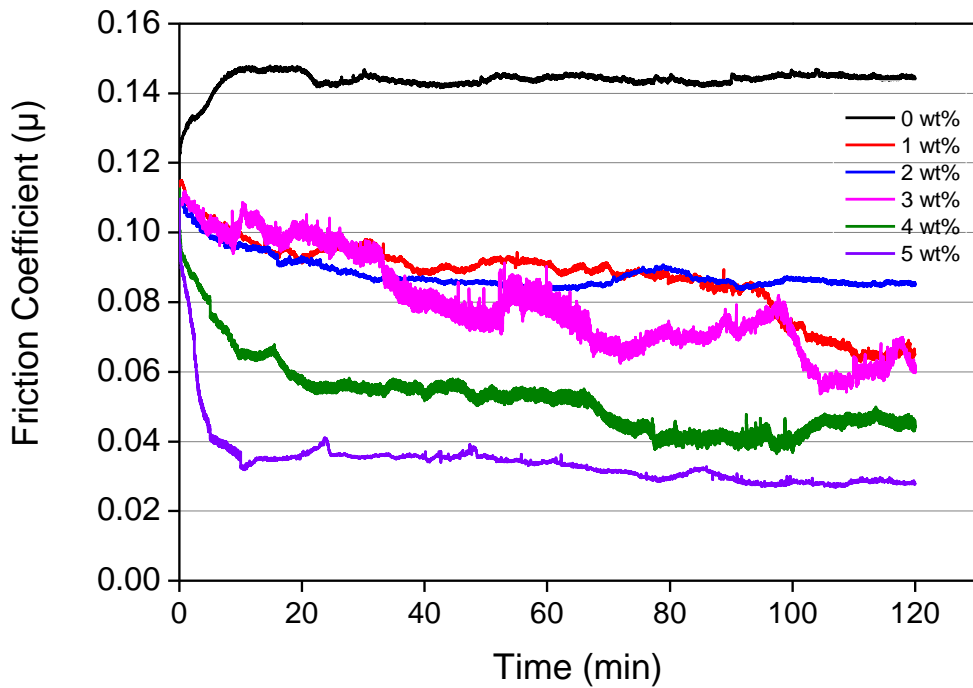
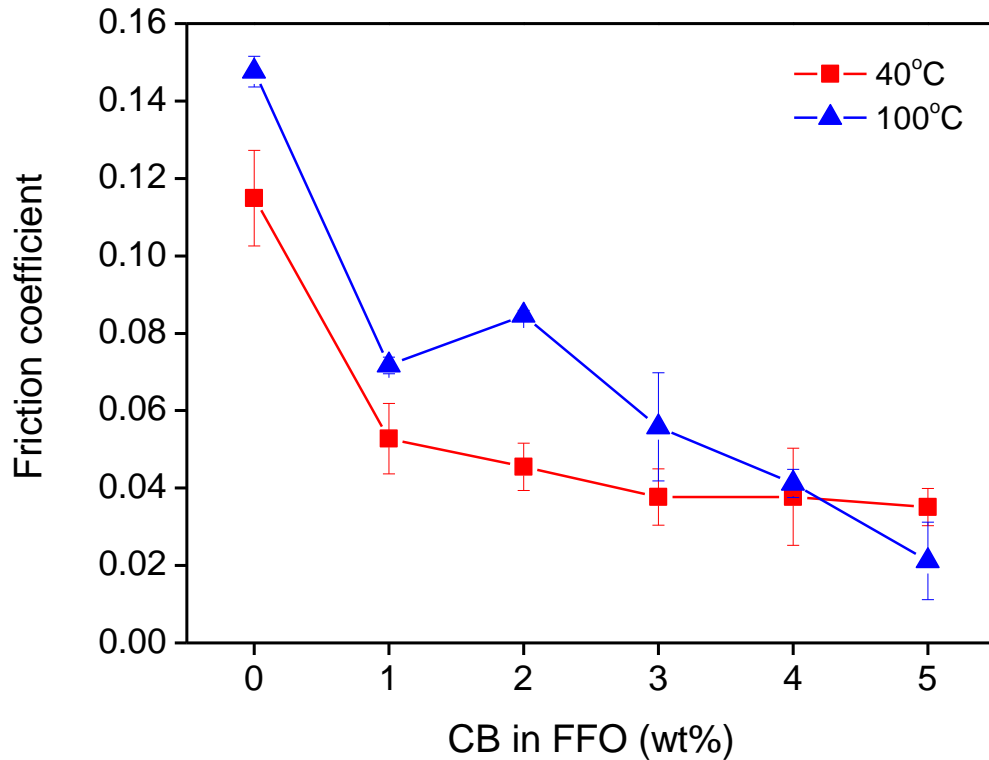


Figure 6-3. Friction coefficient as a function of time for various CB levels in FFO. Tests were conducted at 500 rpm, 0.83 GPa, 100°C.



**Figure 6-4. Friction as a function of CB content in FFO. The friction values are an average of friction coefficient during the last 30 minutes of tests. The error bars on the each points show the repeatability of tests.**

A rapid drop in friction was observed when CB was added to FFO. As mentioned in section 6.2, the viscosity of the oil did not significantly change at different CB levels at a given temperature. Thus the friction behaviour observed in FFO with the CB could not be sufficiently explained by changes in the viscosity of the oil. The friction results indicate that the presence of CB in the oil could be responsible for the low friction observed. From the wear results in Section 6.5, it is evident that reduction in friction comes at the price of high wear. This can be explained by changing the lubrication regime from boundary to mixed due to the high wear in the presence of CB.

## 6.5 Wear results

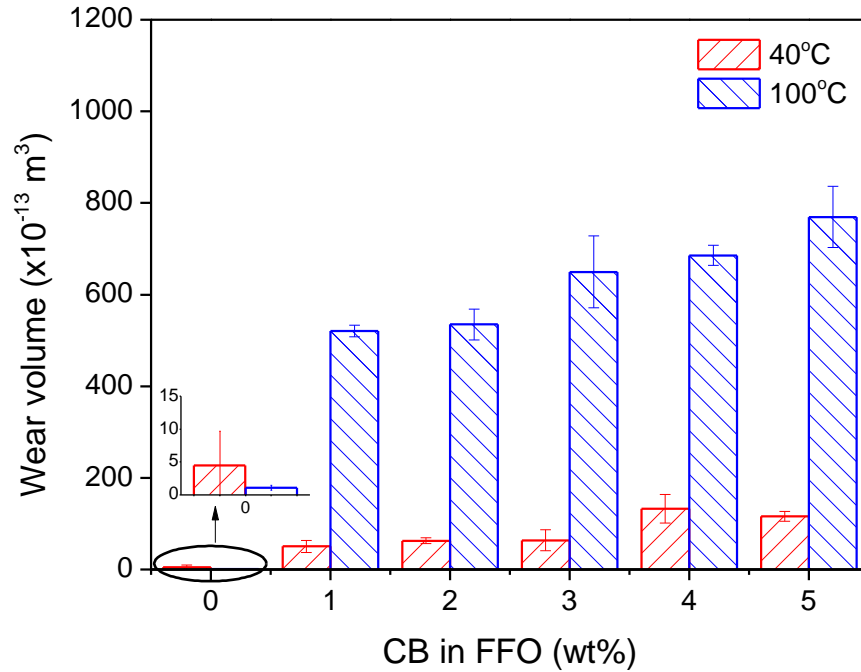
Figure 6-5 shows the wear volume loss on the ball samples after two hours of tests at 40°C and 100°C. As expected, the lowest wear occurred when no CB was present in the FFO. In tests without CB, wear was lower at 100°C than at 40°C. Since the viscosity of the FFO (without CB) was higher at 40°C than at 100°C (Figure 6-1), it is expected that the oil film thickness would be thicker at 40°C than at 100°C. Due to the thinner oil film at the higher temperature there is more asperity-to-asperity contact which would promote wear. However more wear was observed at 40°C than at 100°C despite the oil film being thicker at the lower temperature. This can be explained by formation of more effective antiwear films at higher temperatures. The formation of the antiwear films in the presence of FFO is discussed in detail in Section 6.6.

Figure 6-6 shows optical images of wear scars generated on the balls at varying CB levels and temperatures. As the initial roughness of the disc was high, it was difficult to measure wear volumes on the discs. The smallest wear scar was observed using FFO, the wear scars appeared to be covered with a brown film. At 40°C, this brown film was patchy and not covering the whole wear scar, however at 100°C the whole wear scar was covered with a dark brown film. This brown film formed on the wear scar can justify the low wear observed by FFO in Figure 6-5.

Figure 6-5 shows that the addition of CB to FFO resulted in an increase in the wear volume loss. Higher wear was observed at 100°C than at 40°C. It was also observed that the wear scar diameter increased significantly with the addition of CB in the oil (Figure 6-6). Observations from optical microscope images showed good agreement with the wear results.

At similar CB content levels, the wear scar diameters were larger at 100 °C than at 40 °C. In the presence of CB, grooves were also observed in the wear scar and there was also no sign of a brown film in the wear scar. The increase

in wear with CB level has also been reported in previous studies in tests conducted with FFO [118, 121] as well as in tests conducted with model oils containing P- and S- based antiwear and extreme pressure additives [114].



**Figure 6-5. Wear volume loss on balls at varying CB content in FFO for tests conducted at 40°C and 100°C. The error bars on the each points demonstrate the repeatability of tests.**

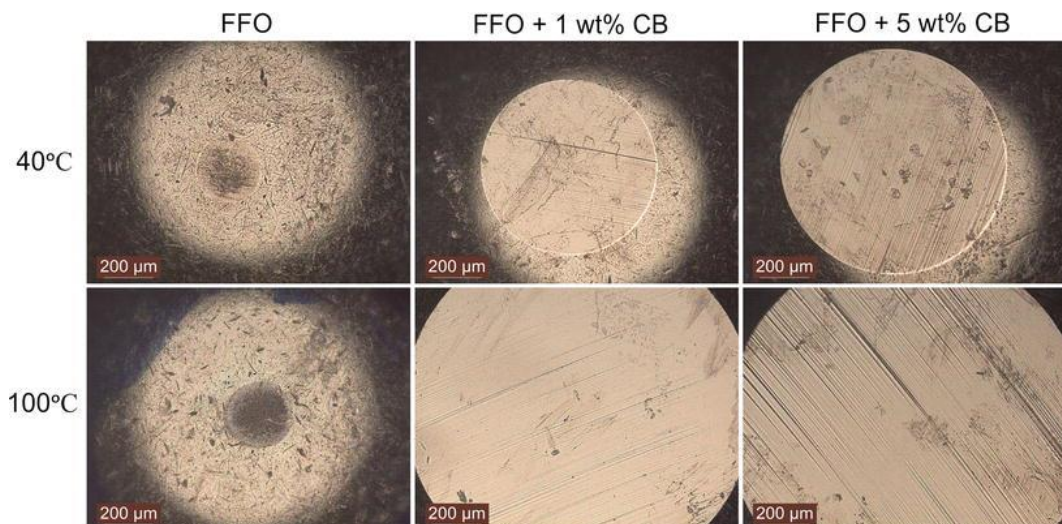


**Figure 6-6. Optical images of the wear scars formed on balls after tests with FFO, 1wt% CB and 5wt% CB at 40°C and 100°C.**

## 6.6 Surface characterisation

To verify the observations from optical images, Raman spectra and SEM-EDX were conducted at different regions within generated wear scars. Representative spectra of Raman analysis of wear scars after tests conducted with FFO are shown in Figure 6-7.

At both 40°C and 100°C it was observed that the wear scars were composed of phosphates as can be seen by the broad peak at 900-1100  $\text{cm}^{-1}$  [169]. The presence of phosphate films in the wear scars was due to decomposition of ZDDP additive which was present in the FFO. The Raman spectra show a broad peak at 200-400  $\text{cm}^{-1}$  which indicates the presence of iron sulfide (FeS) [170]. The Raman results also show a broad peak in the region of 700-800  $\text{cm}^{-1}$  and a sharp peak at 670  $\text{cm}^{-1}$  which indicate the presence of calcium hydroxide and  $\text{Fe}_3\text{O}_4$  respectively [171, 172]. Broad peaks belonging to amorphous carbon were also observed at 1373  $\text{cm}^{-1}$  and 1575  $\text{cm}^{-1}$  [161]. In previous studies, the formation of ZDDP tribofilms containing phosphate have been reported which provides wear protection [173]. In a previous study by Morina *et al.* [174], the tests were conducted with mineral oil containing only ZDDP and it was observed that wear decreased by increasing the temperature. This is in agreement with the wear results in this study where FFO has been used. This suggests that the effect of temperature on antiwear performance of ZDDP is consistent in both BO and FFO. Thus, the presence of the ZDDP tribofilms within the wear scars in the test with FFO explains the low wear observed in Figure 6-5.

The presence of Zn, P and S in the wear scars was also confirmed by SEM-EDX analysis. SEM-EDX analysis showed that the amount of Zn, P and S elements were more uniform and higher at 100°C than 40°C (see Figure 6-8). This can be related to the brown tribofilm which uniformly formed on the wear scar at 100°C as shown in Figure 6-6. Thus, it is possible that in the absence of CB, a thicker and more effective antiwear film is formed at 100°C than the

tribofilm at 40°C. This would explain the higher wear observed at 40°C than at 100°C. In tests with FFO without CB, it was observed that the wear volume loss at 40°C was almost five times higher than at 100°C.

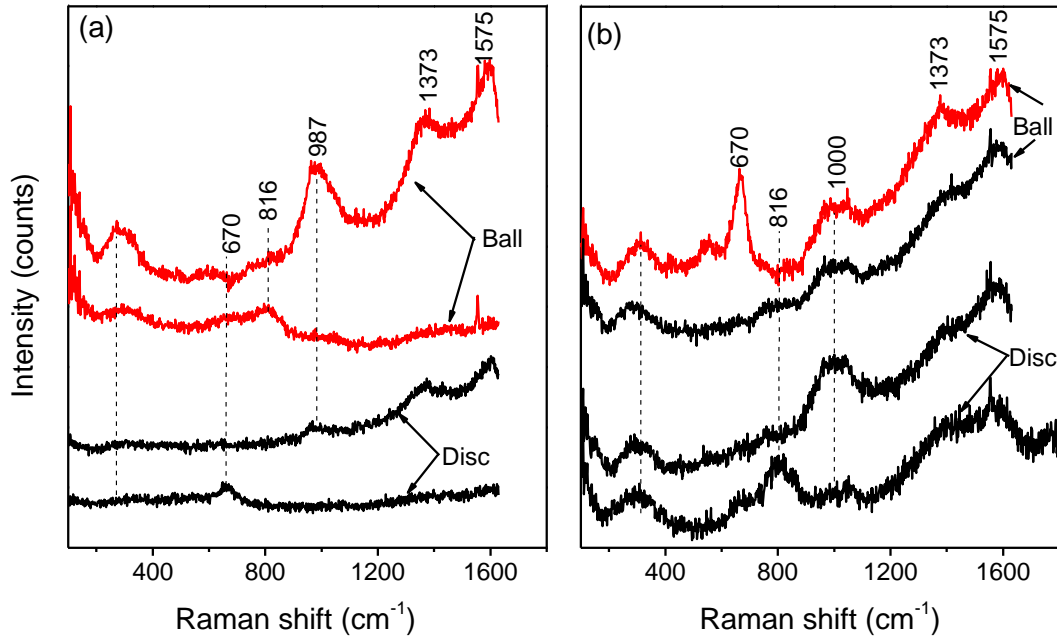


**Figure 6-7. Raman spectra obtained from different positions on tribopair samples after tests with FFO at (a) 40°C and (b) 100°C.**

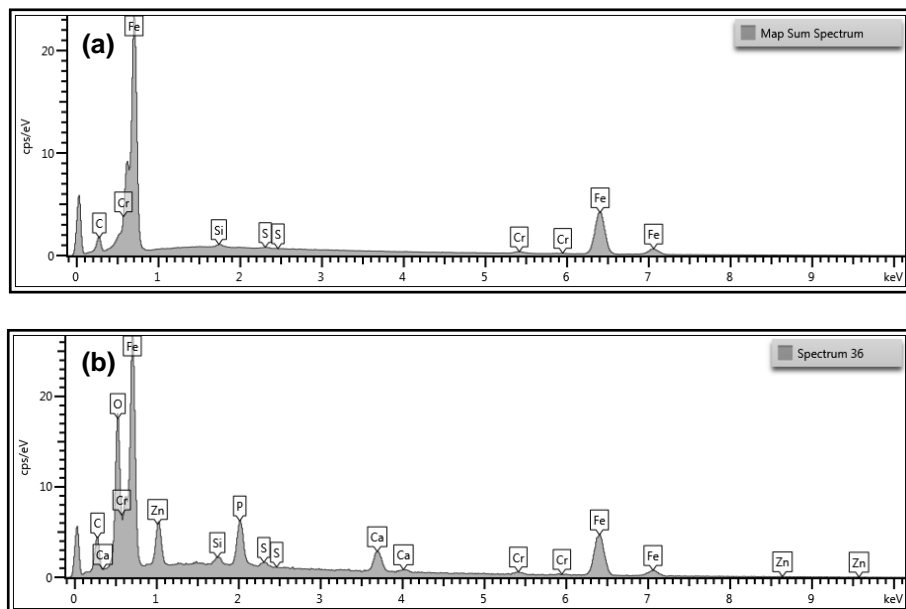


**Figure 6-8. EDX spectra obtained from wear scar formed by FFO at (a) 40°C and (b) 100°C.**

Figure 6-9 shows representative Raman spectra obtained from wear scars on ball and disc after tests with FFO containing 5 wt% CB. These spectra only showed the presence of calcium hydroxide ( $810\text{ cm}^{-1}$ ),  $\text{Fe}_3\text{O}_4$  ( $670\text{ cm}^{-1}$ ) and FeS ( $300\text{ cm}^{-1}$ ) [175]. Phosphate peaks previously observed in tests with FFO were not observed in the presence of CB particles in oil. Zn, P and S compounds were also not detected by SEM-EDX analysis (Figure 6-10). As phosphate films are well-known for their antiwear properties, the absence of the films would explain the high wear observed when CB was present. Below are the possible reasons for lack of phosphate in tribofilm in the presence of CB:

1. Phosphate films were removed by the CB as soon as they were formed.
2. The formation of phosphate films was inhibited in the first place probably due to adsorption of the additive on CB particles in the oil phase as has been previously suggested.

The possibility of these two processes occurring at the contact interface is discussed in greater detail in Section 6.7.

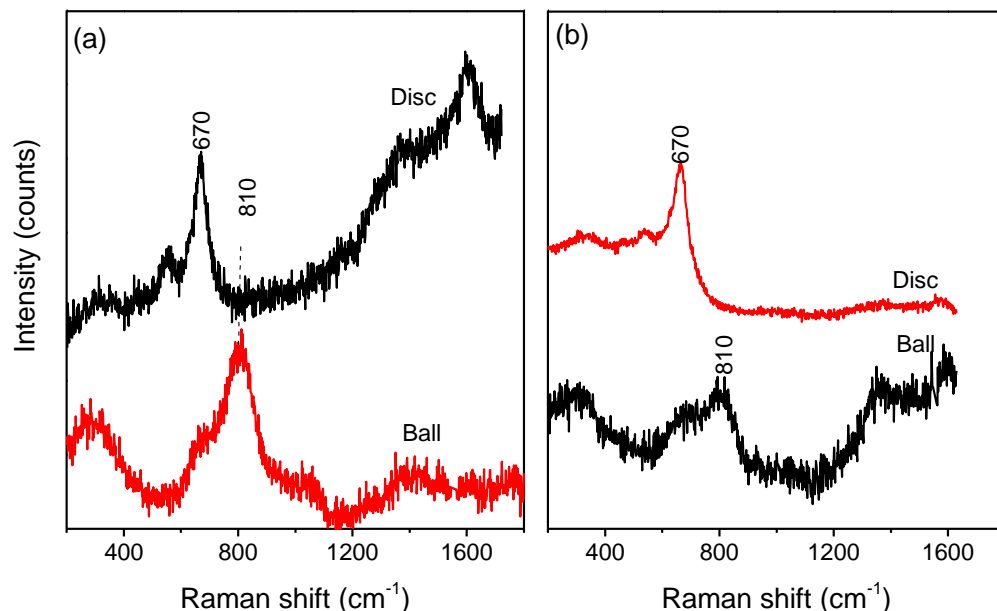


**Figure 6-9. Raman spectra of tribopair wear scars after tests with FFO containing 5 wt% CB for tests conducted at (a) 40°C and (b) 100°C.**

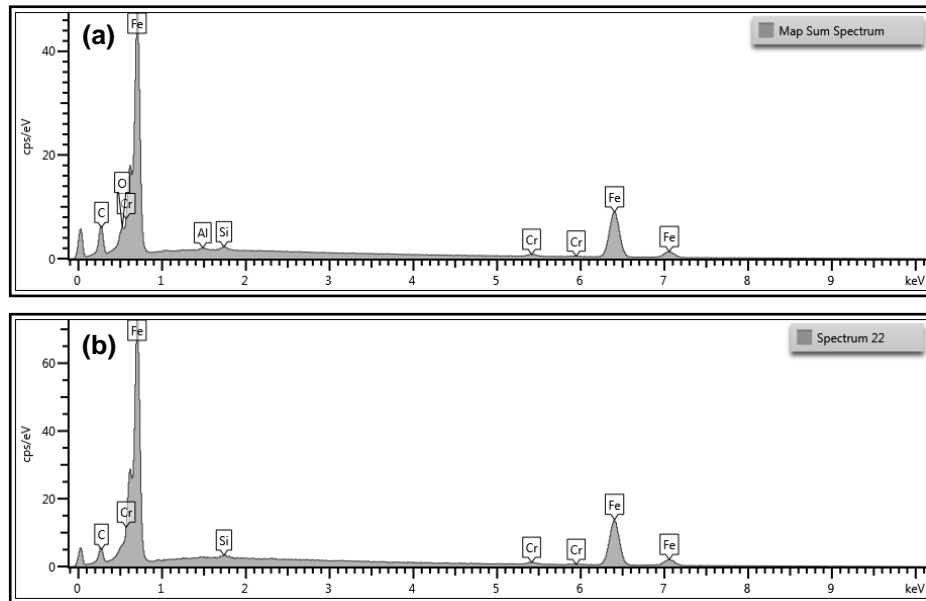


**Figure 6-10. EDX spectrum obtained from wear scar formed by FFO containing 5 wt% CB at (a) 40°C and (b) 100°C.**

## 6.7 Wear mechanism

### 6.7.1 Abrasion of antiwear tribofilms and steel substrate

To simulate the wear that would be generated on the steel substrate due to the presence of CB, tests were conducted using base oil (BO) containing CB. As the BO did not contain any additives the resulting wear would be due to abrasion by the CB particles.

Tribological tests were conducted using 5 wt% of CB concentration at 100°C, at the speed of 500 rpm, under 0.83 GPa pressure for two hours. The tests were only conducted at 100°C and 5 wt% CB since the highest wear was observed in these conditions. It should be noted that the viscosities of FFO and BO at 100°C were 0.006 and 0.003 Pa.s respectively. After adding 5 wt% CB to the oils, the viscosities of FFO and BO were 0.008 and 0.007 Pa.s respectively. Boundary lubrication regime was achieved at these test conditions.



Figure 6-11 (a) shows wear results obtained from tests with BO compared to those from FFO. In the absence of CB, the wear was higher in tests with BO than with FFO as expected since no antiwear films were formed in tests with BO. Addition of CB to the BO resulted in the wear volume loss increasing by  $179 \times 10^{-13} \text{ m}^3$ . In tests with FFO, the wear volume loss increased by  $768 \times 10^{-13} \text{ m}^3$  when CB was added. If  $179 \times 10^{-13} \text{ m}^3$  of the wear volume loss in tests with BO+CB is attributed to wear loss due to third-body abrasion by CB, there is still a large proportion of wear volume loss ( $589 \times 10^{-13} \text{ m}^3$ ) which is unexplained and unaccounted, see Figure 6-11(b).

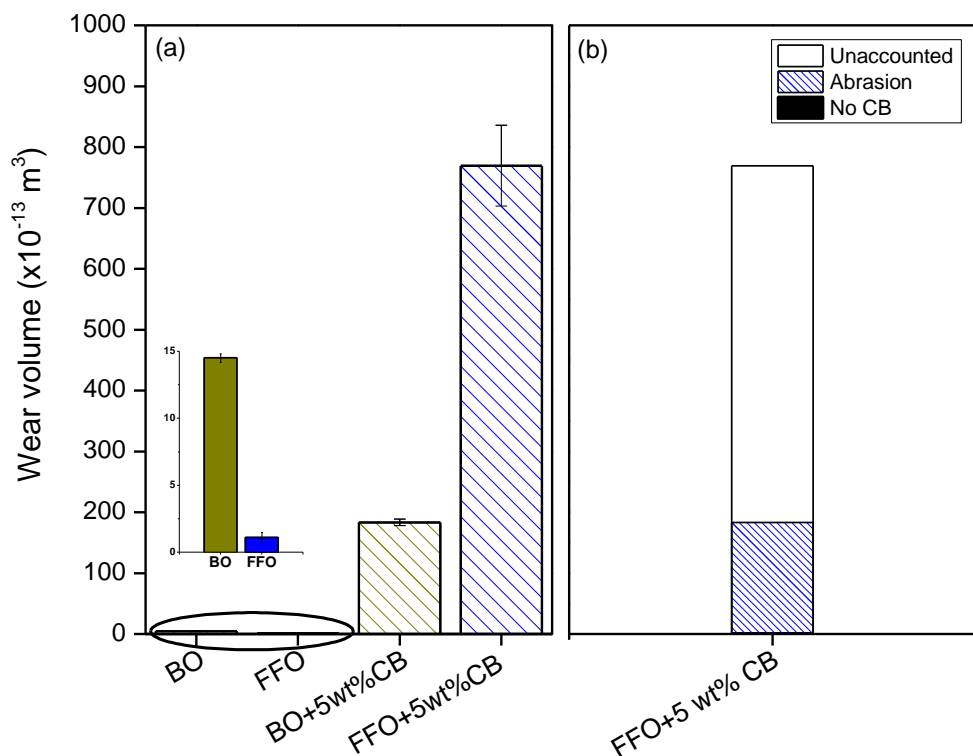


**Figure 6-11. (a) Wear results of BO and FFO with 5wt% CB (b) proportion of wear accounted by abrasion in FFO + 5wt % CB- The black bar for No CB in (b) cannot be seen in the bar chart since the wear volume is very small in comparison to the overall wear volume. All tests were conducted at 100°C for 2h.**

It should be highlighted that in the current study the BO did not contain any additives while FFO did contain additives such as dispersant, detergent, anti-

wear, friction modifier and etc. The role of dispersant additive is to keep the particles dispersed in the oil and prevent agglomeration. The BO did not have any dispersant, therefore the lower wear observed in BO+CB compared to FFO+CB can be attributed to the CB agglomeration due to lack of dispersant in BO+CB. The role of dispersant in BO containing CB is investigated in more detail in section 6.7.1.1.

### 6.7.1.1 Effect of dispersant

There are some reports [72, 114] that suggest that the presence of dispersant can affect the wear behaviour of oils containing CB. Lack of dispersant additive in BO could cause less CB particles to go through the contact, resulting in lower wear than FFO+CB [114]. Figure 6-12 shows optical images of wear scars generated on the balls with BO and FFO containing 5wt% CB at 100°C. The sign of abrasive wear can be seen on the wear scar generated with FFO+CB but not on BO+CB. This suggests that less particles might go through the contact due to CB agglomeration in BO.

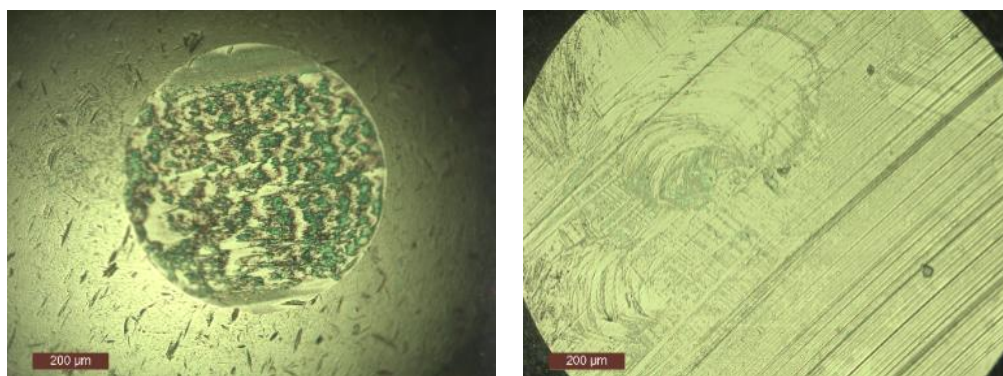


**Figure 6-12. Optical images of the wear scars formed on balls after tests with (a) BO+5wt% CB and (b) FFO+5wt% CB at 100°C.**

In order to investigate the effect of dispersant in CB-contaminated oil, tests were conducted with 2 wt% dispersant in BO containing 5wt% CB. Addition of 2 wt% dispersant in BO resulted in an increase in wear volume loss by

$345 \times 10^{-13} \text{ m}^3$ , this was a 48% increase compared to BO+5 wt% CB. These results thus show that wear increases in the presence of dispersants. However, the wear was still much lower than FFO+CB. If  $345 \times 10^{-13} \text{ m}^3$  of the wear volume loss in tests with FFO+CB is attributed to wear loss due to third-body abrasion by CB, there is still a large proportion of wear volume loss ( $423 \times 10^{-13} \text{ m}^3$ ) which remains unexplained and unaccounted, see Figure 6-13.

It is assumed that if the high wear observed in the oils containing CB was due to abrasion of the tribofilm and the steel substrate, then BO and FFO would have similar wear volume loss. However, from the results of this study, it can be seen that abrasion alone as a mechanism cannot explain the high wear observed in oils containing antiwear additives.

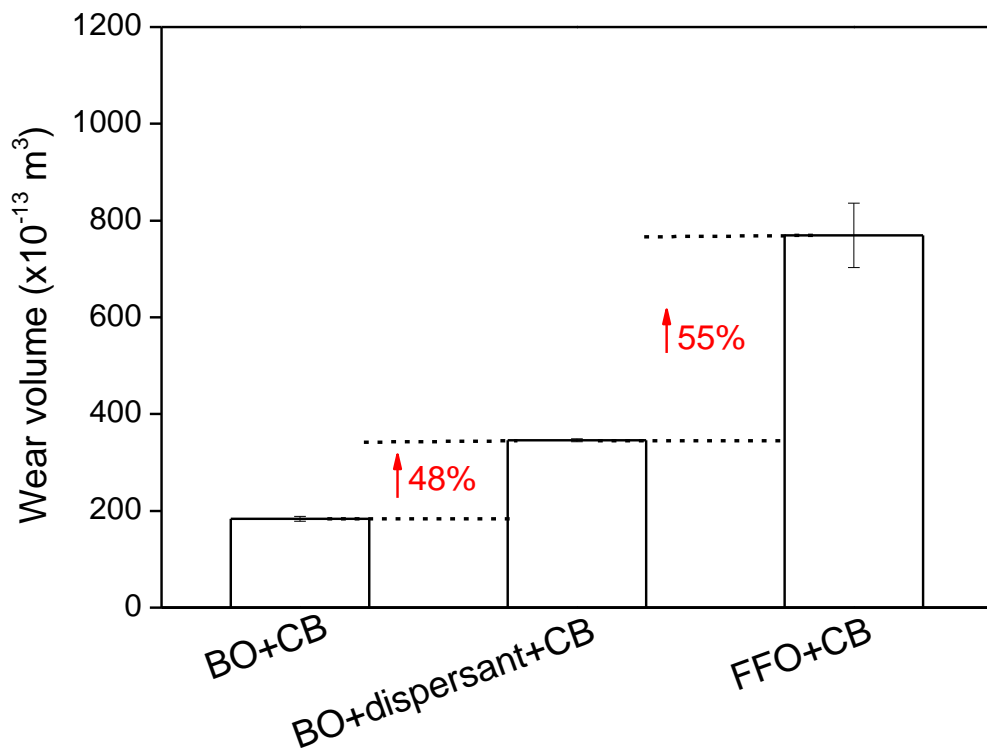


Figure 6-13. Wear results of BO and FFO with 5wt% CB.

### 6.7.2 Additive adsorption

To investigate antiwear additive adsorption on CB in FFO, 5wt% CB was added to FFO and homogeneously mixed in an ultrasonic bath for 30 minutes. The oil was then heated on a hot plate at 100°C for two hours to allow additive adsorption to take place. The heated oils were allowed to cool down before being centrifuged at 12,000 rpm for one hour to separate CB particles from the oil. The resulting oil was then used in tribological tests. The tests were conducted at 100°C for two hours. It should be noted that the results in the later chapters show that ageing the oil for 2 hours has no effect on the properties of oil, however partial ZDDP adsorption is occurred.

The heated and filtered oil sample is hereafter designated as H&F. Tests with H&F oils provide wear results after adsorption of additive due to the heating process and also eliminate the effect of abrasion wear by CB particles due to the filtering process using centrifugation. The results in the next chapter with model oil (base oil containing ZDDP and CB) showed that CB can be completely removed from the oil after centrifuging.

Figure 6-14 shows wear results after tests with the H&F oil sample compared to the FFO containing different levels of CB. It can be seen that filtering the oil reduced the wear obtained in comparison to FFO+5 wt% CB. Although lower wear was observed in the H&F sample, the wear was still much higher than that observed in FFO without CB (see Figure 6-5). The higher wear in the H&F sample can be attributed to three factors (1) reduction in ZDDP concentration due to partial additive adsorption on CB particles (2) abrasion by remaining CB particles (3) antagonistic interaction between remaining CB particles and the ZDDP additives.

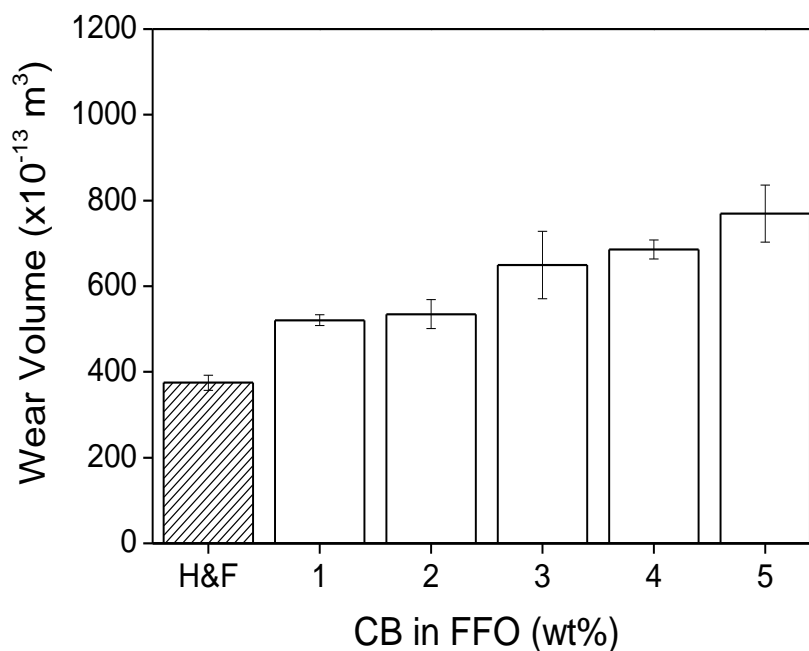


**Figure 6-14. Wear volume loss for tests conducted with H&F and FFO containing various CB levels. Tests were conducted at 100°C for 2h.**

In the H&F sample, the CB particles were removed and ZDDP was still present whereas ZDDP was not present in BO+5 wt% CB+2 wt% dispersant and the CB content was significantly higher. Despite these differences, the wear observed in the H&F sample was similar to that observed in tests with BO+5 wt% CB+2wt% dispersant (see Figure 6-13).

The high wear in BO+5 wt% CB+2 wt% dispersant can be attributed to abrasion by CB particles but similar high wear in the H&F sample cannot be justified by abrasion due to a significantly lower CB content. It is therefore unlikely that the first two factors presented above were responsible for the high wear observed in the H&F sample. Heating the oil for two hours in the presence of CB can lead to a proportion of the additives being adsorbed on CB. The remaining additives would interact negatively with CB resulting in excessive wear. Therefore, the antagonistic interaction between ZDDP and CB is the main factor that caused high wear in the H&F sample. This mechanism will be discussed in Chapter 10 in detail.

## 6.8 Summary

In this chapter, the tribological performance of steel-on-steel contact with CB- contaminated oil under boundary lubrication conditions was investigated. The following key points can be drawn from this part of the study:

- Viscosity of the oils increased by adding CB in the oils. However, this increase in viscosity became negligible as the temperature increased from 20°C to 100°C.
- The presence of CB particles in the oil reduced friction coefficient. These results indicate that CB particles in the oil were responsible for the low friction observed.
- In the tribological tests, wear increased in the existence of CB particles in the oil at both temperatures. It was also demonstrated that more CB particles in the oil result in higher wear. The effect of temperature on wear in the presence of CB particles was also significant. Wear was considerably higher at 100°C than 40°C.
- Abrasion by CB was not the dominant mechanism causing high wear. Adsorption of additives did not provide a reasonable explanation for high wear in tests with oils containing CB. Therefore, these two mechanisms by CB do not sufficiently explain high wear in oils containing CB. The results presented in this chapter provide evidence that the wear in the presence of CB cannot be simply explained by considering an abrasive mechanism, instead an interaction between the antiwear additives and CB has to be taken into account.
- These results show that the combination of additives and CB particles is responsible for the high wear observed and plays a significant role in soot-induced wear.

## Chapter 7 Antiwear additive adsorption mechanism on soot

### 7.1 Introduction

When soot enters the engine oil, the additives in the oil can adsorb onto it thereby reducing the availability of additives to form antiwear tribofilm. It has been reported [72] that no elements of tribofilm were observed in the wear scar when soot was present in the oil. The results from Chapter 6 were also in line with this finding. Additive adsorption mechanism has been stated in previous studies [127], however there has been no experimental proof on the adsorption of antiwear additive, *i.e.* ZDDP, on CB particles. In this chapter, antiwear additive adsorption on CB particles are investigated. To do this, base oil (BO) was used to exclude the effect of other additives that are present in FFO. ZDDP was added to the BO and then the mixture, which will be referred to as the model oil, was aged with CB particles. The resulting samples were analysed using ICP and FTIR analysis techniques. Finally, the CB particles were filtered out and analysed using EDX.

### 7.2 Base oil (group III mineral oil) and ZDDP additive

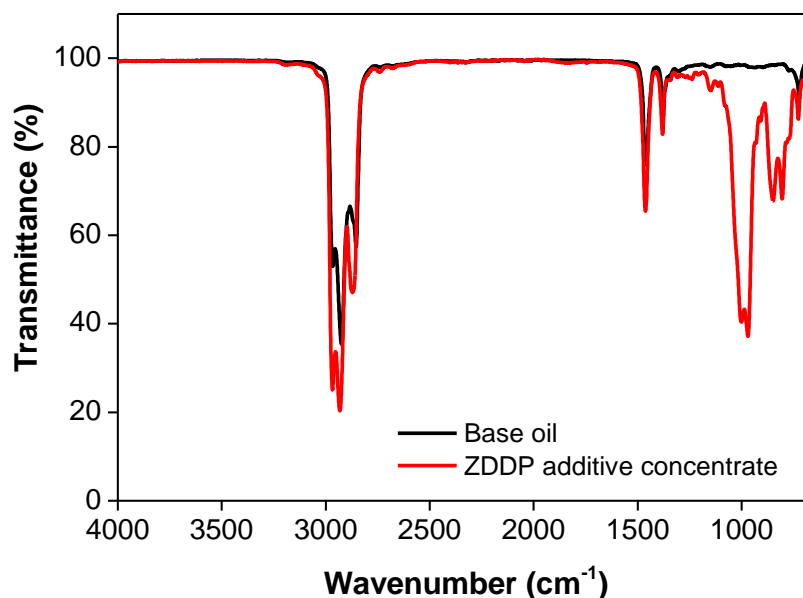
Table 7-1 shows the different levels of ZDDP concentration in the model oils used for the experiments of this study. A hot plate and a stirrer were used to mix the ZDDP additive with the BO at 60°C for 30 minutes. Some of the ZDDP concentration used in this study are higher than the standard ZDDP concentrations in FFO, however these values were only used to validate the suitability of the analysis methods used in this chapter.

Figure 7-1 shows the FTIR spectra of the BO and ZDDP used in this study. IR bands between 2850-3000  $\text{cm}^{-1}$  and 1385-1500  $\text{cm}^{-1}$  are attributed to alkyl C-H stretching and C-H bending respectively. The peak at 722  $\text{cm}^{-1}$  is also attributed to alkyl chains [176]. These three main peaks, which are from the

base stock hydrocarbons, were present in both BO and ZDDP. The peak region from 950 to 1020  $\text{cm}^{-1}$  in ZDDP is the most relevant to this study. Within this region strong bands associated with P-O-(C) vibrations in ZDDP are adsorbed [177]. This peak is the main difference between the BO and ZDDP spectra.

**Table 7-1. ZDDP concentration in base oil.**

Base oil	Mineral oil III
ZDDP concentration (wt%)	0.5,1,3 and 5



**Figure 7-1. FTIR spectra of BO and ZDDP additive concentrate.**

Figure 7-2 shows FTIR spectra of the model oils with different concentrations of ZDDP. It can be clearly seen that the P-O-(C) peak around 950-1020  $\text{cm}^{-1}$  appears by adding more concentrations of ZDDP to the BO. Figure 7-3 indicates the zinc concentration in the BO after blending process using ICP. The BO had no additives therefore all the zinc concentration came from the ZDDP additive. It can be seen that there was a linear relationship between the



added ZDDP values in the BO and zinc concentration measured by ICP. Both ICP and FTIR analyses indicated that these methods are appropriate to measure the level of ZDDP in oils. Therefore, these methods are used in this study to investigate the ZDDP adsorption on CB particles.

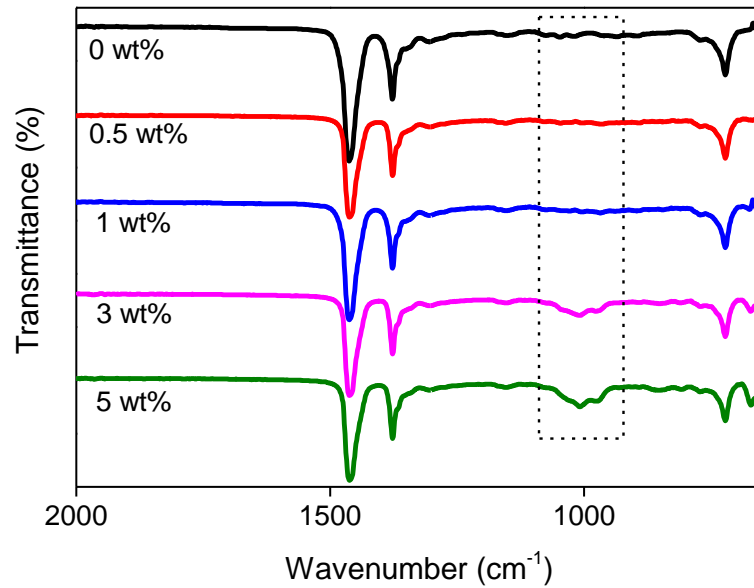


**Figure 7-2. FTIR spectra of model oils containing various concentration of ZDDP. It shows that P-O-C band appears by increasing the concentration of ZDDP in BO.**

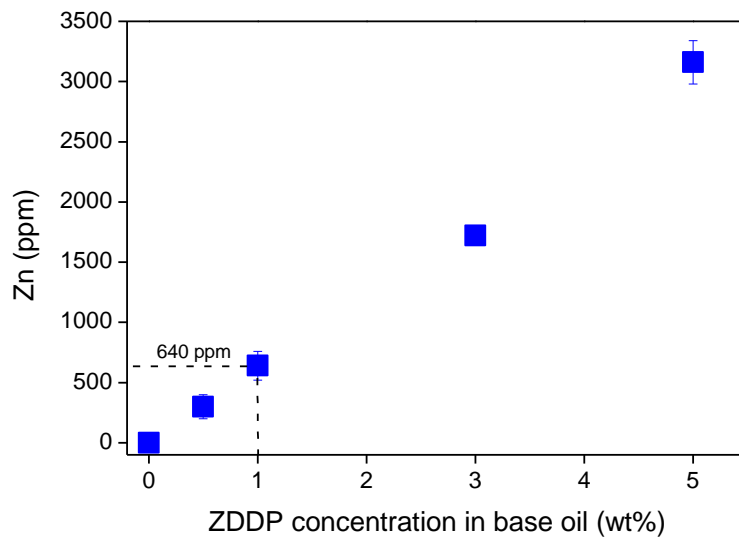


**Figure 7-3. ICP results showing zinc concentration in BO as a function of ZDDP in BO.**

### 7.3 Oil degradation in presence of CB

In this section, all experiments were conducted using 1 wt% ZDDP in BO which is a realistic ZDDP concentration in oil. Two different levels of CB, 1 wt% and 5 wt%, were added to the oil. Then, the oil samples were aged for 2 hours and 96 hours using the method explained in Chapter 4. The two-hour ageing period was chosen because the tribotests are conducted for two hours. Therefore the two-hour aged sample can indicate how much additives adsorbed on CB particles during the tribotests. The longer ageing time, 96 hours, was also selected as the standard ageing time of the oils in this study as explained in Chapter 4. The aged oil samples were centrifuged at 12,000 rpm for one hour to separate CB particles from the oil. Figure 7-4 shows the images of aged oils after removing the CB particles.

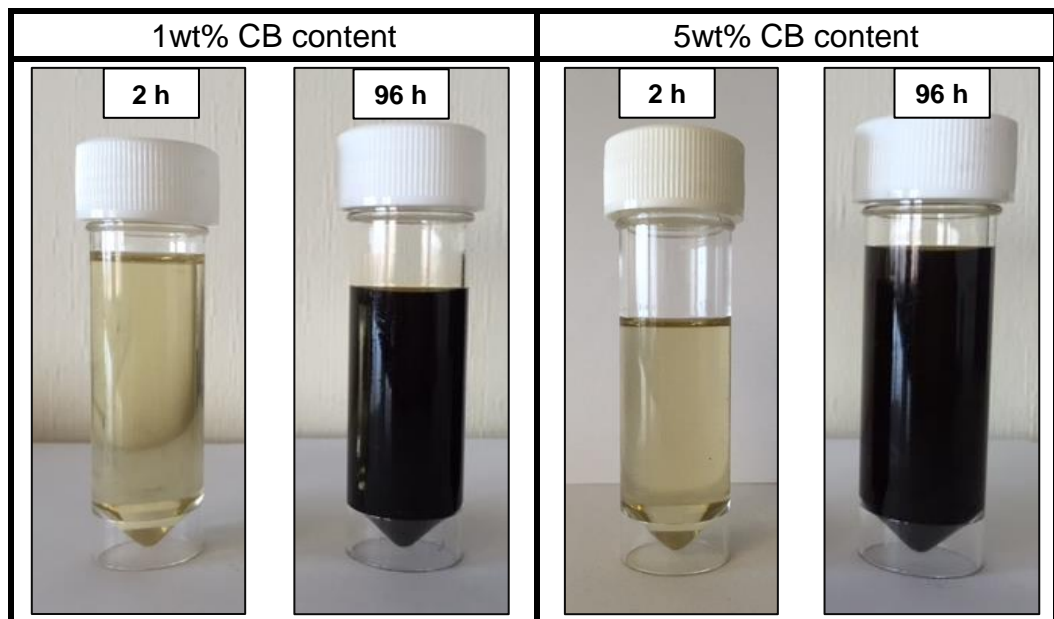


**Figure 7-4. Aged oils (BO+ 1wt% ZDDT) containing 1wt% and 5wt% CB. the oils were aged for 2 and 96 hours. The images were taken after removal of CB particles using the centrifuge.**

It can be seen that there was no CB particles left in oil samples aged for two hours after centrifuging. This can confirm that all the CB particles were

completely removed from the oil and this was an appropriate method to separate the CB particles from the oil. The dark colour of aged oil samples after 96 hours shows that the oil has experienced some level of degradation. This change in colour was not seen after two hour ageing process. Further analyses will be conducted on both oil samples and the removed CB particles are presented in section 7.4.

## **7.4 ZDDP additive adsorption during the ageing process**

### **7.4.1 FTIR analysis**

Figure 7-5 shows the FTIR spectra of aged oils (BO + 1wt% ZDDP) in the presence of 1 wt% and 5 wt% CB particles after 2 and 96 hours of ageing process. FTIR analysis was conducted to investigate the additive adsorption on CB particles in oil samples during the ageing process. It is worth noting that CB particles were removed from the oil using the centrifuge as mentioned in section 7.3. Results showed the existence of P-O-(C) peak around 950-1020  $\text{cm}^{-1}$  after 2 hours of ageing.

These results indicate that additive adsorption has partially occurred after two hours of ageing since there was still sign of ZDDP in oil. However, this peak, P- O- (C), disappeared after 96 hours of ageing regardless of CB concentration. This shows that the ZDDP additives were mostly adsorbed on CB particles after 96 hours of ageing.

As mentioned in Chapter 3 Section 3.15, the exposure of oil compounds to the high temperature and source of oxygen results in oxidation products. Figure 7-5 shows that the oxidation peak at 1720  $\text{cm}^{-1}$  appeared for 96-hour aged oil samples which indicates that the oil samples have gone through a degradation process. As observed in Figure 7-4, the colour of aged oils was also dark after 96 hours of ageing which shows the first sign of oil degradation.

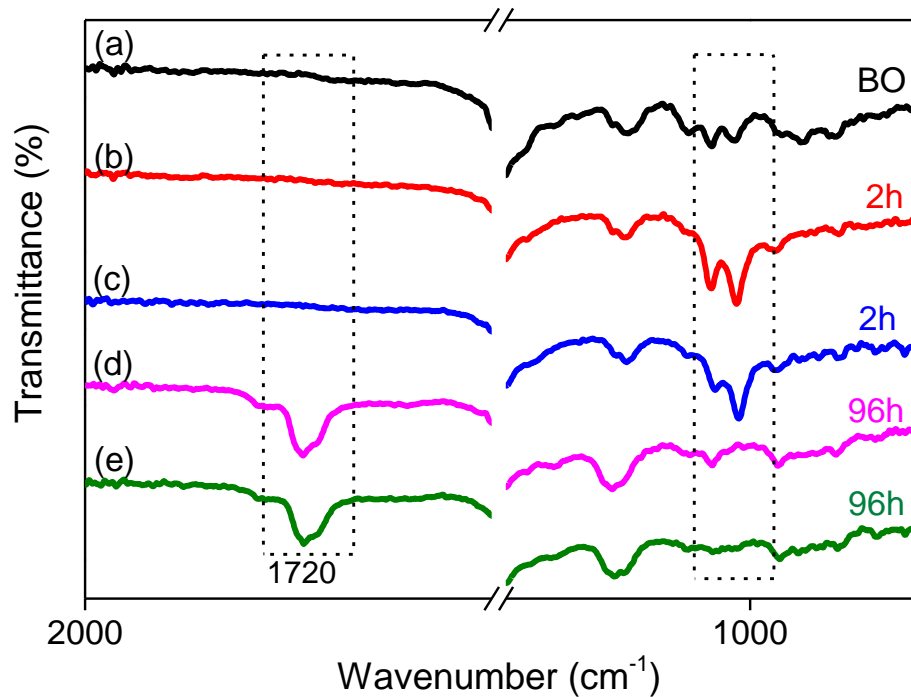


**Figure 7-5. FTIR spectra of oils after 2 h and 96 h of ageing. The oil is BO containing 1wt% ZDDP which is then mixed with 1wt% CB and 5wt% CB. FTIR spectra of (a) base oil, and aged oils containing (b) 1 wt% CB (c) 5wt% CB (d) 1wt% CB and (e) 5wt% CB.**

#### 7.4.2 ICP analysis

The aged oil samples were further analysed using ICP to investigate the zinc concentration from ZDDP additive after removing the CB particles. Figure 7-6 shows the zinc concentration in the aged oil samples in the presence of 1wt% and 5wt% CB particles. It can be seen that the fresh oil (BO +1wt% ZDDP) contained 640 ppm zinc. The aged oil with 1wt% CB particles after 2 hours of ageing showed slightly lower amount of zinc. However, adding more levels of CB particles, *i.e.* 5wt%, reduced the zinc concentration significantly by approximately 55% after two hours of ageing.

These results showed that additive adsorption partially occurred at high levels of CB, 5 wt%, after two hours of ageing. After 96 hours of ageing, no zinc remained in both samples regardless of CB concentration. These results indicate that as the ageing time increased more additives were adsorbed on the CB particles. FTIR results in section 7.4.1 showed signs of oil degradation after 96 hours of aging; therefore, the reduction in zinc concentration in Figure 7-6 can be also related to the additive depletion.

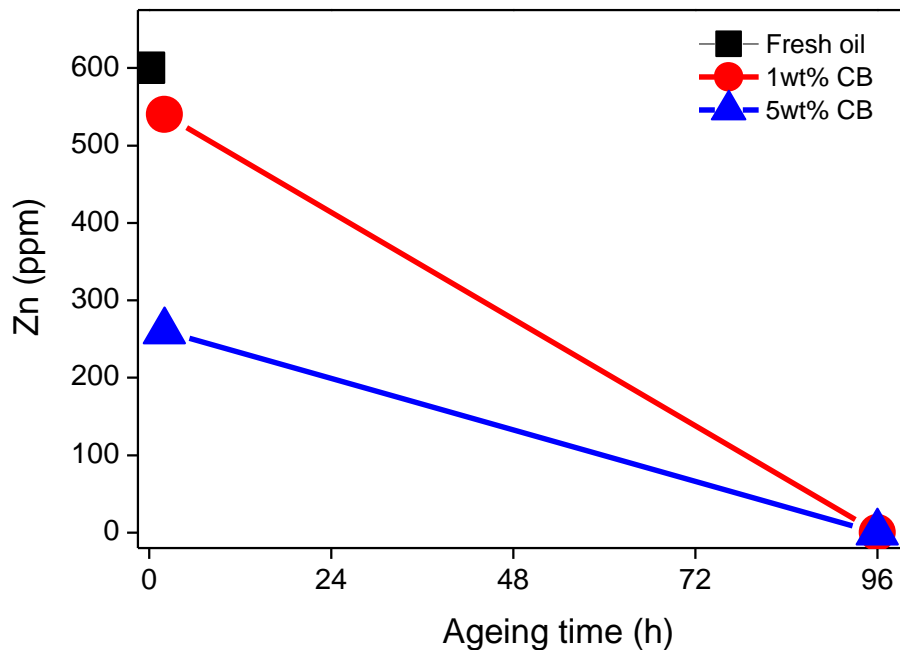


**Figure 7-6. Zinc concentration in oil (BO+1wt% ZDDP) in the presence of 1wt% and 5wt% CB particles after ageing for 2 h and 96 h using ICP. CB particles were removed from the oil samples by centrifuging before ICP analysis.**

### 7.4.3 Chemical composition of CB particles

To further investigate the additive adsorption mechanism, EDX analysis was conducted on the CB particles extracted from the aged oils. As explained in section 7.3, the aged oils were centrifuged at 12,000 rpm for one hour to separate CB particles from the oil. Then the removed CB particles were dried in an oven at 60°C to enable the EDX analysis on these particles to be

undertaken. It is worth noting that the exact values reported with EDX are not precise since these values vary from spot to spot. This technique was only used to investigate the existence of ZDDP elements in CB particles after ageing.

EDX data was also obtained from fresh (*i.e.* unused) CB Monarch 120 particles for comparison. Results of EDX spectrum showed that Monarch 120 particles were mainly composed of carbon, oxygen and a very low level of sulphur. EDX was carried out on ten different spots to check the uniformity of the compositions.

Figure 7-7 and Figure 7-8 show the EDX spectra of phosphate and zinc content in CB particles, respectively. EDX analysis on the CB particles from the aged oils revealed the presence of phosphorus and zinc which are elements of ZDDP. The presence of these elements on CB particles indicates that these elements were adsorbed on CB particles during the ageing process.

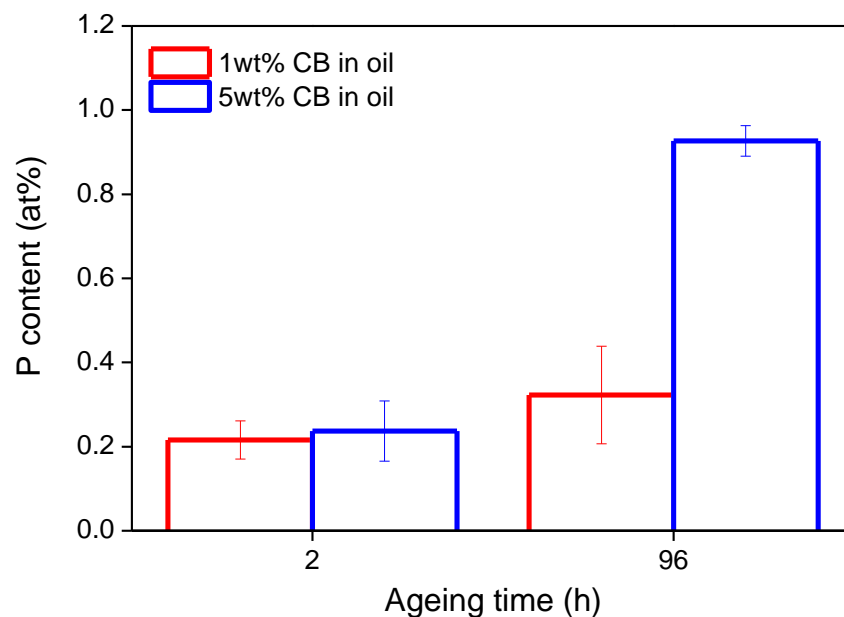


**Figure 7-7. Phosphorous content in CB particles after ageing for 2 and 96 hours**

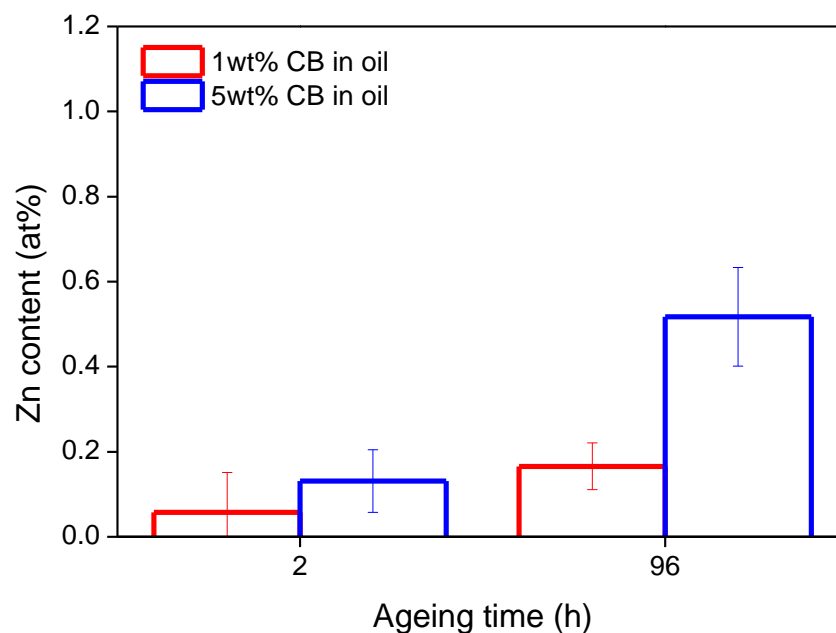


**Figure 7-8. Zinc content in CB particles after ageing for 2 and 96 hours**

## 7.5 Summary

CB particles are polar in nature and have a significant surface activity. Therefore, there is a possibility of chemical interactions between CB and oil additives [178]. The results obtained in this part of the study are in line with this statement; and as demonstrated, the additive adsorption on CB particles is one of the mechanisms occurring in the presence of CB in the oil. In summary:

- Additive adsorption of ZDDP on CB particles is dependent on test conditions such as the concentration of CB in oil and the ageing period of oil.
- Higher concentration of CB and longer ageing process increase the additive adsorption on CB particles. This can be related to the higher surface area of CB with higher levels of CB in oil which leads to more additive adsorption.

- The results from this chapter showed that the antiwear additives (ZDDP) adsorbed on CB particles and there was a chemical reaction between CB surface and additives in the oil.



## **Chapter 8 The effect of diesel contamination on tribological performance of fully formulated engine oils**

### **8.1 Introduction**

In comparison to soot, there has been less focus on the effect of diesel fuel contamination in oils. This chapter aims to investigate the effect of engine oil diluted by diesel fuel on friction and wear performance of the fully formulated engine oil (FFO) in the boundary lubrication regime. Tribological tests were conducted using ball-on-disc tribometer under unidirectional sliding conditions at 40°C and 100°C. Temperature and diesel fuel concentration were the variables of the tests. The diesel fuel dilution rates were chosen as 0, 3, 5 and 10 wt%, in order to simulate real engine conditions [106]. It is worth noting that up to 5 wt% of diesel fuel in the engine oil is considered as an acceptable level [106]. Higher levels of diesel are considered as unacceptable levels and 10 wt% is deemed as danger level [106].

In this study, in addition to the acceptable levels, 10 wt% diesel concentration was also considered as a severe condition. All tribological tests were conducted at the speed of 500 rpm, under 0.83 GPa contact pressure for two hours. All tests were conducted at least two times to check for repeatability.

### **8.2 Physical properties of oils**

Figure 8-1 shows the viscosity of oil samples diluted with various levels of diesel using a rheometer at ambient temperature, 40°C and 100°C. Diesel was dissolved in FFO with a stirrer and a hot plate for 30 minutes. An ultrasonic bath was used for 30 minutes prior to tests to ensure all oil samples were uniform.

From the results in Figure 8-1, it can be seen that viscosity of oil samples reduced by adding diesel to FFO. Higher levels of diesel in FFO reduced the viscosity further and 10 wt% diesel in FFO showed the lowest viscosity at any given temperature. The variation in viscosity of oil samples with different levels of diesel was noticeable at ambient temperature and 40°C, however this variation in viscosity became negligible at 100°C. It should be noted that the viscosity of diesel fuel was 0.004 Pa.s at room temperature. The viscosity of diesel reduced to 0.002 Pa.s and 0.001 Pa.s at 40°C and 100°C, respectively.

The viscosity of oils decreased by increasing the temperature from ambient to 100°C as expected. According to the published results [106] addition of diesel to the engine oil leads to the oil dilution which reduce viscosity and increase wear. It is worth noting that the FFO used in this study is synthetic oil and It is believed [106, 179] that synthetic oils have a better stability comparing to the mineral oil when diluted with diesel.

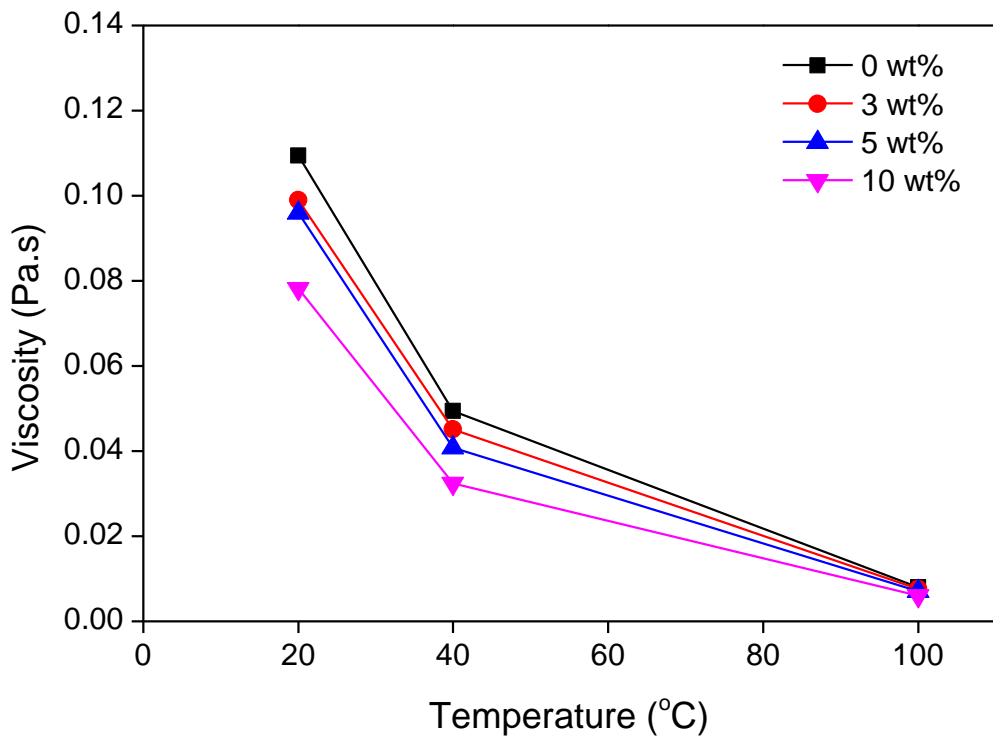


**Figure 8-1. Viscosity of oils at varying diesel levels as a function of temperature.**

### 8.3 Calculation of lambda ratio ( $\lambda$ )

Lambda values were calculated for all oil samples containing various levels of diesel fuel at both 40°C and 100°C using Equation 2-6 and Equation 2-8. Table 8-1 shows that the initial lambda values for all oil samples were less than one ( $\lambda < 1$ ) at both temperatures. This indicates that all tests were started in the boundary lubrication regime. The Lambda value decreased when more diesel was added to FFO at both temperatures. The Lambda values at 100°C were approximately one third of lambda values at 40°C. The lower lambda values at 100°C indicate that the samples experienced more severe lubrication regime at higher temperature.

**Table 8-1. Lambda ratio for oils containing various levels of diesel contamination.**

<b>Diesel in FFO (wt%)</b>	<b><math>\lambda</math> at 40°C</b>	<b><math>\lambda</math> at 100°C</b>
0	0.68	0.19
3	0.64	0.19
5	0.60	0.18
10	0.51	0.16

### 8.4 Friction results

Figure 8-2 and Figure 8-3 show the friction curves obtained during tests with different levels of diesel in FFO at 40°C and 100°C respectively. The friction coefficient was relatively stable for all oils during the two-hour tests. The tests which were conducted with fresh FFO showed the highest friction values at both temperatures. The addition of diesel contamination to FFO reduced friction. The 3 wt% diesel in oil showed the lowest friction coefficients at 40°C and 100°C. The higher concentration of diesel in the FFO increased friction further, however the friction values were still less than fresh FFO at both temperature.

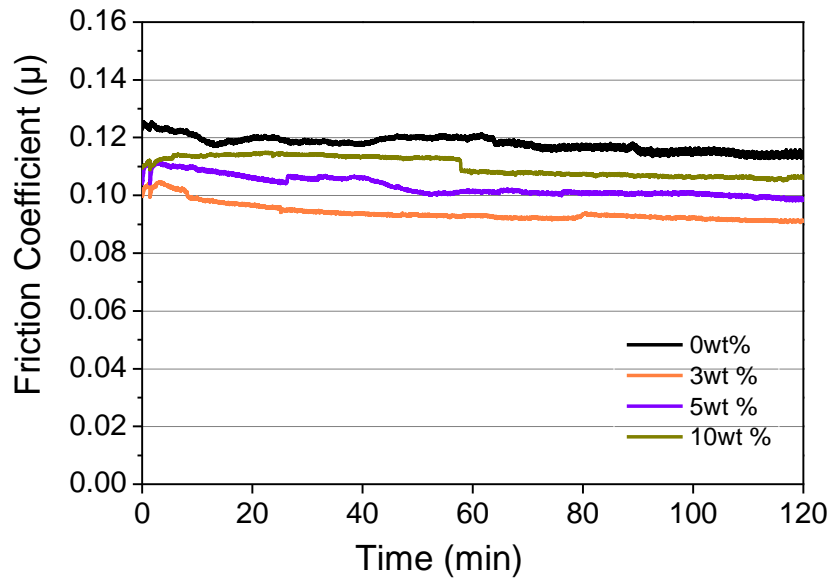


**Figure 8-2. Friction curves obtained during tests with various diesel levels in FFO. Tests were conducted at 0.83 GPa, 40°C.**

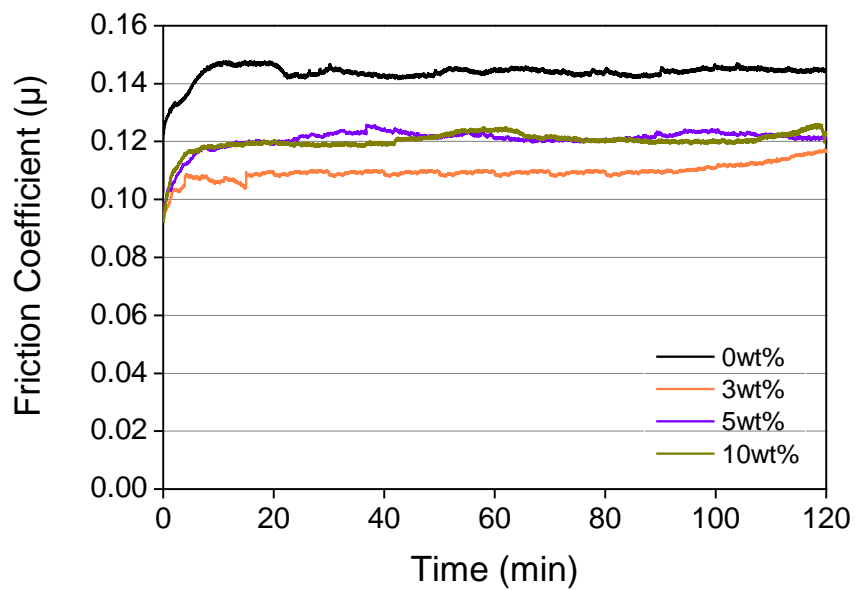


**Figure 8-3. Friction curves obtained during tests with various diesel levels in FFO. Tests were conducted at 0.83 GPa, 100°C.**

Figure 8-4 shows the average friction coefficient values for the last 30 minutes (steady-state condition) of the test with different diesel concentration at 40°C and 100°C. In general, friction coefficient at 100°C was higher than friction coefficient at 40°C. As aforementioned, the highest friction value was

observed with the uncontaminated oil at both temperatures. Dilution of the oil by diesel reduced friction at both temperatures. This reduction in friction can be attributed to the lubricity of diesel which was present in oil.

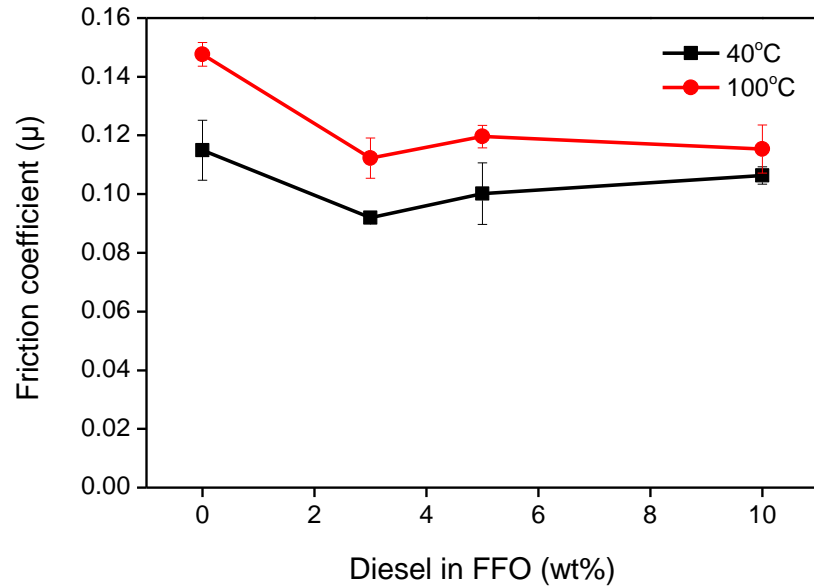


**Figure 8-4. Friction as a function of diesel content in FFO. The friction values are an average of friction coefficient during the last 30 minutes of tests. The error bars on the each points show the repeatability of tests.**

## 8.5 Wear results

Figure 8-5 shows the wear volume loss of the ball samples after two hours of tests at 40°C and 100°C. In tests without diesel, wear was lower at 100°C than at 40°C. A possible explanation for this can be the formation of more effective antiwear films at higher temperatures. The formation of the antiwear films in FFO is discussed in more detail in section Section 8.6.

One of the notable outcomes of these experiments was that diesel-contaminated oil showed lower wear values than FFO. Since the viscosity of diesel-contaminated oil was lower than FFO at any given temperature (Figure 8-1), higher wear was expected due to more asperity-to-asperity contact in the oil diluted with diesel. The results of this study are in contrast to this

assumption. The wear volume decreased by introducing diesel contamination in the FFO at 40°C. Higher levels of diesel in FFO reduced the wear further at 40°C. There was no significant difference in wear volume of samples with different level of diesel contamination at 100°C.

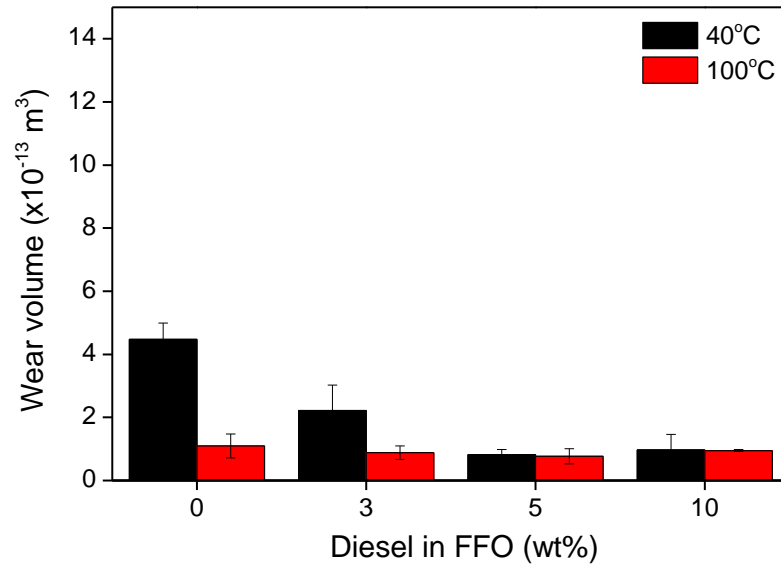


**Figure 8-5. Wear volume loss on balls at varying diesel content in FFO for tests conducted at 40°C and 100°C. The error bars on the each points show the repeatability of tests.**

Figure 8-6 shows representative optical images of the wear scars after tribological tests with FFO and 10 wt% diesel-contaminated oil at 40°C and 100°C. These images indicate that the wear scars appeared to be covered by a brown film. At 40°C, this brown film was patchy and was not covering the entire wear scars; however at 100°C the whole wear scar on the balls were completely covered with dark brown films in both FFO and diesel-contaminated oil. This can be attributed to the formation of a better tribofilm at higher temperature than lower temperatures due to additive decomposition [180]. In other words, the antiwear additives in FFO protect the rubbing surfaces at high temperature regardless of diesel content in the oil. This can justify the low wear observed at 100°C than 40°C regardless of diesel

concentration in the oil. Further investigation on this using EDX and Raman analysis will be presented in section 8.6.

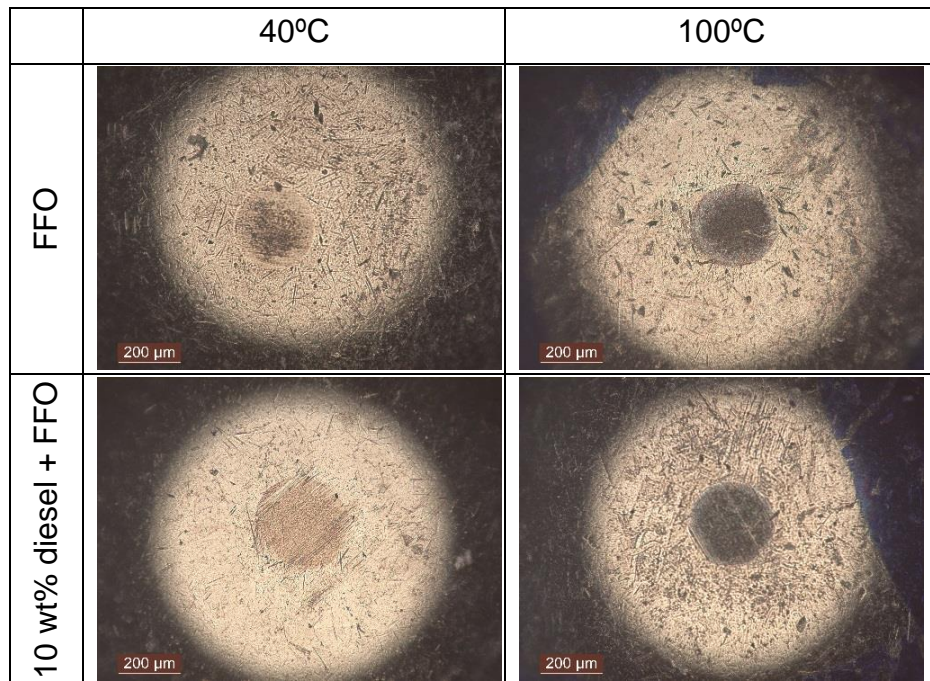


**Figure 8-6. Optical images of ball wear scars after two hour tests with FFO and 10 wt% diesel- contaminated oil.**

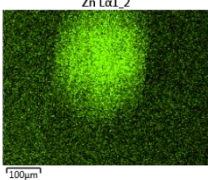
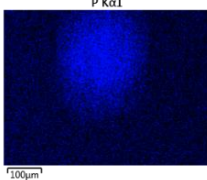
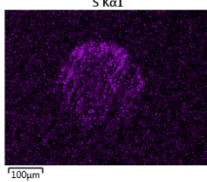
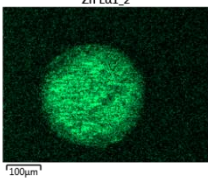
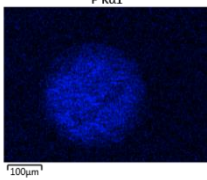
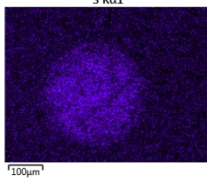
## 8.6 Chemical composition of tribofilm

This section provides information on the chemical composition of tribofilm using EDX and Raman.

### 8.6.1 EDX analysis

To verify the observations from wear results and optical microscope images, EDX analysis was conducted inside the wear scar. Four different positions inside the wear scar were selected to check the uniformity of the elements. EDX information revealed sulphur concentration (atomic %) of 0.03 on wear scar of diesel contaminated oil at 40°C. Higher concentrations of ZDDP tribofilm elements such as Zn, P, and S were detected on the wear scar at higher temperature. These elements were not observed at 40°C. This can be

attributed to the patchy structure of tribofilm as shown in Figure 8-6. EDX revealed sulphur, zinc and phosphorus concentrations (atomic %) of 0.05, 0.16 and 0.06 in the wear scar of FFO at 100°C. Even higher concentrations (atomic %) of sulphur (0.08) in the wear scar was detected with diesel-contaminated sample. Figure 8-7 shows EDX mapping of the wear scar formed on the ball samples with FFO and 10 wt% diesel in FFO. In diesel-contaminated oil, EDX results showed the existence of sulphur element in tribofilm at both temperatures. This was the only difference between FFO and diesel contaminated oil. Thus, the low wear observed with diesel-contaminated oil (see Figure 8-5) can be justified by the existence of sulphur from diesel fuel in the tribofilm which can protect the surfaces from wear.

Sample		Zn	P	S
FFO	40°C	ND	ND	ND
	100°C			ND
10 wt% diesel	40°C	ND	ND	
	100°C			

**Figure 8-7. EDX mapping of the Zn, P and S on ball wear scars formed by FFO and FFO + 10 wt% diesel. ND-not detected.**



## 8.6.2 Raman analysis

Figure 8-8 shows Raman spectra obtained from the generated wear scars after the tests with FFO containing 10 wt% diesel at 40°C and 100°C. Spectra from the disc wear scars showed iron oxide peaks and less intense peaks in the 900- 1000  $\text{cm}^{-1}$  region. Spectra from the ball wear scars showed very intense peaks at 343 and 379  $\text{cm}^{-1}$  which are assigned to  $\text{FeS}_2$  [181, 182]. Spectra from tribopair wear scars generated with oil containing 10 wt% diesel at 100°C showed slightly different spectra than those obtained at 40°C. The high intense  $\text{FeS}_2$  peaks observed in tests at 40°C on the ball wear scars were not observed at 100°C. A broad peak of  $\text{FeS}$  was observed in the region 300-400  $\text{cm}^{-1}$ . The peaks at 670  $\text{cm}^{-1}$  are associated to  $\text{Fe}_3\text{O}_4$ . A prominent peak at 1038  $\text{cm}^{-1}$  was observed.

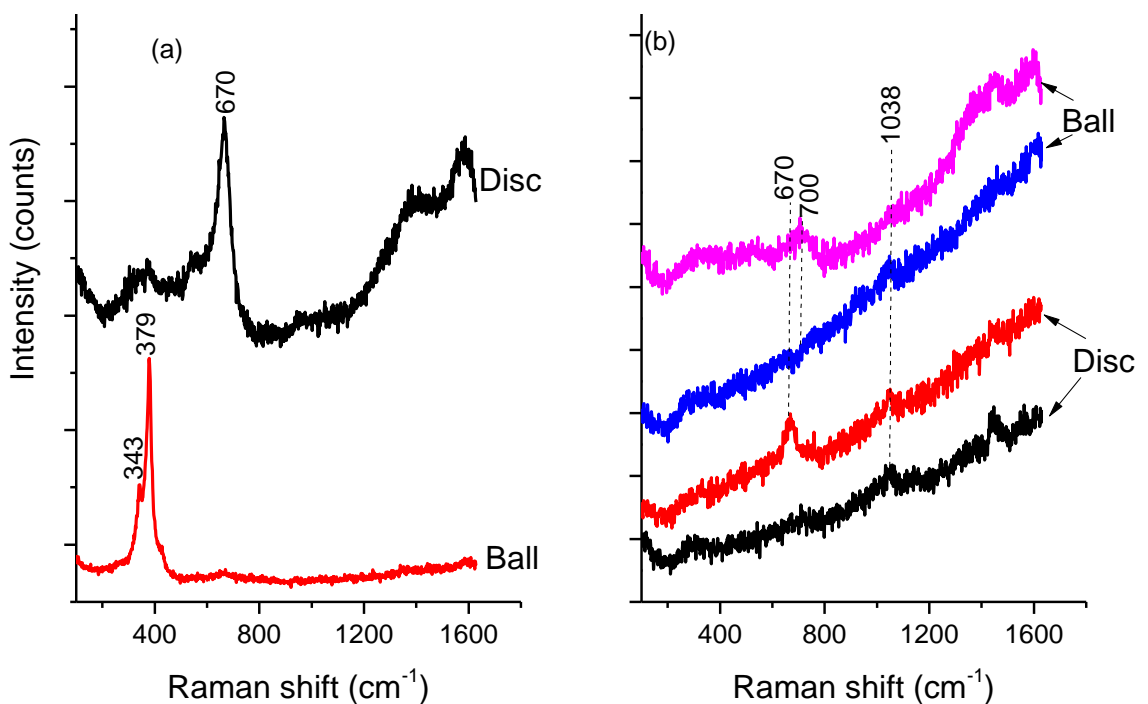


**Figure 8-8. Raman spectra obtained from different positions on tribopair samples with FFO containing 10 wt% diesel after tests at (a) 40°C and (b) 100°C.**

## 8.7 Role of diesel on wear mechanism

The results obtained in section 8.5 and section 8.6 showed that diesel-contaminated oil can reduce the wear. It is important to investigate whether the lower wear was due to the presence of diesel in FFO or antiwear additives in FFO. To investigate this further, the tests were conducted using BO containing 5 wt% diesel. As the BO does not contain any additives the formation of tribofilm would be attributed to the presence of diesel.

## 8.8 Physical properties of oils

Figure 8-9 shows the viscosity of BO diluted with 5 wt% diesel using a rheometer at ambient temperature, 40°C and 100°C. It can be seen that the viscosity of BO was much lower than FFO. The addition of 5 wt% diesel in BO reduced the viscosity further. All tests were conducted in the boundary lubrication regime. Since the viscosities of BO and BO+5 wt% diesel were lower than FFO, the experiments conducted with these lubricants experienced more severe contact conditions.

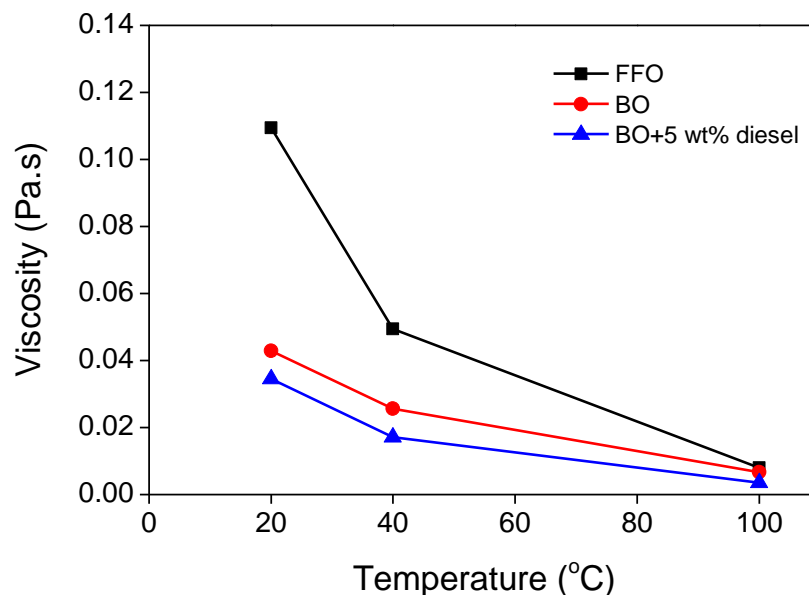


Figure 8-9. Viscosity of oils as a function of temperature.

### 8.8.1 Wear results

Figure 8-10 shows the wear volume loss obtained from the ball samples after two hours of tests at 40°C and 100°C. Results showed that BO had the highest wear volume compared to the diesel-contaminated oil at both 40°C and 100°C. In tests without diesel, wear was higher at 100°C than at 40°C. This can be attributed to the lower viscosity of BO at 100°C than 40°C.

Notably, the wear volume decreased by introducing 5 wt% diesel contamination in BO at both temperatures. This reduction in wear can be attributed to the existence of diesel in oil since BO had no additives. However, this requires further investigation on the tribofilm formed on the wear scar which will be explained in section 8.8.2.

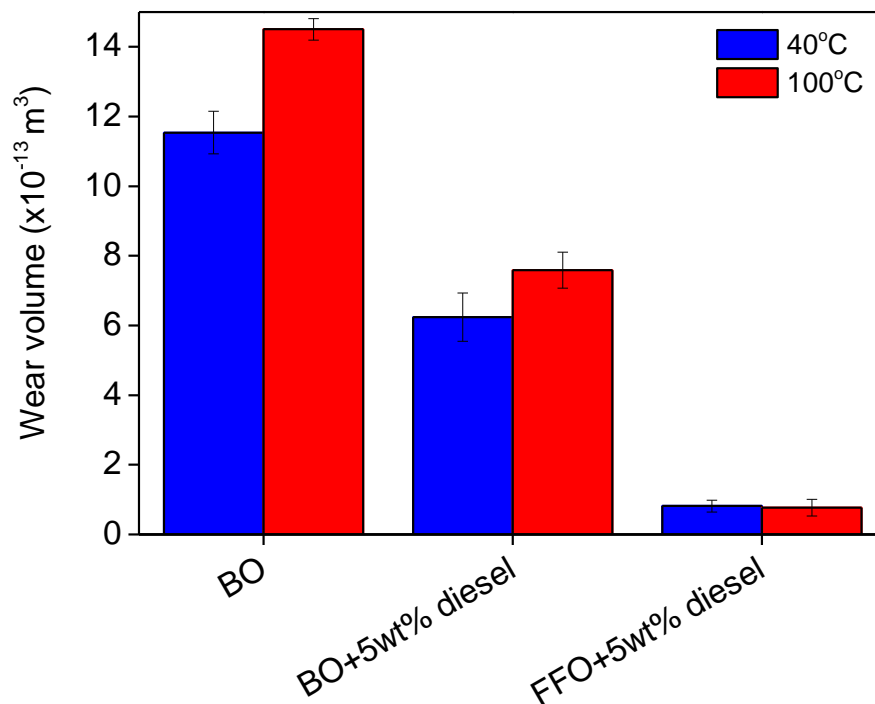
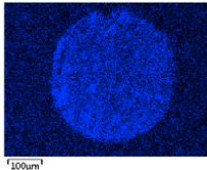
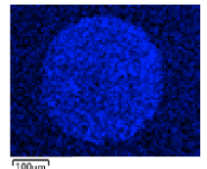


Figure 8-10. Wear volume loss on balls with BO and BO+5wt% diesel for tests conducted at 40°C and 100°C. The error bars on the each points show the repeatability of tests.

### 8.8.2 EDX analysis

EDX analysis was conducted to assess the elemental composition of the wear scar formed by BO and BO + diesel. EDX analysis on the wear scar formed by BO revealed no additives elements at both temperature since the BO did not contain any additives. EDX information on the wear scar of BO + diesel samples revealed sulphur concentrations (atomic %) of 0.04 and 0.05 at 40°C and 100°C, respectively. EDX were conducted at several points within the generated wear scars to verify these observations. Figure 8-11 shows the EDX mapping of wear scar formed on the ball samples. The mapping images showed sulphur elements inside the wear scar with diesel-contaminated oil at both temperatures. The existence of sulphur element in BO+diesel can be attributed to the diesel composition. As mentioned in section 3.13.1 diesel fuel contains sulphur. The presence of sulphur in diesel fuel was also confirmed by Raman analysis as shown in Section 4.2.4 .

Sample		S
BO	40°C	ND
	100°C	ND
BO + 5 wt% diesel	40°C	
	100°C	

**Figure 8-11. EDX mapping of the ball wear scars formed by BO and BO + 5 wt% diesel. Sulphur element was detected on the samples diluted with diesel. ND-not detected.**

## 8.9 Summary

In this phase of this research the tribological performance of steel-on-steel contact with diesel-contaminated oil under boundary lubrication conditions was investigated. In summary, the following key points can be drawn from this part of the study:

- Viscosity of both FFO and BO reduced by adding diesel to the oils.
- The addition of diesel to FFO reduced friction coefficient slightly at both 40°C and 100°C.
- In general, wear was lower at high temperature. This can be attributed to enhanced antiwear tribofilm formation at high temperature.
- Wear decreased when diesel was added to the oils. This can be explained by the varying chemical composition of oil when diesel was present.
- The improved wear performance in the presence of diesel was related to the formation of a better tribofilm containing sulphur, supplied by diesel, which protects surfaces.

## **Chapter 9 The effect of oil degradation on tribological performance of vane-rotor contact**

### **9.1 Introduction**

Previous studies [38, 183] have shown excessive wear on the key components of VDVP such as slide ring, vanes and rotor. The failure analysis of VDVP in Chapter 5 of this study also revealed sign of severe wear on these components. Based on the results presented in Chapter 5 and the review of the literature, it is believed that oil contamination could be responsible for the high wear observed in this system. It is therefore important to understand how contaminants influence friction and wear of vane-rotor contact. However, it is not clear how oil contamination and degradation affect the tribological performance of the oil [2].

In this chapter, firstly, the impact of carbon black and diesel contaminants on the bulk properties of the oil during ageing process will be investigated. This will be done using rheometer and Fourier Transform Infrared Spectroscopy (FTIR). Secondly, the performance of these oils on the friction and wear of vane-rotor contact under boundary lubrication condition will be evaluated. The experiments in this section were designed to replicate the contact between vane and rotor on VDVP. Vane and rotor samples were cut from the real vane pump. The details of samples were explained in Chapter 4, Section 4.4.2.1. The tribotests were conducted using TE77 tribometer under reciprocating sliding conditions. Tribotests were conducted at the following test conditions: 2 hours, 100°C, 0.83 GPa and 25 Hz. The wear mechanism and chemical nature of tribofilm formed in tribological tests were verified using Scanning Electron Microscopy/Energy Dispersive X-ray spectroscopy (SEM/EDX) and Raman spectroscopy.

## 9.2 Oil analysis

The physical and chemical properties of FFO used in this study were explained in Chapter 4. The effect of diesel and carbon black contaminants in FFO were considered during the ageing process. The details of oil degradation experiments were also provided in Chapter 4. Table 9-1 illustrates the test matrix for thermo-oxidative degradation tests. Figure 9-1 shows the visual inspection of oil degradation during the ageing process for 96 hours. It can be clearly seen that as the oxidation time increased the colour of the sample darkens. This is one of the clearest signs of oil degradation.

**Table 9-1. Contaminants and their level in the test matrix.**

Factors	Level (weight %)	Samples name	Ageing time
Oxidation	No contamination	AFFO	96 hours (sampling every 24 hours)
Diesel	1 wt%	1% D	
CB	1 wt%	1% CB	
CB and diesel	1 wt% each	1% CB&D	
CB and diesel	2 wt% each	2% CB&D	

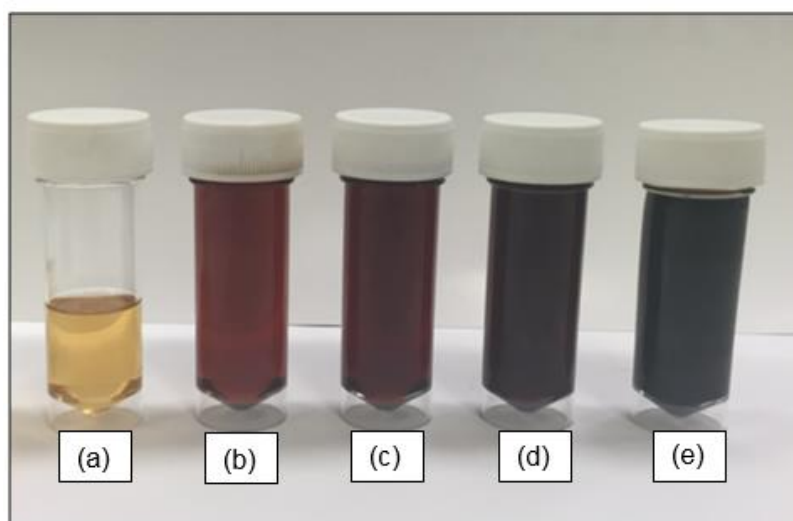


**Figure 9-1. Visual inspection of (a) fresh FFO and oils after different oxidation time: (b) 24h, (c) 48h, (d) 72h, (e) 96h.**

### 9.2.1 Viscosity results

The viscosity of all oil samples were measured using rheometer at 40°C and 100°C. Figure 9-2 and Figure 9-3 show the dynamic viscosity of oils containing various contaminants at 40°C and 100°C respectively.

It can be observed that the viscosity of the oils increased during the ageing process by the oxidation process and the addition of CB contamination as expected. Diesel contamination slightly reduced viscosity of the oils due to the fuel dilution [184]. As diesel decreases the viscosity and CB particles increase viscosity of oil, there was no notable change in the viscosity of oils which were contaminated with both CB and diesel fuel. In addition, at higher temperatures there was no significant difference in the viscosity of oil samples with various contaminants.

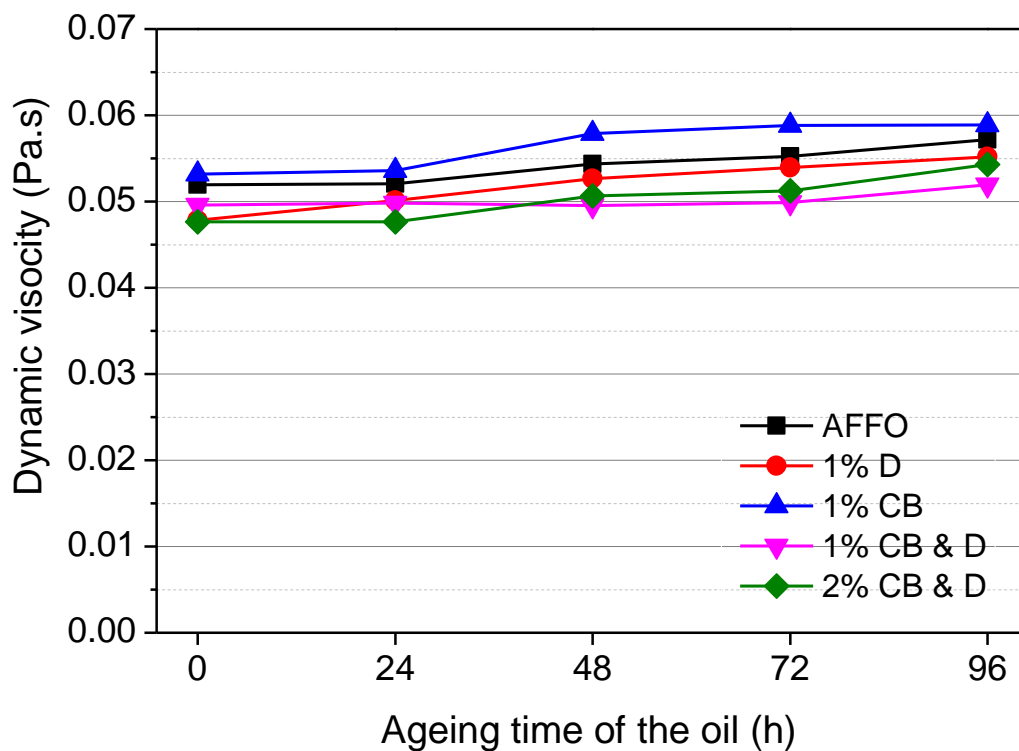


Figure 9-2. Dynamic viscosity of aged oil samples at different ageing time at 40°C.



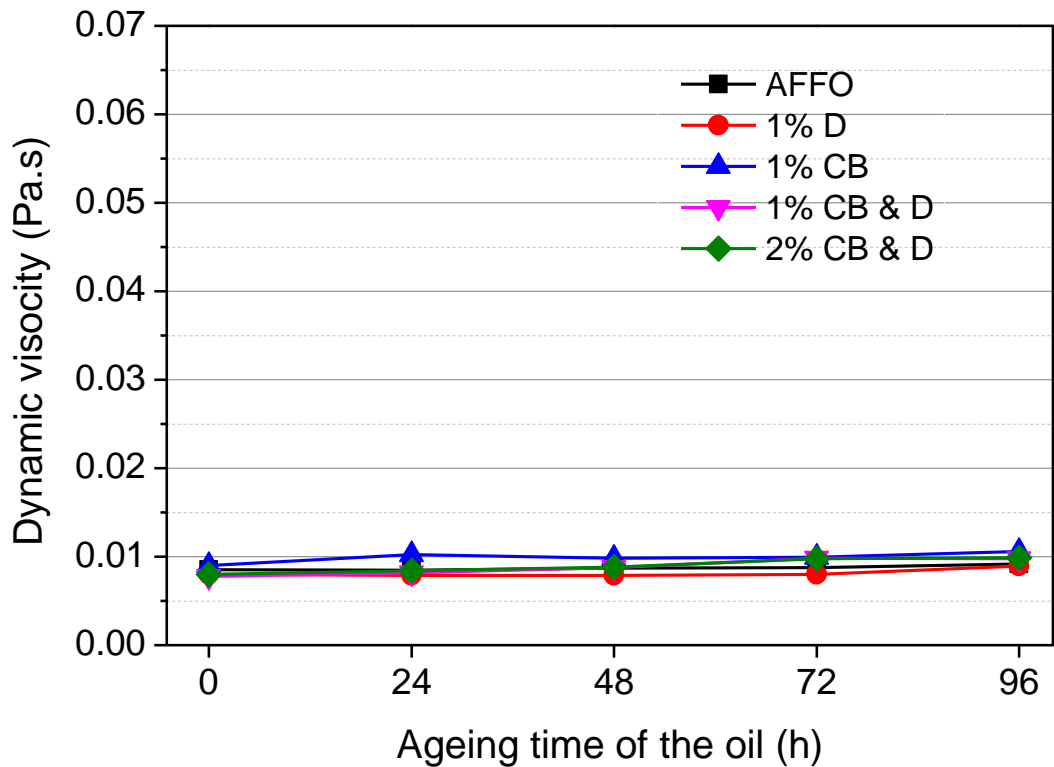
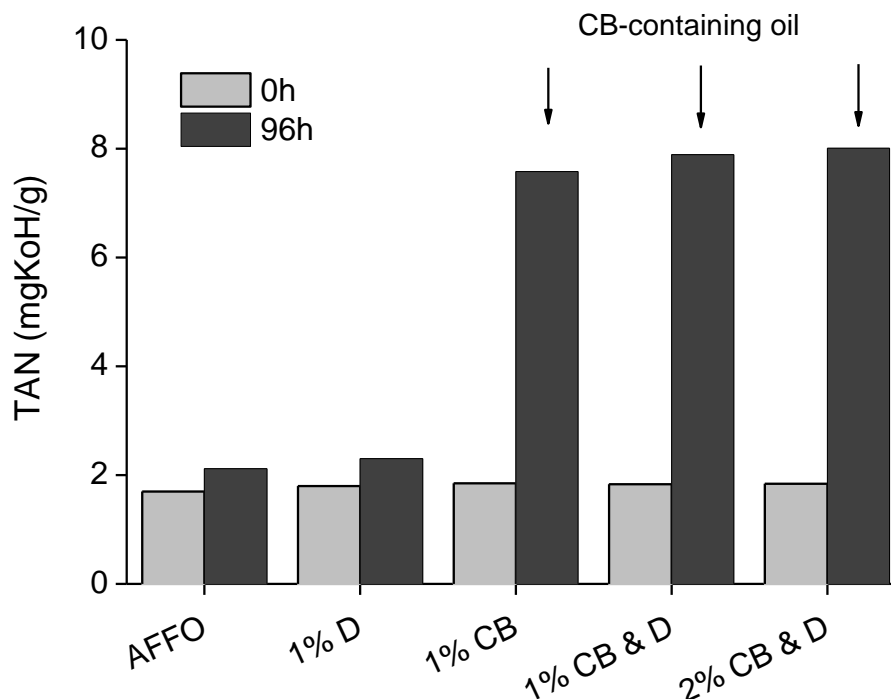


Figure 9-3. Dynamic viscosity of aged oil samples at different ageing time at 100°C.

### 9.2.2 Total Acid Number (TAN)

Figure 9-4 shows total acid number (TAN) values for the fresh oils and aged oils after 96 hours of ageing. The results showed that TAN values increased during the ageing process from 1.7 to the maximum of 8.01 KOH/g. It is notable that an increase in TAN was significant when CB particles were present in the oil during the ageing process. This can be related to the formation of acids in the oil when CB particles were present.



**Figure 9-4. TAN value comparison for aged oil samples.**

### 9.2.3 FTIR results

The effects of oxidation, diesel and carbon black contaminants in FFO during the ageing process were investigated using FTIR. There are a large number of tests and results, however only the selected spectra at 0 hour and 96 hours are presented here. Each FTIR spectrum is the result of four scans at  $4.0 \text{ cm}^{-1}$  resolution.

Figure 9-6 (a) shows FTIR spectrum of FFO at 0 h and 96 h. Infrared spectra of the aged oil due to oxidation showed similar absorption bands at 0 h and 96 h. IR bands between  $2850\text{-}3000 \text{ cm}^{-1}$  and  $1385\text{-}1500 \text{ cm}^{-1}$  are attributed to alkyl C-H stretching and C-H bending respectively. The spectrum at  $722 \text{ cm}^{-1}$  is also attributed to alkyls chains [176]. These three main peaks which are from the base stock hydrocarbons were present in all oil samples. In this section, the focus is more on the fingerprint region ( $650\text{-}1800 \text{ cm}^{-1}$ ) to determine if additive depletion has occurred during the ageing process.

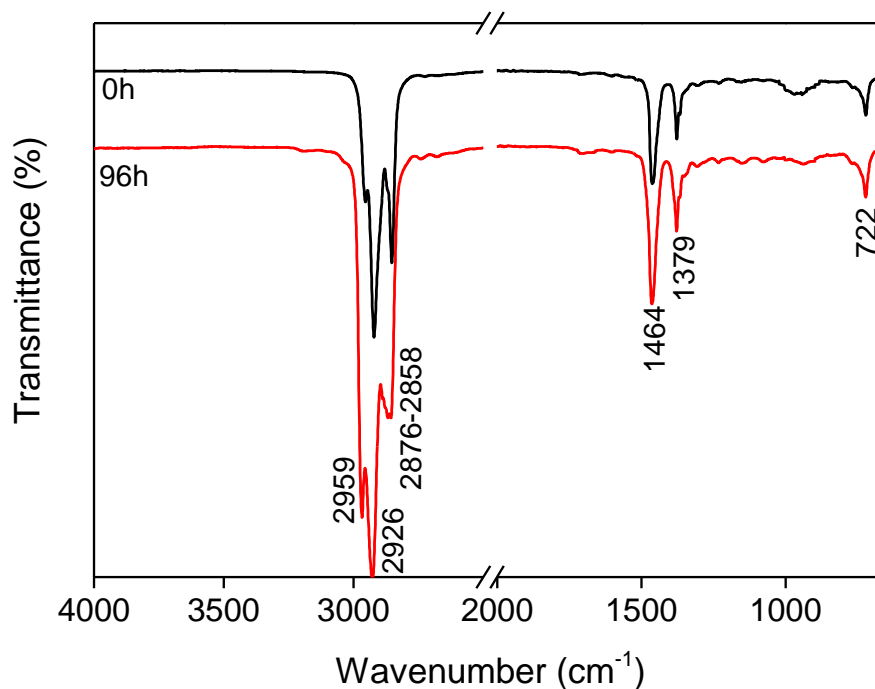


**Figure 9-5. FTIR spectrum of fresh FFO and aged FFO after 96 hours.**

Antiwear ( $970\text{ cm}^{-1}$ ), antioxidants ( $1080\text{ cm}^{-1}$ ), viscosity improvers ( $1162\text{ cm}^{-1}$ ), dispersants ( $1232\text{ cm}^{-1}$ ) are known through literature (Figure 9-6) [185, 186]. P-O-C bond from ZDDP additive in oil is located at  $920\text{-}1050\text{ cm}^{-1}$  region and the P=S bond is around  $950\text{-}1040\text{ cm}^{-1}$  [187]. In the current study, the peak at  $970\text{ cm}^{-1}$  is attributed to ZDDP. FTIR peaks showed a reduction in the intensity of infrared peak at  $970\text{ cm}^{-1}$  after 96 hours of ageing. Intensity of the bands at  $1080\text{ cm}^{-1}$  and  $1162\text{ cm}^{-1}$  increased and broadened. Such increase in intensity and band broadening after 96 hours of the ageing can be attributed to the formation of several oxidation products during the ageing process [188]. In addition, an increase in the carbonyl absorbency at  $1720\text{ cm}^{-1}$  (carboxylic acid) was observed.

For diesel contamination, as can be seen in Figure 9-7 a new peak appeared during the ageing process. This peak is attributed to the sulphate peak ( $1040\text{ cm}^{-1}$ ). Sulphate compounds can either be related to the sulphur in diesel fuel or the oxidation of sulphur from the additives in FFO [189]. Since this peak was not observed in the aged FFO, therefore the existence of this spectrum

can be due to sulphur in diesel. It should be noted that the oxidation peak at  $1720\text{ cm}^{-1}$  appeared in diesel-contaminated oil after 96 hours of ageing.

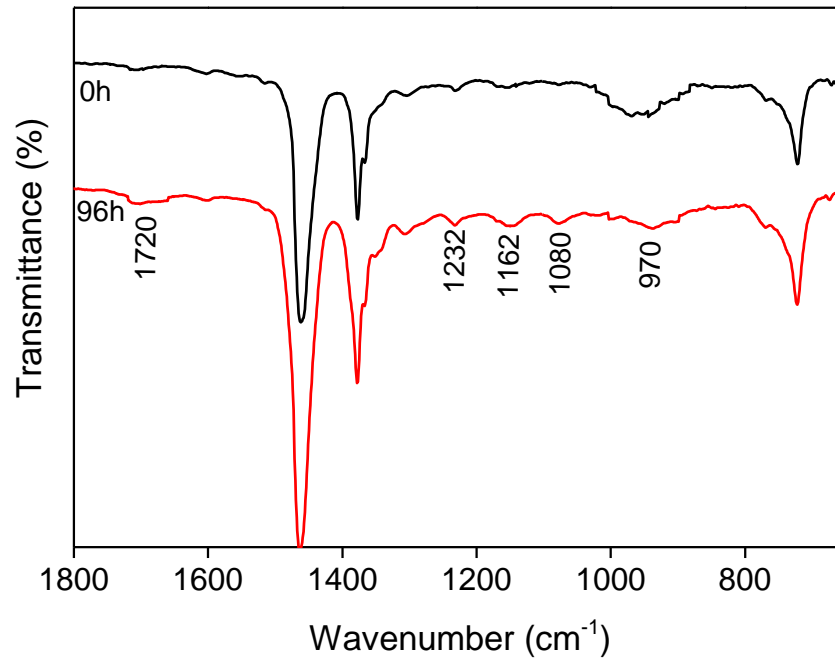


Figure 9-6. FTIR spectrum of fresh FFO and aged FFO fingerprint region.

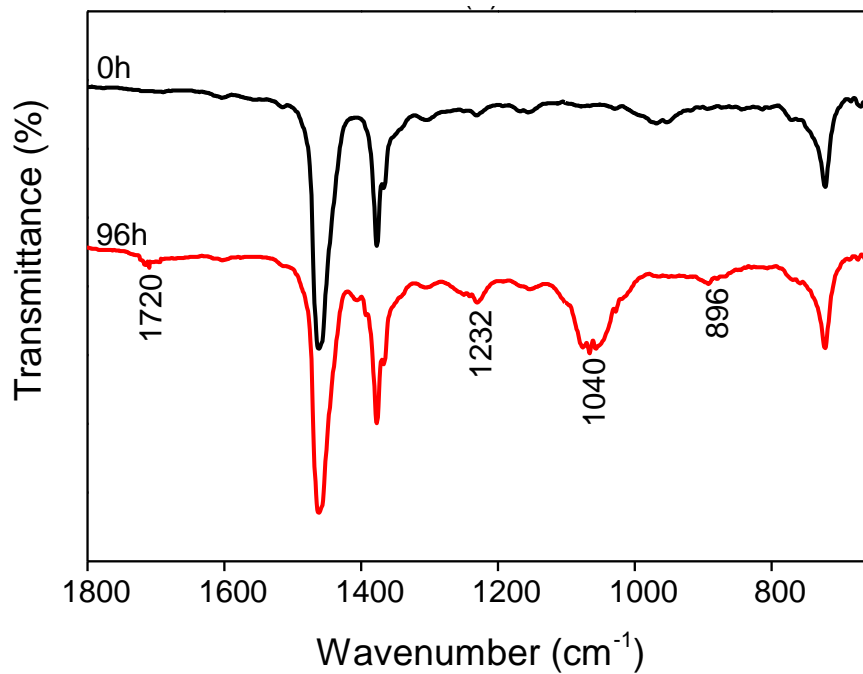
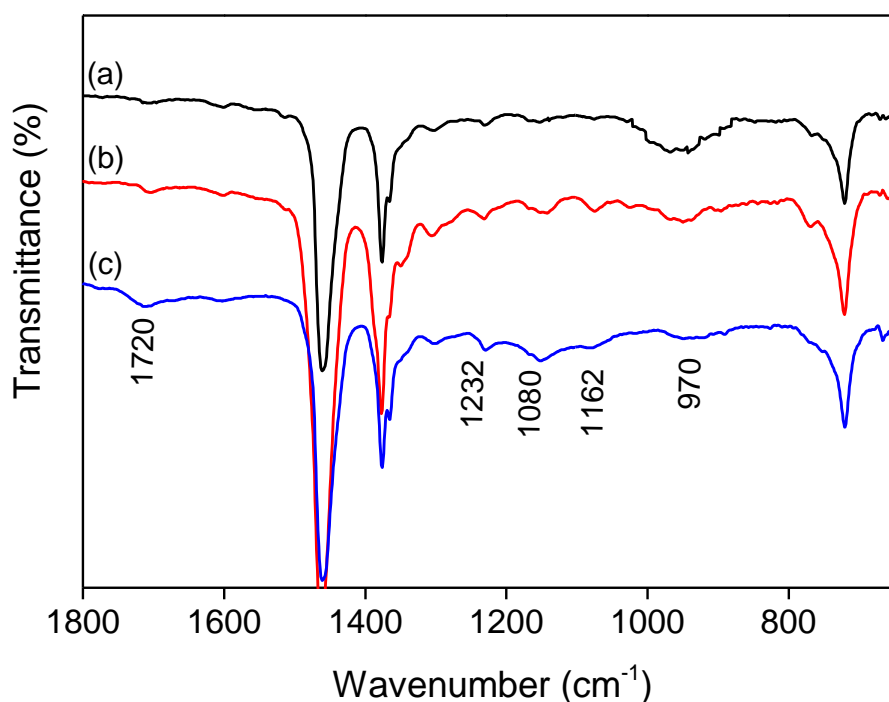


Figure 9-7. FTIR spectrum of fingerprint region for diesel contaminated oil at 0 h and 96 h.

Figure 9-8 shows the FTIR spectrum of FFO, contaminated oil with 1wt% and 2wt% CB and diesel. It can be seen that the intensity of antiwear additives peak which is around  $970\text{ cm}^{-1}$  is reduced after 96 hours of ageing. It has been reported that antiwear additives interact negatively with CB [114]. Thus, this result suggests that additive depletion has occurred during the ageing process in the presence of CB. It can also be seen that oxidation peak at  $1720\text{ cm}^{-1}$  also appeared after 96 hours of ageing in the oil with both CB and diesel contaminants.



**Figure 9-8. FTIR spectrum of (a) fresh FFO, (b) aged oil with 1wt % CB and diesel and (c) aged oil with 2 wt% CB and diesel.**

### 9.3 Tribotests under reciprocating sliding conditions

#### 9.3.1 Effect of contaminants on friction and wear

The effect of contaminants in FFO were investigated on the friction and wear behaviour of vane-rotor contact in tribological tests. Figure 9-9 indicates the

average friction coefficient values for the last 30 minutes of the tests (steady state friction) and wear coefficients calculated using Equation 2-11.

It can be seen that FFO and diesel-contaminated oil showed the highest friction coefficient. There was a slight reduction in both friction and wear by adding 1 wt% diesel in FFO. This reduction in friction and wear was also observed in results presented in Chapter 8.

When 1 wt% CB was added to the FFO, nearly 8% reduction in friction was observed. The same reduction in friction was observed when both CB and diesel were added to the oil. Also, higher levels of CB and diesel in oil decreased the friction further. In terms of wear, the results show that CB-contaminated oil significantly increased wear, which is consistent with the other literature [118, 121]. The combination of CB and diesel contamination increased the wear further. The higher levels of contaminant in oil also led to higher wear, as expected.

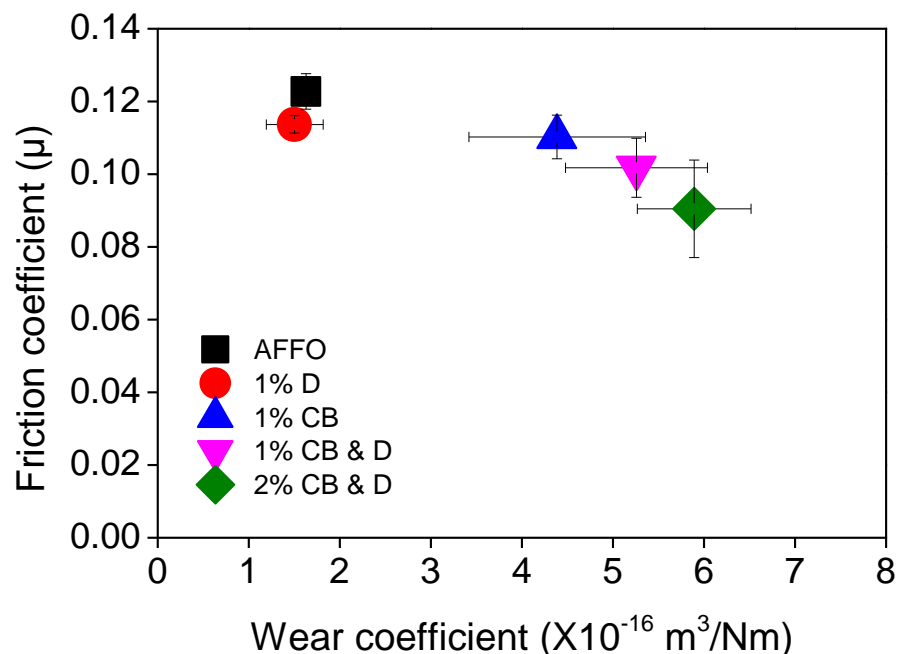


**Figure 9-9. The effect of contaminants on friction and wear at 0 h oil ageing. The error bars on the each points demonstrate the repeatability of tests. All tests were conducted at 100°C.**

### **9.3.2 Effect of oil degradation on friction and wear**

In this section, the combined effect of contaminants and the ageing of the oil on friction and wear will be studied. Figure 9-10 indicates the average friction coefficient values for the last 30 minutes of the tests (steady state friction). Figure 9-11 shows the wear coefficient as a function of ageing time of the oil for various contaminated oil.

As can be seen in Figure 9-10 and Figure 9-11, in terms of aged FFO, friction and wear were fairly unaffected during the ageing process. It is usually expected that oxidation leads to an increase in viscosity of oil. However, the variation in viscosity depends on the formulation of oil, level and type of additives in the oil [190].

With diesel contamination the friction coefficient did not change significantly. However, a notable result was obtained on wear with the diesel contamination. The wear coefficient reduced by the ageing process. This was the only time where with diesel contamination a lower wear coefficient was observed in comparison to the uncontaminated oil.

The greatest effect on friction and wear was observed with CB contamination. The friction and wear coefficients for tests containing CB contaminant were fluctuating and therefore the error bars were larger compared to the oil without CB. These spikes could be due to the random nature of the large particles going through the contact interface. Friction coefficient initially reduced by introducing CB into the FFO which was explained in 9.3.1. The same tests were conducted for combination of contaminants (CB and diesel) to examine if these contaminants interact with each other. The coefficient of friction initially reduced by introducing CB and diesel in oil. As discussed previously, this reduction in friction is mostly due to the existence of CB in oil. However the friction increased during the ageing process with combination of CB, diesel and oxidation.

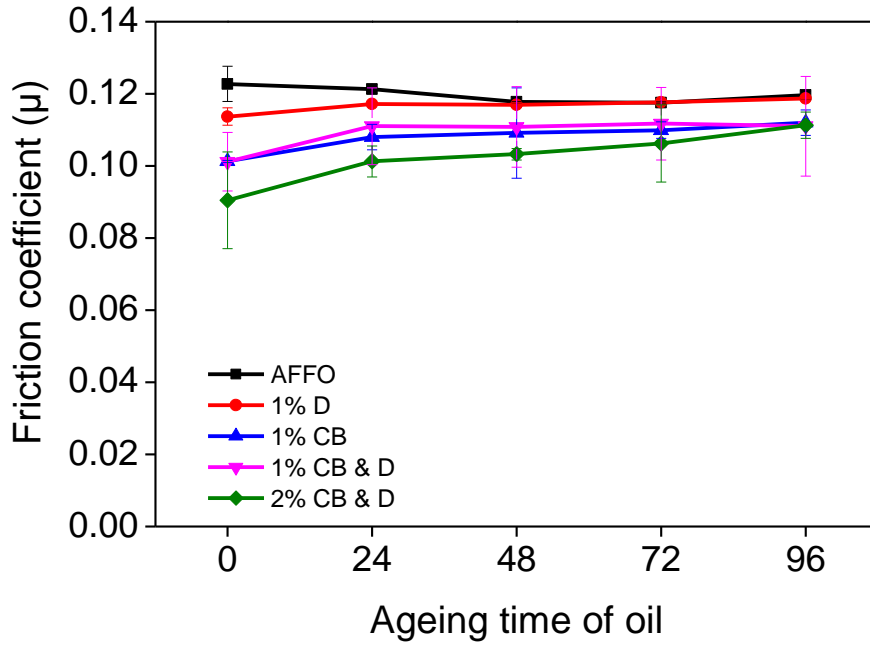


Figure 9-10. Steady state friction coefficient as a function of ageing time of the oil with aged oil due to oxidation, 1wt% diesel, 1wt% CB, 1wt% CB and diesel, and 2wt% CB and diesel. The error bars on the each points show the repeatability of tests. All tests were conducted at 100°C.

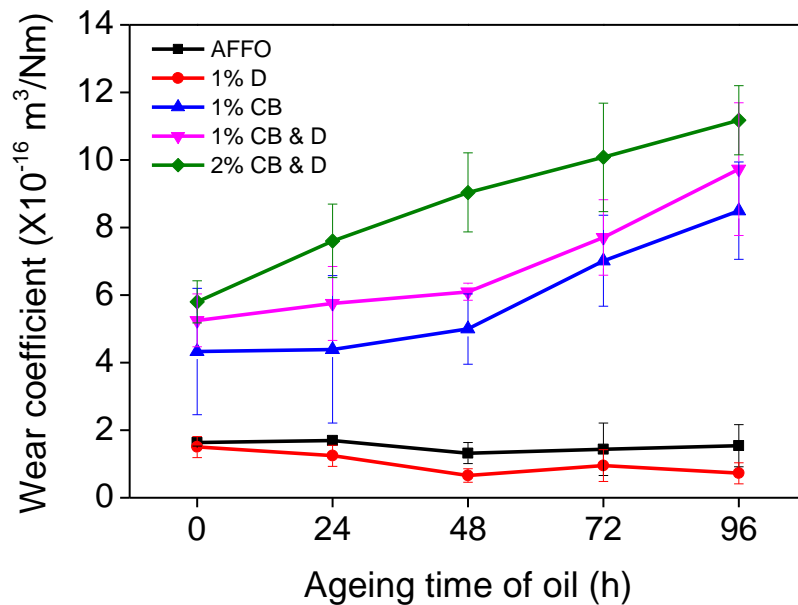


Figure 9-11. Wear coefficient as a function of ageing time of the oil with aged oil containing various contaminants. Wear measurements were conducted on the vane samples. All tests were conducted at 100°C.



## 9.4 Surface characterisation

In this section, SEM/EDX and Raman analysis on the worn surfaces are shown. These analyses can help to understand the mechanisms of reactions, morphology and elemental composition of the worn surfaces lubricated with contaminated and aged oils.

Figure 9-12 shows the SEM images of wear scars formed using FFO and diesel contaminated oil at 0 h and 96 h. The wear scar in Figure 9-12(a) showed slightly or nearly no marks on the surface. The arrow on the image indicates the sliding direction. There are other scratches on the sample which are possibly from the manufacturing since they are not in line with the sliding direction. EDX information on the wear track formed by FFO revealed the existence of Zn, P, and S elements with concentration of 0.41%, 0.19% and 0.15% by atomic% respectively. It should be noted that these values change from point to point of wear scar. This clearly illustrates the heterogeneous nature of tribofilm.

Figure 9-12(b) shows SEM image of wear scar formed by diesel-contaminated oil. In the presence of diesel, EDX showed a higher concentration of S in tribofilm. These results have also been confirmed by Raman analysis.

Figure 9-13 indicates the Raman spectra obtained from the wear scar formed after test with FFO at both 0 h and 96 h. The Raman spectra also showed the presence of iron sulphide (FeS) evidenced by the broad peak at  $200\text{-}400\text{ cm}^{-1}$ . The peaks observed at  $670\text{ cm}^{-1}$  and  $800\text{ cm}^{-1}$  were assigned to Iron (III) oxide ( $\text{Fe}_3\text{O}_4$ ) and calcium hydroxide respectively. Phosphate peak can be seen at  $987\text{ cm}^{-1}$  and zinc phosphate peak observed at  $1040\text{ cm}^{-1}$  [169]. The same peaks were observed within the wear scar of aged FFO after 96 h of ageing with lower intensity.

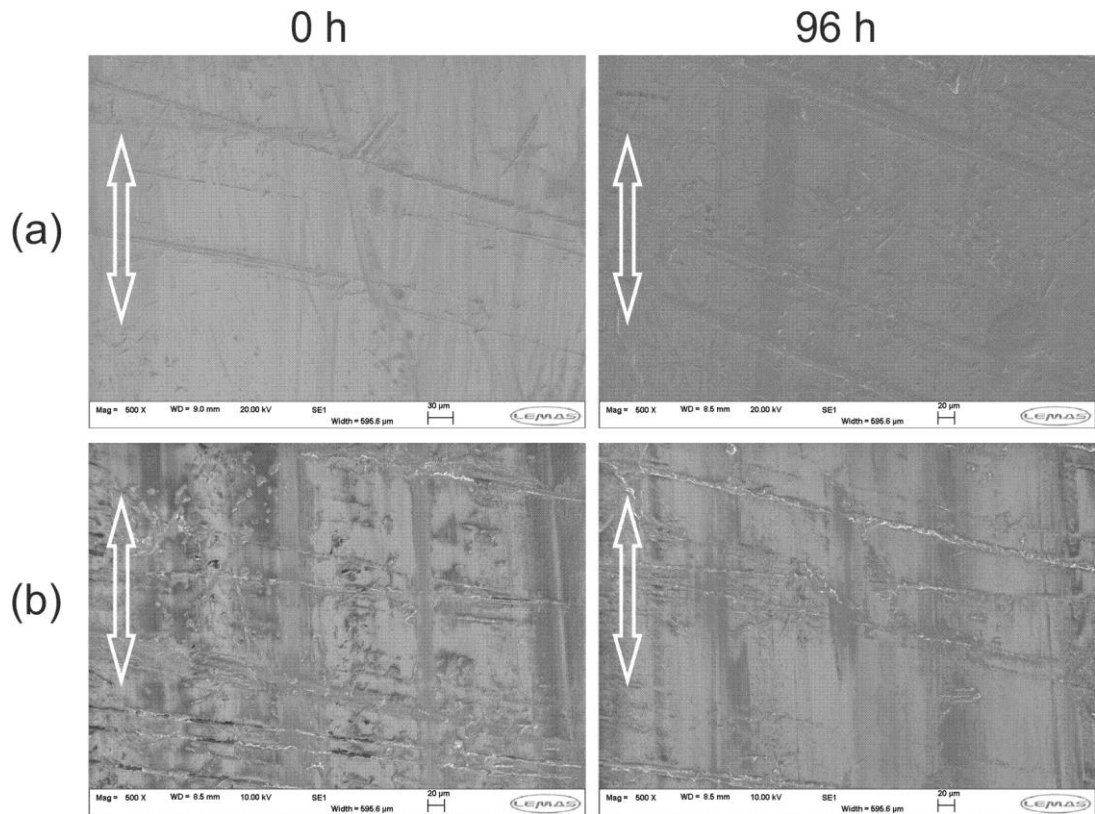


**Figure 9-12. SEM images of wear scar formed by (a) FFO (b) 1wt% diesel-contaminated oil at 0 h and 96 h of oil ageing.**

Figure 9-14 shows Raman spectra obtained from wear scar after tests with diesel contaminated oil at 0 h and 96 h. These spectra showed similar peaks presented in wear scar by FFO.

Figure 9-15(a) and Figure 9-15(b) show the wear scar on the vane sample formed using aged oil with %1 wt CB at 0h and 96 h respectively. It can be seen that abrasion increases during the ageing process from 0 h to 96 h. The same increase in abrasion was also observed for combination of contaminants. The wear was much more severe when the oil was contaminated and aged with both CB and diesel (see Figure 9-15(c) and Figure 9-15(d)).

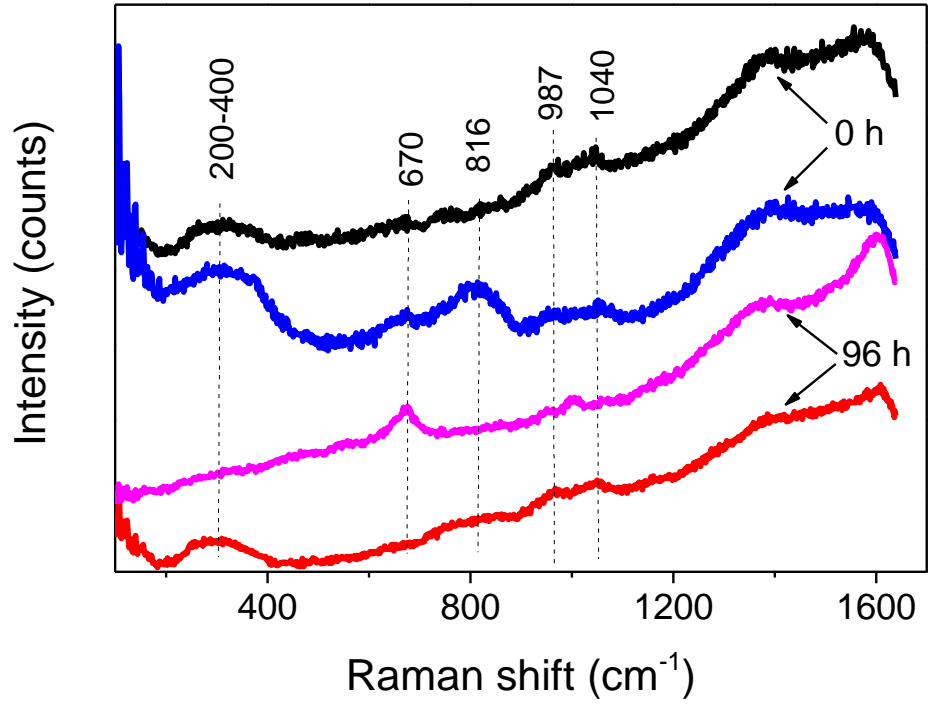


Figure 9-13. Raman spectra of wear scars after tests with aged FFO at 0 h and 96 h of oil ageing.

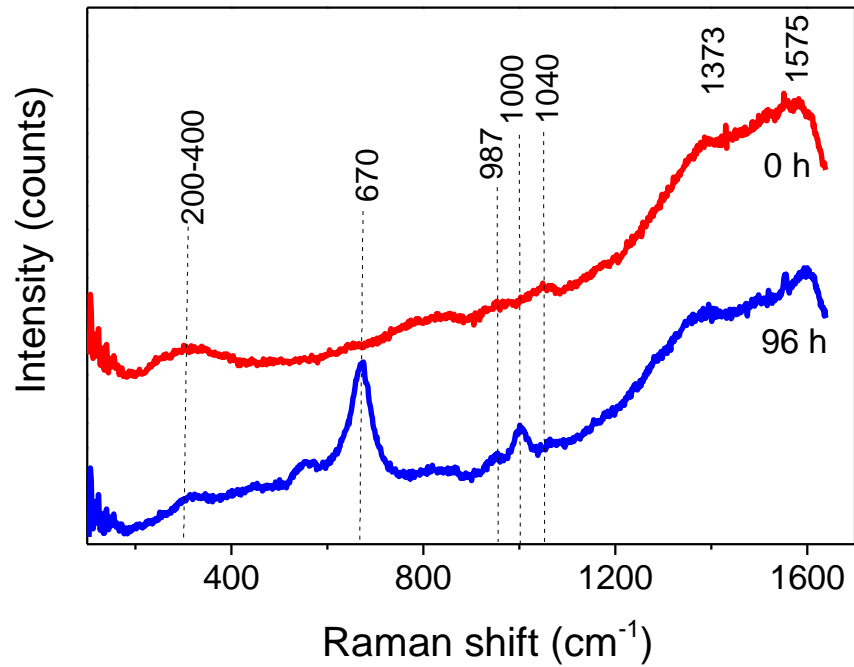
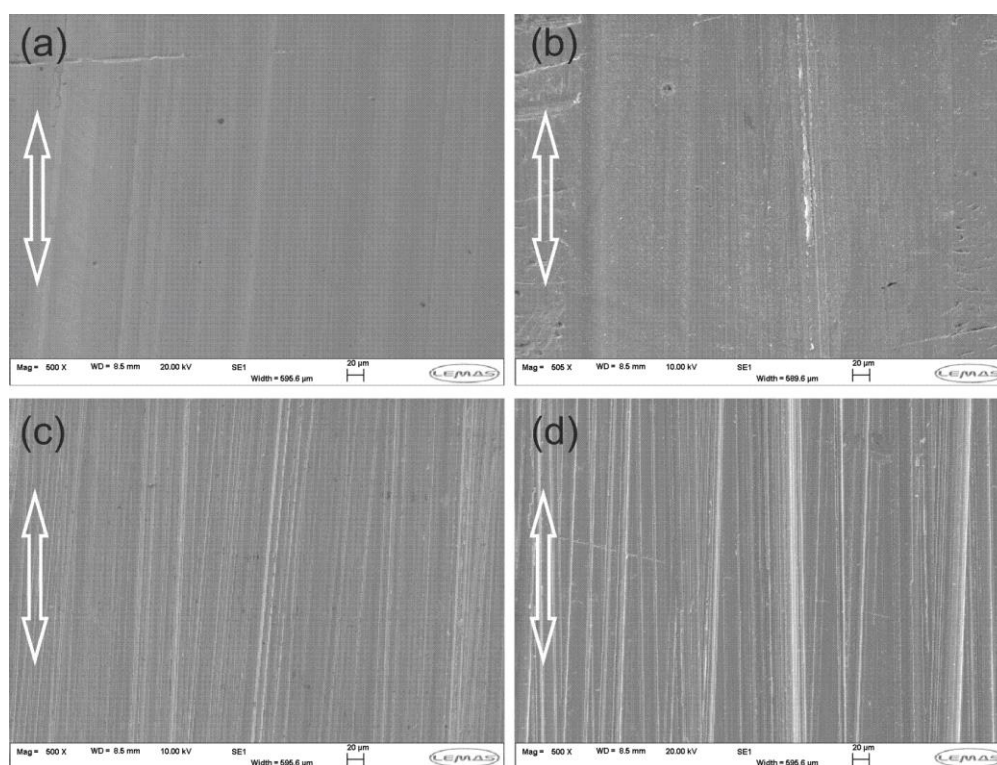


Figure 9-14. Raman spectra of wear scars after tests with 1wt% diesel-contaminated oil at 0 h and 96 h.

EDX results revealed no elements of Zn, P and S after 96 h of ageing on these samples. Figure 9-16(a) and (b) show Raman spectra obtained from wear scar after tests with 1wt% CB and 1wt% CB and diesel at 0 h and 96 h of ageing time respectively. It can be seen that the generated wear scars were mainly composed of iron oxides after 96 h; haematite ( $\text{Fe}_2\text{O}_3$ ) and magnetite ( $\text{Fe}_3\text{O}_4$ ). The peaks at  $222\text{ cm}^{-1}$ ,  $291\text{ cm}^{-1}$  and  $404\text{ cm}^{-1}$  were assigned to  $\text{Fe}_2\text{O}_3$  and the peak at  $670\text{ cm}^{-1}$  was assigned to  $\text{Fe}_3\text{O}_4$ . The carbon peaks were also observed on the contact region at  $1375\text{-}1575\text{ cm}^{-1}$ . These results are in line with high wear observed when CB was present in oil after 96 h of ageing in section 9.3.2. The same results were observed for 2wt% CB and diesel contaminated oil.



**Figure 9-15. SEM images of wear scar with aged oil with 1wt% CB at (a) 0 h, (b) 96 h, (c) aged oil with 1wt% CB and diesel (d) aged oil with 2wt% CB and diesel.**

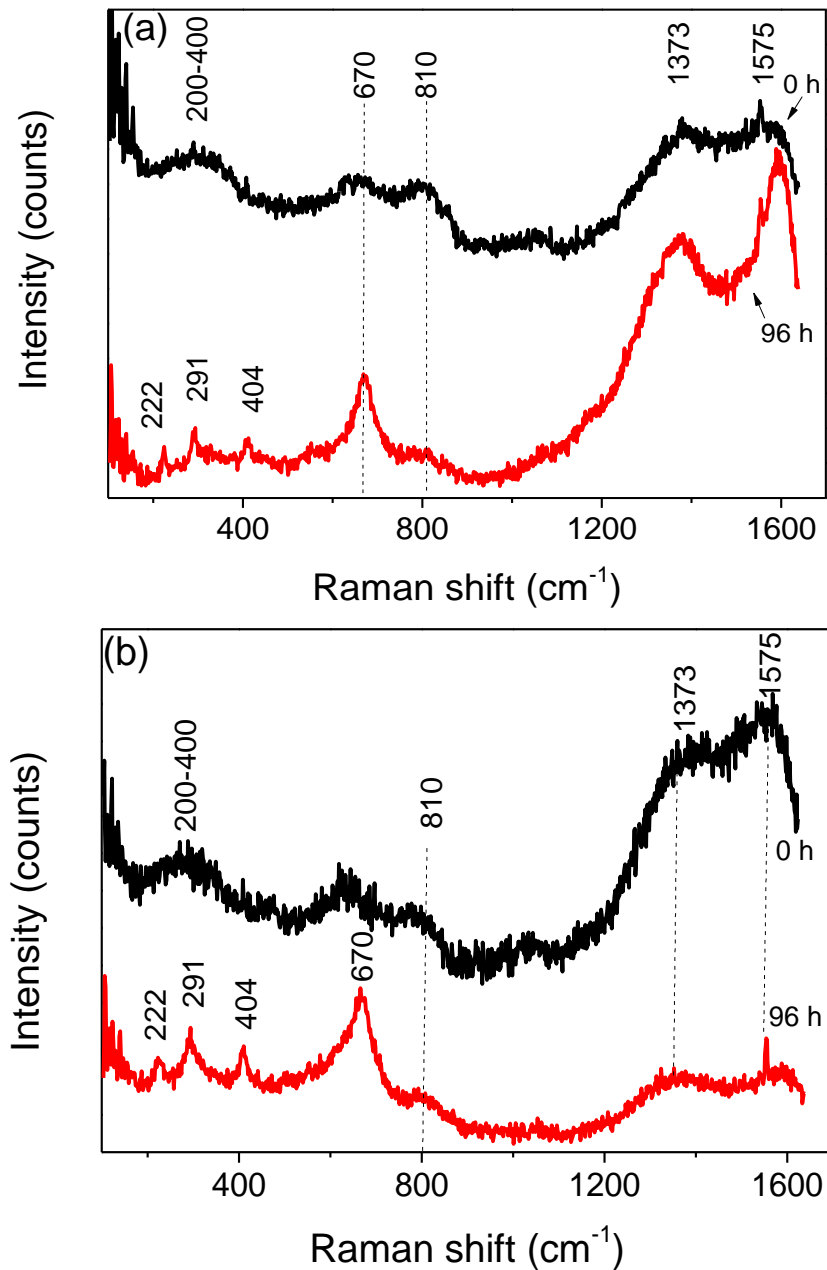


Figure 9-16. Raman spectra of wear scars after tests with (a) 1wt% CB and (b) 1wt% CB and diesel contaminated oil.

## 9.5 The effect of contaminants on wear mechanism

Based on the results obtained in the previous sections of this chapter, further experiments were carried out in order to investigate the antagonistic effect of diesel and soot contamination on wear. Table 9-2 shows the test matrix and

the aim of these experiments. Figure 9-17 indicates the average friction coefficient values for the last 30 minutes of the tests and wear coefficients calculated using Equation 4-3.

**Table 9-2. Text matrix for ageing the oil.**

Name		Test condition	Aim
T1	□	Aged oil with no contaminant for 96 h then add 1 wt% CB before the test	To establish the relationship between abrasion ageing of the oil
T2	△	Aged oil with no contaminant for 96 h then add 2 wt% CB before the test	
T3	⬡	Aged oil with 1wt% diesel for 96 h then add 1 wt% CB before the test	To investigate the antagonistic effect of contaminants on wear
T4	☆	Aged oil with 1wt% CB for 96 h then add 1 wt% diesel before the test	
T5	○	Filter the aged oil with 2 wt% CB and diesel contaminants	To understand how oil functions after removing the CB contaminants

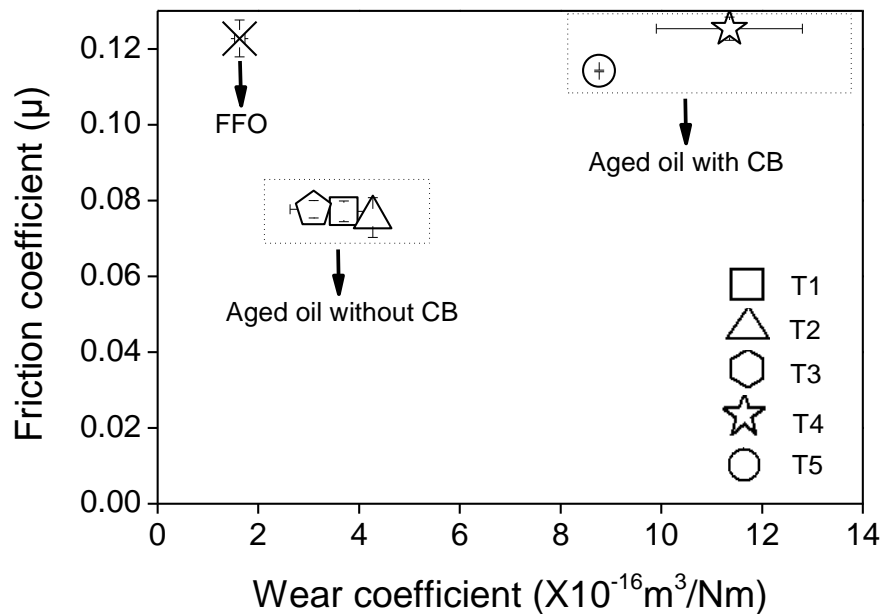


**Figure 9-17. Friction and wear coefficient of tests. Wear measurements were conducted on vane samples. Error bars show repeatability of tests.**

### 9.5.1 Effect of abrasion by CB

Tests T1 and T2 were conducted using aged FFO for 96 hours once with 1wt% and once with 2wt% concentration of CB. These tests were conducted to establish why abrasion increases during the ageing process. Figure 9-17 indicates that friction reduced for both T1 and T2 tests compared to the FFO. The CB particles increased the wear and higher CB concentration resulted in higher wear as expected. Figure 9-18(a) shows the wear scar formed using aged oil with 1wt% CB for 96 hours. Figure 9-18(b) and Figure 9-18(c) indicate the SEM images of wear scar for tests T1 and T2 respectively. There are a number of scratches in the direction of sliding on the wear scar produced during tests T1 and T2 however the wear is not as severe as wear scar shown in Figure 9-18(a). These results indicate that when 1wt% CB was present in the oil during the ageing process, approximately 42% higher wear was observed in comparison to the test in which 1wt% CB was added to the aged FFO Figure 9-18(b). That is to say although in both tests 1wt% CB was present in the oil, the wear behaviours were different.

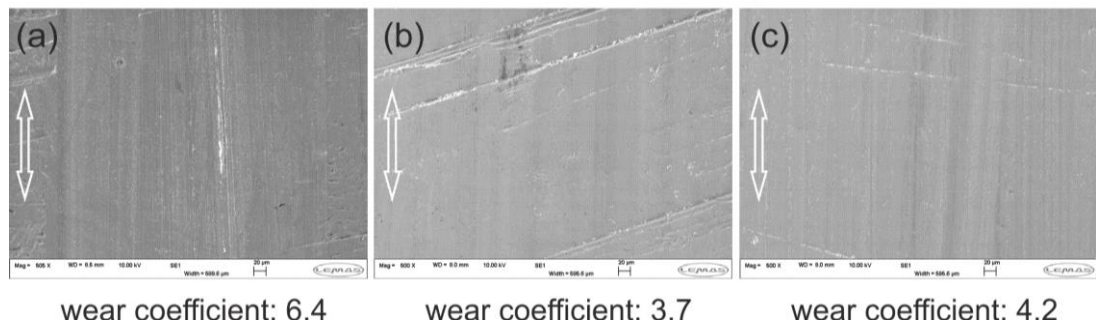


**Figure 9-18. SEM images of wear scar on vane with (a) aged oil with 1wt% CB for 96 and aged FFO for 96h then adding(a) 1 wt% CB (b) 2wt% CB - Wear coefficient unit is ( $\times 10^{-16} \text{ m}^3/\text{Nm}$ ).**

### 9.5.2 Antagonistic effect of contaminants on wear

T3 and T4 were conducted to investigate the antagonistic effect of diesel and CB contaminants on wear (explained in Table 9-2). As can be seen from

Figure 9-17, similar concentration of CB in oil resulted in significantly different wear.

Figure 9-19(a) and Figure 9-19(b) show SEM images of the wear scar with T3 and T4 tests. From the SEM images it can be seen that the wear was significantly severe when the oil was aged with 1wt% CB for 96 hours and then the diesel was added just before the test. The reverse sequence resulted in less wear. Wear coefficient was approximately 73% higher in T4 than T3. In addition, the generated wear scar was about 5  $\mu\text{m}$  deep in T4. It is believed [114] that abrasion by soot can either be due to the rubbing metallic surfaces or by rubbing the tribofilms formed on the surface. The latter mechanism was occurred in test T3. Tribofilms are softer than steel and therefore they are more vulnerable to abrasion by soot [131]. However, in tests T4 both tribofilm and metallic surface were removed and resulted in a severe wear. Table 9-3 summarises the results from this section.

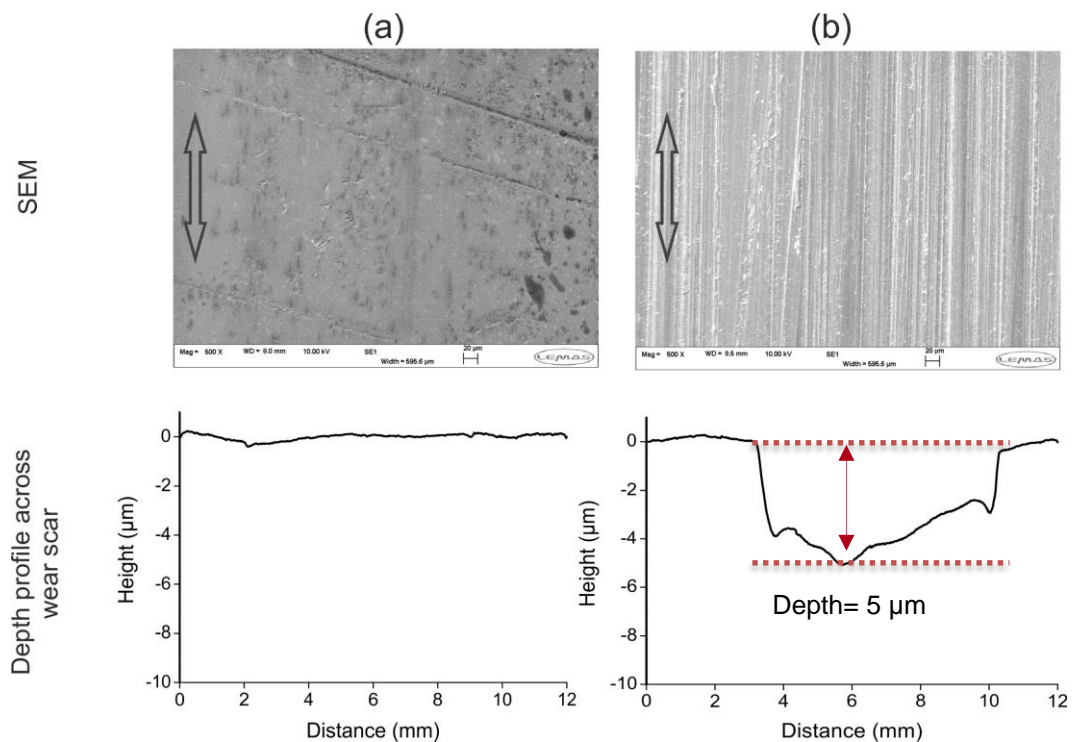


Figure 9-19. SEM images and wear scar depth for tests (a) T3 and (b) T4.



**Table 9-3. Summary of antagonistic effect of contaminants on wear**

Test	T3	T4
Causes of ageing	<ul style="list-style-type: none"> <li>• Oxidation</li> <li>• Diesel</li> </ul>	<ul style="list-style-type: none"> <li>• Oxidation</li> <li>• CB particles</li> </ul>
contaminants added after ageing (96h)	CB	Diesel
Effect of added contaminants	Abrasion	Oil dilution
Conclusions	<ul style="list-style-type: none"> <li>• Not severe wear</li> <li>• Abrasion by CB was probably not the dominant mechanism of producing high wear</li> <li>• Tribofilm removal by CB particles</li> </ul>	<ul style="list-style-type: none"> <li>• Severe wear</li> <li>• Antiwear additives properties is lost during the ageing process as a result of additive adsorption</li> <li>• No tribofilm formed, therefore CB particles abrade steel surface</li> </ul>

### 9.5.3 Effect of filtration on oil performance

The aged oil with 2 wt% CB and diesel was filtered to investigate how oil would function after removing of the CB particles. The filtration was conducted for one hour with the speed of 12000 rpm to remove the CB particles as far as practical. Tests with such oil provide wear results in which the effect of CB particles (third-body abrasion) was eliminated. As can be seen in Figure 9-20, the removal of CB from oil resulted in lower wear (21% reduction) compared to the unfiltered oil.

Figure 9-21 indicates the SEM images of wear scar formed by filtered and unfiltered oils. The wear coefficient was still high and the scratches on the wear scars prove that abrasion was taking place in both tests. Therefore, the lack of tribofilm on the wear scars and metal-on-metal contact can be responsible for the high wear observed. This statement was confirmed by

Raman analysis which only indicated iron oxide peaks in the wear scar (Figure 9-22).

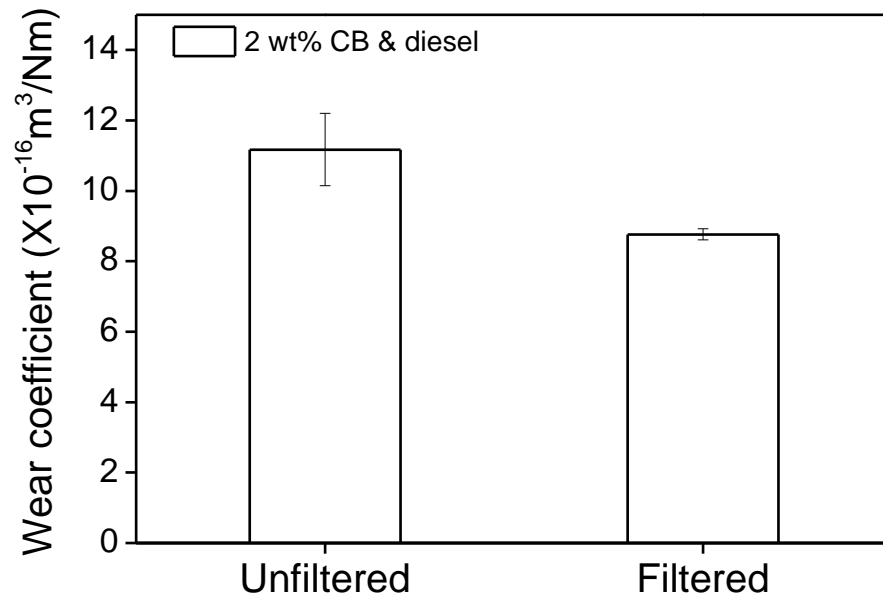


Figure 9-20. Wear coefficient for tests conducted with unfiltered and filtered FFO containing 2 wt% CB and diesel.

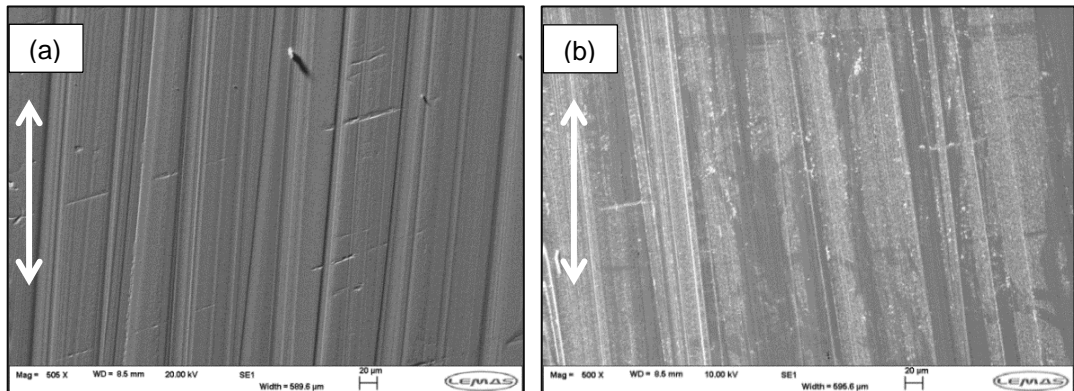
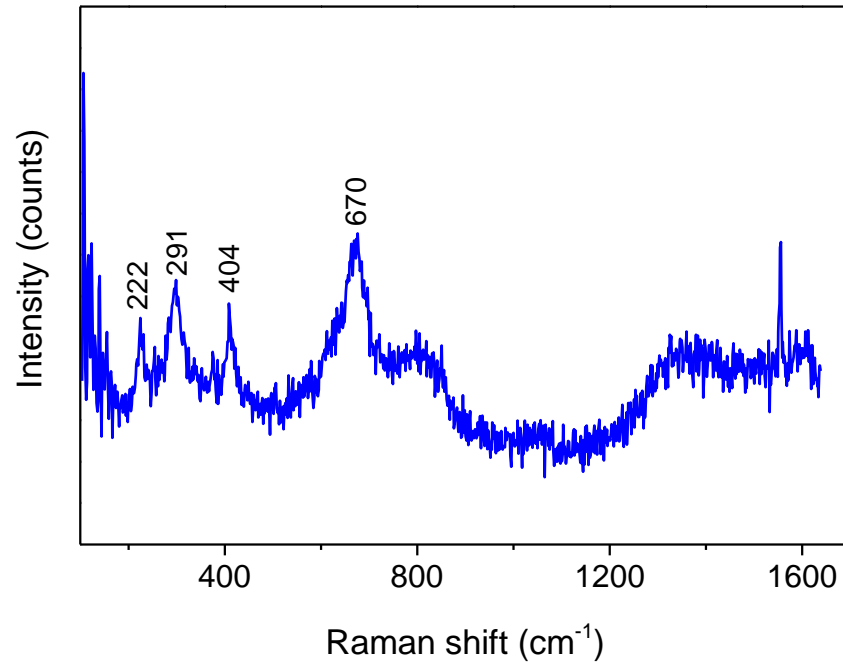


Figure 9-21. The wear scar formed on vane samples by aged oil with %2wt CB and diesel (a) non-filtered (b) filtered.



**Figure 9-22. Raman spectra of wear scar of vane sample after tests with the filtered oil (T5).**

## **9.6 Summary**

In this study friction and wear behaviour of vane-rotor contact were studied using various contaminants and varying ageing times. The results from FTIR, SEM/EDX and Raman analysis together provided a consistent explanation of the wear mechanism and surface chemistry. The following conclusions can be drawn from the results presented in this study:

- Viscosity of the oils increased slightly during the ageing process, however there was no significant variation in the viscosity of oils with various contaminants at higher temperature.
- Total acid number increased during the ageing process. The increase in TAN was significantly high when CB was presence in the oil during the ageing process.

- Wear significantly increased during the ageing process when the CB contaminates the oil.
- Removal of CB particles from the oil reduced wear slightly, however wear was still high. This showed that abrasive mechanism by CB particles (*i.e.* mechanical action) was not the main factor contributing in high wear. Therefore, additive depletion and additive adsorption by CB particles (*i.e.* chemical action) have been the dominant mechanisms which promote wear.
- When surfaces are lubricated by diesel-contaminated oil, wear and friction decreased slightly due to the lubricity of diesel which contains sulphur components.
- In the presence of all contaminants, higher wear was observed due to the antagonistic effect of contaminants in FFO.

## Chapter 10 Discussion

In the first phase of this study (Chapter 5), a comprehensive failure analysis on the failed VDVP was conducted. The results showed that oil contamination could be one of the potential causes of the severe wear observed which has led to the failure of the pump. In the literature review, it was discussed that several studies have reviewed the effect of different design parameters on the performance of VDVP. However, no study has investigated the effect of oil contamination on tribological performance of VDVP. Therefore, this study has explored the effect of oil contaminations such as soot and diesel on tribological performance of contacts in the boundary lubrication regime, which is the most dominant lubrication regime in VDVP.

On the other hand, many studies have investigated the effect of oil contamination, in particular soot, on friction and wear behaviour of contacts. However less studies have considered the combined effect the oil ageing process in the presence of these contaminants, which is considerably closer to a real condition. Thus, this research has also investigated the effect of oil contamination on the oil properties and tribological performance of contacts during the ageing process. In this part of the study, the actual samples from VDVP were used in order to ensure the tests simulate the real pump conditions as far as practical.

In this chapter, the following topics will be discussed:

(1) The effect of CB contamination on the properties of oil and tribological performance of contacts (refer to results presented in Chapter 6); specifically:

- The link between low friction and CB contamination
- The link between sliding configuration and friction
- Corrosive-abrasive wear induced by CB contamination

(2) Tribological performance of diesel-contaminated oils in the boundary lubrication regime

(3) The effect of ageing duration on tribological performance of contaminated oils

### 10.1 The effect of CB on the bulk properties of oils

The results presented in Chapter 6 demonstrated that adding CB to FFO increased the viscosity of the oil. However, as temperature increased the difference between the viscosities of the oil samples containing different levels of CB became negligible as shown in Figure 10-1. Green *et al.* [121] reported that addition of CB to FFO increased the viscosity of the oils consistently in both 40 and 100°C. However, these results are in conflict with another study by Hu *et al.* [72] who showed that viscosity of FFO did not change significantly when CB was added. The results presented in Chapter 6 are also in line with Hu *et al.* [72].

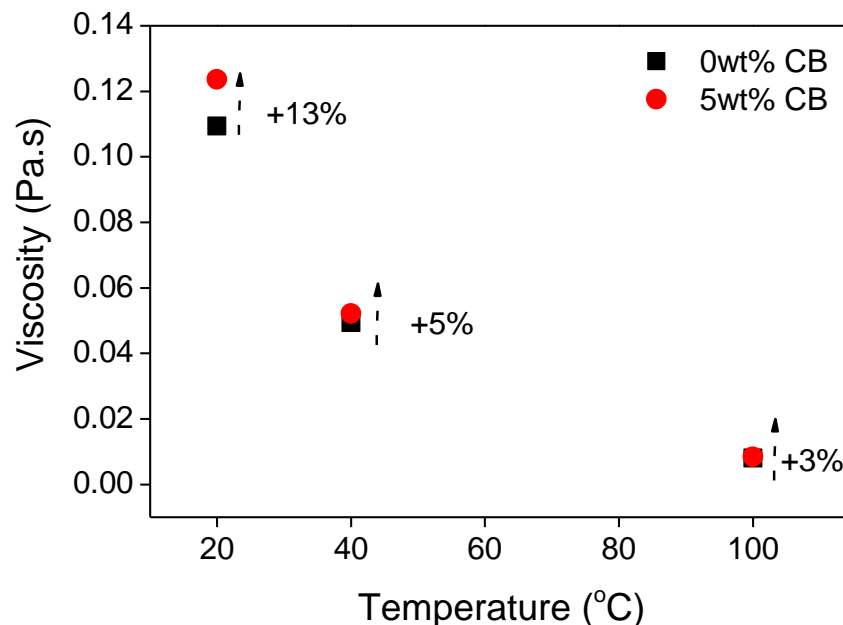
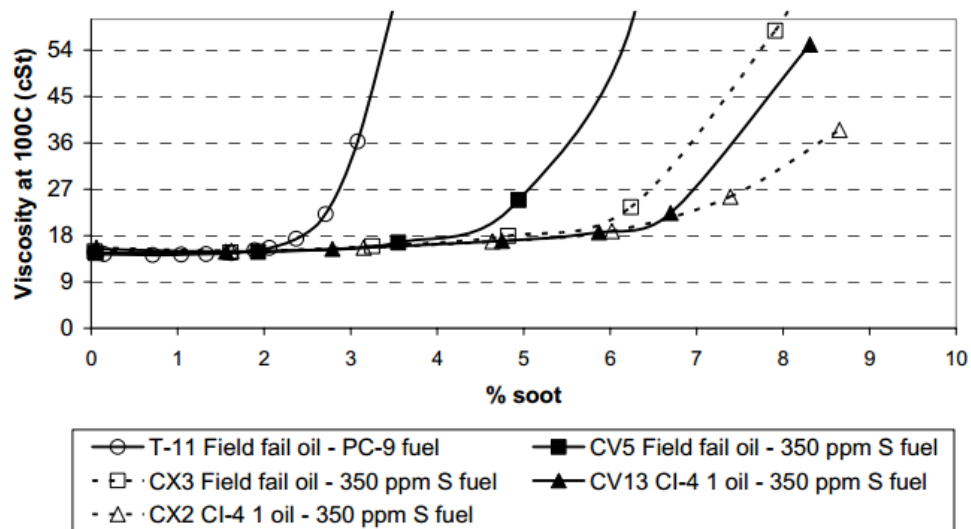


Figure 10-1. Variation in viscosity of FFO and FFO+5wt% CB at different temperatures.

Duncan *et al.* [191] found that different types of engine oils contaminated with soot had different trend in viscosity. The viscosity of some oils increased significantly at lower levels of soot. However, viscosity of the other oils did not even change with 6 wt% soot (Figure 10-2). This variation in viscosity of the oils depends on the oil properties, such as additives. Viscosity modifiers have proven to be beneficial in controlling the soot-related viscosity changes [190]. Other additives such as polymers and dispersants are found to be effective in dispersing the soot particles in the engine oil in order to prevent viscosity changes [192]. Devlin *et al.* [133] showed that oils containing polymers and dispersants have excellent viscosity control in the presence of soot particles.

Thus, it can be concluded that the viscosity of FFO used in this study did not increase significantly when CB was added in high temperatures due to viscosity modifier additives in FFO. As such, the presence of CB in oils did not have any significant influence on the lubrication regime in the experiments (see Table 6-1). Therefore, it can be argued that the difference between friction and wear results is related to the tribochemistry of samples.



**Figure 10-2. Comparison of viscosity of different oils in the presence of soot. Experiments were conducted in engine tests with different oils [191].**

## 10.2 The link between friction and CB contamination

In the previous studies [72, 118, 121-123] there have been contradictory reports on the influence of soot or CB on friction performance. As summarised in Table 3-1, it was observed that friction coefficient varied significantly depending on the test conditions. Liu *et al.* [122] showed that friction behaviour of oils containing soot is very much dependent on their formulation.

In the current study, the results showed a drop in the friction coefficient (Figure 6-2 and Figure 6-3). As mentioned in Section 10.1, the viscosity of the oils did not change significantly with different CB levels at a given temperature. Thus, the decrease in friction coefficient by adding CB in the oils could not be related to the changes in the viscosity. Therefore, the existence of CB particles in the oils should be responsible for the lower friction.

Some studies [110, 118] have found that CB can only reduce the friction when it is uniformly dispersed in the oil using dispersants. In absence of a dispersant, CB agglomerates at the inlet of the tribocontact and causes oil starvation which results in high friction [118]. Fujita *et al.* [125] proved that oils with a better ratio of dispersant to soot reduced friction further. This was explained by the particles passing through the surfaces more uniformly and removing the high friction ZDDP tribofilm and reducing friction. Thus, at the contact interface, CB is able to reduce friction by the following mechanisms:

1. Removing the high friction ZDDP tribofilm formed on the surfaces.
2. Passing through the contacts and acting as a friction modifier since it has a similar structure to graphite which is a well-known solid lubricant.

Thus it can be argued that the low friction observed in this study (when CB was added to the oil) was due to good dispersion since the FFO contained dispersants. The high friction ZDDP tribofilm was then removed by CB particles and these particles could act as a solid lubricant. This is in line with



the chemical analysis of tribofilm in Section 6.6 which confirmed that there was no element of ZDDP tribofilm inside the wear scar when oil contained CB.

In this study, experiments with FFO+CB were conducted under both unidirectional sliding (see Chapter 6) and reciprocating sliding conditions (see Chapter 9). The results showed that the nature of the sliding contact is another factor that can affect the frictional results. In the following section the implication of these two conditions will be discussed in detail.

### **10.3 The link between sliding configuration, friction and wear**

The results presented in Chapter 6 showed a significant reduction in friction when CB particles were present in FFO in unidirectional sliding ball-on-disc experiments. In contrast, significantly less reduction in friction was observed in reciprocating sliding experiments using TE77 presented in Chapter 9. The test conditions were set such as the contact pressure, test duration, oil and CB content were similar in both experiments.

Figure 10-3 compares friction results obtained under unidirectional sliding and reciprocating sliding. One possible reason for obtaining higher friction under reciprocating condition can be that CB particles could not easily pass through the surface due to the constant change in the direction of the movement. In other words, the oil displaced by the contact during the forward stroke is not fully replaced during the reverse stroke. Therefore the CB particles are less likely to be present at the contact to act as solid lubricants. In contrast, in the unidirectional sliding condition, the CB particles are consistently pushed by the oil to the contact surfaces. Figure 10-4 illustrates the schematics of both contacts in tribotests. These results can also explain the conflicting friction values reported in the previous studies summarised in Table 3-1 where different sliding configurations were used.

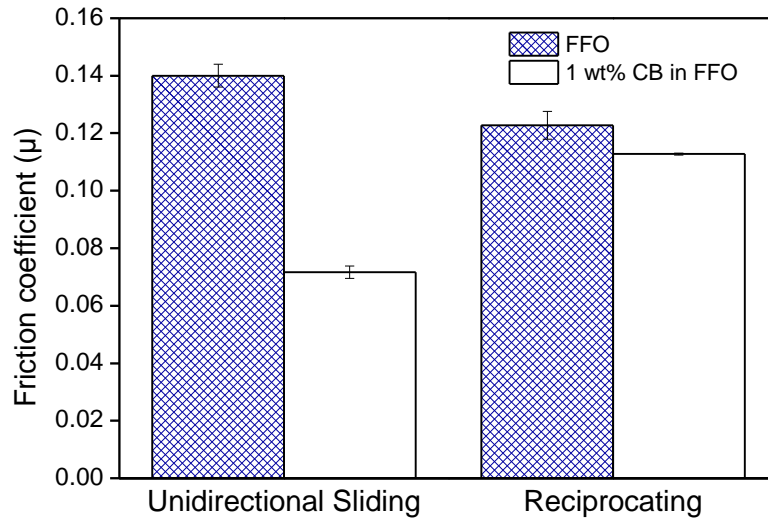


**Figure 10-3. Friction comparison of FFO and FFO+1wt% CB at different sliding configurations. Two hours tests at 100°C.**

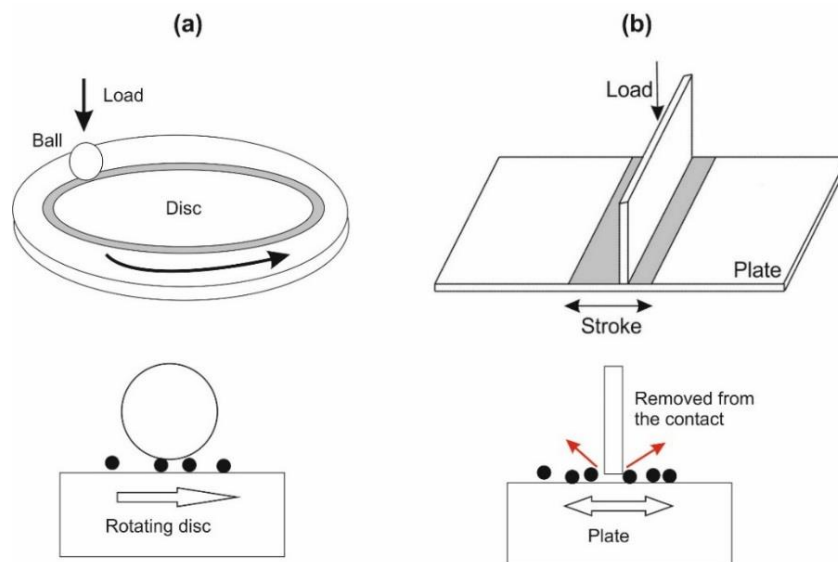


**Figure 10-4. Geometric configuration of tribosystems used in (a) unidirectional sliding (b) reciprocating tests.**

Figure 10-5 compares the wear results of FFO and FFO+1wt% CB in different sliding conditions. It can be seen that aside from the friction results, the wear results provide further evidence of more CB particles in the contact areas under the unidirectional sliding condition.

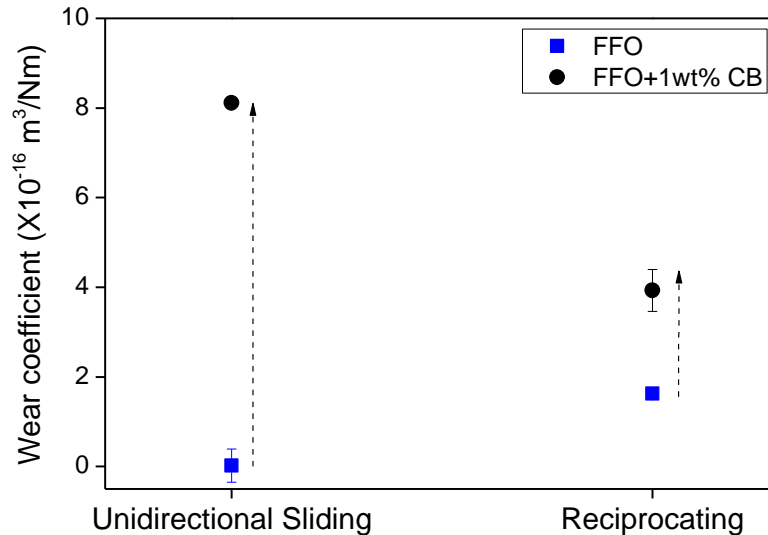


**Figure 10-5. Wear performance of FFO and FFO+1wt% CB at different sliding configurations under two hour tests at 100°C.**

### 10.4 Wear mechanism induced by carbon black

It has been reported that ZDDP antiwear films are rapidly removed in the presence of CB [114]. The lack of ZDDP tribofilms in tests with FFO+CB can be due to either abrasion; or antiwear additive adsorption on CB particles [72]. The results presented in Chapter 6 demonstrated that abrasion was not the main wear mechanism where oil contained CB particles. Also, the results in Chapter 7 showed that additive adsorption on CB particles was not significant after two hours tests. Thus, abrasion and additive adsorption mechanisms do not necessarily explain the high wear induced by CB in FFO.

Olomolehin *et al.* [114] observed that wear increased by more than 2000 times when ZDDP was added to model oils (mineral oil + dispersant) containing 5 wt% CB. They also showed that the combination of ZDDP with CB in base oil gave significantly higher wear than either ZDDP or CB alone. As a result, they proposed that the interaction between ZDDP and CB was responsible for high wear observed in the oils containing phosphorous-based and sulphur-based additives. This antagonist interaction between ZDDP and CB is known as a

corrosive-abrasive wear process. Uy *et al.* [115] demonstrated that the presence of CB in various oils had different wear results. They showed that for one type of oil, FFO+CB had higher wear than a model oil containing CB. The model oil was composed of base oil, dispersant and viscosity improver. They justified these results with the antagonistic interaction of ZDDP and dispersant in FFO.

In this study, the wear results are in agreement with Olomolehin *et al.* [114]. Figure 6-13 in Chapter 6 showed that FFO+CB had much higher wear than model oil+CB. The results from this study back up the corrosive-abrasive mechanism suggested by Olomolehin *et al.* [114]. In this research, it is believed that this mechanism is likely to be responsible for the exceptionally high wear observed with FFO containing CB since extremely high wear was only observed with FFO and not with BO.

In the corrosive-abrasive mechanism, the phosphorous or sulphur-based tribofilms which are formed on the steel substrate are easily removed through abrasion by CB particles leaving a nascent metal surface. The steel substrate can become prone to wear by CB particles due to the lack of protective tribofilm. This metal surface can also form iron oxide which can react with sulphur in ZDDP. It has also been reported that active sulphur has a significant effect on increasing wear [147]. In summary, ZDDP reacts with the surface to form tribofilm however the film is constantly removed by CB particles. Since the formation of the tribofilm involves intermixing of the substrate (Fe) with the additive, the removal of the antiwear films also results in the removal of the substrate. The cycle of formation of tribofilm by the additives and removal by CB particles continues and promotes wear (Figure 10-6).

This mechanism would explain the higher wear observed in FFO in comparison to BO. With BO, unlike FFO, no antiwear tribofilms were continually formed and removed; and the wear in tests with BO is purely due to the bore-polishing effect of the CB.

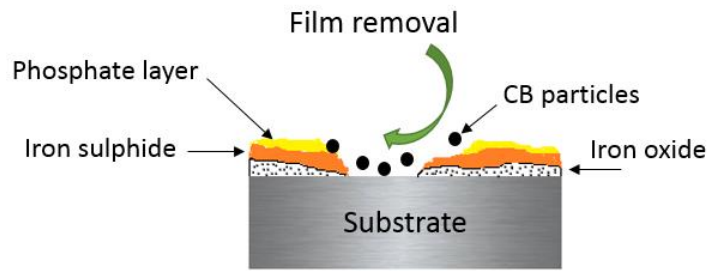


**Figure 10-6. Schematic image of corrosive-abrasive wear mechanism by CB particles- adopted from Booth *et al.* [147].**

Figure 10-7 shows the important parameters that influence on the corrosive-abrasive wear mechanism. There are two processes that occur simultaneously in the corrosive-abrasive wear mechanism; *i.e.* tribofilm formation and tribofilm removal by CB particles. The rate of tribofilm formation would be determined by parameters such as temperature while the rate of tribofilm removal would be determined by CB content. The wear results obtained is dictated by the rates of the two processes. It has been suggested [114] that the rate of tribofilm formation is the rate-determining step in the corrosive-abrasive wear process. This means that high wear would be observed at higher temperatures and vice versa. However, there has been no experimental proof for this effect [114].

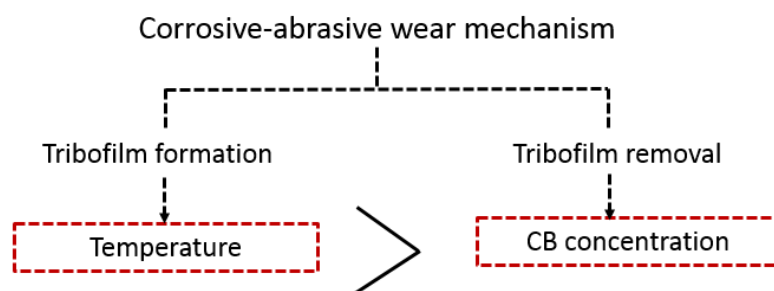


**Figure 10-7. Important factors in corrosive-abrasive wear mechanism.**

By analysing results obtained in this study at varying temperatures and CB content levels it is possible to determine which process has been the rate-determining step in the wear process. At a given temperature, increasing the

CB concentration resulted in an increase in wear. The increase in wear can be attributed to the increase in the rate of tribofilm removal as the amount of abrasives at the contact increases. Also, at any given CB content level, significantly higher wear was observed at 100°C than 40°C. Thus, it was observed that the effect of temperature on wear was more significant than the effect of CB content (see Figure 10-8).

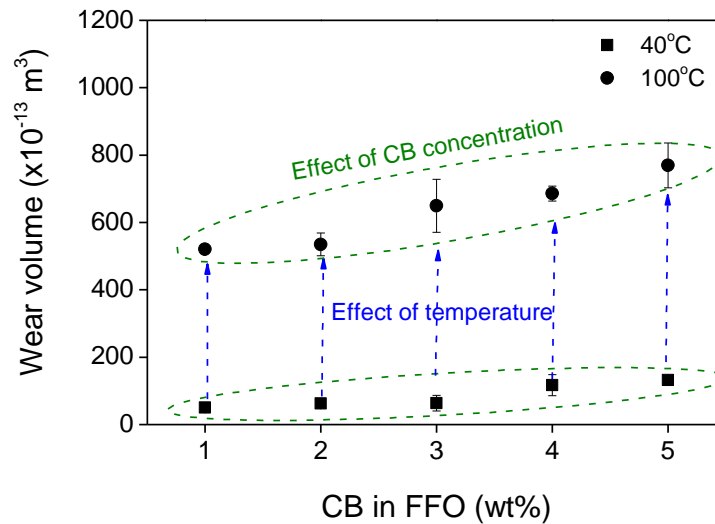


**Figure 10-8. Effect of CB concentration and temperature on wear.**

These results indicate that the rate of tribofilm formation had a higher impact on wear than the rate of tribofilm removal. This observation can be explained by the fact that at higher temperatures, additive decomposition is faster and the surfaces are more reactive to additives. Thus, the rate of tribofilm formation is more significant at higher temperatures than at lower temperatures [180]. Consequently, the faster tribofilm replenishment at the higher temperature is quickly followed by tribofilm removal causing higher wear.

The results of this study therefore confirm that the rate of tribofilm formation is indeed the rate determining step in the corrosive-abrasive mechanism. This is the first time that such a mechanism has been proved experimentally and

highlights the importance of tribochemical reactions between carbon black particles and P-based and S-based additives in the oils.

### **10.5 The effect of diesel fuel on wear reduction and tribofilm formation**

The effect of diesel contamination in the FFO on tribological behaviour of contacts under boundary lubrication regime was investigated in Chapter 8. In general, FFO diluted with diesel fuel showed lower friction and wear at both 40°C and 100°C temperatures. Higher levels of diesel in FFO reduced the wear further at 40°C, however there was no significant difference in wear with different level of diesel at 100°C. Surface analysis results in Section 8.6 clearly showed that a more uniform tribofilm was formed at 100°C. This is thought to be due to the activation of additives in FFO at high temperature which then form a protective film regardless of diesel concentration.

As explained in Chapter 3, diesel fuel contains a long chain of hydrocarbon “tail” and other elements at the “head” which have a beneficial lubricity effect on diesel. The lubricity of diesel fuel is due to the existence of polar heads such as sulphur [101, 193]. Unlike the hydrocarbon tails, these heads tend to escape from the non-polar hydrocarbons and form a bond with other polar elements such as the additives in FFO, metal and degradation particles [103].

Agarwal *et al.* [101] reported that the diesel fuel has a lubricity characteristic due to the additives which contain a range of chemicals with active surfaces. They described that these additives have an affinity for metal surfaces and form boundary films to protect metal [101]. The mixture of both diesel fuel and additives in FFO leads to a competition between the additives and fuel compounds for reacting with the metal surfaces [103]. Therefore, it is possible that diesel compounds, which are polar, competitively adsorb on the surfaces and protect surfaces [194, 195].

The lower wear observed with oil containing diesel indicates that sulphur in the diesel fuel interact with the metal surface to form iron sulphide and reduce wear. The formation of FeS on the metal surface was shown to be effective on reducing wear since it has a load carrying effect [196]. The EDX results in Chapter 8 demonstrated the presence of sulphur in all the wear scars formed with diesel in oil. Raman analysis also indicated the formation of FeS film throughout the wear scar. The presence of sulphur on the wear scar of samples using BO+diesel confirmed that sulphur in diesel can interact with the metal and protect the surfaces (Figure 8-11).

Thus, the reason for the lower friction and wear observed in the presence of diesel contamination can be attributed to the lubricity of diesel fuel.

## **10.6 Effect of ageing on tribological behaviour of oils**

In this study, the effects of the ageing process on the bulk properties of FFO with both diesel and CB contaminants were investigated. In addition, the tribological performance of FFO and tribochemistry of wear scars were studied in detail. This section provides a detailed discussion on the results presented in Chapter 9.

### **10.6.1 Effects of ageing process and contamination on oil**

The results presented in Figure 9-2 and Figure 9-3 showed an increase in the viscosity of oils during the ageing process. This increase was expected due to the oxidation of the oil [197]. George *et al.* [190] stated that the variation in viscosity depends on the formulation of oil, type of additives and their concentration in the oil. As explained in Table 2-1, additives in FFO protect the oil from oxidation and acid formation [8]. In addition, the FFO used in this study was a synthetic oil which is proven to be more resistant to oxidation than mineral oils [198].



It was observed that the total acid number (TAN) of oils has changed based on the type of contaminants (see Figure 9-4). The ageing process was conducted on the high temperature and in the presence of oxygen that together provide a suitable environment for oxidation of oil. As explained in Chapter 3 Figure 3-26, the oxidation of oil results in formation of organic acids. The increasing trend of TAN in aged oils can be attributed to the oxidation of the oil constituents and formation of carboxylic acids [197, 199]. Thus, the formation of carboxylic acid during the ageing process is a good indicator of oil degradation. FTIR results presented in Section 9.2.3 clearly demonstrated the formation of this band at  $1720\text{ cm}^{-1}$  after 96 of ageing for all samples. The presence of this peak was stronger in the samples containing CB (Figure 9-8).

From the results presented in Chapter 9, it can be seen that TAN increased by approximately four times when CB was present in the lubricant during the ageing process (see Figure 9-4). This is in agreement with the literature which suggests that oxidation of oils is enhanced in the presence of soot. This has been explained by two potential mechanisms as follows:

- The acidic nature of CB particles, which interact with oxygen during the ageing process, accelerate the degradation process of the oil to form inorganic acids [200].
- The presence of metallic catalyst during the ageing process and source of oxygen are two important factors that could cause oxidation to occur in carbon black surface areas. Metallic catalysts are known to influence the rate of oxidation of carbon black particles. It has been suggested that the oxygen disrupts the crystalline structure of the CB to a depth of 10 to 20 Å from the surface. This leads to change of  $sp^2$  hybrid bonding to  $sp^3$  which is more acidic [201].

The exact chemical process of CB oxidation is outside the scope of this study, however, the results presented in this study are in line with this theory. In general, these results suggest that under high temperature condition and

exposure to air, oil has gone through oxidation and experienced more severe degradation. This is in line with higher wear results observed with CB contamination, which will be discussed in next section.

### 10.6.1.1 Effects of ageing on friction and wear

The comparison of the friction and wear results of the fresh and aged oils samples (Figure 9-11) indicate that additives in oil were still effective even after ageing and oxidation processes. FTIR results showed that the chemical structure of additives did not change during the ageing process. All peaks were still present even after the ageing process. This behaviour is thought to be due to the anti-oxidant additives in FFO which delayed the oxidation process [8]. Penchaliah *et al.* [123] reported that oxidation of the oil for 10 hours at 170°C had a negligible effect on wear as shown in Figure 10-9(a). They also showed a variation in friction coefficient with different levels of oxidation (Figure 10-9(b)). However, they could not explain the reason for this variation in friction. They believed that increasing viscosity results in higher friction level associated with the formation of viscous tribofilm under hydrodynamic lubrication regime [123]. It is worth noting that in the current study all experiments were conducted under boundary lubrication regime in which chemical composition of lubricants have a greater effect than physical properties of lubricants.

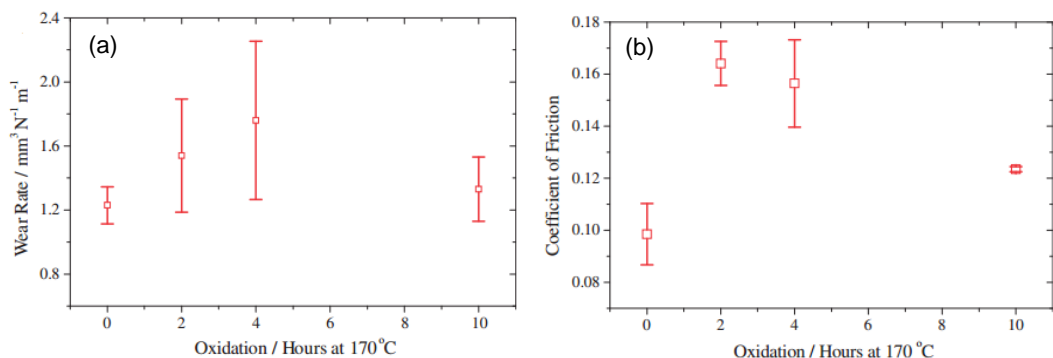


**Figure 10-9. Wear and friction behaviour of oil under 10 hours of oxidation [123]**

There have been several debates on the effect of ageing on the tribological performance of oils containing ZDDP. Devlin *et al.* [202] showed that tribofilm characteristics are different when using fresh oil and aged oils. Barnes *et al.* [203] stated that the degradation of ZDDP could either increase or decrease wear based on different mechanisms. Fuller *et al.* [83] showed that preheated ZDDP at temperature of 150°C up to 24 hours resulted in higher wear than fresh oil. Coy *et al.* [204] reported that the aged oils containing ZDDP provided better wear performance than the fresh oils. A lot of previous research works [49, 69] have shown that the antiwear protection ability of ZDDP in the oil is due to its decomposition. They believed that the ageing of the oil results in decomposition of ZDDP which reduces the wear.

Devlin *et al.* [202] examined different types of ZDDP additives to understand the relationship between ZDDP structure and performance of aged oils. It has been shown that different types of ZDDP additive decompose at different rates and the decomposition products have different tribofilm properties. Therefore, it has been concluded that the ability of ZDDP additives to reduce friction and wear greatly depend on the engine operating conditions and ZDDP structure.

In this study, the EDX and Raman analysis on the wear scar of vane samples (Figure 9-13) indicate the presence of phosphate films even after ageing. This is attributed to the decomposition of ZDDP additive in FFO. The presence of phosphate and zinc phosphate tribofilm within wear scars even after 96 hours of ageing is consistent with the low wear observed by FFO in Figure 9-11.

#### **10.6.1.2 Effect of diesel contamination on tribological performance of lubricants**

Friction and wear slightly decreased with diesel-contaminated oil. Similar results obtained in Chapter 8. This low wear can also be attributed to the sulphur which lead to the lubricity of oils as explained in Section 10.5 [101, 193]. A new sulphate peak at 1040  $\text{cm}^{-1}$  was appeared in FTIR spectra after

96 hours of ageing oil with diesel (Figure 9-7). The formation of this peak can be attributed to the interaction of additives and sulphur in diesel during the ageing process. EDX and Raman analysis for diesel contaminated oil confirmed the existence of tribofilm on the wear scars even after 96 h of ageing. The lower wear observed with diesel-contaminated oil is believed to be related to the existence of sulphur composition in diesel fuel which promotes formation of a better tribofilms.

### **10.6.1.3 Aged oil with carbon black**

The highest effect on wear was observed when CB particles were present in FFO during the ageing process. Wear increased significantly during the ageing process from 0 to 96 hours. EDX and Raman did not show any elements of ZDDP tribofilm in the wear scars. This can be attributed to the lack of tribofilm due to either abrasion or the additive adsorption during the ageing process. Various mechanisms have been proposed for CB such as removal of tribofilm by mechanical action (abrasion) [131] or the interaction of CB and additives by chemical action during the ageing process [143]. These mechanisms will be discussed in more detail in the following sections.

- **Effects of abrasion**

Many studies [110, 123, 129, 130, 132] have reported that the increase in wear by soot was related to the abrasive nature of soot. In this study, the experiments presented in Section 9.5.1 demonstrated that the tests which were conducted with the same levels of CB particles (1wt%) showed different levels of wear. Figure 10-10 compares the wear coefficient and the average depth of wear scars on sample using different oils. The difference between the wear results with oils containing 1%wt CB suggests that abrasion is not the dominant wear mechanism, since similar wear would be expected with the same concentration of CB. Even higher levels of CB (2wt%) showed less amount of wear in comparison to the aged oil which contained 1wt% CB

during the ageing process. Thus, it can be concluded that the high wear observed in aged oil containing 1wt% CB cannot be simply justified by abrasion. These results suggest that the existence of CB in the oil will not necessarily cause severe wear during the tribological tests due to abrasion or mechanical action. Thus, the results presented in this study contradict the concept that suggests abrasion-induced wear is the main mechanism [110, 123, 129, 130, 132].

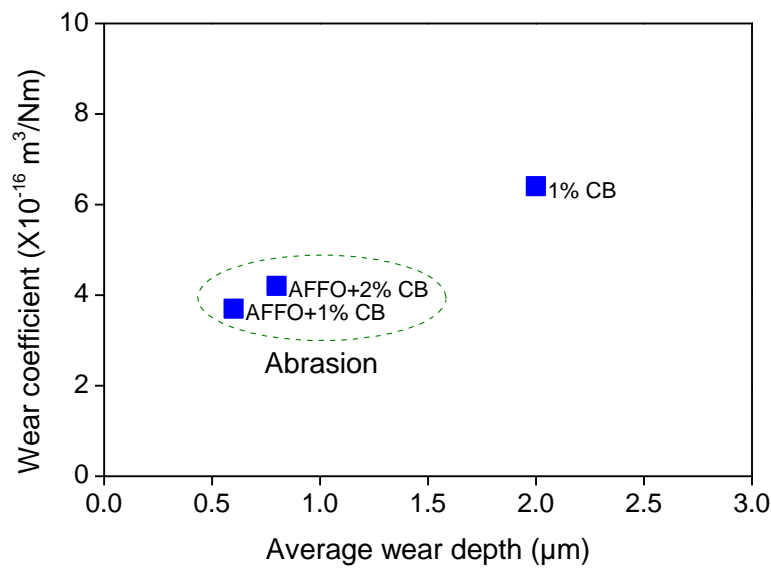


**Figure 10-10. Wear coefficient and average wear depth of wear scar of vane samples using aged FFO with 1wt% CB, aged FFO then adding 1wt% and 2wt% CB.**

- **Antiwear additive adsorption**

The difference in wear results as shown in Figure 10-10 [110, 129, 130, 132] can be explained by additive adsorption mechanism on soot particles [107, 127]. The results presented in 9.5.3 demonstrated that removing the CB particles from the oil reduced wear only by 21%. Thus, the high wear observed indicates that another mechanism were responsible for the high wear which is more dominant than abrasion effect. Rounds [127] suggested that soot particles adsorb the decomposition products of antiwear additives leading to high wear. The results presented in Chapter 7 demonstrated that ZDDP

additive adsorption on CB particles occurred after 96 h of ageing. Hosonuma *et al.* [142], Berbezier [140] and Gautam [143] believed that the oil could still perform with the remaining phosphorus compounds within the oils after zinc-containing compound adsorption by soot. The results presented in this study are in contrast with this statement. Raman analysis on the wear scar of T5 test did not show any ZDDP elements in the tribofilm. Therefore, the high wear and the lack of tribofilm on the wear scar suggest that even after removing of the particles the oil was not able to generate tribofilm. Considering the fact that additive adsorption occurs during the ageing process, these results suggest that additive adsorption is more dominant than abrasion. In other words “additive adsorption” and “corrosive-abrasive mechanism” (which was explained in Section 10.4) are the key wear mechanisms.

### **10.6.2 Ageing oil with diesel and carbon black**

The wear results in Figure 9-11 showed that the combination of CB and diesel had an antagonistic effect on wear compared to the individual effect of each contaminants on wear. The tests in Section 9.5.2 were investigated this mechanism.

As discussed in Section 10.6.1, the oil properties were not affected by diesel contamination during the ageing process. Thus, when CB was added to the aged oil in test T3, the most likely wear mechanism was abrasion of tribofilm formed on the surfaces by CB particles as shown in Figure 10-11.

When CB was present in FFO during the ageing process and then diesel was added before the tests, there are a combination of factors that produce high wear; such as the interaction between contaminants and additives during the ageing process (mainly additive adsorption), abrasion by CB particles, corrosive-abrasive mechanism and oil dilution by diesel. As discussed in Section 10.5, diesel in oil did not have a negative effect on wear. Therefore, it

can be concluded that the combination of additive adsorption, abrasion and corrosive-abrasive mechanisms produced the higher wear in T4 (Figure 10-11). In this section, comparison of T3 and T4 indicates that the additive adsorption of CB and corrosive-abrasive mechanism which are both chemical wear are dominant mechanisms compared to abrasion.

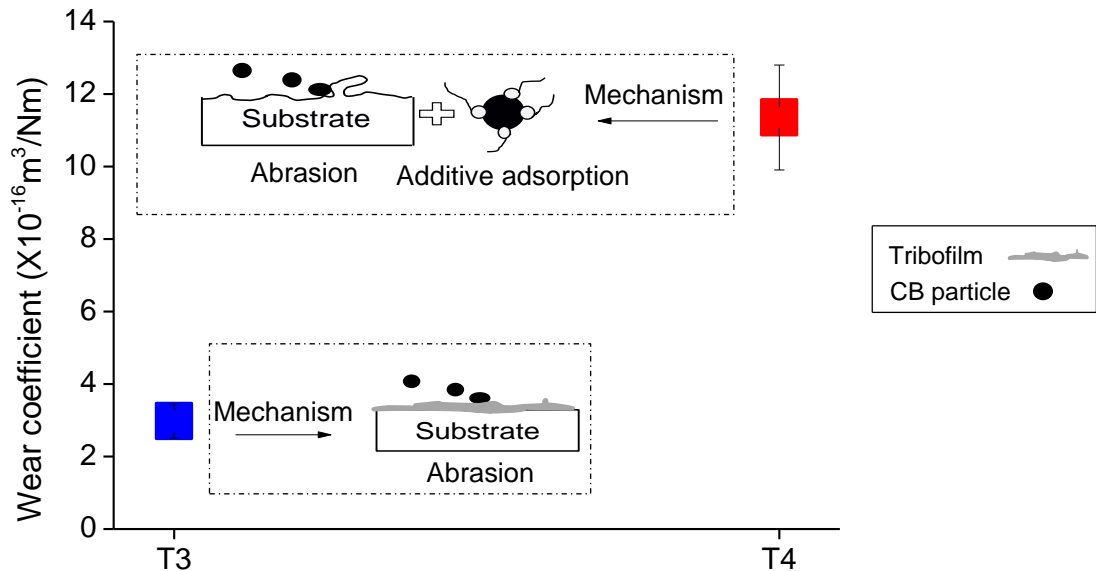


**Figure 10-11. Comparison of wear results and potential wear mechanism between T3 (aged diesel-contaminated oil then adding 1wt% CB) and T4 (aged CB-contaminated oil Then adding 1wt% diesel)**

In summary, the results presented in Chapter 9 indicate that the ageing process on its own did not have a significant effect on the performance of FFO used in this study. However, when CB was present in FFO during the ageing process it led to more severe wear. This study contradicted all previous studies that suggested that abrasion (*i.e.* mechanical action) by CB particles is the main mechanism producing high wear in engine components [110, 129, 130, 132]. This study proves the role of more dominant wear mechanisms in the presence of CB particles, *i.e.* “antiwear additives adsorption” and “corrosive-abrasive wear”, which both have a chemical nature.

## **Chapter 11 Conclusions and future work**

### **11.1 Conclusions**

This chapter summarises the conclusions derived from the various works presented in this thesis. This study has provided an insight into the effect of oil contamination on tribological behaviour of contacts in the boundary lubrication regime. Finally, this chapter provides a series of recommendations for future works on this subject.

The key findings of this research are summarized in the following sections.

#### **11.1.1 Effects of contaminants and ageing on the bulk properties of FFO**

Three main conclusions have been derived with regards to the effects of CB and diesel on the bulk properties of FFO, which are summarised in this section.

##### **11.1.1.1 Effects of contaminants on the viscosity of oils**

- Overall, the viscosity of the oils decreased by increasing the temperature from 20°C to 100°C. At ambient temperature (20°C), the viscosity of the oils increased by adding more CB concentration in the oil. However, this increase in viscosity became negligible at higher temperatures.
- The viscosity of oil decreased by adding higher levels of diesel. However this variation in viscosity became negligible at 100°C.



#### **11.1.1.2 Effects of oil ageing on the viscosity of oils**

- There was an increase in viscosity of all oil samples from 0 h to 96 h during the ageing process. This is due to the oxidation of oils during ageing process.

#### **11.1.1.3 Effects of oil ageing on the TAN values**

- TAN values of different oil samples through ageing process has generally increased. There was a slight increase in the TAN values of AFFO and diesel-contaminated oil. This shows that the FFO used in this study contains effective anti-degradation additive
- The changes in TAN values are found to be linked to the existence of CB in the oils during the ageing process. The aged oil with CB particles showed significantly higher TAN values after the ageing process. This can be attributed to the acidic nature of CB which accelerate the degradation process and the formation of acids.
- The change in TAN was highly dependent on the type of contaminant that presents in the oil during the ageing process.

#### **11.1.2 Effect of CB on the tribological performance of oil**

- The tribological performance of oil contaminated with different CB concentration was studied in Chapter 6. It was observed that friction reduced in the presence of CB which was explained with two mechanisms: 1) removal of high friction ZDDP tribofilm by CB 2) CB particles act as a friction modifier.
- The effect of CB on friction behaviour was dependent on the type of contact. It was observed that while CB in FFO provided friction reduction in unidirectional linear sliding conditions, similar friction reduction was not observed in reciprocating sliding conditions. This

was explained by the presence of more CB particles within the sliding interface due to the nature of contact.

- The effect of CB on wear was the main focus of this study. It was observed that the increase of CB levels resulted in higher wear at both 40°C and 100°C. Although there was no significant change in viscosity of the oils with various CB levels, the wear behaviour was different. The higher CB levels lead to higher wear and wear was also much higher at higher temperature. It can be concluded that the effect of temperature on wear was significant in the presence of CB. The high wear observed in the existence of CB cannot simply explained by abrasion. The reason was explained in section 6.7. These results proves that corrosive-abrasive mechanism occurs.
- There was a chemical reaction between CB surface and antiwear additives in the oil; which leads to antiwear additive to be adsorbed on CB particles. This mechanism is dependent on test conditions such as the concentration of CB oil and the ageing time of the oil.
- Higher concentration CB and longer ageing process increased the additive adsorption. This is believed to be related to the higher surface area of CB with higher levels of them in oil which leads to more additive adsorption.

### **11.1.3 Effects of diesel on tribological performance of oil**

- Addition of diesel to FFO reduced friction coefficient slightly at both 40°C and 100°C. This reduction in friction with diesel contaminated oil can be attributed to the lubricity of diesel present in the oil.
- Wear reduced when the oil diluted by diesel. The experiments conducted by BO+diesel, excluding the effect of additives, confirmed that the reduction in wear was due to the presence of diesel. This

statement can be explained by the lubricity of diesel fuel due to the existence of polar heads such as sulphur.

#### **11.1.4 Effects of ageing process on the tribological performance of oil**

- Ageing process on its own did not have a significant effect on the performance of FFO used in this study.
- Wear decreased slightly when oil was aged with diesel. Therefore, the lower wear was attributed to the variation in tribofilm formation and lubricity of diesel fuel due to the existence of sulphur in diesel.
- Wear increased significantly when CB was present in the oil during the ageing process. The interaction of additives and CB during the ageing process causes additive adsorption on CB particles. Therefore, for the first time it was discovered that this is the dominant mechanisms which promote wear (i.e. chemical action) in comparison to abrasion by CB particles (i.e. mechanical action).

#### **11.2 Recommendations for future work**

There are a number of variables and parameters in this study such as CB concentration, diesel, friction, wear, viscosity, TAN, tribofilm, ageing time. Detailed study of the combined effect of all these parameters can be very complex and time consuming. There are still various aspect of oil contamination which were not investigated in the current work, mainly due to time constraints. Possible future works on this subject are as follows:

- Investigate the corrosive-abrasive mechanism using various FFO, containing different levels of S-based and P-based additives, mixed with CB. This will elucidate the corrosive-abrasive wear mechanism
- Exclude the effect of other additives in corrosive-abrasive mechanism and conduct the experiments with base oil, antiwear additives and CB.

This will help to understand the exact interaction and mechanism between soot and antiwear additives in corrosive-abrasive mechanism.

- Study the entrainment of CB particles in different sliding condition. Modelling of these contact will help to consider various factors, such as configuration, velocity of oil, speed and CB particle size at the same time. All these factors will have an impact on the friction and wear behaviour of contacts in the presence of CB particles.
- Study the behaviour of other types of fuels in oil to investigate friction and wear behaviour of contact.
- Investigate the mechanism in which CB increases TAN values during the ageing process.
- Change the ageing condition to understand the effect of these conditions on oil properties and tribological behaviour of oils. For example, reducing the temperature and increasing the ageing duration.
- Develop a practical method for using soot extracted from a real engine with consistent properties in the experiments.

## References

1. K. Holmberg, P. Andersson, and A. Erdemir, *Global energy consumption due to friction in passenger cars*. Tribology International, 2012. **47**(0): p. 221-234.
2. A. Comfort, *An Introduction to Heavy-Duty Diesel Engine Frictional Losses And Lubricant Properties Affecting Fuel Economy – Part I* in SAE Powertrain & Fluid Systems Conference & Exhibition. 2003, SAE International
3. Y. Nakamura, K. Tomizawa, T. Onishi, T. Hashimoto, M. Sato, T. Tatani, A. Akamatsu, H. Inaba, and R. Aoki, *Development of Fuel Economy Engine Oil for Heavy Duty Diesel Engine*. 2015, SAE International 2015-01-2034.
4. J. Bennett and D. Chudasama, *The Use of Low Viscosity Oils to Improve Fuel Economy in Light Duty Diesel Engines*. 2000, SAE International 2000-01-2054.
5. R. I. Taylor, *Heavy Duty Diesel Engine Fuel Economy: Lubricant Sensitivities*. 2000, SAE International 2000-01-2056.
6. K. M. Jefferd, J. S. Rogerson, D. E. Copp, R. L. Brundle, and M. A. Huntly, *The Impact of Lubricants on Heavy Duty Diesel Engine Fuel Economy and Exhaust Emissions*. 2000, SAE International 2000-01-1983.
7. W. van Dam, T. Miller, G. M. Parsons, and Y. Takeuchi, *The Impact of Lubricant Viscosity and Additive Chemistry on Fuel Economy in Heavy Duty Diesel Engines*. SAE Int. J. Fuels Lubr., 2011. **5**(1): p. 459-469.
8. S. Aldajah, O.O. Ajayi, G.R. Fenske, and I.L. Goldblatt, *Effect of exhaust gas recirculation (EGR) contamination of diesel engine oil on wear*. Wear, 2007. **263**(1–6): p. 93-98.
9. D. OuYang, W. Cai, L. He, and Y. Li, *Two Types of Variable Displacement Oil Pump Development*. Proceedings of the FISITA 2012 World Automotive Congress. Vol. 190. 2013: Springer Berlin Heidelberg. 1357-1368.

10. F. Frendo, N. Novi, and R. Squarcini. *Numerical and experimental analysis of variable displacement vane pumps*. in *AITC-AIT 2006- 5th International Conference on Tribology*, . 2006. Italy.
11. G. Stachowiak and A. W. Batchelor, *Engineering tribology*. 2005. p. 832.
12. Tabor, D., *History of tribology: D.Dowson*. Tribology International, 1979. **12**(3): p. 146.
13. Martin, P., *Introduction to Tribology, Lecture notes*. 2011.
14. B.J. Hamrock, B. Jacobson, and S.R. Schmid, *Fundamentals of Machine Elements*. 1999: Thomas Casson.
15. T.A. Stolarski and S. Tobe, *Rolling contacts*. 2000, London: Professional Engineering Pub.
16. K.L. Johnson, *Contact Mechanics*. 1985, Cambridge Cambridge University Press.
17. Booth, J.E., *The Feasibility of using electrostatic charge condition monitoring for lubricant additive screening*. 2008, University of Southampton.
18. A.A. Lubrecht, C. HVenner, and F. Colin, *Film thickness calculation in elasto-hydrodynamic lubricated line and elliptical contacts: the Dowson, Higginson, Hamrock contribution*. Engineering Tribology, 2008. **223**.
19. Roelands, C., *Correlational aspects of the viscosity-temperature-pressure relationship of lubricating oils*. 1966, PhD thesis, Technische Hogeschool Delft, The Netherlands.
20. B.J. Hamrock and D. Dowson, *Elastohydrodynamic Lubrication of Elliptical Contacts for Materials of Low Elastic Modulus I—Fully Flooded Conjunction*. Journal of Lubrication Technology, 1978. **100**(2): p. 236-245.
21. S.M Hsu and R.S. Gates, *Boundary lubricating films: formation and lubrication mechanism*. Tribology International, 2005. **38**(3): p. 305-312.
22. M. Priest and C.M. Taylor, *Automobile engine tribology - approaching the surface*. Wear, 2000. **241**(2): p. 193-203.

23. C.M. Allen and E. Drauglis, *Boundary layer lubrication: monolayer or multilayer*. *Wear*, 1969. **14**(5): p. 363-384.
24. Stachowiak, G.W., A.W. Batchelor, and ScienceDirect, *Engineering tribology*. 3rd ed. 2005, Amsterdam ; Boston: Elsevier Butterworth-Heinemann.
25. G. Stachowiak, *Wear: materials, mechanisms and practice*. 2005: Wiley.
26. G.E. Totten, D. D.K. Wills, and D.G. Feldmann, *Hydraulic failure analysis: fluids, components, and system effects*. 2001, West Conshohocken, PA: ASTM.
27. H.C. Meng and K.C. Ludema, *Wear models and predictive equations: their form and content*. *Wear*, 1995. **181–183, Part 2**(0): p. 443-457.
28. E. Rabinowicz, *Friction and Wear of Materials*. 2nd ed. 1995, New York: Wiley.
29. Mortier, R.M. and S.T. Orszulik, *Chemistry and technology of lubricants*. Second ed. Friction, wear and the role of additives in their control, ed. C.H. Bovington. 1997, London: Blackie Academic & Professional.
30. H.A. Spikes, *Additive-additive and additive-surface interactions in lubrication*. *Lubrication Science*, 1989. **2**(1): p. 3-23.
31. M. Cavallari, *A Lumped Parameter Model for the Pressure and Vibration Analysis of Variable Displacement Vane Pumps*. 2011, Università degli Studi di Ferrara.
32. Powertrain, M., *Variable Displacement Variable Pressure Vane Pump System*. 2007.
33. H. Martin, *Design of hydraulic components and systems*. 1995, London: Ellis Horwood. (240)p ; 24 cm.
34. R. Gellrich, A. Kunz, G. Beckmann, and E. Broszeit, *Theoretical and practical aspects of the wear of vane pumps Part A. Adaptation of a model for predictive wear calculation*. *Wear*, 1995. **181–183, Part 2**(0): p. 862-867.
35. L. Bachus and A. Custodio, *Know and understand centrifugal pumps*. 1st ed. 2003, Oxford ; New York: Elsevier.

36. A. Kunz, R. Gellrich, G. Beckmann, and E. Broszeit, *Theoretical and practical aspects of the wear of vane pumps Part B. Analysis of wear behaviour in the vickers vane pump test*. *Wear*, 1995. **181–183, Part 2(0)**: p. 868-875.
37. M. Teodorescu, D. Taraza, N.A. Henein, and W. Bryzik, *Simplified Elasto-Hydrodynamic Friction Model of the Cam-Tappet Contact*. 2003, SAE International.
38. E. Mucchi, A. Agazzi, G. D'Elia, and G. Dalpiaz, *On the wear and lubrication regime in variable displacement vane pumps*. *Wear*, 2013. **306(1–2)**: p. 36-46.
39. Y. Inaguma and A. Hibi, *Theoretical Analysis of Mechanical Efficiency in Vane Pump*. *Mechanical Engineering Science*, 2005. **219(11)**: p. 1269-1278.
40. Inaguma., Y. and A. Hibi, *Reduction of friction torque in vane pump by smoothing cam ring surface*. *Journal of Mechanical Engineering Science*, 2007. **221**: p. 527-534.
41. Inaguma, Y., *Reduction of friction torque in vane pumps by using physical vapour deposition-coated vane*. *Mechanical Engineering Science*, 2010. **224(11)**: p. 2449-2458.
42. K. A. Blencoe and J. A. Williams, *The contact of rough surfaces carrying pressure sensitive boundary layers*, in *Tribology Series*. 2000, Elsevier. p. 45-56.
43. T. Koivula, R. Karjalainen, A. Ellman, and M. Vilenius, *The effect of oil type on wear in fluid power components*. ASTM International, 2001.
44. G.E. Totten, S.R. Westbrook, and R.J. Shah, *Fuels and lubricants handbook: technology, properties, performance, and testing*. 2003: ASTM International.
45. Inaguma, Y., *Oil temperature influence on friction torque characteristics in hydraulic pumps*. *Mechanical Engineering Science*, 2011. **0(0)**: p. 1-15.
46. D.M. Pirro, M. Webster, and E. Daschner, *Lubrication Fundamentals, Revised and Expanded*. Third ed. 2016.



47. H. Kaleli and Y. Berthier, *The mechanism of layer formation and the function of additives used in fully formulated engine crankcase oils*, in *Tribology Series*. 2002, Elsevier. p. 189-197.
48. M.A. Nicholls, T. Do, P.R. Norton, M. Kasrai, and G.M. Bancroft, *Review of the lubrication of metallic surfaces by zinc dialkyl-dithiophosphates*. *Tribology International*, 2005. **38**(1): p. 15-39.
49. P.A. Willermet, D.P. Dailey, R.O. Carter Iii, P.J. Schmitz, and W. Zhu, *Mechanism of formation of antiwear films from zinc dialkyldithiophosphates*. *Tribology International*, 1995. **28**(3): p. 177-187.
50. J.M. Martin, C. Grossiord, T. Le Mogne, and J. Igarashi, *Transfer films and friction under boundary lubrication*. *Wear*, 2000. **245**(1–2): p. 107-115.
51. Z. Yin, M. Kasrai, G.M. Bancroft, K.F. Laycock, and K.H. Tan, *Chemical characterization of antiwear films generated on steel by zinc dialkyl dithiophosphate using X-ray absorption spectroscopy*. *Tribology International*, 1993. **26**(6): p. 383-388.
52. Nehme, G., R. Mourhatch, and P.B. Aswath, *Effect of contact load and lubricant volume on the properties of tribofilms formed under boundary lubrication in a fully formulated oil under extreme load conditions*. *Wear*, 2010. **268**(9–10): p. 1129-1147.
53. H. Spikes, *The History and Mechanisms of ZDDP*. *Tribology Letters*, 2004. **17**(3): p. 469-489.
54. S. Berkani, F.Dassenoy, C. Minfray, M. Belin, B. Vacher, J. M. Martin, H. Cardon, G. Montagnac, and B. Reynard, *Model formation of ZDDP tribofilm from a mixture of zinc metaphosphate and goethite*. *Tribology International*, 2014. **79**: p. 197-203.
55. H. Fujita, R. P. Glovnea, and H. A. Spikes, *Study of Zinc Dialkydithiophosphate Antiwear Film Formation and Removal Processes, Part I: Experimental*. *Tribology Transactions*, 2005. **48**(4): p. 558-566.
56. S. Kosarieh, A. Morina, E. Lainé, J. Flemming, and A. Neville, *Tribological performance and tribochemical processes in a DLC/steel system when lubricated in a fully formulated oil and base oil*. *Surface and Coatings Technology*, 2013. **217**(0): p. 1-12.

57. M. Aktary, M.T. McDermott, and G.A. McAlpine, *Morphology and Nanomechanical Properties of ZDDP Antiwear Films as a Function of Tribological Contact Time*. Tribology Letters, 2002. **12**(3): p. 155-162.
58. J.M. Martin, C. Grossiord, T. Le Mogne, S. Bec, and A. Tonck, *The two-layer structure of Zndtp tribofilms: Part I: AES, XPS and XANES analyses*. Tribology International, 2001. **34**(8): p. 523-530.
59. M. Crobu, A. Rossi, F. Mangolini, and N.D. Spencer, *Tribochemistry of Bulk Zinc Metaphosphate Glasses*. Tribology Letters, 2010. **39**(2): p. 121-134.
60. Bec, S., A. Tonck, J.M. Georges, R.C. Coy, J.C. Bell, and G.W. Roper, *Relationship between mechanical properties and structures of zinc dithiophosphate anti-wear films*. Proceedings of the Royal Society of London. Series A: Mathematical, Physical and Engineering Sciences, 1999. **455**(1992): p. 4181-4203.
61. N.J. Mosey, T.K. Woo, M. Kasrai, P.R. Norton, G.M. Bancroft, and M.H. Müser, *Interpretation of experiments on ZDDP anti-wear films through pressure-induced cross-linking*. Tribology Letters, 2006. **24**(2): p. 105-114.
62. Ghanbarzadeh, A., *Mechano-Chemical Modelling of Boundary Lubrication*, in *School of Mechanical Engineering, PhD thesis*. 2016, University of Leeds. p. 297.
63. R. C. Watkins, *The antiwear mechanism of zddp's. Part II*. Tribology International, 1982. **15**(1): p. 13-15.
64. Aktary, M., M.T. McDermott, and J. Torkelson, *Morphological evolution of films formed from thermooxidative decomposition of ZDDP*. Wear, 2001. **247**(2): p. 172-179.
65. A. Morina, J.H. Green, A. Neville, and M. Priest, *Surface and Tribological Characteristics of Tribofilms Formed in the Boundary Lubrication Regime with Application to Internal Combustion Engines*. Tribology Letters, 2003. **15**(4): p. 443-452.
66. M. A. Nicholls, T. Do, P.R. P. R. Norton, G. M. Bancroft, M. Kasrai, T.W. Capehart, Y.-T. Cheng, and T. Perry, *Chemical and Mechanical Properties of ZDDP Antiwear Films on Steel and Thermal Spray Coatings Studied by XANES Spectroscopy and Nanoindentation Techniques*. Tribology Letters, 2003. **15**(3): p. 241-248.

67. Willermet, P.A. and S.K. Kandah, *Some observations on the role of oxygen in lubricated wear*. Lubrication Science, 1993. **5**(2): p. 129-147.
68. S.H. Choa, K.C. Ludema, G.E. Potter, B.M. Dekoven, T.A. Morgan, and K.K. Kar, *A model of the dynamics of boundary film formation*. Wear, 1994. **177**(1): p. 33-45.
69. Yin, Z., M. Kasrai, M. Fuller, G.M. Bancroft, K. Fyfe, and K.H. Tan, *Application of soft X-ray absorption spectroscopy in chemical characterization of antiwear films generated by ZDDP Part I: the effects of physical parameters*. Wear, 1997. **202**(2): p. 172-191.
70. A. Rossi, M. Eglin, F. M. Piras, K. Matsumoto, and N. D. Spencer, *Surface analytical studies of surface-additive interactions, by means of in situ and combinatorial approaches*. Wear, 2004. **256**(6): p. 578-584.
71. J. M. Palacios, *Films formed by antiwear additives and their incidence in wear and scuffing*. Wear, 1987. **114**(1): p. 41-49.
72. E. Hu, X. Hu, T. Liu, L. Fang, K.D. Dearn, and H. Xu, *The role of soot particles in the tribological behavior of engine lubricating oils*. Wear, 2013. **304**(1–2): p. 152-161.
73. Williams, J.A., *The Behaviour of Sliding Contacts Between Non-Conformal Rough Surfaces Protected by 'Smart' Films*. Tribology Letters, 2004. **17**(4): p. 765-778.
74. Taylor, L., A. Dratva, and H.A. Spikes, *Friction and Wear Behavior of Zinc Dialkyldithiophosphate Additive*. Tribology Transactions, 2000. **43**(3): p. 469-479.
75. S. Jahanmir, *Wear Reduction and Surface Layer Formation by a ZDDP Additive*. Journal of Tribology, 1987. **109**(4): p. 577-586.
76. L. Taylor, H. Spikes, and H. Camenzind, *Film-Forming Properties of Zinc-Based and Ashless Antiwear Additives*. 2000, SAE International.
77. L.J. Taylor and H.A. Spikes, *Friction-Enhancing Properties of ZDDP Antiwear Additive: Part II—Influence of ZDDP Reaction Films on EHD Lubrication*. Tribology Transactions, 2003. **46**(3): p. 310-314.
78. J. Sheasby, T. Caughlin, A. Blahey, and K. Laycock, *A reciprocating wear test for evaluating boundary lubrication*. Tribology International, 1990. **23**(5): p. 301-307.

79. Cann, P. and A. Cameron, *Studies of thick boundary lubrication — influence of zddp and oxidized hexadecane*. Tribology International, 1984. **17**(4): p. 205-208.
80. H.L. Adams, M.T. Garvey, U.S. Ramasamy, Z. Ye, A. Martini, and W. Tysoe, *Shear-Induced Mechanochemistry: Pushing Molecules Around*. The Journal of Physical Chemistry C, 2015. **119**(13): p. 7115-7123.
81. J.M. Martin, T. Onodera, C. Minfray, F. Dassenoy, and A. Miyamoto, *The origin of anti-wear chemistry of ZDDP*. Faraday Discuss, 2012. **156**: p. 311-23; discussion 413-34.
82. T. Onodera, Y. Morita, A. Suzuki, R. Sahnoun, M. Koyama, H. Tsuboi, N. Hatakeyama, A. Endou, H. Takaba, M. Kubo, C.A. Del Carpio, C. Minfray, J.M. Martin, and A. Miyamoto, *A theoretical investigation on the abrasive wear prevention mechanism of ZDDP and ZP tribofilms*. Applied Surface Science, 2008. **254**(23): p. 7976-7979.
83. M.L. Fuller, M. Kasrai, G.M. Bancroft, K. Fyfe, and K.H. Tan, *Solution decomposition of zinc dialkyl dithiophosphate and its effect on antiwear and thermal film formation studied by X-ray absorption spectroscopy*. Tribology International, 1998. **31**(10): p. 627-644.
84. H. Fujita and H. Spikes, *The influence of soot on lubricating films*, in *Tribology Series*, G. Dalmaz, A.A. Lubrecht, D. Dowson, and M. Priest, Editors. 2003, Elsevier: Lyon. p. 37-43.
85. Smeeth, M., H. Spikes, and S. Gunsell, *Performance of Viscosity Index Improvers in Lubricated Contacts*. Langmuir, 1996. **12**(19): p. 4594-4598.
86. M. T. Devlin, S. Li, T. Burgess, and T-C. Jao, *Film Formation Properties of Polymers in the Presence of Abrasive Contaminants*. 2002, SAE International 2002-01-2793.
87. Z. Pawlak, *Tribochemistry of lubricating oils* 1st ed. 2003: Elsevier. 382.
88. F.G. Rounds, *Additive Interactions and Their Effect on the Performance of a Zinc Dialkyl Dithiophosphate*. A S L E Transactions, 1978. **21**(2): p. 91-101.
89. Y. Wan, M. L. Suominen Fuller, M. Kasrai, G. M. Bancroft, K. Fyfe, J. R. Torkelson, Y. F. Hu, and K. H. Tan, *Effects of detergent on the chemistry of tribofilms from ZDDP: studied by X-ray absorption spectroscopy and*

XPS, in *Tribology Series*, M.P.G.D. D. Dowson and A.A. Lubrecht, Editors. 2002, Elsevier. p. 155-166.

90. P.A. Willermet, *Some engine oil additives and their effects on antiwear film formation*. Tribology Letters, 1998. **5**(1): p. 41-47.
91. P. A. Willermet, D. P. Dailey, R. O. Carter, P. J. Schmitz, W. Zhu, J. C. Bell, and D. Park, *The composition of lubricant-derived surface layers formed in a lubricated cam/tappet contact II. Effects of adding overbased detergent and dispersant to a simple ZDTP solution*. Tribology International, 1995. **28**(3): p. 163-175.
92. M. Kasrai, M. S. Fuller, G. M. Bancroft, and P. R. Ryason, *X-Ray Absorption Study of the Effect of Calcium Sulfonate on Antiwear Film Formation Generated From Neutral and Basic ZDDPs: Part 1— Phosphorus Species*. Tribology Transactions, 2003. **46**(4): p. 534-542.
93. M. Kasrai, M. S. Fuller, G. M. Bancroft, E. S. Yamaguchi, and P. R. Ryason, *X-Ray Absorption Study of the Effect of Calcium Sulfonate on Antiwear Film Formation Generated From Neutral and Basic ZDDPs: Part 2 — Sulfur Species*. Tribology Transactions, 2003. **46**(4): p. 543-549.
94. M. A. Nicholls, G. M. Bancroft, P. R. Norton, M. Kasrai, G. De Stasio, B.H. Frazer, and L.M. Wiese, *Chemomechanical Properties of Antiwear Films Using X-ray Absorption Microscopy and Nanoindentation Techniques*. Tribology Letters, 2004. **17**(2): p. 245-259.
95. M. Shiomi, J. Mitsui, K. Akiyama, K. Tasaka, M. Nakada, and H. Ohira, *Formulation Technology for Low Phosphorus Gasoline Engine Oils*. 1992, SAE International.
96. G. C. Smith and J. C. Bell, *Multi-technique surface analytical studies of automotive anti-wear films*. Applied Surface Science, 1999. **144–145**: p. 222-227.
97. M.R. Cho and D.C. Han, *Vane tip detachment in a positive displacement vane pump*. KSME International Journal, 1998. **12**(5): p. 881-887.
98. Parker, D.B., *Positive displacement pumps-performance and application*, in *11th International Pump Users Symposium*. 1994.

99. M. Rundo and N. Nervegna, *Geometry Assessment of Variable Displacement Vane Pumps*. Journal of Dynamic Systems, Measurement, and Control, 2006. **129**(4): p. 446-455.
100. J. Foder and F. Ling, *Friction Reduction in an IC Engine through Improved Filtration and a New Lubricant Additive*, "Lubrication Engineering". 1985 October: p. 614-618.
101. S. Agarwal, V.K. Chhibber, and A.K. Bhatnagar, *Tribological behavior of diesel fuels and the effect of anti-wear additives*. Fuel, 2013. **106**: p. 21-29.
102. V.S. Azev and A.V. Sereda, *Influence of sulfur compounds on antiwear properties of diesel oils*. Chemistry and Technology of Fuels and Oils, 2009. **45**(3): p. 170-176.
103. J. Yan, T. Shamim, S.K Chou, U. Desideri, and H. Li, *Clean, Efficient and Affordable Energy for a Sustainable Future*. Applied Energy, 2016. **75**: p. 111-117.
104. S. Capone, M. Zuppa, D.S. Presicce, L. Francioso, F. Casino, and P. Siciliano, *Metal oxide gas sensor array for the detection of diesel fuel in engine oil*. Sensors and Actuators B: Chemical, 2008. **131**(1): p. 125-133.
105. I. Cesur, V. Ayhan, A. Parlak, Ö. Savaş, and Z. Aydin, *The Effects of Different Fuels on Wear between Piston Ring and Cylinder*. SAGE, Advances in Mechanical Engineering, 2014.
106. D. Ljubas, H. Krpan, and I. Matanoviæ, *Influence of engine oils dilution by fuels on their viscosity, flash point and fire point*. Nafta, 2010. **61**(2): p. 73-79.
107. D. A. Green and R. Lewis, *The effects of soot-contaminated engine oil on wear and friction: a review*. Automobile Engineering 2008. **222**(9): p. 1669-1689.
108. Clague, A.D.H., J.B. Donnet, T.K. Wang, and J.C.M. Peng, *A comparison of diesel engine soot with carbon black*. Carbon, 1999. **37**(10): p. 1553-1565.
109. GmbH, R.B., *Bosch Automotive handbook*. 9th ed. 2014, Karlsruhe: Robert Bosch GmbH.

110. M. Ratoi, R. C. Castle, C. H. Bovington, and H. A. Spikes, *The influence of soot and dispersant on ZDDP film thickness and friction*, *Lubrication Science* 17. 2004: p. 25-43.
111. M.F. Guo, Z.B. Cai, Z.C. Zhang, and M.H. Zhu, *Characterization and lubrication performance of diesel soot nanoparticles as oil lubricant additives*. RSC Advances, 2015. **5**(123): p. 101965-101974.
112. Sharma, V., D. Uy, A. Gangopadhyay, A. O'Neill, W.A. Paxton, A. Sammut, M.A. Ford, and P.B. Aswath, *Structure and chemistry of crankcase and exhaust soot extracted from diesel engines*. Carbon, 2016. **103**: p. 327-338.
113. Uy, D., M.A. Ford, D.T. Jayne, A.E. O'Neill, L.P. Haack, J. Hangas, M.J. Jagner, A. Sammut, and A.K. Gangopadhyay, *Characterization of gasoline soot and comparison to diesel soot: Morphology, chemistry, and wear*. Tribology International, 2014. **80**: p. 198-209.
114. Y. Olomolehin, R. Kapadia, and H. Spikes, *Antagonistic Interaction of Antiwear Additives and Carbon Black*. Tribology Letters, 2010. **37**(1): p. 49-58.
115. D. Uy, A.E. O'Neill, S.J. Simko, and A.K. Gangopadhyay, *Soot-additive interactions in engine oils*. Lubrication Science, 2010. **22**(1): p. 19-36.
116. A.Y. Watson and P.A. Valberg, *Carbon black and soot: two different substances*. American Industrial Hygiene Association 2001. **62**: p. 218-228.
117. T.C. Jao, S. Li, K. Yatsunami, S.J. Chen, A.A. Csontos, and J.M. Howe, *Soot characterisation and diesel engine wear*. Lubrication Science, 2004. **16**(2): p. 111-126.
118. P. Ramkumar, L. Wang, T. J. Harvey, R. J. K. Wood, K. Nelson, E. Yamaguchi, J.J. Harrison, and H.E.G. Powrie, *The Effect of Diesel Engine Oil Contamination on Friction and Wear*, in *World tribology congress, 3rd 2005; WTC2005-63854*. 2005.
119. CC. Kuo, C. A. Passut, T. C. Jao, A. A. Csontos, and J. M. Howe, *Wear Mechanism in Cummins M-11 High Soot Diesel Test Engines*. 1998, SAE International 981372.

120. A.D.H. Clague, J.B. Donnet, T.K. Wang, and J.C.M. Peng, *A comparison of diesel engine soot with carbon black*<sup>1</sup>. *Carbon*, 1999. **37**(10): p. 1553-1565.
121. Green, D.A. and R. Lewis, *Effect of soot on oil properties and wear of engine components*. *Journal of Physics D: Applied Physics*, 2007. **40**(18): p. 5488.
122. Liu, C., S. Nemoto, and S. Ogano, *Effect of Soot Properties in Diesel Engine Oils on Frictional Characteristics*. *Tribology Transactions*, 2003. **46**(1): p. 12-18.
123. R. Penchaliah, T J. Harvey, R J K. Wood, K. Nelson, and H E G. Powrie, *The effects of diesel contaminants on tribological performance on sliding steel on steel contacts*. *Engineering Tribology*, 2011. **225**.
124. Penchaliah, R., T. Harvey, R. Wood, K. Nelson, and H. Powrie, *The effects of diesel contaminants on tribological performance on sliding steel on steel contacts*. *Proceedings of the Institution of Mechanical Engineers, Part J: Journal of Engineering Tribology*, 2011. **225**(8): p. 779-797.
125. H. Fujita and H.A. Spikes, *Study of Zinc Dialkyldithiophosphate Antiwear Film Formation and Removal Processes, Part II: Kinetic Model*. *Tribology Transactions*, 2005. **48**(4): p. 567-575.
126. F. Chiñas-Castillo and H.A. Spikes, *The Behavior of Diluted Sooted Oils in Lubricated Contacts*. *Tribology Letters*, 2004. **16**(4): p. 317-322.
127. Rounds, F.G., *Soots from used diesel-engine oils: their effects on wear as measured in 4-ball wear tests*. 1981, SAE International.
128. D.A. Green and R. Lewis, *Investigation of Soot Contaminated Lubricant Wear Mechanisms*. 2007, SAE International.
129. M. Torrance, *Wear of lubricated steel in the presence of dispersed carbon*, in *IMEchE Mission of Tribology Conference*. 2004.
130. P.R. Ryason, I.Y. Chan, and J.T. Gilmore, *Polishing wear by soot*. *Wear*, 1990. **137**(1): p. 15-24.
131. W. Cadman and J.H. Johnson, *The study of the effect of exhaust gas recirculation on engine wear in a heavy-duty diesel engine using analytical ferrography* SAE International, 1986.



132. I, N., H. Endo, H. Nakamura, and H. Yano, *Soot and Valve Train Wear in Passenger Car Diesel Engines*, SAE Technical Paper 831757. SAE International, 1983.
133. C. C. Devlin, C. A. Passut, R. L. Campbell, and T.C. Jao, *Biodiesel Fuel Effect on Diesel Engine Lubrication*. 2008, SAE International 2008-01-2375.
134. Gautam, M., K. Chitoor, S. Balla, and M. Keane, *Contribution of Soot Contaminated Oils to Wear-Part II*. 1999, SAE International.
135. M. Gautam, M. Durbha, K. Chitoor, M. Jaraiedi, N. Mariwalla, and D. Ripple, *Contribution of Soot Contaminated Oils to Wear*. 1998, SAE International.
136. T. Skurai and K. Yoshida, *Tribological Behaviour of Dispersed Phase Systems*, in *International Tribology*. 1987.
137. D.A. Green, R. Lewis, and R.S. Dwyer-Joyce, *Wear effects and mechanisms of soot-contaminated automotive lubricants*. Engineering Tribology, 2006. **220**: p. 159-169.
138. H. Sato, N. Tokuoka, H. Yamamoto, and M. Sasaki, *Study of wear mechanism by soot contaminated in engine oil*. SAE International, 1999.
139. F.G. Rounds, *Carbon: Cause of Diesel Engine Wear?* . SAE International, 1977.
140. I. Berbezier, M. Martin, and Ph. Kapsa, *The role of carbon in lubricated mild wear*. Tribology International, 1986. **19**(3): p. 115-122.
141. S. Corso and R. Adamo, *The Effect of Diesel Soot on Reactivity of Oil Additives and Valve Train Materials*. SAE Paper, 1984.
142. K. Hosonuma, K. Yoshida, and A. Matsunaga, *The decomposition products of zinc dialkyldithiophosphate in an engine and their interaction with diesel soot*. Wear, 1985. **103**(4): p. 297-309.
143. M. Gautam, K. Chitoor, M. Durbha, and J.C. Summers, *Effect of diesel soot contaminated oil on engine wear — investigation of novel oil formulations*. Tribology International, 1999. **32**(12): p. 687-699.
144. J.K. Mowlem and J.C. Edwards, *Lubricant additive chemistry effects of diesel engine soot on wear performance as studied by XPS and solid-*

state NMR, in *Colloid and Surface Science Symposium*. 2002: Pennsylvania State University.

145. D. M. Stehouwer, H. L. Fang, D. Wooton, and H. Martin, *Interaction Between Fuel Additive and Oil Contaminant: (I) Field Experiences*. 2003, SAE International.
146. H. L. Fang, D. M. Stehouwer, and J. C. Wang, *Interaction Between Fuel Additive and Oil Contaminant: (II) Its Impact on Fuel Stability and Filter Plugging Mechanism*. 2003, SAE International.
147. J. E. Booth, K. D. Nelson, T. J. Harvey, R. J. K. Wood, L. Wang, H. E. G. Powrie, and J. G. Martinez, *The feasibility of using electrostatic monitoring to identify diesel lubricant additives and soot contamination interactions by factorial analysis*. *Tribology International*, 2006. **39**(12): p. 1564-1575.
148. W. Tuszynski, R. Michalczewski, W. Piekoszewski, and M. Szczerek, *Effect of ageing automotive gear oils on scuffing and pitting*. *Tribology International*, 2008. **41**(9–10): p. 875-888.
149. G.C. Offunne, A.U. Maduako, and C.M. Ojinnaka, *Studies on the ageing characteristics of automotive crankcase oils*. *Tribology International*, 1989. **22**(6): p. 401-404.
150. D. Troyer *Lubricant Lifecycle Management - Part 1*, in *Machinery Lubrication*. 2007.
151. Ancho, L.C. *Oxidation in lubricant base oils*. 2006 [cited 2016 19 August].
152. Metrics, F. *Oil Degradation Mechanisms*. 2012 [cited 2016 1 August]; Available from: <http://www.fluidmetrics.com/degradation.html>.
153. K.L. Kreuz, *Gasoline Engine Chemistry as Applied to Lubricant Problems*. *Lubrication Science*, 1969. **55**: p. 53-46.
154. X. Zhang, H. Murrenhoff, P. Weckes, and W. Hölderich, *Effect of temperature on the ageing behaviour of unsaturated ester-based lubricants*. *Journal of Synthetic Lubrication*, 2004. **21**(1): p. 1-11.
155. S. Beyer-Faiss and T.G. Horb, *Test Method for Simulating the Aging and Oxidation Stability of Lubricants*, in *Practicing Oil Analysis*. 2005.

156. W.D. Phillips, *The high-temperature degradation of hydraulic oils and fluids*. Journal of Synthetic Lubrication, 2006. **23**(1): p. 39-70.
157. S. Bec, A. Tonck, J.M. Georges, R.C. Coy, J.C. Bell, and G. W. Roper, *Relationship between mechanical properties and structures of zinc dithiophosphate anti-wear films*. Proceedings of the Royal Society of London A: Mathematical, Physical and Engineering Sciences, 1999. **455**(1992): p. 4181-4203.
158. P.A. Willermet, S.K. Kandah, W.O. Siegl, and R.E. Chase, *The Influence of Molecular Oxygen on Wear Protection by Surface-Active Compounds*. ASLE Transactions, 1983. **26**(4): p. 523-531.
159. H. Spedding and R.C. Watkins, *The antiwear mechanism of ZDDP's. Part I*. Tribology International, 1982. **15**(1): p. 9-12.
160. D. Uy, S.J. Simko, R.O. Carter III, R.K. Jensen, and A.K. Gangopadhyay, *Characterization of anti-wear films formed from fresh and aged engine oils*. Wear, 2007. **263**(7-12): p. 1165-1174.
161. J.S. Zabinski and N.T. MacDevitt, *Raman Spectra of Inorganic Compounds Related to Solid State Tribochemical Studies*. USAF Wright Laboratory Report No. WL-TR-96-4034., 1996.
162. International, A., *Standard test method for corrosiveness and oxidation stability of hydraulic oils*. 2010.
163. S. Korcek, R.K. Jensen, and M.D. Johnson, *Assessment of the useful life of current long-drain and future low-phosphorus engine oils*. Tribotest, 2003. **9**(3): p. 197-207.
164. C.X. Li, *Weat Testing and Wear Measurement*. Surface Engineering: University of Birmingham.
165. Y. Perez Delgado, K. Bonny, P. De Baets, P. D. Neis, O. Malek, J. Vleugels, and B. Lauwers, *Impact of wire-EDM on dry sliding friction and wear of WC-based and ZrO<sub>2</sub>-based composites*. Wear, 2011. **271**(9-10): p. 1951-1961.
166. D. Lin-Vien, N.B. Colthup, W.G. Fateley, and J.G. Grasselli, *The Handbook of infrared and raman characteristic frequencies of organic molecules*. 1991: Academic Press.

167. B. Graça and J. Seabra, *Improving realibility of wind turbine gearboxes throught oil analysis, Unit of Tribology, Vibrations and Industrial Maintenance*, in *International Conference on Experimental Mechanics*. 2012: Porto, Portugal.
168. G.E. Totten and V.J.D. Negri, *Handbook of Hydraulic Fluid Technology*. Second ed. Vol. 2. 2011, GB: CRC Press.
169. S. Berkani, F. Dassenoy, J.M. Martin, H. Cardon, G. Montagnac, and B. Reynard, *Structural Changes in Tribo-Stressed Zinc Polyphosphates*. *Tribology Letters*, 2013. **51**: p. 489-498.
170. D.N. Khaemba, A. Neville, and A. Morina, *A methodology for Raman characterisation of MoDTC tribofilms and its application in investigating the influence of surface chemistry on friction performance of MoDTC lubricants*. *Tribology Letters*, 2015. **59**(3): p. 1-17.
171. D. Chiriu, P.C. Ricci, A. Polcaro, P. Braconi, D. Lanzi, and D. Nadali, *Raman Study on Pompeii Potteries: The Role of Calcium Hydroxide on the Surface Treatment*. *Journal of Spectroscopy*, 2014. **2014**: p. 10.
172. T.Y. Kwon, T. Fujishima, and Y. Imai, *FT - Raman spectroscopy of calcium hydroxide medicament in root canals*. *International endodontic journal*, 2004. **37**(7): p. 489-493.
173. A. Morina, A. Neville, M. Priest, and J.H. Green, *ZDDP and MoDTC interactions and their effect on tribological performance – tribofilm characteristics and its evolution*. *Tribology Letters*, 2006. **24**(3): p. 243-256.
174. A. Morina and A. Neville, *Tribofilms: aspects of formation, stability and removal*. *Journal of Physics D: Applied Physics*, 2007. **40**(18): p. 5476.
175. Berkani, S., F. Dassenoy, C. Minfray, J.-M. Martin, H. Cardon, G. Montagnac, and B. Reynard, *Structural Changes in Tribo-Stressed Zinc Polyphosphates*. *Tribology Letters*, 2013. **51**(3): p. 489-498.
176. Lin-Vien D, C.N., Fateley WG, Grasselli JG., *The handbook of infrared and Raman characteristic frequencies of organic molecules*. 1991, New York: Academic Press.
177. J.S. Tse, Y. Song, and Z. Liu, *Effects of Temperature and Pressure on ZDDP*. *Tribology Letters*, 2007. **28**(1): p. 45-49.

178. Rudnick, L.R., *Synthetics, Mineral oils, and Bio-Based Lubricants: Chemistry and Technology*. 2005: Taylor & Francis.
179. Y. A. Gur'yanov, *Criteria for Limiting Contamination of Motor Oil by Fuel*. 2007. **43**(1): p. 30-36.
180. N. N. Gosvami, J.A. Bares, F. Mangolini, A.R. Konicek, D.G. Yablon, and R.W. Carpick, *Mechanisms of antiwear tribofilm growth revealed in situ by single-asperity sliding contacts*. *Science*, 2015. **348**(6230): p. 102-106.
181. S. Ushioda, *Raman scattering from phonons in iron pyrite (FeS<sub>2</sub>)*. *Solid State Communications*, 1972. **10**(3): p. 307-310.
182. H. Vogt, T. Chattopadhyay, and H.J. Stolz, *Complete first-order Raman spectra of the pyrite structure compounds FeS<sub>2</sub>, MnS<sub>2</sub> AND SiP<sub>2</sub>*. *Journal of Physics and Chemistry of Solids*, 1983. **44**(9): p. 869-873.
183. M. Hirata and H. Watanabe, *Wear in Vane Pump Test*. *A S L E Transactions*, 1979. **22**(4): p. 342-348.
184. B.H. Song and Y.H. Choi, *Investigation of variations of lubricating oil diluted by post-injected fuel for the regeneration of CDPF and its effects on engine wear*. *Journal of Mechanical Science and Technology*, 2008. **22**(12): p. 2526-2533.
185. M. Diaby, M. Sablier, A. Le Negrate, M. El Fassi, and J. Bocquet, *Understanding carbonaceous deposit formation resulting from engine oil degradation*. *Carbon*, 2009. **47**(2): p. 355-366.
186. J. Martínez and A.C. Aguiar, *Analytical Supercritical Fluid Extraction*, in *Analytical Separation Science*. 2015, Wiley-VCH Verlag GmbH & Co. KGaA.
187. A. Kupareva, P. Mäki-Arvela, H. Grénman, K. Eränen, R. Sjöholm, M. Reunanen, and D.Y. Murzin, *Chemical Characterization of Lube Oils*. *Energy & Fuels*, 2013. **27**(1): p. 27-34.
188. Y. Arai and D.L. Sparks, *ATR-FTIR Spectroscopic Investigation on Phosphate Adsorption Mechanisms at the Ferrihydrite-Water Interface*. *Journal of Colloid and Interface Science*, 2001. **241**(2): p. 317-326.
189. M.C. Garry and J. Bowman, *FT-IR Analysis of Used Lubricating Oils – General Considerations*. Thermo Fisher Scientific Inc, 2007.

190. S. George, S. Balla, V. Gautam, and M. Gautam, *Effect of diesel soot on lubricant oil viscosity*. Tribology International, 2007. **40**(5): p. 809-818.
191. D.A. Duncan, M. Rees, A.L Szabo, and L. Williams, *Soot-Related Viscosity Increase - Further Studies Comparing the Mack T-11 Engine Test to Field Performance*. 2005, SAE International.
192. S. Li, M. T. Passut, M. T. Devlin, and T. C. Jao, *Diesel soot particles dispersion by oil soluble surfactants*, in *Fifth World Surfactants Congress 2000*: Firenze.
193. Wei, D.P., *The lubricity of fuels, I. Wear studies on diesel fuel components*. 1986. **2**: p. 79-87.
194. H.L. Costa and H. Spikes, *Effects of Ethanol Contamination on Friction and Elastohydrodynamic Film Thickness of Engine Oils*. Tribology Transactions, 2015. **58**(1): p. 158-168.
195. J. Hancsok, L. Bartha, I. Molnar, J. Auer, J. Baladincz, and Z. Kocsis. *Interactions between modern engine oils and reformulated fuels*. in *Technische Akademie Esslingen International Tribology Colloquium Proceedings*. 2004.
196. M. T. Costello and M. Kasrai, *Study of surface films of overbased sulfonates and sulfurized olefins by X-Ray Absorption Near Edge Structure (XANES) spectroscopy*. Tribology Letters, 2006. **24**(2): p. 163-169.
197. A. Agoston, C. Ötsch, and B. Jakoby, *Viscosity sensors for engine oil condition monitoring—Application and interpretation of results*. Sensors and Actuators A: Physical, 2005. **121**(2): p. 327-332.
198. S. Amat, Z. Braham, Y. Le Dréau, J. Kister, and N. Dupuy, *Simulated aging of lubricant oils by chemometric treatment of infrared spectra: Potential antioxidant properties of sulfur structures*. Talanta, 2013. **107**: p. 219-224.
199. B. Rahimi, A. Semnani, A. Nezamzadeh-Ejhieh, H. Shakoory Langeroodi, and M. Hakim Davood, *Monitoring of the Physical and Chemical Properties of a Gasoline Engine Oil during Its Usage*. Journal of Analytical Methods in Chemistry, 2012. **2012**: p. 8.

200. T.J. Fabish and M.L. Hair, *The dependence of the work function of carbon black on surface acidity*. Journal of Colloid and Interface Science, 1977. **62**(1): p. 16-23.
201. C.W. Snow, D.R. Wallace, L.L. Lyon, and G.R. Crocker, *Influence of hydrogen content on oxidation of carbon blacks*. Carbon, 1959.
202. M. T. Devlin, T. Dvorsak, K. Garelick, J. M. Guevremont, G. Guinther, K. Hux, J. T. Loper, and R. Sheets, *Effect of Fluid Aging on ZDDP Tribofilm Formation and Tribofilm Properties*. International Automotive Forum & SAE-China Congress, 2010.
203. A.M. Barnes, K.D. Bartle, and V.A. Thibon, *A review of zinc dialkyldithiophosphates (ZDDPS): characterisation and role in the lubricating oil*. Tribology International, 2001. **34**(6): p. 389-395.
204. R.C. Coy and R.B. Jones, *The Thermal Degradation and EP Performance of Zinc Dialkyldithiophosphate Additives in White Oil*. ASLE Transactions, 1981. **24**(1): p. 77-90.